

**VERSLAGEN EN VERHANDELINGEN**

REPORTS AND TRANSACTIONS

**NATIONAAL LUCHT- EN RUIMTEVAART-  
LABORATORIUM**

NATIONAL AEROSPACE LABORATORY NLR

**THE NETHERLANDS**

\*

**XXXIII - 1968**

VV(1968)33

## PREFACE

This volume of Reports and Transactions of the National Aerospace Laboratory NLR contains a selection of reports completed in recent years.

These reports have been prepared in connection with investigations carried out under contract for the Netherlands Aircraft Development Board (NIV). The permission for publication is herewith acknowledged. In addition to the selected reports which are collected at more or less regular intervals in the volumes of Reports and Transactions numerous others are published on subjects studied by the NLR.

A complete list of publications issued from 1921 through 1967 is available upon request.

Amsterdam, April 1968

A. J. Marx

(General Director)

## CONTENTS

NLR-TR M. 2143

D. BROEK

The residual strength of aluminium alloy sheet specimens containing fatigue cracks or saw cuts.

NLR-TR M. 2145

D. BROEK

The residual strength of cracked sheet. Tests interrupted after intermediate slow crack growth.

NLR-TR M. 2148

J. SCHIJVE AND P. DE RIJK

The effect of 'ground-to-air cycles' on the fatigue crack propagation in 2024-T3 alclad sheet material.

NLR-TR M. 2149

D. BROEK AND F. A. JACOBS

The static strength of aluminium alloy sheet specimens containing blunt notches.

NLR-TR M. 2152

D. BROEK

The effect of finite specimen width on the residual strength of light alloy sheet.

NLR-TR M. 2154

D. BROEK AND A. NEDERVEEN

The influence of the loading rate on the residual strength of aluminium alloy sheet specimens.

NLR-TR M. 2156

J. SCHIJVE AND P. DE RIJK

The crack propagation in two aluminium alloys in an indoor and an outdoor environment under random and programmed load sequences.

NLR-TR M. 2160

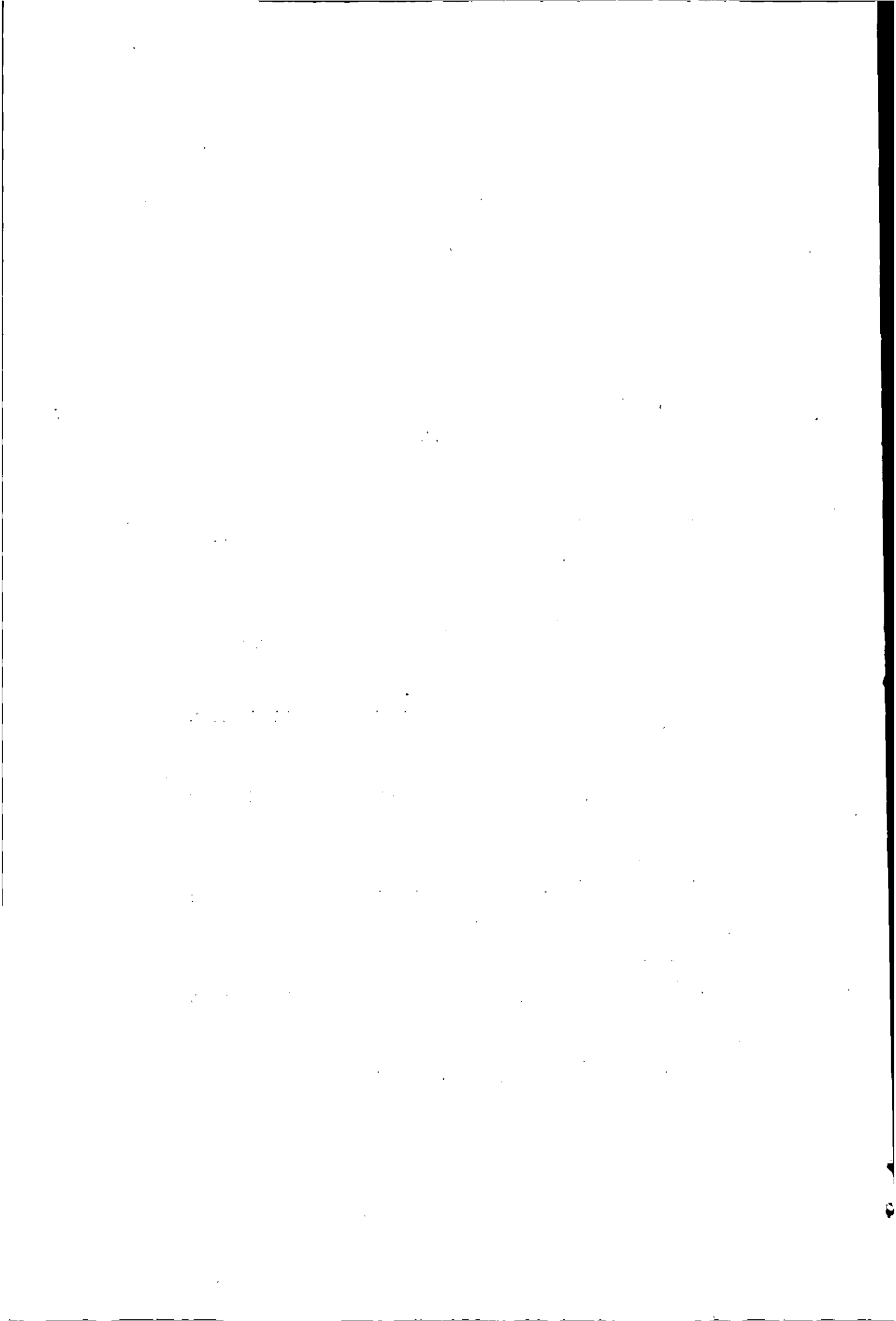
D. BROEK

The effect of the sheet thickness on the fracture toughness of cracked sheet.

NLR-TR M. 2162

J. SCHIJVE AND P. DE RIJK

The fatigue crack propagation in 2024-T3 alclad sheet materials from seven different manufacturers.



REPORT NLR-TR M. 2143

# The residual strength of aluminium alloy sheet specimens containing fatigue cracks or saw cuts

by

D. BROEK

## Summary

Specimens of 2024-T3 and 7075-T6 aluminium alloy sheet containing fine saw cuts appear to have the same residual strength as specimens with fatigue cracks of the same length. The stress level at which the fatigue cracks were grown does not affect the residual strength properties.

Stop holes drilled at the crack tip postpone the onset of slow crack growth to a higher stress. If slow crack growth precedes fracture the residual strength is not affected by the acuteness of the initial crack, and there always is slow crack growth if the stress that initiates slow crack growth is not raised to or beyond the residual strength of a specimen with a fatigue crack of equal initial length.

## Contents

	Page	$\sigma_{0.2}$	0.2% yield strength
1 Introduction	1	$\sigma_c$	critical fracture stress (residual strength)
2 Experimental details	2	$\sigma_i$	stress to initiate slow crack growth
2.1 Materials and specimens	2	$\sigma_{nett}$	fracture stress based on nett cross section
2.2 Testing technique	2	$\sigma_u$	ultimate tensile strength
3 Test results	3		All stresses, except $\sigma_{nett}$ , are based on gross area.
4 Discussion	3		<b>Units</b>
5 Conclusions	8		length mm (1 inch = 25.4 mm)
6 References	8		force kg (1 lb = 0.454 kg)
2 tables			stress kg/mm <sup>2</sup> (1000 psi = 0.703 kg/mm <sup>2</sup> )
13 figures			

## List of symbols

$E$	modulus of elasticity
$2l$	crack length
$2l_0$	initial crack length
$2l_c$	critical crack length at fracture
$S_a$	stress amplitude in a fatigue test
$S_m$	mean stress in a fatigue test
$U$	elastic energy
$W$	plastic energy
$2w$	specimen width
$\alpha, \beta, p$	constants
$\delta$	elongation
$\rho$	radius of crack tip

## 1 Introduction

In specimens for residual strength tests the crack is often simulated by a saw cut made by a fine fret saw, because the production of fatigue cracks is time consuming. A saw cut, though very fine, has a blunt tip which implies that the stress concentration at the tip may be of lower intensity than the stress concentration at the sharp tip of a fatigue crack. This might well affect the result of a residual strength test, thus reducing the value of the test. The aim of the present investigation was to study this effect and to determine whether a saw cut as a simulation of a crack could give reliable residual strength results for aluminium alloy sheets.

A fatigue crack, grown at a large stress amplitude, may have a somewhat blunter tip than a fatigue crack developed at low stresses. It has been suggested in the literature that this might affect the residual strength. This problem was also studied in the present investigation. Furthermore a few preliminary tests were carried out to get some information on the effectiveness of drilling stop holes at the crack tips in gaining a higher residual strength.

**2 Experimental details**

**2.1 Materials and specimens**

The materials tested were 2024-T3 and 7075-T6 alclad sheet of 2 mm thickness, having the following static properties (averages of 8 test for each material)

	$\sigma_{0.2}$ (kg/mm <sup>2</sup> )	$\sigma_u$ (kg/mm <sup>2</sup> )	$\delta$ (2 in.) (%)
2024-T3	+1.4	+0.6	
	36.4	47.6	18
	-1.6	-1.0	
7075-T6	+0.8	+0.4	
	51.4	55.2	12
	-0.9	-0.4	

The specimens were cut to a size of 680 x 300 mm (fig. 1) and provided with a central transverse crack or saw cut. Three types of cracks were used, as illustrated in fig. 1. The length of the initial crack  $2l_0$  was either 45 or 90 mm for the 2024-T3 specimens and either 25 or 60 mm for 7075-T6 specimens. The specimens with fatigue cracks were first provided with a short fine saw cut and then fatigued in a hydraulic Amsler pulsator of 50 tons capacity. The initial saw cut was of such a length that an additional fatigue crack of 15 mm at both ends of the saw cut was necessary to obtain the required total crack length. The specimens were fatigued at a mean

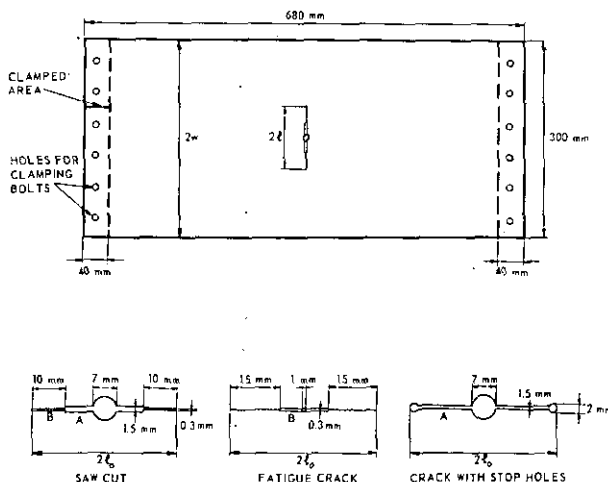


Fig. 1 The specimen

Saw cuts A were made by means of a jig saw (saw cut width 1.5 mm). Saw cuts B were made by means of a jeweller's fret saw (saw cut width 0.3 mm).

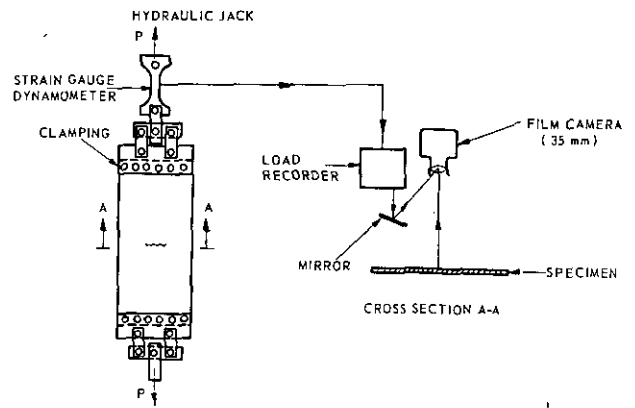


Fig. 2 Arrangement of test

stress  $S_m = 8$  kg/mm<sup>2</sup>, and a stress amplitude  $S_a = 2.5$  kg/mm<sup>2</sup> for the low-fatigue-load cracks, and at a stress amplitude  $S_a = 6.5$  kg/mm<sup>2</sup> for the high-fatigue-load cracks. For each type of crack and at each crack length two specimens were used for both materials, leading to a total number of 32 tests.

**2.2 Testing technique**

The residual strength tests were carried out in an ad hoc test set-up. The specimen ends were bolted in a "fir-tree" clamping device and loaded in tension by a hydraulic jack of 50 tons capacity (fig. 2). A strain gauge dynamometer in combination with a strip chart recorder provided the load records.

During the test the specimen was filmed (14 frames per second) to record the slow stable crack growth preceding fracture and the critical crack length at fracture. Through a mirror arrangement the load recorder was filmed simultaneously (fig. 2) and the load at the onset of slow crack growth could thus be determined from the film. The duration of a test was between 1 and 2 minutes.

There could be some doubt as to the usefulness of crack growth observations at the specimen surface from cinematographic records, since the crack might be longer in the interior of the specimen than at the surface. This was checked by sectioning a specimen that

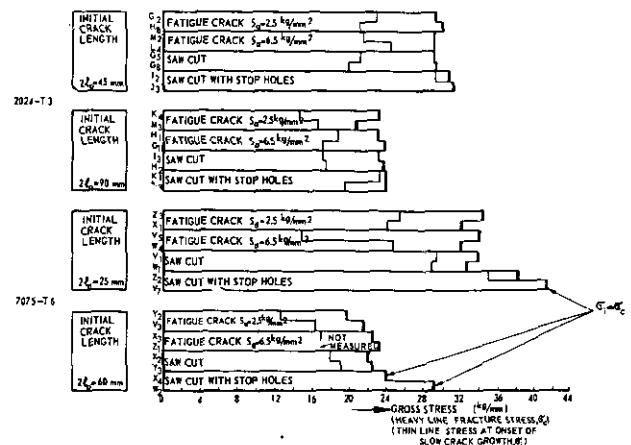


Fig. 3 Stresses for crack growth and fracture

had shown a small amount of slow crack growth and had been unloaded before fracture. The curvature of the crack front was determined by measuring the crack length microscopically in a number of sections parallel to the sheet surface. It turned out that in the interior of the specimen the crack was at most 1 mm longer than at the surface and it may be concluded that, for the (thin) sheet used in the present investigation, filming gives reliable crack growth records.

### 3 Test results

The test results are collected in table 1 and plotted as bar graphs in figs. 3 and 4. The most important technical result, viz. the fracture stress is plotted as a function of initial crack length in fig. 5. In this figure also results of ref. 1 are plotted (obtained from similar specimens of the same batch of material). Furthermore the stress to initiate slow crack growth is plotted as a function of crack length in fig. 6.

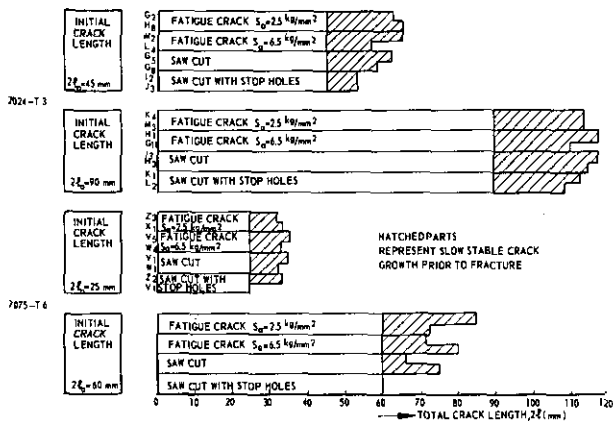


Fig. 4 Slow (stable) crack growth and critical crack length

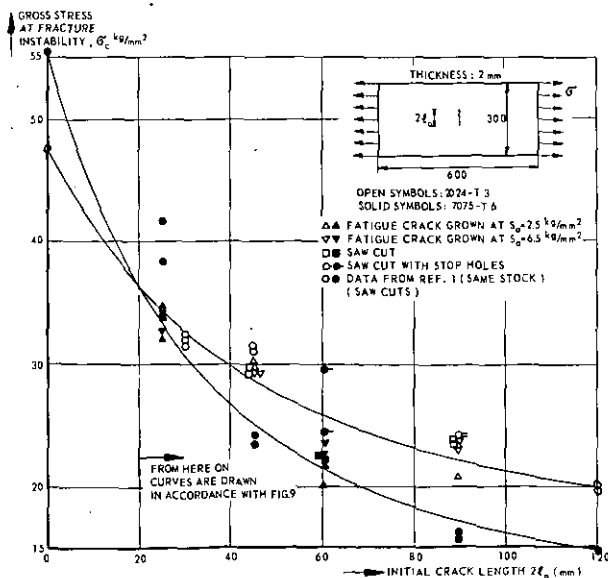


Fig. 5 The fracture stress

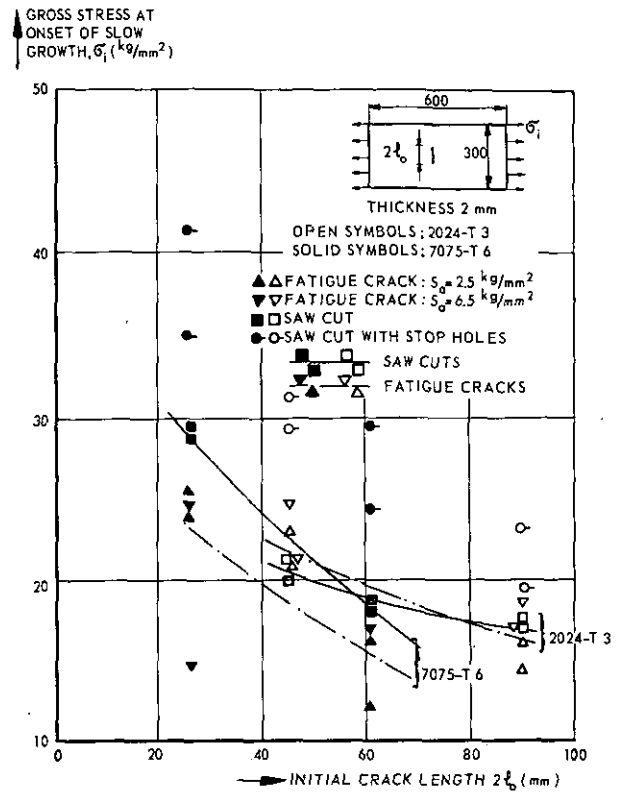


Fig. 6 The stress at the onset of slow crack growth

### 4 Discussion

As for the technical implications of the present results it can be concluded that the simulation of cracks by fine saw cuts gave reliable values for the residual strength of 2024-T3 and 7075-T6 aluminium alloy sheet specimens, as used in the present investigation. Stop holes increased the residual strength, in the case of the 7075-T6 alloy. Possibly larger stop holes would have given even better results, which will be discussed later in this chapter. The stress level during fatigue crack growth did not affect the residual strength properties which is not surprising in view of the results for the saw cuts. This is confirmed by data obtained in ref. 2, presented here in fig. 7. Fig. 7 even suggests a trend opposite to what would be expected, i.e. that high fatigue loads would give slightly worse results at small crack lengths. It is felt, however, that this is a more or less fictitious result, since at high fatigue loads the crack front may have a larger curvature and the crack length in the interior of the (fairly thick) specimen might have been somewhat larger than observed at the surface. This would shift the data points for the high fatigue loads in fig. 7 in the direction of those for the low fatigue loads.

Some more data concerning the comparison of saw cuts and fatigue cracks, obtained from refs. 3 and 4, are given in fig. 8. For the 7075 alloy in fig. 8a there seems to be a large difference between saw cuts and fatigue cracks. The sheet width used for the specimens of fig. 8a is not given in ref. 3 but a small sketch of the specimens

TABLE 1  
Test results

Specimen	Material	Type of crack	Initial crack length $2l_0(\text{mm})$	$\sigma_i$ kg/mm <sup>2</sup>	Critical crack length $2l_c(\text{mm})$	$\sigma_c$ kg/mm <sup>2</sup>	$\frac{\sigma_c}{\sigma_u}$
G2	2024-T3 ( $\sigma_u = 47.6 \text{ kg/mm}^2$ )	— $S_a = 2.5$	45	23.2	62.5	29.5	0.62
H8			45	21.2	65	30.1	0.63
M2		— $S_a = 6.5$	47	21.5	65	29.4	0.62
L4			45	24.7	57	29.4	0.62
G5		=== saw cut	45	21.4	63	29.4	0.62
G8			44.5	20.0	58	29.6	0.62
I2		○—○ stop holes	44	29.6	53	30.9	0.65
J3			44	31.3	53	31.4	0.66
M3	— $S_a = 2.5$		90	14.8	114	20.7	0.435
K4			90.5	16.5	114	23.4	0.49
G11	— $S_a = 6.5$		90	18.9	118	23.8	0.50
H1			90.5	17.2	110	23.2	0.49
H2	=== saw cut		89	17.2	117	23.7	0.50
I3			89	17.5	115	23.9	0.505
K1	○—○ stop holes		90	23.4	113	24.1	0.51
L2			90	19.7	109	24.1	0.51
X1	7075-T6 ( $\sigma_u = 55.2 \text{ kg/mm}^2$ )	— $S_a = 2.5$	25	25.8	32	32.1	0.58
Z3			25	24.1	33.5	34.6	0.625
V5	— $S_a = 6.5$		25	14.8	35.5	34.4	0.625
W4			25	24.8	32.5	32.3	0.585
V1	=== saw cut		24.5	29.7	35	34.0	0.615
W1			25	29.1	32	32.8	0.595
Z2	○—○ stop holes		24	35.2	33	38.3	0.695
V7			24	41.8	24	41.8	0.761
V3	— $S_a = 2.5$		60	12.4	85	21.6	0.39
Y2			60	16.3	72	19.9	0.36
X3	— $S_a = 6.5$		60	17.0	71	22.6	0.41
Z1			60		80	23.3	0.42
X2	=== saw cut		59.5	18.1	66	22.1	0.40
Y3			59.5	19.0	75	22.4	0.405
X4	○—○ stop holes		59	24.3	59	24.3	0.44
W2			59	29.5	59	29.5	0.535

is presented, suggesting that the specimens with fatigue cracks had a larger width than the specimens with saw cuts. Moreover this sketch indicates that the specimens with fatigue cracks had a crack at one specimen edge only. Therefore it is felt that the data points in fig. 8a are not comparable. Fig. 8b gives an indication that the conclusions drawn from the present tests cannot be generalized for other materials.

Important features emerging from the present tests are the influences of saw cuts and stop holes on the stress  $\sigma_i$  for the initiation of slow crack growth (figs. 3 and 6).

For both 2024-T3 and 7075-T6 stop holes are effective in raising  $\sigma_i$  and so are saw cuts in the case of 7075-T6 specimens. Apparently the stress concentration at a stop hole or the tip of a saw cut is lower than at an actual crack tip, causing slow crack growth to start at a higher gross stress. If slow crack growth occurs it is immaterial whether this crack growth started at a blunt or a sharp crack; in both cases the same fracture stress and the same critical crack length are observed. If the stop holes are able to postpone the initiation of crack growth to a stress equal to or higher than the fracture

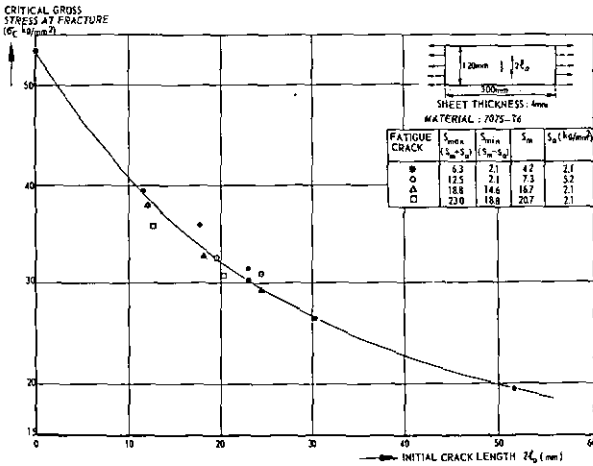


Fig. 7 Residual strength of specimens with fatigue cracks grown at different fatigue loads (ref. 2)

strength in the case of absence of stop holes no slow crack growth is observed (table 1) and fracture occurs immediately when the crack starts to extend.

These observations are an interesting support to the crack growth criteria proposed in ref. 5. It was suggested in ref. 5 that slow crack growth starts when the stress at the crack tip exceeds a certain critical value. This criterion leads to:

$$\sigma_l \sqrt{\frac{l}{\rho}} = \text{constant} \quad (1)$$

in which  $\rho$  is the tip radius of an elliptical crack with semi-major axis  $l$ . It was further stated that during slow crack growth the condition

$$\frac{\partial U}{\partial l} + \frac{dW}{dl} = 0 \quad (2)$$

should be fulfilled and the criterion for fracture instability as proposed in ref. 5 reads properly written:

$$\left. \begin{aligned} \frac{\partial U}{\partial l} + \frac{dW}{dl} &= 0 \\ \frac{\partial^2 U}{\partial l^2} + \frac{d^2 W}{dl^2} &= 0 \end{aligned} \right\} \quad (3)$$

In these equations  $\partial U/\partial l$  is the elastic energy release during a crack extension  $dl$  (energy available for crack extension) and  $dW/dl$  is the energy consumption during a crack extension  $dl$  (associated with plastic work). Adopting the hypothesis of Krafft and co-workers (ref. 6), which states that  $dW/dl$  is a function of the amount of slow crack growth only, one can rewrite eqs. (3) in the form (see ref. 5):

$$\sigma_c l_0^p = \text{constant} \quad (4)$$

where  $l_0$  is the initial crack length,  $\sigma_c$  is the critical stress (at fracture) and  $p$  is a constant.

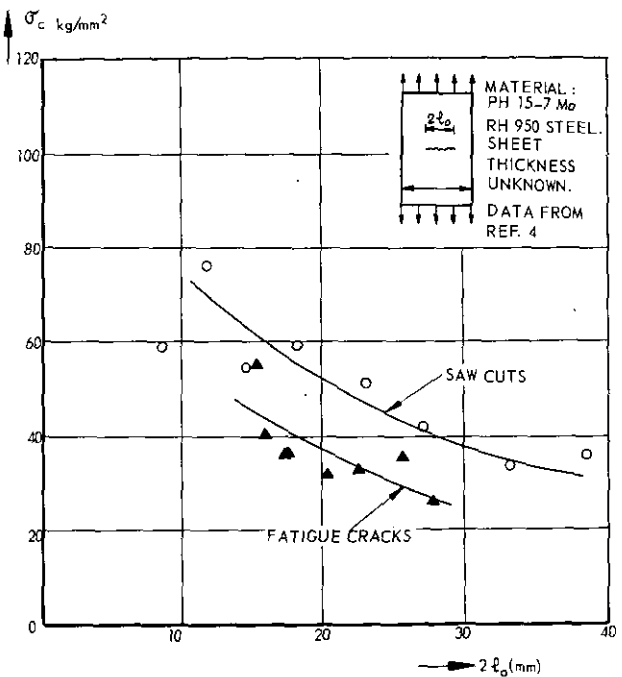
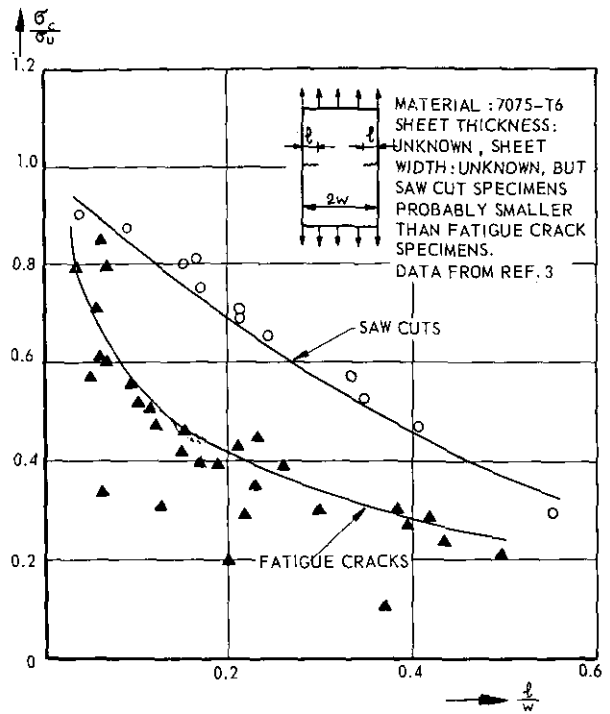


Fig. 8 Results of residual strength tests as presented in refs 3 and 4.

Eq. (4) is valid for an infinite sheet. Therefore it can be checked with test results only if no finite width effect is involved, i.e. only results of specimens with small ratios  $l/w$  should be considered. Then, according to fig. 9, the criterion of eq. (4) is found to be obeyed with reasonable accuracy.

Fig. 10 is the basis for the derivation of eq. (4).  $dW/dl$  is plotted as a function of the crack extension  $l-l_0$  (ref. 6) and  $\partial U/\partial l$  as a function of the instantaneous crack length  $l$ ; the slope of the lines for  $-U/\partial l$  is proportional to  $\sigma^2$  (see eq. in fig. 10). At a stress  $\sigma_1 < \sigma_c$  and an initial crack length  $l_0$  the possible value of  $\partial U/\partial l$  is

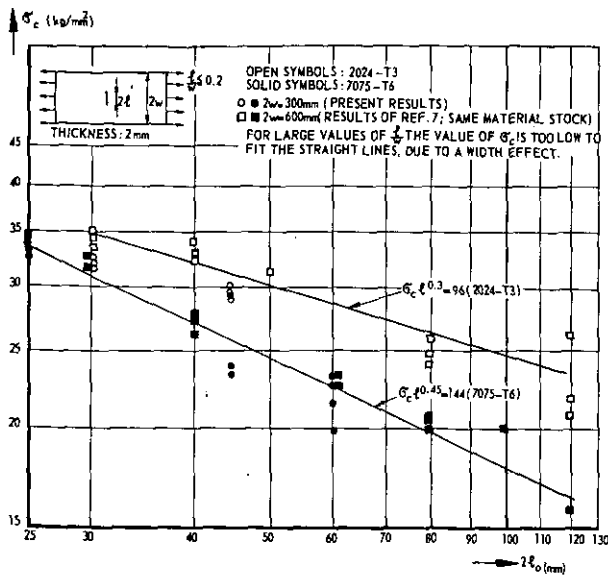


Fig. 9 The relation between residual strength and crack length

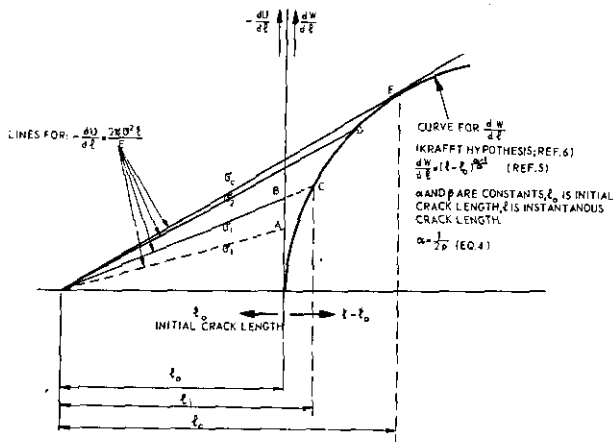


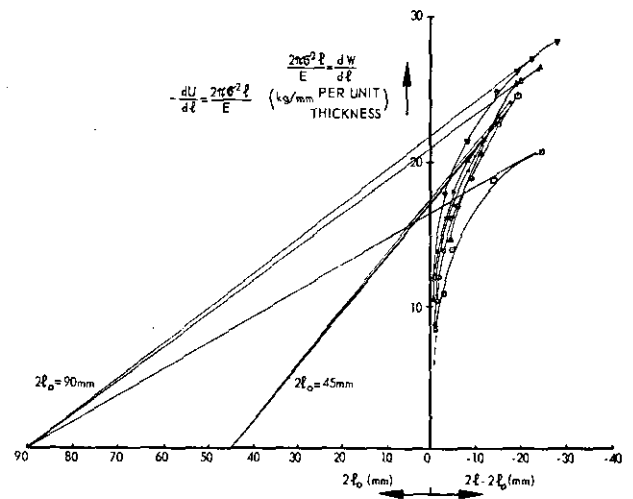
Fig. 10 Energy criteria for crack growth

represented by point A. However, crack extension does not occur ( $dl=0$ ). Let the criterion for the onset of slow crack growth be fulfilled at a stress  $\sigma_1$ . The value for  $-\partial U/\partial l$  at the onset of crack growth is represented by point B. There is some oversupply of energy giving a discrete crack extension to the length  $l_1$  where  $\partial U/\partial l$  and  $dW/dl$  are balanced (point C). Such a discrete crack extension (to  $l_1$ ) at the onset of slow crack growth, generally associated with a distinct burst or pop-in, was often observed and in most of the present tests as well. During further increase of the stress there is a continuous balance between  $\partial U/\partial l$  and  $dW/dl$  giving the appropriate gradual crack extension. When the stress  $\sigma_c$  is reached the crack length is  $l_c$  (point E). Further crack extension (at constant stress) now gives an increasing oversupply of energy and fracture instability occurs (eqs. 3).

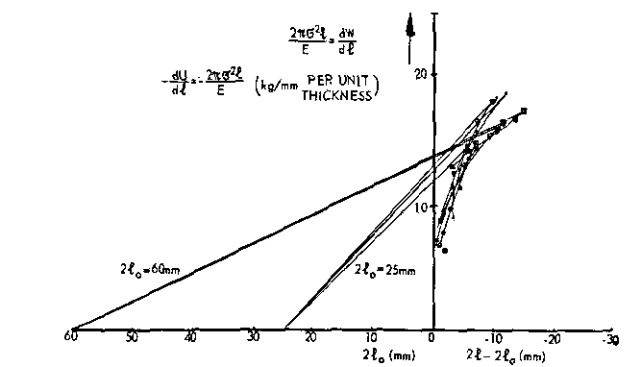
A blunt tip of the initial crack postpones slow crack growth to a stress, say  $\sigma_2 > \sigma_1$ . From then on the behaviour is the same as for a short initial crack. If the tip of the initial crack is so blunt that crack growth is postponed

to a stress equal to or higher than  $\sigma_c$ , immediate fracture occurs (fig. 10) as soon as the crack starts to extend.

The curve for  $dW/dl$  could be obtained from the present investigation. From simultaneous film readings of stress and crack length during slow crack growth the values of  $-\partial U/\partial l = 2\pi\sigma^2 l/E$  could be calculated ( $E$  is modulus of elasticity). Since during slow crack growth  $\partial U/\partial l + dW/dl = 0$  (points C, D, E in fig. 10) the curve for  $dW/dl$  is obtained also. For a number of specimens the calculated points are plotted in fig. 11. This figure shows that indeed fracture occurs when eqs. (3) are fulfilled and that the curve for  $dW/dl$  is of the form shown in fig. 9. The curve for  $dW/dl$  should be the same for all specimens. It might be argued that this is not the case in fig. 11. It should be noted, however, that scatter in  $\sigma_c$  and in the amount of slow crack growth is unavoidable and partly due to light variations in material properties and to limited accuracy of measurement. The scatter of these two variables cumulates in the value of  $\sigma_c^2 l$  and it is seen from fig. 11a that for tests with the same initial crack length ( $2l_0 = 90$  mm) the scatter in  $\sigma_c^2 l$  may already be large. The scatter will also be partly due to an effect of finite specimen width. The latter effect tends to give too low values of  $\sigma_c$  at large crack lengths, which might be responsible for the



a. 2024-T3 SPECIMENS



b. 7075-T6 SPECIMENS

Fig. 11  $dW/dl$  as observed from the present test results

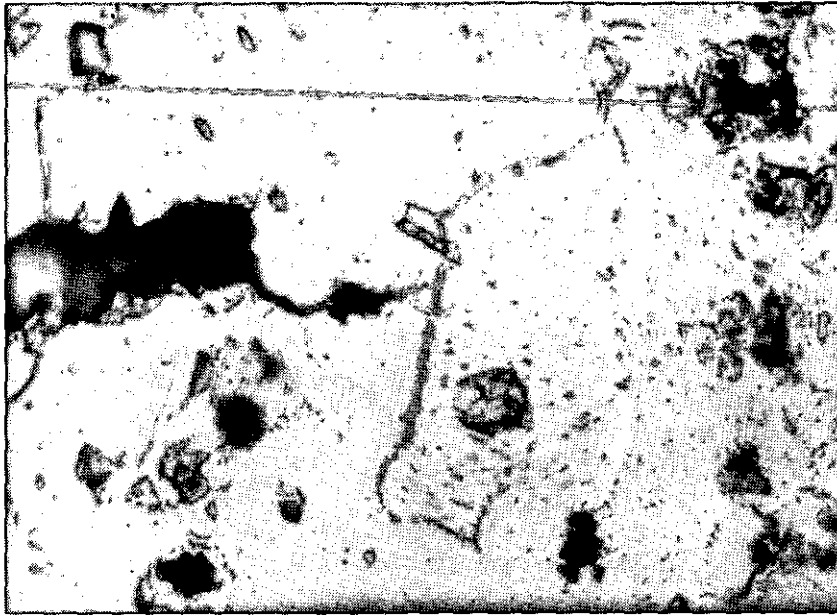


Fig. 12 Slow crack growth starting from a fatigue crack ( $\times 1000$ ). Note blunting of fatigue crack

discrepancy between the curves for  $2l_0 = 60$  mm and for  $2l_0 = 25$  mm in fig. 11b. It can be concluded that there is reason to believe that the Krafft hypothesis (ref. 6) of an invariant curve for  $dW/dl$  as a function of  $l-l_0$  is

obeyed by the present specimens, giving support to the fracture criteria of eqs. 2-4 (ref. 5).

In this connection it is interesting to refer to fig. 12, which shows that at the onset of slow crack growth the fatigue crack has blunted considerably. The newly formed crack is quite sharp, which might point to a difference between the original crack and the slow-growth crack. This observation could give some ground to the hypothesis that  $dW/dl$  is a function of slow crack growth only.

An important conclusion can be drawn on the effectiveness of stop holes. Apparently stop holes can increase the fracture strength only if they are able to increase  $\sigma_i$  to a value above  $\sigma_c$ , pertaining to the case without stop holes. It should be pointed out then what determines the value of  $\sigma_i$ . In the previous discussion the criterion has been given by eq. (1). Evaluation of this criterion for the specimens with stop holes is carried out in table 2. An almost constant value for  $\sigma_i\sqrt{l}/\sigma_c$  is indeed obtained. A further check should be made by testing various types of stop holes.

The minimum diameter for stop holes to have a beneficial effect depends upon the type of material and is smaller for the less ductile 7075-T6 alloy. The explanation is that a ductile alloy is able to deform plastically to a large extent thus blunting a sharp crack tip and reducing the stress concentration to the level of that at a large stop hole. In a material with a very low ductility, very small stop holes may have a considerable effect already as is shown in fig. 13 obtained from ref. 8. A very small root radius of the crack is sufficient to raise  $\sigma_i$  above  $\sigma_c$ , and thus increase the fracture strength.

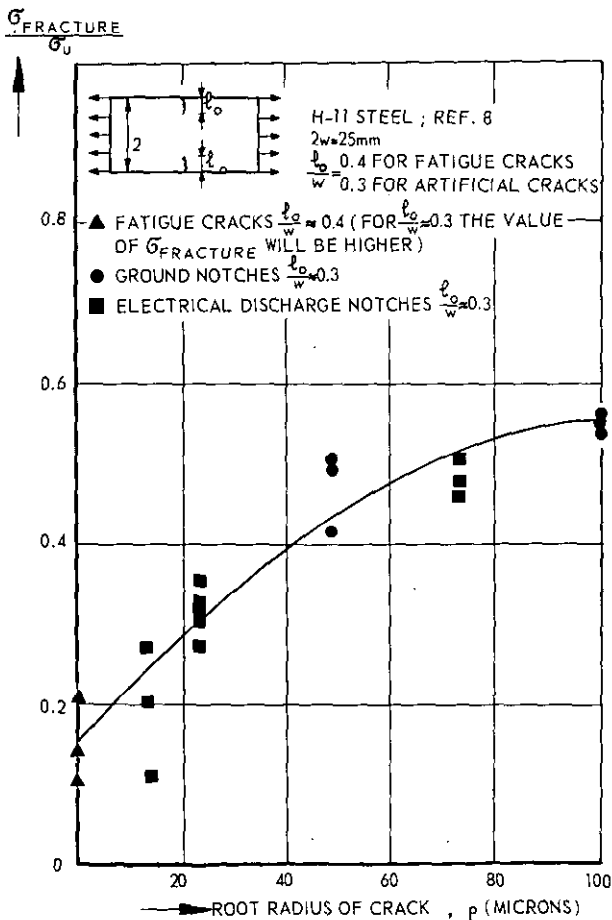


Fig. 13 Test results of ref. 8

TABLE 2  
The criterion for the initiation of crack growth

Type of crack	2024-T3				7075-T6			
	$2l_0$ (mm)	$\sigma_i$ (kg/mm <sup>2</sup> )	$\sigma_i/l_0/\rho$ (kg/mm <sup>2</sup> )	$\sigma_i/l_0^*$ (kg/mm <sup>3/2</sup> )	$2l_0$ (mm)	$\sigma_i$ (kg/mm <sup>2</sup> )	$\sigma_i/l_0/\rho$ (kg/mm <sup>2</sup> )	$\sigma_i/l_0^*$ (kg/mm <sup>3/2</sup> )
stop holes $\rho = 1$ mm	45	29.6	140		25	35.2	124	
	45	31.3	148		25	41.8	148	
	90	23.4	157		60	24.3	133	
	90	19.7	132		60	29.5	161	
saw cuts	45	21.4		101	25	29.7		105
	44.5	20.0		95	25	29.1		103
	90	17.2		115	60	18.1		99
	90	17.5		117	60	19.0		104
fatigue cracks	45	23.2		110	25	25.8		91
	45	21.2		101	25	24.1		85
	47	21.5		104	25	14.8		52
	45	24.7		117	25	24.8		88
	90	14.8		99	60	12.4		68
	90	16.5		111	60	16.3		89
	90	18.9		127	60	17.0		93
	90	17.2		115	60	—		—

\*) For fatigue cracks and saw cuts  $\rho$  cannot be defined, but is assumed to be a constant for any length of a particular type of crack.

## 5 Conclusions

From an experimental investigation on the residual strength of 2024-T3 and 7075-T6 specimens of 300 mm width and 2 mm thickness the following conclusions can be drawn:

- In specimens for residual strength tests the initial fatigue crack may be simulated by a fine saw cut. This may give slightly unconservative results for the stress at the onset of slow crack growth, but reliable results are obtained for the critical crack length and the residual strength (critical gross stress at fracture).
- The fatigue loads at which the fatigue cracks were formed do not affect the results of the residual strength test.
- Stop holes at the crack tips increase the stress for the initiation of slow crack growth, but have no favourable effect on the residual strength, unless they are so large that the onset of crack growth is postponed to a stress higher than the fracture stress for the case without stop holes. In the latter case immediate fracture occurs as soon as the crack starts to extend. In other words: if slow crack growth precedes fracture the critical stress is not affected by the acuteness of the initial crack and there always is slow crack growth, provided that crack extension starts at a stress below the critical stress of a specimen with a fatigue crack of the same initial length.

- The tests confirmed the crack growth criteria proposed in ref. 5.

## 6 References

- This investigation has been performed under contract with the Netherlands Aircraft Development Board (N.I.V.)
- BROEK, D., The effect of sheet thickness on fracture toughness of light alloy sheet. To be published as NLR report M. 2160.
  - NIEUWENHUIZEN, M.P., Private communication. Royal Netherlands Aircraft Factories "Fokker".
  - CRISTENSEN, R.H., Fatigue cracking, fatigue damage and their detection. Metal Fatigue p. 391. Un. of Calif. Engng. Extension Series. Ed. by Sines and Waisman, Mc Graw-Hill, 1959.
  - CRISTENSEN, R.H., Cracking and fracture in metals and structures. Proceedings of the crack-propagation symposium, Cranfield 1961, Vol. II pp. 326-374. Cranfield, the College of Aeronautics, 1962.
  - BROEK, D., The residual strength of cracked sheet and structures. NLR report M. 2135, Aug. 1964.
  - KRAFFT, J.M., SULLIVAN, A.M., BOYLE, R.W., Effect of dimensions on fast fracture instability of notched sheets. Proceedings of the crack-propagation symposium, Cranfield 1961, Vol. I, pp. 8-28. Cranfield, the College of Aeronautics, 1962.
  - BROEK, D., The effect of finite specimen width on the residual strength of light alloy sheet. NLR report M. 2152.
  - Special ASTM Committee, Fracture testing of high-strength sheet materials. 3rd report of committee. Materials Research and Standards 1, 11 (Nov. 1961) pp. 877-885.

REPORT NLR-TR M.2145

# The residual strength of cracked sheet - Tests interrupted after intermediate slow crack growth

by

D. BROEK

## Summary

Residual strength tests were performed on 2024-T3 and 7075-T6 aluminium alloy sheet specimens of 600 mm width. After the cracks had shown some stable slow growth the specimens were unloaded and then reloaded. Unloading appeared to have no effect on the residual strength.

## Contents

	Page
List of symbols	
1 Introduction.	
2 Experimental details.	
3 Test results.	
4 Discussion.	
5 Technical implication of the test results.	
6 The present results and the energy criterion for fracture.	
7 Conclusions.	
8 References.	
2 tables.	
10 figures	

## Symbols

$2l$	— crack length
$2l_0$	— initial crack length
$2l_{01}$	— crack length at first interruption of the test
$2l_{02}$	— crack length at second interruption of the test
$2l_c$	— crack length at fracture instability
$U$	— elastic energy
$W$	— plastic energy
$\alpha, p$	— numerical constants
$\delta$	— elongation
$\sigma_{0.2}$	— 0.2% yield strength
$\sigma_c$	— critical fracture stress (residual strength)
$\sigma_i$	— stress to initiate slow crack growth
$\sigma_{i1}$	— stress to re-initiate crack growth after first interruption of test
$\sigma_{i2}$	— stress to re-initiate crack growth after second interruption of test

$\sigma_{r1}$	— stress at first interruption of test
$\sigma_{r2}$	— stress at second interruption of test
$\sigma_u$	— ultimate tensile strength
$\sigma_y$	— yield strength

All stresses are based on gross area

## Units

length mm (1 inch = 25.4 mm)  
 force kg (1 lb = 0.454 kg)  
 stress kg/mm<sup>2</sup> (1000 psi = 0.703 kg/mm<sup>2</sup>)

## 1 Introduction

Consider a sheet containing a central transverse crack (of length  $2l_0$ ) loaded in tension. At a certain value  $\sigma_i$  of the gross stress the crack will start to extend slowly. The stress can still be increased under continuous gradual slow crack growth until at a certain crack length  $2l_c$  and a gross stress  $\sigma_c$  fracture instability occurs. Both the stress  $\sigma_i$  to initiate crack growth and the fracture stress  $\sigma_c$  are lower if the initial crack is longer. The amount of slow crack growth is larger for longer initial cracks.

The slow crack growth preceding fracture is interesting from a theoretical point of view and is not well understood. From an engineering point of view the phenomenon gives rise to an important problem: A high load in service may induce slow growth of an existing crack. A longer crack then remains, having possibly a lower residual strength. Several of such loads

This investigation has been performed under contract with the Netherlands Aircraft Development Board (N.I.V.)

might impair the residual strength so much that fracture might occur at loads which previously only induced slow crack growth.

It seemed worthwhile to investigate the effect of high preloads on the residual strength. Therefore tests were carried out on large aluminium alloy sheet specimens. Firstly the residual strength curve was determined. In a second test series the specimens were loaded until the cracks had shown a certain amount of slow crack growth. The tests were then interrupted by fully unloading the specimens, after which the specimens were fractured by reloading. A number of tests were interrupted twice in this way.

This report gives the results of the tests and a discussion from a technical point of view. The results are also used to check the criteria for slow crack growth and fracture as presented in ref. 1 and 2.

## 2 Experimental details

The materials tested were 2024-T3 Alclad and 7075-T6 Clad sheets of 2 mm thickness, having the following static properties (averages of 8 tests):

	$\sigma_{0.2}$ (kg/mm <sup>2</sup> )	$\sigma_u$ (kg/mm <sup>2</sup> )	$\delta_{2in}$ %
2024-T3	36.4 <sup>+1.4</sup> -1.6	47.6 <sup>+0.6</sup> -1.0	18
7075-T6	51.4 <sup>+0.8</sup> -0.9	55.2 <sup>+0.4</sup> -0.4	12

The specimens were cut to a size of 1280 × 600 mm (51 × 24 in, see fig. 1) and provided with a fine central transverse saw cut, made by means of a jeweller's fret saw. It was shown in ref. 3 for aluminium alloy sheet that this saw cut can simulate a fatigue crack for the purpose of residual strength tests. The stress to initiate slow crack growth was slightly higher for a saw cut than for a fatigue crack, but once slow crack growth had started the behaviour was the same (same  $\sigma_c$  and  $l_c$ ).

The residual strength tests were carried out in an ad hoc test set-up. The specimens were loaded in tension by means of a hydraulic jack of 50 tons capacity. A strain gauge dynamometer in combination with a strip chart recorder provided the load records. During the test the specimen was filmed continuously (at 14 frames per second) to record the slow crack growth. Through a mirror arrangement the load recorder was filmed simultaneously (fig. 1). From the cinematographic records the relation between stress and crack length during slow growth and the crack length at the interruption of the tests could be determined. As was pointed out in ref. 3 for the thin sheets used in the present investigation filming gives reliable crack growth records.

Fig. 1 Test arrangement.

## 3 Test results

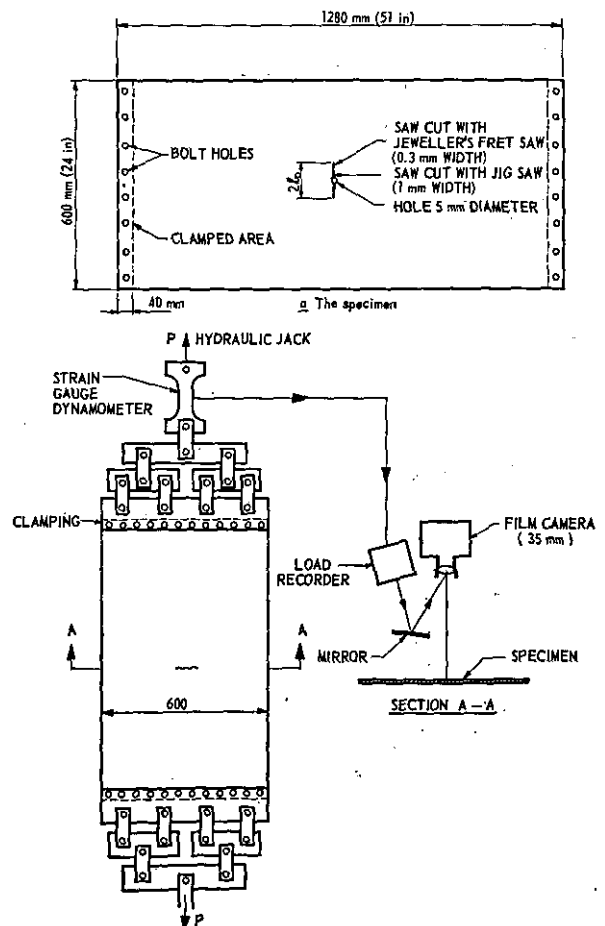
The test results are collected in table 1 for the 2024-T3 alloy and in table 2 for the 7075-T6 alloy. In these tables the results of the interrupted tests are compared with two series of continuous tests. As appears from tables 1 and 2 a number of tests were interrupted twice. The residual strength curves (the fracture stress as a function of initial crack length) are plotted in figs. 2 and 3. In these figures the results of the interrupted tests are also shown, again as a function of initial crack length.

The slow crack growth curves are given in figs. 4 and 5. For the continuous tests only average curves are given in order to avoid confusion. Only two curves of each series of 4 interrupted tests are plotted (The results of the other tests are similar and the characteristic points of these curves are given in tables 1 and 2).

Finally in figs. 6 and 7 the critical crack length is plotted as a function of the initial crack length.

## 4 Discussion

From the residual strength curves in figs. 2 and 3 it can be concluded that one or two interruptions of a residual strength test have no influence on the residual strength. A better appreciation of the results can be obtained from figs. 4 and 5. For the discussion of these



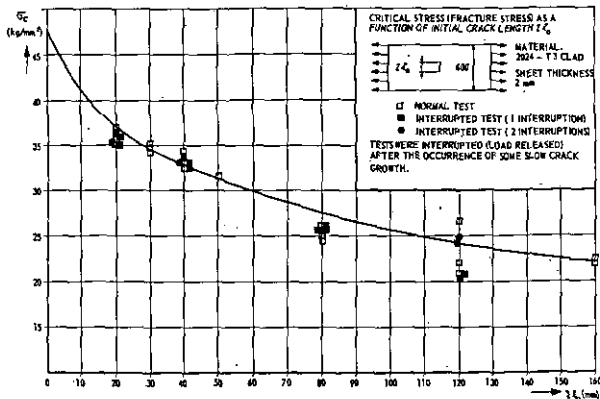


Fig. 2 Influence of unloading and reloading on the residual strength.

figures reference is made also to fig. 8. There are two distinct ways in which a specimen might behave when it is reloaded after a load release to  $\sigma = 0$ .

Suppose the initial crack length is  $2l_0$  (fig. 8) and the specimen is unloaded after the crack has grown to a length  $2l_{01}$ . At reloading, one of the following two extreme possibilities can happen:

- The specimen behaves as a new specimen with an initial crack length  $2l_{01}$ . Consequently, slow crack growth is initiated at a stress  $\sigma_1^*$  in accordance with the curve for the start of slow crack growth (fig. 8) and fracture occurs at a stress  $\sigma_c^*$ , which is the fracture stress belonging to an initial crack length  $2l_{01}$  (fig. 8).
- There is no influence of unloading and the crack continues to grow as soon as the stress  $\sigma_r$  is reached,

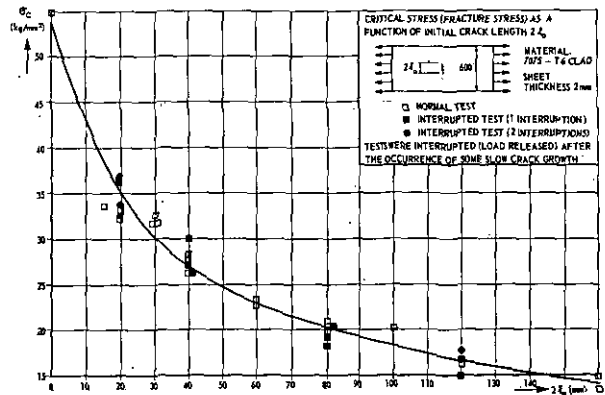


Fig. 3 Influence of unloading and reloading on the residual strength.

$\sigma_r$ , being the stress at which the test was interrupted.

Figs. 4 and 5 show that after an interruption there is no initiation of slow crack growth in accordance with the curve for the start of slow crack growth, though crack growth is continued at a stress somewhat below  $\sigma_r$ .

Soon after the re-initiation of crack growth the original slow growth curve is followed again. The specimen apparently "remembers its load history and ignores the unloading".

It seems reasonable to conclude that if the interrupted tests had been carried out as continuous tests crack propagation curves would have been obtained similar to the dotted curves given in figs. 4 and 5.

At the moment of the interruption of the test a plastic zone of a certain size has formed at the crack tip (fig.

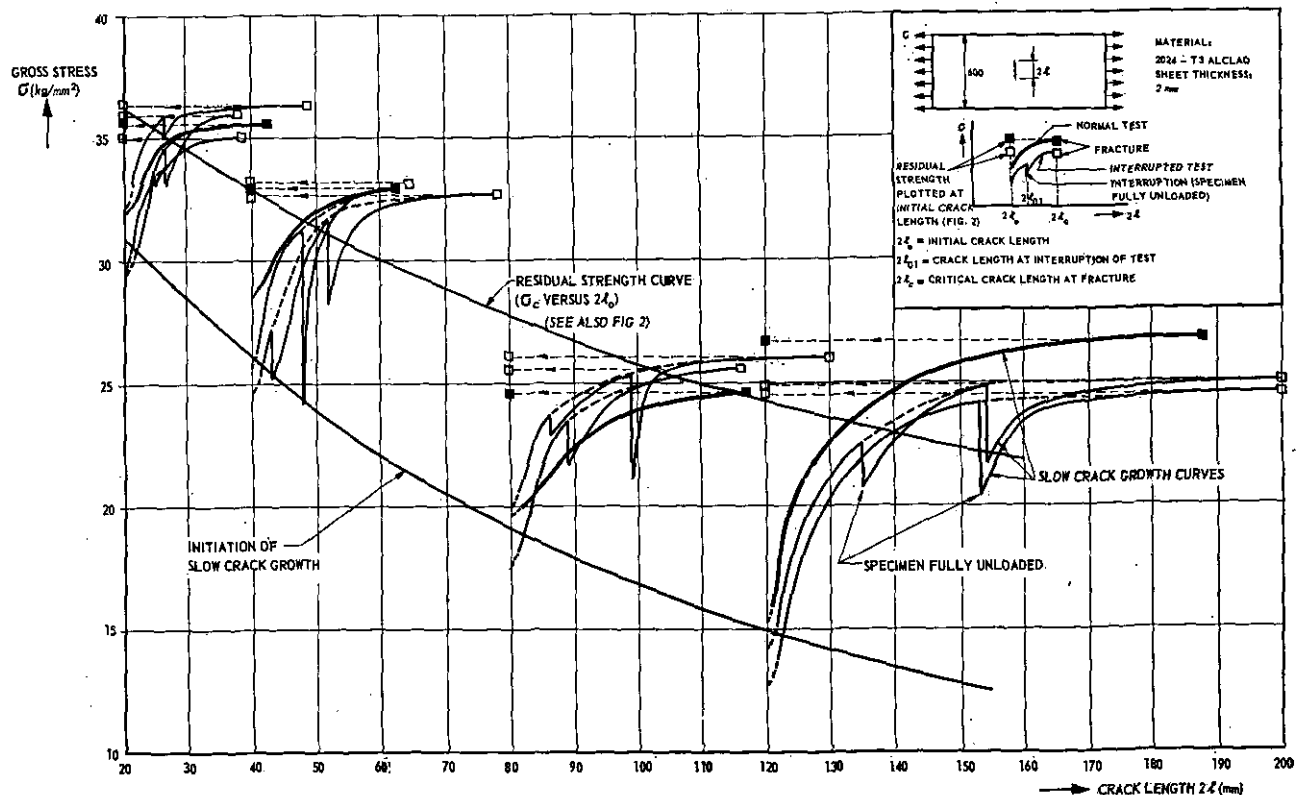


Fig. 4 Influence of unloading to zero stress on slow crack growth.

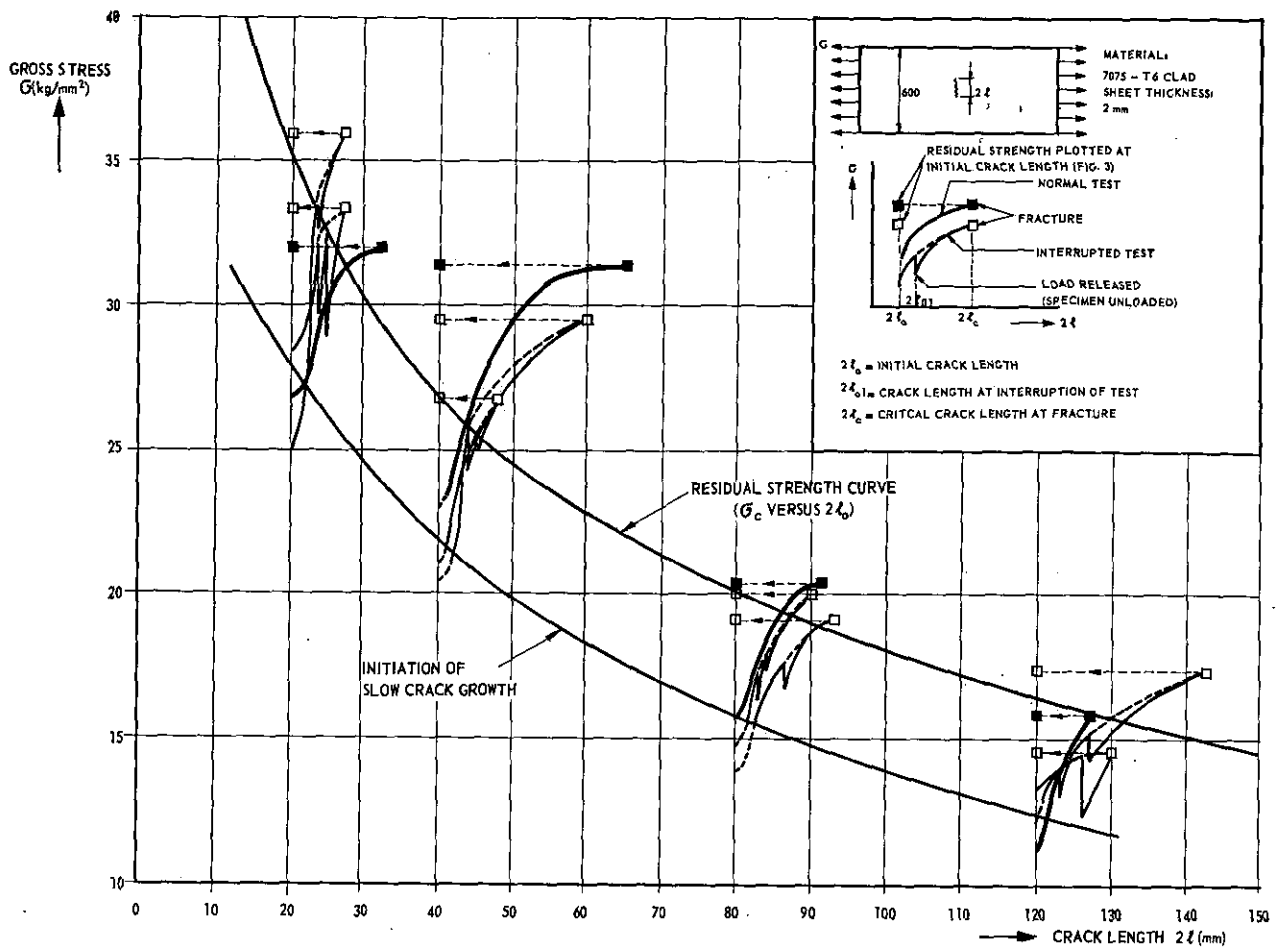


Fig. 5 Influence of unloading to zero stress on slow crack growth.

9a). Now it is assumed for a moment that at unloading only elastic deformations take place. The stress distribution at the crack tip in an unloaded specimen then is as shown diagrammatically in fig. 9b. At reloading the stresses at the crack tip are lower than in fig. 9a, as long as the nominal stress is below  $\sigma_r$ . At a stress  $\sigma$ , the stress

distribution of fig. 9a is again obtained. The stresses at the crack tip are highly decisive for the occurrence of crack growth and before unloading the stress distribution of fig. 9a was necessary to maintain crack growth. Then it is plausible that at reloading the re-initiation of crack growth is postponed until the stress distribution is the same as before unloading, i.e. until the stress  $\sigma$  is reached.

Of course unloading is not fully elastic. Reversed plastic flow will take place in a small region at the crack

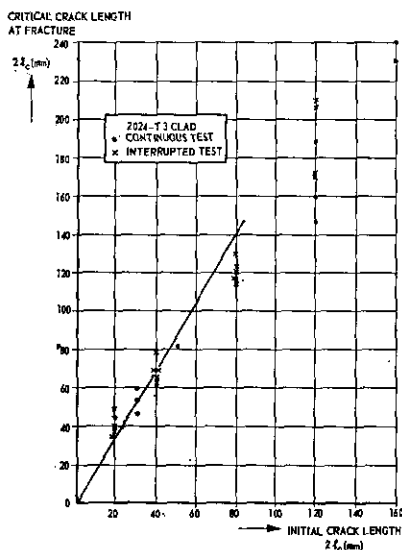


Fig. 6 Relation between critical crack length and initial crack length.

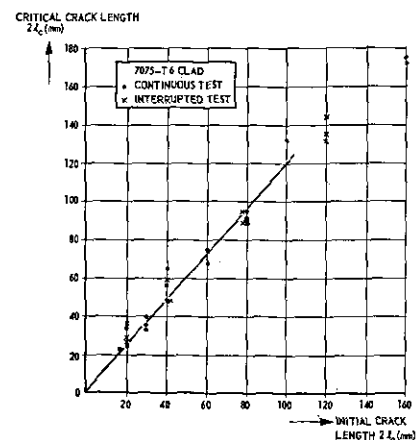


Fig. 7 Relation between critical crack length and initial crack length.

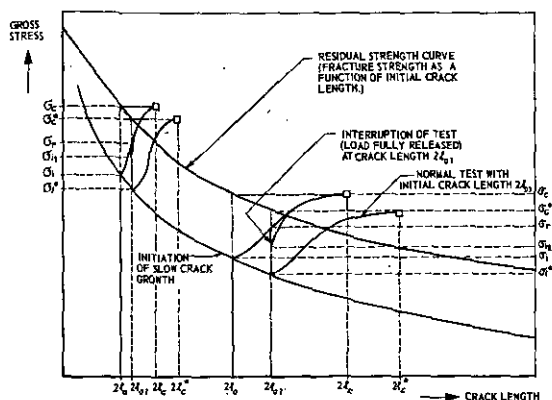


Fig. 8 Possible crack propagation curves at reloading after interruption of residual strength tests.

tip and the stress distribution will resemble that in fig. 9c. At reloading the stress at the crack tip will reach the value of fig. 9a at a nominal stress lower than  $\sigma_r$ . Then it may be expected that the re-initiation of crack growth also takes place at a stress below  $\sigma_r$ . When the crack has grown through the small region in which reversed plastic flow has occurred there is no longer an influence of the unloading on the stress distribution and the situation is similar again to the situation in a continuous test. This might explain why at reloading slow crack growth started at a stress somewhat below  $\sigma_r$ , and why soon after re-initiation of crack growth the original crack propagation curve was followed again.

### 5 Technical implication of the test results

The fail-safe qualities of an aircraft include that under the presence of a crack of a certain length a certain high load can be safely resisted. When a crack of this ultimate length is actually present in service it may show some slow growth if a high load, lower than the failsafe load, is met. Though the ultimate crack length is exceeded now the residual strength is still sufficient as may be concluded from the present test results. The high load that induced slow crack growth has introduced residual compressive stresses at the crack tip (fig. 9c) which are known (refs. 4, 5) to slow down the rate of crack propagation under subsequent fatigue loading. Therefore it may be expected that during some time after the occurrence of slow static crack growth the residual strength is not impaired, not even if a second high load induces some further slow crack growth.

Though this conclusion may be reassuring it must be expected that a number of successive high loads could well affect the residual strength. This is a consequence of the fact that in the present tests slow crack growth was re-initiated at a stress lower than the stress at which the test was interrupted (figs. 4 and 5). Now consider the case when previous loads have extended the crack to a length almost equal to the critical crack length. At subsequent loading and initiation of crack growth

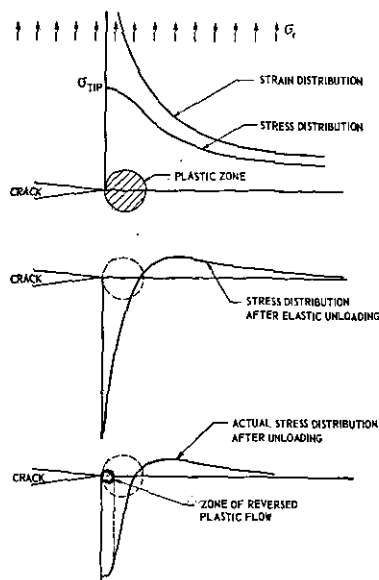


Fig. 9 Stress distribution at crack tip after unloading.

the crack length will exceed the critical crack length already at stresses lower than the fracture stress. Then fracture might occur at a lower stress. It is not likely, however, that between two inspections so many high loads are met. The same situation will be obtained if one single high load extends the crack to almost the critical length but it is a case of low probability that then before the next inspection a second high load of the magnitude of the fail-safe load would occur.

It should be concluded that high preloads generally will not affect the residual strength, but that in certain extreme cases a reduction of the strength must be expected.

### 6 The present results and the energy criterion for fracture

In refs. 1 and 2 it was concluded that the energy criterion for fracture reads:

$$\left. \begin{aligned} \frac{\partial U}{\partial l} + \frac{dW}{dl} &= 0 \\ \frac{\partial^2 U}{\partial l^2} + \frac{d^2 W}{dl^2} &= 0 \end{aligned} \right\} \quad (1)$$

in which  $\frac{\partial U}{\partial l}$  is the energy released during a crack extension  $dl$  and  $\frac{dW}{dl}$  is the energy consumed during a crack extension  $dl$ .

Eqs. (1) could be evaluated by-making use the observation that critical crack length  $l_c$  is proportional to the initial crack length  $l_0$ , i.e.:

$$l_c = \alpha l_0 \quad (2)$$

As a result of this the following relation was obtained

between the fracture stress  $\sigma_c$  and the initial crack length  $l_0$ :

$$\sigma_c l_0^p = \text{constant} \quad (3)$$

in which

$$p = \frac{1}{2\alpha} \quad (4)$$

For the stress  $\sigma_i$  at the onset of slow crack growth the following condition was obtained:

$$\sigma_i l_0^{0.5} = \text{constant} \quad (5)$$

Eqs. (2)–(5) can be checked with the results of the present tests. Figs. 6 and 7 indicate that eq. (2) is reasonably true for small cracks.

The validity of eqs. (3) and (5) is also reasonable as is shown in fig. 10, where both  $\sigma_c$  and  $\sigma_i$  are plotted versus  $l_0$  on a double-logarithmic scale. For very small cracks the results deviate from the straight lines; this is because the residual strength should tend to  $\sigma_u$  for a crack length approaching zero, whereas eqs. (3) and (5) predict infinite stresses at zero crack length. The criteria of eqs. (3) and (5) cannot be valid, however, when the nominal stress is close to or higher than the yield stress, since general yielding will seriously alter the stress distribution. Also for very large cracks the results deviate from the straight lines. This is due to the effect of finite sheet width (ref. 6). For an important range of crack lengths, however, the criteria are reasonably obeyed.

According to fig. 10 the exponent  $p$  in eq. (3) appears to be 0.27 for the 2024-T3 alloy and 0.41 for the 7075-T6 alloy. Then eq. (4) predicts values for  $\alpha$  of 1.85 and 1.22 respectively. The lines drawn in figs. 6 and 7 give

values of 1.75 and 1.20 respectively, which is felt to be a very good agreement. Also in figs. 6 and 7 deviations from the straight lines occur at large values of the crack length. This may again be due to a width effect (ref. 6).

## 7 Conclusions

Residual strength tests were performed on 2024-T3 and 7075-T6 aluminium alloy sheet specimens of 600 mm width and 2 mm thickness. In one test series the specimens were unloaded after a certain amount of stable crack growth had occurred and then reloaded. The following conclusions can be drawn from the test results:

- The interruption of a residual strength test by unloading to zero stress and reloading has no influence on the residual strength. At reloading slow crack growth starts at a stress somewhat below the stress at which the test was interrupted but soon after the reinitiation of crack growth the original crack propagation curve is followed again. The critical fracture stress and the critical crack length are the same for a continuous test and an interrupted test on specimens with the same initial crack length.
- The residual strength of structures containing service cracks will not be impaired by one or two high loads which cause a small amount of stable crack extension.
- The test results reasonably obeyed the fracture criterion

$$\sigma_c l_0^p = \text{constant}$$

and the criterion for slow crack growth:

$$\sigma_i l_0^{0.5} = \text{constant.}$$

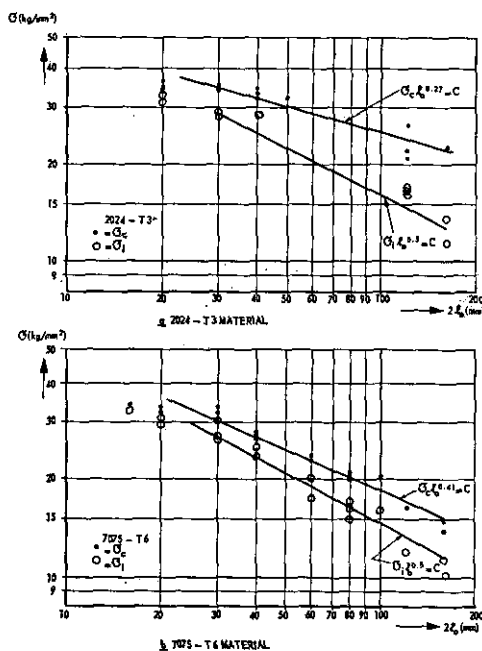


Fig. 10 Check of crack growth and fracture criteria.

## 8 References

- BROEK, D. The residual strength of cracked sheet and structures NLR report TM-M.2135, Aug. 1964.
- BROEK, D. The energy criterion for fracture of sheets containing cracks. Applied Materials Research, 4, 3 (July 1965) pp. 188-189.
- BROEK, D. The residual strength of aluminium alloy sheet specimens containing fatigue cracks or saw cuts. NLR report TR-M.2143, Febr. 1965.
- SCHIJVE, J., BROEK, D. Fatigue-crack propagation under variable amplitude loading. NLR report TN-M.2094, Dec. 1961.
- SCHIJVE, J., BROEK, D. Crack propagation under variable amplitude loading. Aircraft Engineering, Vol. 34 (Nov. 1962) pp. 314-316.
- BROEK, D. The effect of finite specimen width on the residual strength of light alloy sheet. NLR report TR-M.2152, Sept. 1965

TABLE 1  
Test results for 2024-T3 clad material

$2l_0$	First interruption				Second interruption				End of test		Continuous test		
	$\sigma_t$	$\sigma_{r1}$	$2l_{01}$	$\sigma_{t1}$	$\sigma_{r2}$	$2l_{02}$	$\sigma_{t2}$	$2l_c$	$\sigma_c$	$\sigma_t$	$2l_c$	$\sigma_c$	
20	29.5	33.5	26	33.0				39	35.0	*)	37	35.0	
	32.0	35.8	27	35.0				49	36.1	32.5	43	35.4	
	29.5	34.7	27	33.0				38	35.8	20.3	36	36.8	
	30.5	33.9	24	28.3	34.6	26	30.7	36	35.2				
30										26.6	59	34.6	
										29.4	47	34.1	
										29.3	53	35.1	
40	25.8	31.1	48	24.2				65	33.0	28.6	64	34.2	
	24.5	27.1	43	24.9	31.7	52	28.0	78	32.5	28.6	62	33.0	
	26.0	28.9	46	26.7	31.8	52	28.6	68	33.0	*)	*)	32.5	
	26.5	32.2	49	25.4				68	33.6				
50									22.9	81	31.7		
80	17.5	23.4	89	21.7				117	25.4	19.7	117	24.3	
	18.0	24.6	96	23.8				124	25.3	18.0	113	24.9	
	20.0	23.6	87	22.8	25.4	99	20.9	130	25.6	17.8	114	26.0	
	19.6	25.7	103	23.5				121	25.7				
120	14.4	20.9	150	19.4				172	20.4	16.8	188	26.6	
	14.3	20.8	145	14.5				170	20.6	16.6	160	22.0	
	13.0	24.2	153	20.4				205	24.2	15.6	146	20.9	
	14.0	22.4	135	20.8	24.7	154	21.8	209	24.8				
160										13.2	240	21.7	
										11.2	230	22.4	

\*) No value obtained due to fail of motion picture.

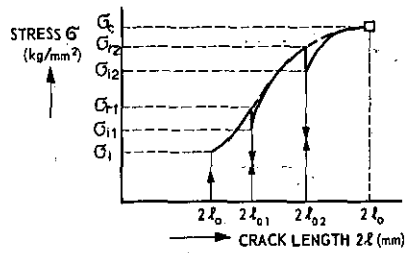
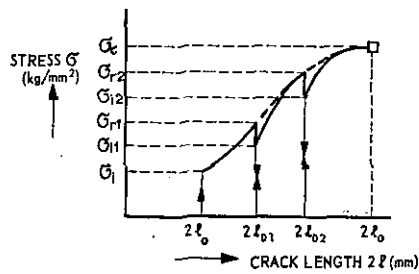


TABLE 2  
Test results for 7075-T6 clad material

$2l_0$	First interruption				Second interruption			End of test		Continuous test		
	$\sigma_i$	$\sigma_{r1}$	$2l_{01}$	$\sigma_{t1}$	$\sigma_{r2}$	$2l_{02}$	$\sigma_{t2}$	$2l_c$	$\sigma_c$	$\sigma_i$	$2l_c$	$\sigma_c$
16										32.4	22	33.7
20	28.5	32.4	24	29.7	32.5	25	29.1	27	33.6	*)	25	33.4
	31.4	31.9	22	31.5	34.3	23	31.3	35	36.8		33	32.0
	24.5	33.3	24	33.3				28	36.1			
	26.6	32.1	26	31.1				28	33.0			
30										26.8	39	31.7
										26.7	35	31.7
										31.1	34	32.7
40	21.3	25.4	46	25.1				48	26.9	*)	57	28.0
	20.5	25.9	45	24.2				59	30.1		65	26.1
	20.6	23.0	44	22.3				53	26.1		48	27.9
60										17.2	75	22.6
										20.0	68	23.2
80	16.6	18.9	88	17.4				88	18.2	14.8	94	19.9
	15.0	17.7	87	17.7				94	19.2	16.9	88	20.9
	16.0	17.6	84	16.4	18.2	85	17.7	90	20.0	15.9	91	20.6
100										15.6	132	20.3
120	13.7	14.7	127	12.8				131	14.7	11.7	127	16.0
	13.0	14.4	124	13.3	15.5	128	15.1	143	17.6			
	13.5	17.2	133	15.5				135	16.5			
160										11.2	174	14.9
										10.0	170	13.3

\*) No value obtained due to fail of motion picture.



Report NLR-TR M-2148

# The effect of ground-to-air cycles on the fatigue crack propagation in 2024-T3 Alclad sheet material

by

J. SCHIJVE and P. DE RIJK

## Summary

Constant-amplitude tests and simplified flight-simulation tests with 10 or 50 gust cycles per flight were performed. The effect of the ground-to-air cycle is compared with the Palmgren-Miner prediction. Optical and electron microscope observations of the fracture are presented.

## Contents

	Page:
List of symbols	
1 Introduction	1
2 Experimental details	2
2.1 The material and the specimens	2
2.2 Load sequences	2
2.3 Testing procedures	2
3 Test results	3
3.1 Crack propagation data	3
3.2 Fractographic observations	3
4 Discussion	8
5 Concluding remarks	9
6 References	9
2 tables	
9 figures	

## List of symbols

$k_c$	— kilocycle = 1000 cycles
$l$	— crack length, defined in figure 1
$l_{tr}$	— crack length, at completion of the transition from 90°-mode of fracture to 45°-mode
$n$	— number of cycles
$n_l$	— number of cycles at crack length $l$
$d/dn$	— crack rate
$N$	— fatigue life (crack propagation life)
$S_a$	— stress amplitude
$S_m$	— mean stress
$S_{min}$	— minimum stress
$S_{max}$	— maximum stress

} gross stress on  
specimen

$S_{0.2}$	— yield stress
$S_u$	— ultimate strength
$\delta$	— elongation
$R$	— stress ratio, $S_{min}/S_{max}$
GTAC	— ground-to-air-cycle
NLR	— Nationaal Lucht- en Ruimtevaartlaboratorium (National Aerospace Laboratory NLR, Amsterdam)
1 mm	— 0.04 inch; 1 inch = 25.4 mm
1 $\mu$	— 0.001 mm
1 kg/mm <sup>2</sup>	— 1,422 psi; 1000 psi = 0.703 kg/mm <sup>2</sup>

## 1 Introduction

Some years ago prototype wing structures of several civil aircraft were tested with a simple flight simulation load sequence (ref. 1). The gust loads were reduced to a single load level and secondly ground-to-air cycles (GTAC) were applied. The load sequence is schematically indicated in fig. 1. Although this sequence now seems to be somewhat oversimplified the application of the GTAC leading to a flight-by-flight simulation was certainly an improvement over older procedures which neglected the GTAC. In several test programs the damaging effect of the GTAC was shown to be considerably larger than predicted by the Palmgren-Miner rule (Ref. 2). This experimental evidence concerned

This investigation has been performed under contract with the Netherlands Aircraft Development Board (NIV).

fatigue lives of specimens and structures. About the effect of the GTAC on crack propagation almost no information was available and it was therefore thought to be feasible to carry out a simple test program exploring the effect. For this purpose crack propagation tests with a load sequence according to fig. 1 were performed.

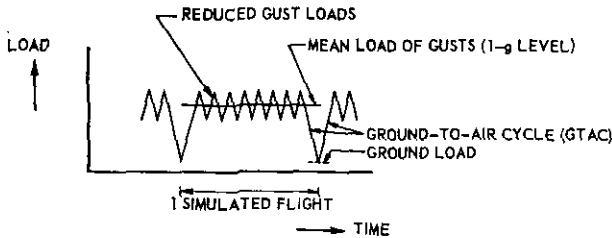


Fig. 1 Load Sequence in a Simplified Flight-Simulation test.

In addition tests with gust-cycles only and tests with GTAC only were also carried out. It then is possible to indicate whether the contribution of the GTAC to the crack propagation is larger than predicted by the Palmgren-Miner rule. Furthermore observations were made on the growth lines on the fracture surfaces. The results of the investigation are presented and discussed in this report.

## 2 Experimental details

### 2.1 The material and the specimens

The specimens were cut from 2024-T3 Alclad sheet material with a thickness of 2 mm (0.08"). The average

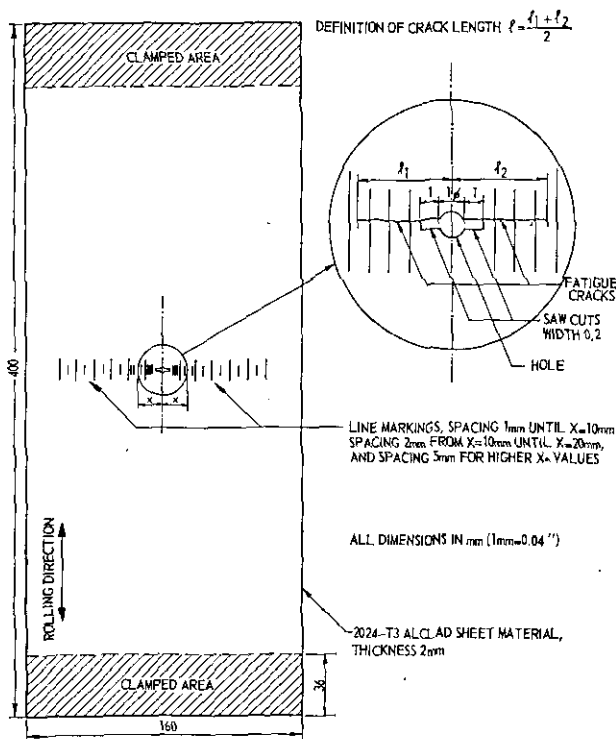


Fig. 2 Sheet specimen for crack propagation.

static properties (8 tests) in the direction of rolling were:

$$S_u : 48.3 \text{ kg/mm}^2 = 68.7 \text{ ksi}$$

$$S_{0.2} : 37.1 \text{ kg/mm}^2 = 52.8 \text{ ksi}$$

$$\delta : 18.9\% \text{ (2 inch gage length)}$$

The type of specimen was the same as for several previous NLR investigations, i.e. a sheet specimen with a small severe central notch for rapid crack initiation.

The dimensions are shown in fig. 2. The width is 160 mm (6.3"). The specimens were locally polished and provided with fine line markings to facilitate the recording of the crack growth. The spacings of the markings are also indicated in fig. 2.

### 2.2 Load sequences

Four test series were carried out (see also fig. 3)

Series	Load sequence	Remarks
a	gust cycles only	$S_m = 9 \text{ kg/mm}^2$ , $S_a = 3 \text{ kg/mm}^2$
b	GTAC only	$S_{max} = 12 \text{ kg/mm}^2$ , $S_{min} = 0.5 \text{ kg/mm}^2$
c	flight simulation	10 gust cycles per flight
d	ditto	50 gust cycles per flight

In each test series there were three similarly tested specimens.

### 2.3 Testing procedures

The specimens were tested in a horizontal Schenck pulsator, type PPD 6 with a capacity of six tons. The machine has a quick drive and a slow drive. The slow drive was used for all tests, since it is impossible to apply the flight simulation with the quick drive (resonance system). The slow drive essentially consists of a reversible screw drive. Reversion of the load is actuated by electric contacts on the spring which is in series with the specimen. The contacts are limiting the stroke of the screw drive. In the flight simulation tests two pairs of contacts were used for the gust cycles and the GTAC respectively. Selection of one of these pairs occurred by the cycle counter of the machine. This auxiliary equipment was built by the NLR.

The frequency of testing was 15.5 cpm for the gust cycles and 8.5 cpm for the GTAC. At such low frequencies tests are progressing fairly slowly and therefore the recording of the crack length was made automatically by taking pictures with a Robot camera at regular time intervals, which also allowed to run the tests overnight. A cycle counter of the machine was simultaneously photographed. Pictures were made at the moment that the load was at its maximum to have a maximum crack opening.

After completion of the test readings of the films were used for plotting crack propagation curves.

### 3 Test results

#### 3.1 Crack propagation data

The central notch initiates two cracks, which are considered as one crack with a length  $l$  defined by  $2l = l_1 + l_2 =$  length from tip to tip, see fig. 2. The differences between  $l_1$  and  $l_2$  were always small. The width of the central notch was 3 mm corresponding to  $l = 1.5$  mm. Crack growth records were started at  $l = 3$  mm which is sufficiently large for a negligible effect of the notch on the subsequent crack propagation.

The crack propagation data have been compiled in table 1, giving numbers of cycles which were read from the crack growth records plotted from the film readings, see previous section. The mean values for each group of three specimens were used for plotting the average crack propagation curves in fig. 4. Table 1 shows that the scatter in each group of three specimens is small, as usual for crack propagation.

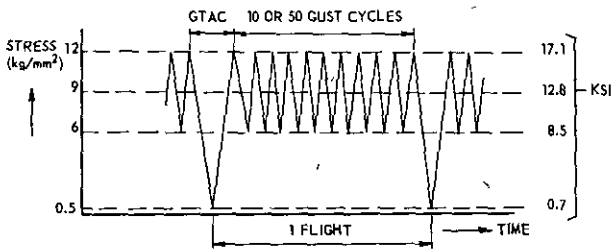


Fig. 3 Load sequence and stresses applied in the crack propagation tests.

In fig. 4 the predicted curves are based on the Palmgren-Miner rule. Indicating the crack rate in a small crack growth interval ( $\Delta l$ ) in (1) a flight simulation test, (2) a test with gusts only and (3) a test with GTAC only by  $(\Delta l/\Delta n)_{flight}$ ,  $(\Delta l/\Delta n)_{gust}$  and  $(\Delta l/\Delta n)_{GTAC}$  respectively it is easily shown that application of the rule to the fatigue lives covered by a crack extension  $\Delta l$  leads to:

$$\left(\frac{\Delta l}{\Delta n}\right)_{flight} = \frac{m \left(\frac{\Delta l}{\Delta n}\right)_{gust} + \left(\frac{\Delta l}{\Delta n}\right)_{GTAC}}{m+1} \quad (1)$$

with  $m$  being the number of gust cycles per flight (and  $m+1$  the number of load cycles per flight). Equation (1) involves that the predicted crack rate is the average value from the crack rates obtained in tests with gusts only and tests with GTAC only, averaged in accordance with the numbers of application in the flight simulation tests. The values of  $(\Delta l/\Delta n)_{flight}$  were calculated for the crack intervals presented in table 1 and integration of (the inverse of) this crack rate yielded the predicted curves in fig. 4. The differences between the predicted curves and the tests results are apparently small although unconservative. The Palmgren-Miner rule was also applied for larger crack intervals, see

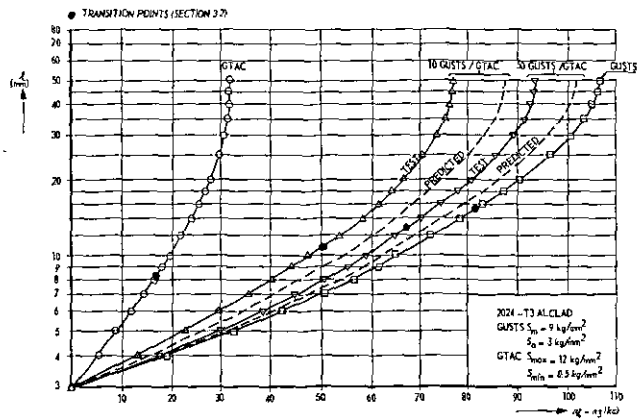


Fig. 4 Crack propagation curves.

table 2, which shows the same trend in the last column.

#### 3.2 Fractographic observations.

On a macroscopic scale the transition from the tensile mode ( $90^\circ$ -mode) to the shear mode ( $45^\circ$ -mode) was again observed. The transition has been described in several previous NLR reports on crack propagation (e.g. refs. 4, 5 and 6). For about 50% of the cracks a double shear fracture was observed, this percentage being lower in previous investigations. An effect of the transition on the crack propagation could not be detected. The crack rate for single and double shear fracture was apparently the same.

The average crack length  $l_{tr}$  at which the transition from the tensile mode to the shear mode was completed has been indicated in fig. 4. The corresponding crack rates at  $l_{tr}$  are in the order of 0.4 mm/kc which is approximately twice as high as found in a previous investigation (ref. 5) for tests at a frequency of 2000 cpm. The same frequency effect on the transition was previously noticed in ref. 6.

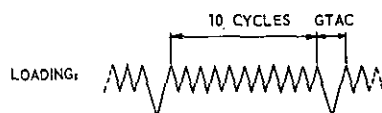
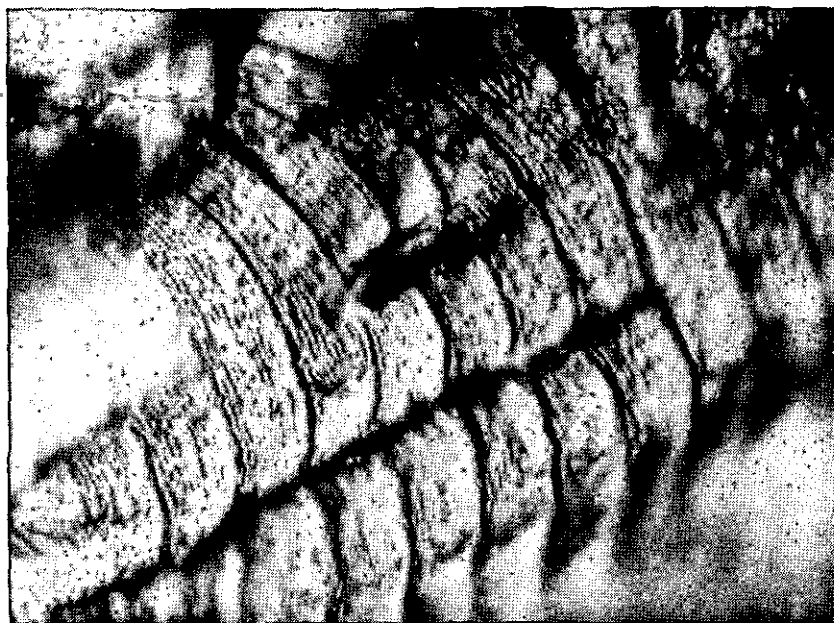
Microscopic observations of the fracture surface revealed the growth lines which indicate the successive positions of the crack front. An example obtained with the optical microscope is shown in fig. 5. At a few locations replicas for the electron microscope were made for two specimens. The electron microscope<sup>1</sup> showed more details of the fracture surface as discussed below. With respect to the growth lines the electron microscope confirmed the observations made by the light optical microscope, see fig. 6, i.e. the growth lines corresponding to the GTAC in the test whit both gust cycles and GTAC could easily be observed and the number of growth lines between the successive GTAC is the same as the corresponding number of gust cycles. It proves that each growth line has to be associated with a single load cycle. This was previously shown in the same way by other investigators (refs. 7, 8 and 9). In

<sup>1</sup> The replicas as well as the electron microscope survey were made by the Metaalinstituut TNO at Delft.

TABLE 1  
Crack propagation data

Type of test	(a) Gust Cycles				(b) G.T.A.C.				(c) Gust + GTAC (10:1)				(d) Gust + GTAC (50:1)				
	Specimen no	A70	A78	A99	mean	A80	A75/A108	A102	mean	A73/A115	A85	A95	mean	A77	A82	A108/A89	mean
<i>l</i> (mm)	Number of cycles																
3	0	0	0	0	0	0	0	0	0	0	0	0	0	0	0	0	0
4	18805	18750	19000	18852	5026	4900	5250	5059	13875	13800	11550	13075	18855	17001	16500	17452	
5	31205	36650	28800	32218	9183	8675	8650	8836	22630	24300	21200	22710	28678	30125	30700	29834	
6	40705	49650	37600	42652	12190	11550	11525	11755	30530	31400	27400	29777	36938	39875	39300	38704	
7	48380	57250	45050	50227	14831	13915	14150	14299	35780	38100	33300	35737	43103	47125	45075	45101	
8	54020	63450	51350	56273	16805	16125	16125	16352	40630	42875	38425	40643	48578	52400	50150	50376	
9	59235	68950	55600	61262	18626	17775	17825	18075	44655	46325	42150	44377	52775	57050	54200	54675	
10	63715	72400	59100	65072	20233	19265	19225	19574	48130	49550	45450	47710	57358	61175	57700	58744	
12	71280	79100	66950	72443	22699	21800	21875	22125	53580	56150	50875	53535	63530	68150	63700	65127	
14	77185	84850	73300	78445	24879	23910	23750	24179	57880	60850	55325	58018	68618	73550	68700	70286	
16	81805	89475	78300	83193	26580	25450	25098	25709	61380	64500	58800	61560	72870	78050	72775	74565	
18	86080	93625	82175	87293	27855	26785	26368	27003	64030	67400	61675	64368	75988	81650	76150	77939	
20	89230	96975	85525	90577	28979	27980	27363	28107	66286	69630	64050	66655	78750	84800	78747	80766	
25	95670	102250	91850	96590	30887	29725	28965	29859	69660	74088	68649	70799	83855	90399	83402	85885	
30	99940	106741	95835	100838	32159	30640	29917	30905	72471	77148	71645	73755	88068	93851	86402	89440	
35	102972	109311	98175	103486	33342	31180	30422	31648	74181	78688	73375	75415	90515	96062	88364	91647	
40	104842	110995	99750	105196	33676	31422	30665	31921	75153	79655	74410	76406	91857	97424	89584	92955	
45	106110	112183	100540	106278	33938	31548	30767	32084	75695	80145	74972	76937	92675	98324	90249	93749	
50	106620	112508	100793	106640	34011	31578	30826	32138	75840	80271	75097	77069	92845	98460	90475	93937	
55	—	112523	100812	—	34029	—	30851	—	75860	80278	75111	77083	92864	98482	90491	93946	
80	106665	112532	100819	106672	34033	31581	30854	32156	75861	80278	75113	77084	92864	98488	90495	93949	

For testseries (c) and (d) the numbers of cycles include both gust cycles and GTAC.



SPECIMEN A 115, FRACTURE SURFACE AT  $l \sim 14$  mm  
 CRACK RATE DERIVED FROM PICTURE :  $dl/dn = 0.55 \mu/c$   
 CRACK RATE DERIVED FROM GROWTH RECORD :  $dl/dn = 0.50 \mu/c$

Fig. 5 Optical micrograph of a fracture surface (magnification 1700  $\times$ )

TABLE 2  
 Damage calculations

Crack growth interval	test series <sup>1</sup>	Life (Kc)	$\frac{n}{N}$ GTAC	$\frac{n}{N}$ Gusts	$\sum \frac{n}{N}$
$l = 3$ mm to $l = 5$ mm	a	32.22			
	b	8.84			
	c	22.71	0.234	0.641	0.88
	d	29.83	0.066	0.908	0.97
$l = 5$ mm to $l = 10$ mm	a	32.85			
	b	10.74			
	c	25.00	0.212	0.692	0.90
	d	28.91	0.053	0.863	0.91
$l = 10$ mm to $l = 40$ mm	a	40.12			
	b	12.35			
	c	28.70	0.211	0.650	0.86
	d	34.21	0.054	0.836	0.89

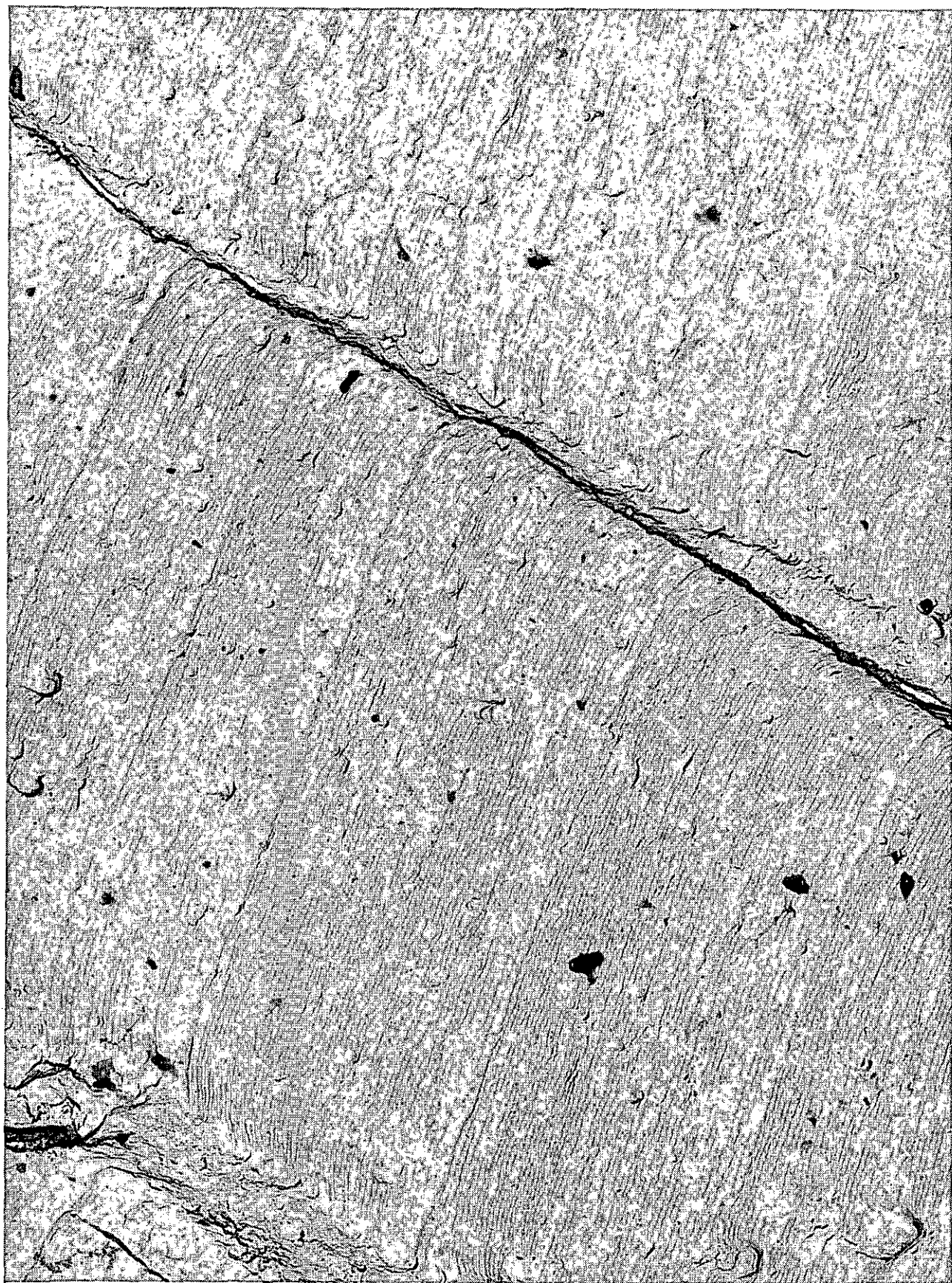
<sup>1</sup> a: gust cycles only, b: GTAC only, c: 10 gust cycles per flight, d: 50 gust cycles per flight.

order to show that crack growth is a continuous process, or in other words that dormant periods are absent, the crack rate derived from the spacing of the growth lines should be equal to the crack rate derived from the crack propagation records. This could most easily be checked with fracture surface data of a specimen with a load sequence with 50 gust cycles + 1

GTAC. For specimen A 77 the spacing between the growth lines of the GTAC corresponding to 51 cycles was measured by averaging a number of such spacings (varying from 1 to 20). The crack rates derived from these measurements have been plotted in fig. 8 as a function of the crack rate (at the same values of the crack length) derived from the crack propagation data. There is approximately a 1 : 1 correlation indicating that crack extension occurred in the major part of the load cycles, dormant periods being virtually absent. The 1 : 1 correlation is much better than shown in fig. 38 of ref. 4 which is a consequence of the more accurate measurements of spacings in the present investigation due to averaging over a much larger number of growth lines.

On the fracture surfaces of specimens loaded by gust cycles and GTAC the growth lines stemming from the GTAC cycles were easily observed, although the differences with the growth lines of the gust cycles became less and less marked at higher values of the crack length and the crack rate. The micrographs did not indicate any interaction effect of the GTAC on the crack growth during the succeeding gust cycles. This is in accordance with the crack propagation data presented in the previous section which showed that only a small interaction effect was found.

Some additional information revealed by the micro-



Load sequence: 50 gust cycles + 1 gtac

Crack length  $l \sim 6$  mm

Crack rate derived from picture:  $dl/dn = 0.11 \mu/c$

Crack rate derived from growth record  $dl/dn = 0.13 \mu/c$

Fig. 6 Electron micrograph of a fracture surface (magnification  $10000 \times$ )



Load sequence: 50 gust cycles + 1 glac  
Crack length  $\sim 21.5$  mm (at transition  $\sim 13$  mm)  
Growth line spacing  $\sim 0.6 \mu$   
Crack rate derived from growth record  $d/dn = 0.8 \mu/c$   
Fig. 7 Electron micrograph of a fracture surface (magnification  
 $10000 \times$ )

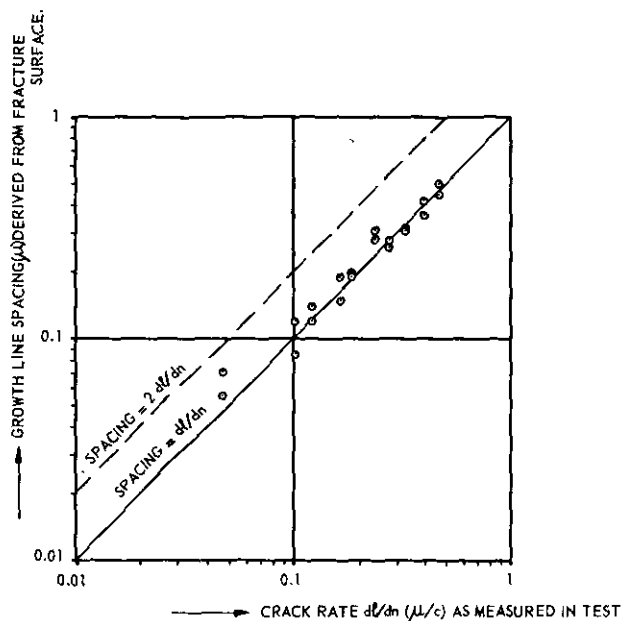


Fig. 8 The growth line spacing measured on the fracture surface of specimen A 77 as a function of the corresponding crack rate derived from the propagation records.

graphs will be summarized below, although it is not the intention to present a discussion on the fracture mechanism at any length.

The growth lines were most clearly observed when the crack length (and the crack rate) was small. For increasing values of the crack length the growth lines became blurred, especially when the transition of the 90°-mode to the 45°-mode had occurred. An example of this is shown in fig. 7. Nevertheless they confirm that also after the transition crack growth occurs in most if not in all cycles.

Between areas with growth lines corridors without these lines were found, especially at the higher values of the crack length. Fig. 7 shows an example between two areas with a mutually perpendicular orientation of the growth lines. Although there are lines in this corridor they are not believed to be growth lines but rather a consequence of a shearing-off fracture connecting the two areas with growth lines. It is not strange that the fatigue fracture along the crack front will show a tendency to grow on different levels, due to the material structure. Since the continuity of the material at both sides of the fracture has to be preserved local shearing-off will occur. The case shown in fig. 7 with growth lines in adjacent areas which are mutually perpendicular is an exception, which is shown for curiosity.

Both figs. 5 and 6 show dark lines approximately perpendicular to the average orientation of the growth lines. At these dark lines the crack growth appears to be lagging behind. From the optical microscope survey the impression was obtained that these dark lines could not be identified as grain boundaries. The dark lines

were also approximately perpendicular to the growth lines if the latter were not perpendicular to the sheet surface. The dark lines might again be a connection between crack growth on two parallel planes (not necessary crystal planes) at slightly different levels. Probably the dark lines are the same as the cliff edges connecting the plateaux with growth lines as described by Forsyth and Ryder in ref. 10.

Another characteristic feature is shown in the upper part of fig. 7. The pitlike area might be the impression of an inclusion. This feature was randomly observed over the fracture surface (electron microscope). No indications were obtained that the pits were associated with an influence on the local crack propagation, contrary to observations of Pelloux (ref. 11) for the aluminium zinc alloy 7178-T6. Some NASA results (ref. 12) for two similar alloys indicated a lower crack rate for the alloy with the higher content of inclusions. Further studies seem to be desirable.

The smallest spacing between successive growth lines observed in the present investigation was about 300 ångstrom or 100 atomic distances. This is in the order of the smallest values reported elsewhere (ref. 4). Smaller values could probably have been detected, but this was not the purpose of the present investigation. The meaning of indicating low values of these spacings was extensively discussed in ref. 4.

#### 4 Discussion

In a previous investigation (refs 3 and 13) on the same material and the same type of specimen (apart of a somewhat larger central notch) the effect of a few high loads interspersed in a constant-amplitude loading at  $S_m \pm S_a = 8.18 \pm 3.27 \text{ kg/mm}^2$  was studied. The effect of three uploads ( $S_{\max} = 19.2 \text{ kg/mm}^2$ ) is shown here in fig. 9.

The effect is dramatic, i.e. the crack propagation after the application of the upload is slowed down most considerably. However, downloads to  $S_{\min} = -2.9 \text{ kg/mm}^2$  applied in a similar test at  $l = 5, 6, 7, 8, 9$ ,

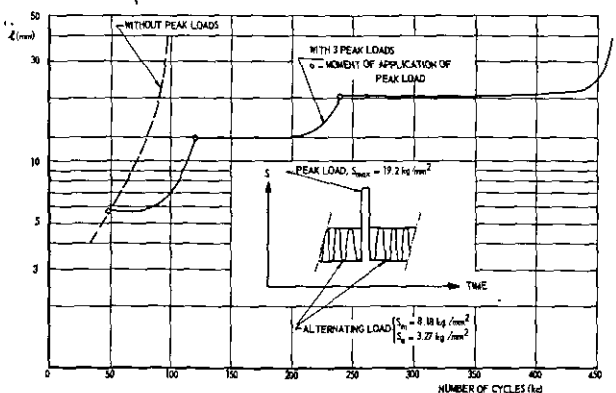


Fig. 9 The effect of peak loads on the crack propagation under constant-amplitude loading (refs 3 and 13).

11, 13, 15, 19, 23 and 29 mm respectively did not have a noticeable effect. In the present testseries such downloads were applied much more frequently, viz. approximately 7000 times in test series (c) and 2000 times in testserie (d). The downloads now had a perceptible effect, but it still was small, see fig. 4 and it was only slightly larger than predicted by the Palmgren-Miner rule.

The large effect of uploads was attributed to negative residual stresses around the tip of the crack. One might ask whether downloads will introduce unfavourable positive residual stresses. Apparently the results show that this is hardly the case which confirms the expectations. The downloads implied an unloading of the specimen and it is not expected that the plastic zone size will increase during the unloading (contrary to what occurs during an upload). Hence it cannot be expected that significant residual stresses, i.e. significant for the subsequent constant-amplitude loading, will be set up. One might speculate that high downloads, inducing a high compressive stress in the sheet specimen could introduce residual tensile stresses around the crack. Although this argument is correct for a notch it does not apply to a crack, since a crack can be closed during compression of the sheet and it will not longer be a stress raiser. This argument was suggested by Illg and McEvily (ref. 14) who confirmed it by comparing crack propagation at  $S_m = 0$  ( $R = -1$ ) and at  $S_{min} = 0$  ( $R = 0$ ) for the same value of  $S_{max}$ .

For completeness it should be added that downloads can reduce the favourable effect of uploads. This was also shown in the previous NLR investigation (refs. 3 and 13) by interspersing in a constant-amplitude test uploads directly followed by a download. The net effect on the crack propagation was still favourable, but it was much less than the effect by the uploads alone.

For practical purposes it may be recapitulated here that fatigue crack propagation under a positive mean stress and some random service load will more frequently meet with favourable (compressive) residual stresses than unfavourable (tensile) residual stresses. The reasons are (1) that the former stresses are more likely to be introduced than the latter ones and (2) closing of the crack under compressive loads opposes the inducing of residual tensile stresses.

## 5 Concluding remarks

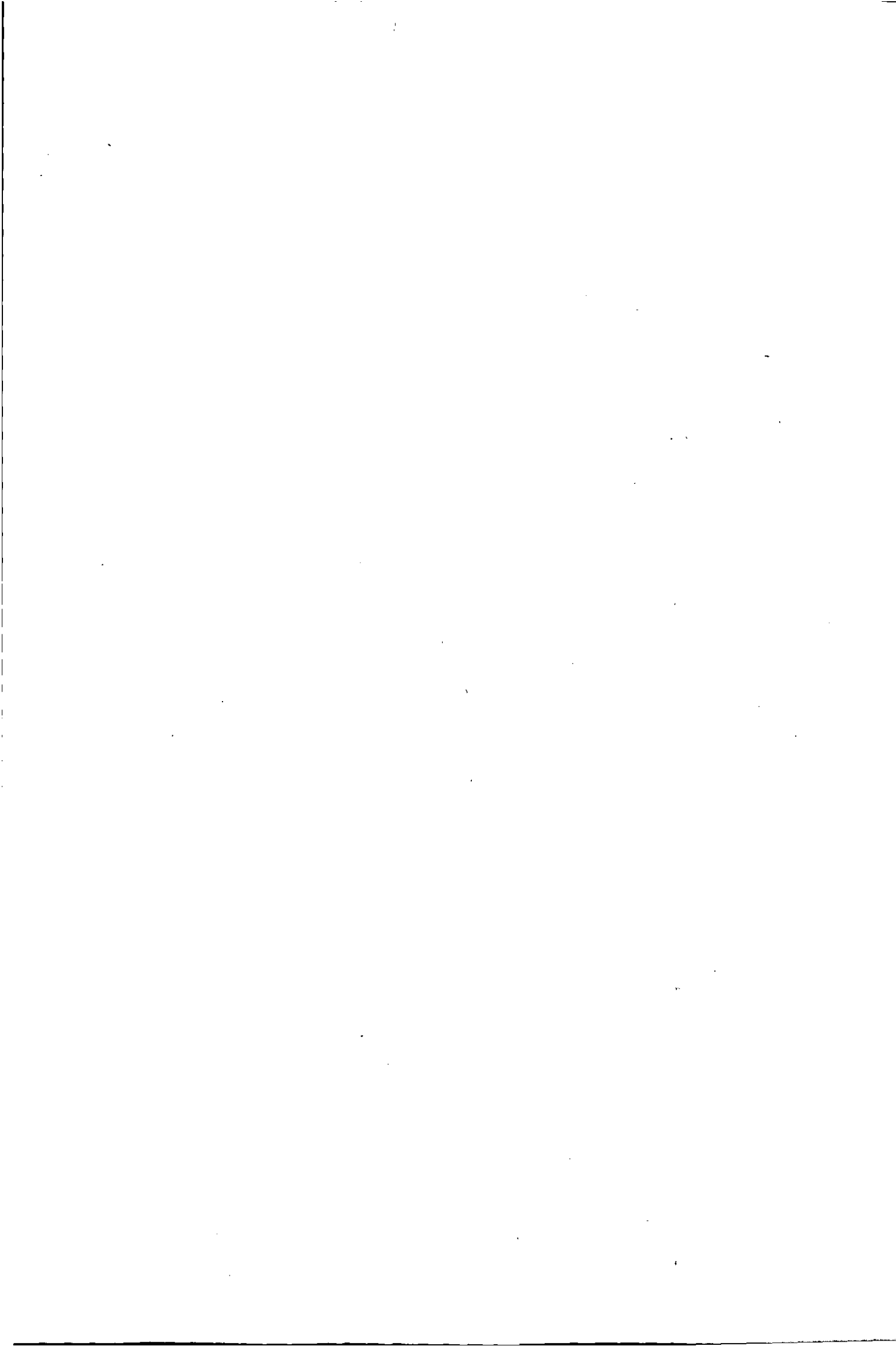
Crack propagation tests were performed on 2024-T3 Alclad sheet specimens. In two test series constant-amplitude loading at  $S_m \pm S_a = 9 \pm 3$  kg/mm<sup>2</sup> was periodically interspersed with downloads to  $S_{min} = 0.5$  kg/mm<sup>2</sup> after each 10 or 50 cycles respectively. This load sequence implied a simplified flight simulation as applied in older prototype testing of aircraft structures, i.e. gust cycles with a constant amplitude and ground-

to-air cycles. The results showed that the crack rate in the flight simulation tests was only some 10% faster than predicted from constant-amplitude test results by the Palmgren-Miner rule. This confirmed existing ideas on the introduction and the effect of residual stresses around the tip of the crack. Under practical conditions an accelerating effect of ground-to-air cycles on the crack propagation need not be feared.

The fractographic observations confirmed that crack extension occurred in most cycles if not in all cycles.

## 6 References

- <sup>1</sup> PLANTEMA, F. J. AND SCHIJVE, J. (Ed.), Full scale fatigue testing of aircraft structures. Symp. Amsterdam, 1959. Pergamon Press 1961.
- <sup>2</sup> SCHIJVE, J. AND JACOBS, F. A., Program-fatigue tests on notched light alloy specimens of 2024 and 7075 material. NLR-TR M. 2070, March 1960.
- <sup>3</sup> SCHIJVE, J., BROEK, D. AND DE RIJK, P. Fatigue-crack propagation under variable-amplitude loading. NLR Report M. 2094, Dec. 1961.
- <sup>4</sup> SCHIJVE, J. Analysis of the fatigue phenomenon in aluminium alloys. NLR-TR M. 2122, April 1964.
- <sup>5</sup> BROEK, D. AND SCHIJVE, J., The influence of the mean stress on the propagation of fatigue cracks in aluminium alloy sheet. NLR-TR M. 2111, Jan. 1963.
- <sup>6</sup> SCHIJVE, J., BROEK, D. AND DE RIJK, P., The effect of the frequency of an alternating load on the crack rate in a light alloy sheet. NLR Report M. 2092, Sept. 1961.
- <sup>7</sup> RYDER, D. A., Some quantitative information obtained from the examination of fatigue fracture surfaces. Roy. Aircraft Est., Techn. Note Met. 288, Sept. 1958.
- <sup>8</sup> LAIRD, C. AND SMITH, G. C., Crack propagation in high stress fatigue. Phil. Mag. (8), vol. 7, p. 847, May 1962.
- <sup>9</sup> MATTING, A. AND JACOBY, G., Ueber das Verhalten von Schweissverbindungen aus Aluminiumlegierungen bei Schwingbeanspruchung. Teil II: Beitrag zum Mechanismus des Schwingungsbruches-Aluminium, vol. 38, p. 309, May 1962.
- <sup>10</sup> FORSYTH, P. J. E. AND RYDER, D. A., Fatigue fracture. Some results derived from the microscopic examination of crack surfaces. Aircraft Engineering, vol. 32, p. 96, April 1960.
- <sup>11</sup> PELLOUX, R. M. N., Fractographic analysis of the influence of constituent particles on fatigue crack propagation in aluminium alloys. Am. Soc. for Metals, Trans. Quart., vol. 57, p. 511, June 1964.
- <sup>12</sup> GLASSMAN, L. H. AND MCEVILY, A. J., Effects of constituent particles on the notch sensitivity and fatigue-crack-propagation characteristics of Al-Zn-Mg alloys. NASA TN D-928, April 1962.
- <sup>13</sup> SCHIJVE, J., Fatigue crack propagation in light alloy sheet material and structures. Advances in Aeronautical Sciences, vol. 3, Pergamon 1961, p. 387. Also NLR Report MP. 195, Aug. 1960.
- <sup>14</sup> ILLG, W. AND MCEVILY, A. J., The rate of fatigue-crack propagation for two aluminium alloys under completely reversed loading. NASA TN D-52, Oct. 1959.



## REPORT TR M.2149

# The static strength of aluminium alloy sheet specimens containing blunt notches

by

D. BROEK and F. A. JACOBS

## Summary

Static tests were carried out on 280 mildly notched specimens of various aluminium alloys. It appears that the nett section fracture stress as a percentage of the ultimate tensile strength is in general higher for materials of lower ductility. This influence of ductility can be reasonably explained on the basis of measured plastic strain distributions. The static strength of aluminium alloys is lower when the elastic stress concentration factor is higher.

<b>Contents</b>	<i>Page:</i>	$t$ — specimen thickness
		$2w$ — specimen width
<b>Symbols</b>	1	$\delta$ — elongation
1 Introduction	1	$\epsilon$ — strain
2 Experimental details	2	$\epsilon_{\max}$ — maximum strain in a specimen
3 Test results and a comparison with results of other investigations	3	$\epsilon_{\text{nett}}$ — average strain in notched section
4 Discussion	4	$\epsilon_{\infty}$ — average strain in unnotched section
4.1 The influence of ductility	4	$\sigma$ — stress
4.2 The difference between blunt and sharp notches	8	$\sigma_{\text{edge}}$ — stress at the edge of the specimen
5 Practical use of the results	8	$\sigma_{\text{nett}}$ — nominal nett section stress
6 Conclusions	9	$\sigma_{\text{nu}}$ — $\frac{\text{fracture load}}{(2w-d)t}$ = fracture stress on nett section
7 References	9	$\sigma_{\max}$ — maximum stress in a specimen
12 tables		$\sigma_u$ — ultimate tensile strength of unnotched material
11 figures		$\sigma_y$ — yield strength
		$\sigma_{0.2}$ — 0.2% yield strength
		$\frac{\sigma_{\text{nu}}}{\sigma_u}$ — static efficiency of a notched specimen

## Symbols

$d$  — hole diameter; width of notch  
 $K_t$  — theoretical elastic stress concentration factor  
 $= \frac{\sigma_{\max}}{\sigma_{\text{nett}}}$

$K_\epsilon$  — strain concentration factor =  $\frac{\epsilon_{\max}}{\epsilon_{\text{nett}}}$  or  $\frac{\epsilon_{\max}}{\epsilon_{\infty}}$

## Units:

length: mm; 1 inch = 25.4 mm.

stress: kg/mm<sup>2</sup>; 1000 psi = 0.703 kg/mm<sup>2</sup>

## 1 Introduction

The residual strength properties of sheets containing sharp notches or cracks depend on the ductility of the sheet material. In general, it can be said that the reduction in strength due to cracks is larger when the ductility of the material is lower. In the presence of blunt notches (like bolt and rivet holes) the reverse seems to be true (ref. 1). The static efficiency (ref. 1) of a tension member containing a notch may be defined as the ratio between the fracture load divided by the nett area and the tensile strength of the unnotched material, i.e.  $\sigma_{\text{nu}}/\sigma_u$ . In the

presence of an open hole the ductile 2024-T3 aluminium alloy shows a static efficiency well below unity, whereas the less ductile 7075-T6 alloy shows a static efficiency only slightly below unity.

The influence of the ductility on the residual strength in the presence of cracks can be explained by noting that the stress concentration at the crack tip can be more effectively reduced by plastic flow in a material of high ductility than in a material of low ductility. The reverse effect in the case of blunt notches cannot be explained in this way and it was concluded in ref. 1 (quote):

"... It seems that the susceptibility of a perforated specimen to strength reduction cannot be explained on the basis of commonly accepted measures of ductility..."

The residual strength in the presence of cracks has been intensively studied during the last decade. In view of the results mentioned above it seems worthwhile to study also the effect of blunt notches. Such a study could deepen the insight in the residual strength problem, especially as to the criterion for fracture. A second argument for such an investigation is that the effect of mild notches on the static strength is of great importance for setting allowable design stresses. In this respect the lower sensitivity for mild notches of the 7075-T6 material as compared with the 2024-T3 material requires further study. An extensive test program has therefore been carried out, the results of which are presented in this report. An explanation of the results based on ductility considerations is given.

## 2 Experimental details

The test programme, consisting of 280 tests, is outlined in table 1.

All alloys tested are familiar alloys, except perhaps the RR-58 alloy. This alloy has been developed for application where structural stability at moderate temperatures is required.

The 2024-material heat treated to maximum hardness was obtained by further artificial ageing of 2024-T3 sheet, by soaking for 2 hours at 195°C leading to a Vickers hardness of  $H_v = 167 \text{ kg/mm}^2$  (hardness of T3 condition:  $H_v = 136 \text{ kg/mm}^2$ ). The overaged material was obtained by soaking the T3 material 6 hours at 195°C giving a hardness of  $H_v = 155 \text{ kg/mm}^2$ . These hardness values are averages of six measurements carried out on a Leitz microhardness tester.

The adhesive bonding cycle as applied to six specimens of test series 6 consisted of heating from 20°C to 160°C in 1 hour, 0,5 hour soaking at the same temperature, cooling to 20°C in 0.5 hour.

The specimens of the extruded material were cut from the flanges of a 7075-T6 hat-section type extrusion and of a 2024-T4 angle-section type extrusion.

The static properties of the materials tested were determined with six tensile specimens for each material. The static properties are given together with the results of the other tests in sec. 3.

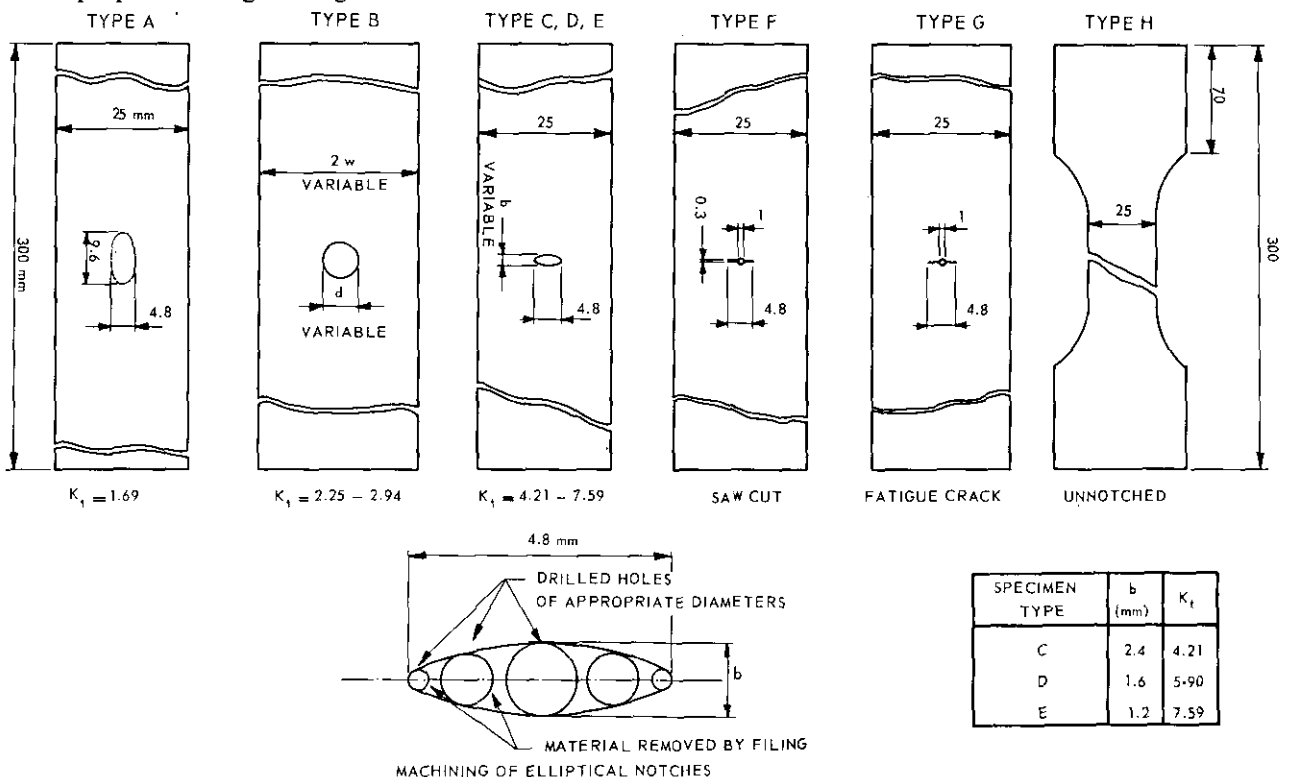


Fig. 1 Survey of specimens

All specimens had a thickness of 2 mm (except the specimens for the study of the thickness effect) and a width of 25 mm (except the specimens for the study of the width effect). The types of specimens used are shown in fig. 1. The specimen used for test series 5 and 6 was type B with a circular hole of 4.8 mm diameter ( $K_t = 2.53$ ). For the investigation on the influence of the stress concentration factor (test series 1) specimens with elliptical notches were used. The way of producing these notches by drilling a number of holes is illustrated in fig. 1. All holes (also in type B specimens) were drilled according to normal workshop practice.

The values for the stress concentration factors as indicated in fig. 1 were obtained from ref. 14. The stress concentration factors for the specimens with elliptical holes were estimated by multiplying the stress concentration factor for an infinite sheet with the same hole by the ratio between the stress concentration factors of a sheet of 25 mm width and an infinite sheet, both with a circular hole having a diameter equal to the transverse axis of the ellipse.

The fatigue cracks in specimen type G were grown in a 2 tons Amsler high frequency pulsator at a mean stress of 8 kg/mm<sup>2</sup> and a stress amplitude of 6.5 kg/mm<sup>2</sup>. The cracks were initiated by a notch consisting of a small hole and a saw cut at both sides, the total length of the notch being 3 mm. The growth of the fatigue cracks from this notch to a total crack length of 4.8 mm from tip to tip on the average required 25,000 cycles for the 2024-T3 specimens, 11,000 cycles for the 7075-T6 specimens and 16,500 cycles for the RR-58 specimens.

The static strength of all specimens was determined in a 20-tons Amsler hydraulic tensile testing machine.

### 3 Test results and a comparison with results of other investigations

The test results are collected in tables 2-6. The effect of the various parameters studied can be most easily appreciated by comparing the values of the static efficiency defined by  $\sigma_{nu}/\sigma_u$ , which are also given in the tables. In tables 2-6 only average values are given for series of 6 similar tests (4 or 5 in a few cases). All individual test results are collected in table 7.

According to table 2 there is a large influence of the stress concentration factor, which is illustrated also in fig. 2, where the results of table 2 are plotted. The values for the specimens with saw cuts are plotted at the applicable value of  $\sigma_{nu}/\sigma_u$ . According to table 3 there is only a slight influence of sheet width if the ratio between hole diameter  $d$  and sheet width  $2w$  is a constant ( $K_t$  constant). Variation of the hole diameter at constant specimen width has a small effect in accordance with the variation of  $K_t$  (see table 4). Riveting has hardly any effect on the static efficiency (table 4). There is also some influence of specimen thickness (table 5) leading to a higher static efficiency for thicker sheets.

According to table 6 the ductility of the material is an important parameter, and indeed it appears that the static efficiency is lower for a more ductile material. This is further illustrated in fig. 3 where the static efficiency is plotted versus the ratio  $\sigma_{0.2}/\sigma_u$  as a measure of ductility ( $\sigma_{0.2}$  is the 0.2% yield strength).

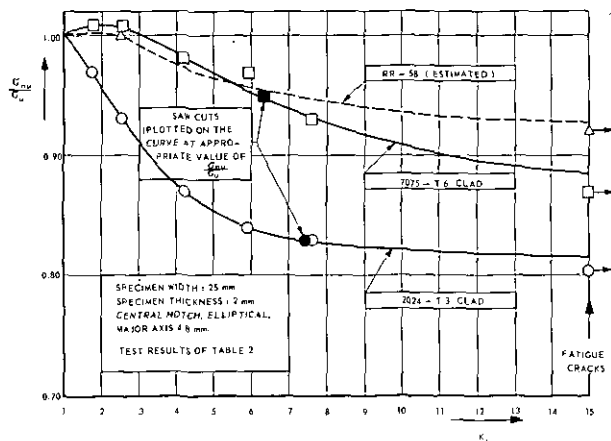


Fig. 2 Influence of stress concentration factor.

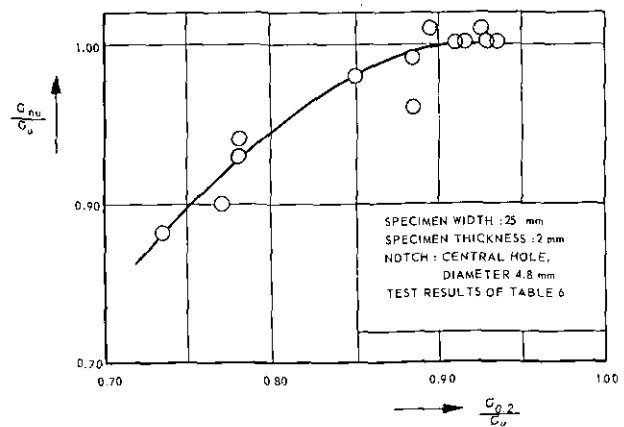


Fig. 3 Influence of material properties.

A large amount of data is available from the literature for comparison with the present results. In fig. 4 results of ref. 2, showing the influence of the stress concentration factor, are compared with the results from the present investigation (presented already in fig. 2). The data from ref. 2 show higher static efficiencies than obtained in the present investigation; the 2024-T3 also shows a static efficiency in excess of one for low values of  $K_t$ . The discrepancy may be due to the fact that the specimens used in ref. 2 were edge notched specimens, whereas centrally notched specimens were used in the present investigation.

Further data on the influence of the stress concentration factor are given in ref. 3. They are presented in table 8

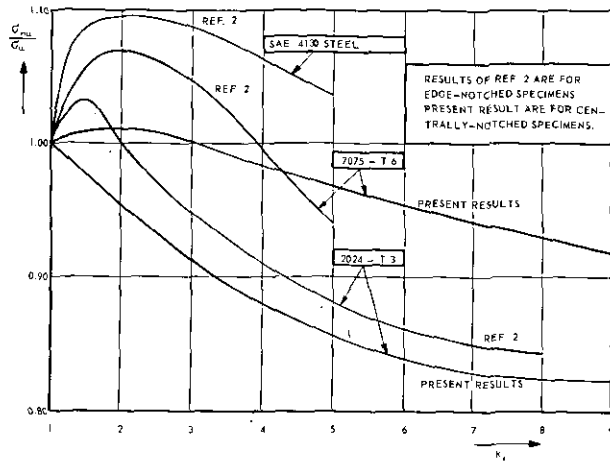


Fig. 4 Influence of stress concentration factor according to ref. 2.

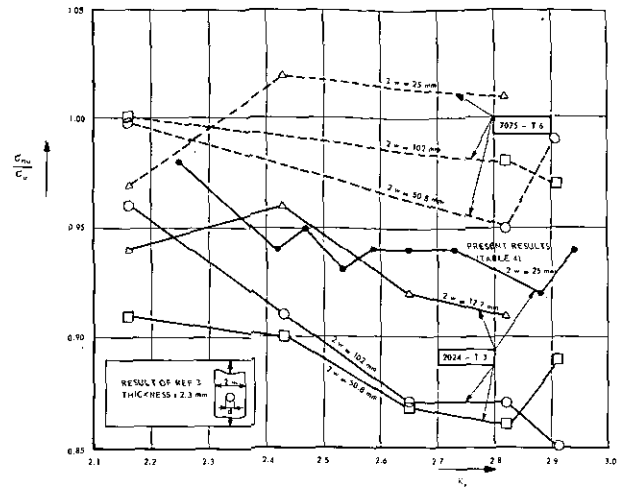


Fig. 5 Influence of sheet width and variation of  $K_t$  due to variation of hole diameter (Ref. 3).

and plotted in fig. 5 together with the results of the present study. Variation of  $K_t$  is due to variation of the hole diameter. Though the data are not very systematical they show a trend of decreasing static efficiency with increasing  $K_t$ , which is in agreement with fig. 2. Fig. 5 also indicates that there is a certain influence of specimen width at constant  $K_t$ . In the present investigation (table 3) only a slight width effect was found.

The influence of the stress concentration factor as found in ref. 1 is shown here in table 9. The data show an increasing static efficiency with decreasing  $K_t$  in accordance with the results previously discussed. It should be noted, however, that this may be partly due to a width effect. The data in table 9 also show the influence of ductility on the static efficiency. There is a trend for a higher static efficiency at a larger ratio  $\sigma_{0.2}/\sigma_w$ , although there are striking exceptions. The same can be said about the results of ref. 6 presented here in table 10. As for the influence of the stress concentration factor the data of table 10 are very unsystematical, which may be due to the fact that edge notches were used with very small root radii.

Finally, some miscellaneous data from ref. 7 are collected in table 11. The results are in agreement with the results of the present investigation as for the influence of the stress concentration factor.

#### 4 Discussion

It is thought that the following conclusions may be drawn from the data presented in the previous section.

- For low stress concentration factors the static efficiency of a notched specimen can be larger than unity, especially where edge notches and aluminium alloys of low ductility are concerned. For stress concentration factors larger than about 3 the static efficiency decreases with increasing stress concentration factor.
- The static efficiency is probably lower for materials with a lower ratio  $\sigma_{0.2}/\sigma_w$ , though the correlation is not fully systematical.
- The static efficiency is somewhat higher for thicker sheets
- At a constant stress concentration factor large specimens are slightly inferior to small specimens as for the static efficiency.

It will prove to be difficult to explain these phenomena. Some tentative thoughts will be presented in sec. 4.1 on the influence of ductility, and in sec. 4.2 the effect of the other parameters will be briefly considered, especially the difference between blunt and sharp notches.

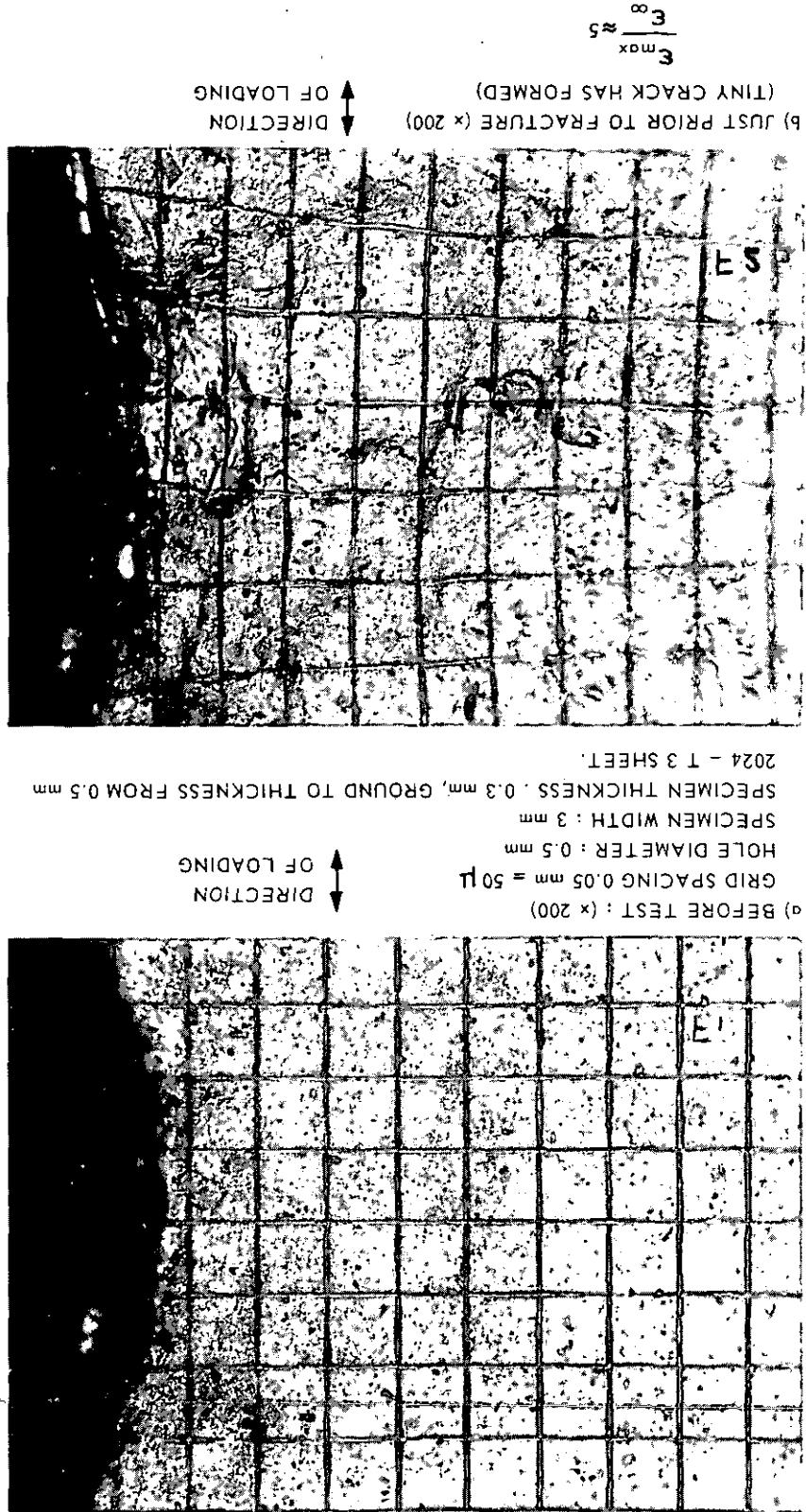
##### 4.1 The influence of ductility

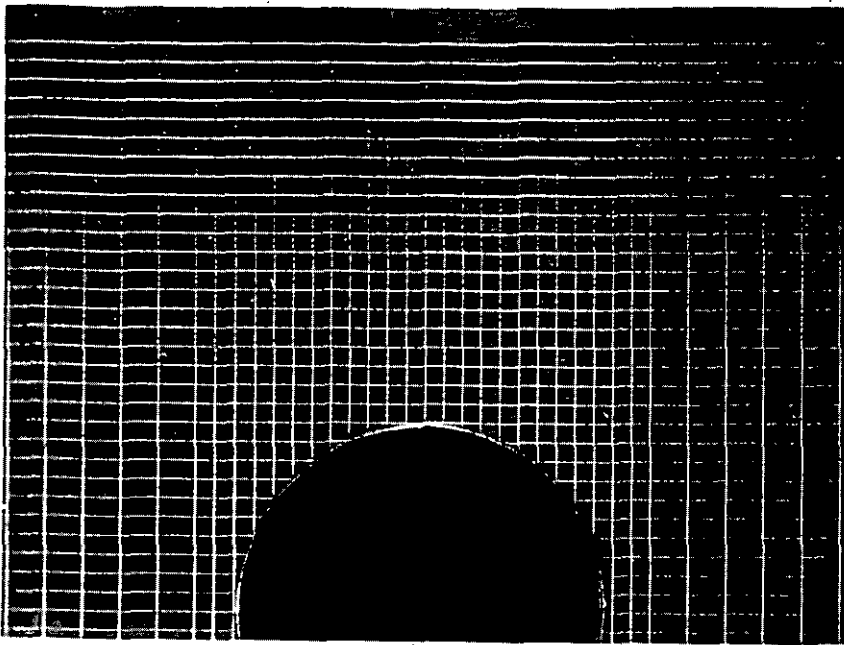
It is thought that the influence of ductility on the static efficiency of notched tensile specimens is strongly related to the effect the ductility has on the stress distribution in the notched section. The stress distribution will be considered first.

The elastic stress and strain distributions at the edge of the hole in a finite sheet are diagrammatically given in fig. 6a. When the stress at the edge of the hole exceeds the yield strength of the material plastic flow will occur, which reduces the stress concentration, but the strain concentration is not reduced (fig. 6b). Calculations made by Stowell (ref. 8) of the elastic-plastic stress and strain distributions around a circular hole in an infinite sheet indicate that the strain concentration factor even increases when plastic flow occurs. This is shown in fig. 7a and it is also shown in this figure that the calculations are confirmed by test results of Griffith (ref. 9). The strain con-

centration factor may attain values in the order of 8. According to Peterson (ref. 10) the strain concentration factor will be reduced again when overall plastic flow takes place, which is illustrated in fig 7b. In general overall plastic flow will occur prior to fracture and the strain concentration at fracture will therefore be lower again. The strain concentration factor was measured on a number of specimens of the present investigation. This was done by means of a grid system inscribed in the specimen with a grid spacing of 0.25 mm. Also a number of tests were carried out on microspecimens with a grid system of spacing 0.05 mm. The latter specimens were fractured in a micro-tensile testing device, which could be manipulated under the optical microscope. Some results of this

Fig. 8 Strain concentration in micro-specimen with a circular hole, loaded in tension.

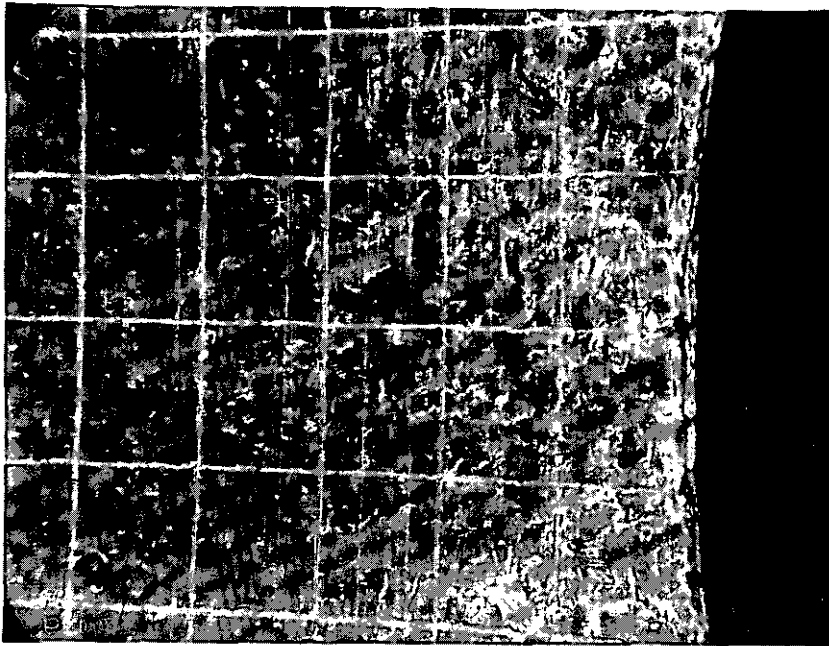




a) SPECIMEN BEFORE TEST. (x 10)  
 GRID SIZE 0.25 x 0.25 mm  
 AND 0.25 x 0.5 mm

← DIRECTION  
 OF LOADING

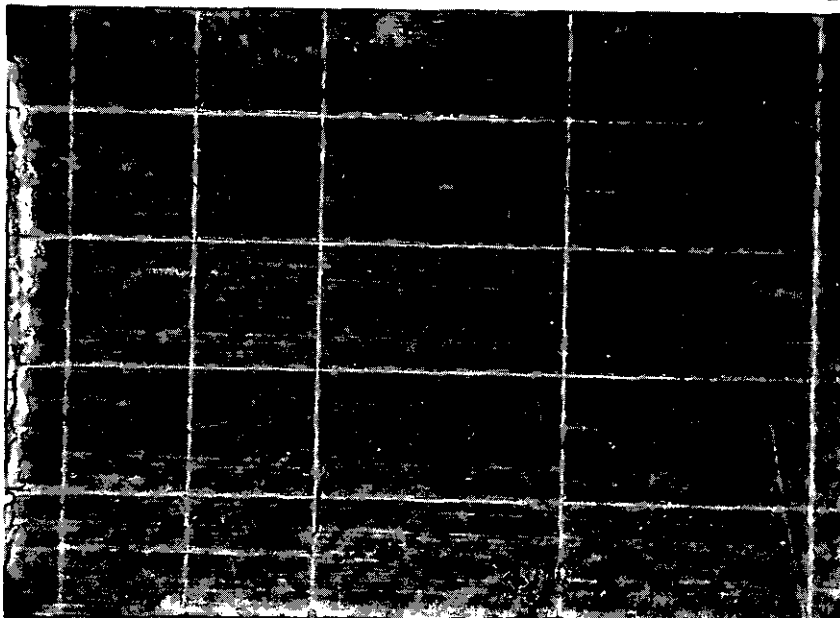
HOLE DIAMETER : 4.8 mm  
 SPECIMEN WIDTH : 25 mm  
 SPECIMEN THICKNESS : 2 mm  
 MATERIAL : 2024 - T3 CLAD



b) JUST PRIOR TO FRACTURE  
 (x 66)  
 TINY CRACK HAS FORMED  
 ALREADY.

↑ DIRECTION  
 OF LOADING

$$\frac{\epsilon_{\max}}{\epsilon_{\infty}} \approx 9$$



c) JUST PRIOR TO FRACTURE.  
 (x 66)  
 MATERIAL REMOTE FROM THE  
 HOLE.

← DIRECTION  
 OF LOADING

Fig. 9 Strain distribution in a 2024-T3 specimen of the present investigation.

4.2 The difference between blunt and sharp notches.

An increasing stress concentration factor will also give an increasing strain-concentration factor at fracture and,

is not high.

determined experimentally and which have no physical meaning. As was shown in ref. 7 the accuracy of the method use of the elastic-plastic stress distribution as calculated by Stowell (ref. 8) and of two constants which should be done already in ref. 11, based on more or less the same assumptions as made here. The analysis of ref. 11 makes criterion. Therefore no attempt will be made to present a quantitative analysis, the more so since this has been previously, but these assumptions are rather dubious from a physical point of view especially as to the fracture It would be possible to make a quantitative analysis of the ductility effect on the basis of the assumptions made is flat at strains larger than about 25% of the fracture strain ( $K_t \approx 4$ ) a high static efficiency is to be expected.

and resembles that of the material with a high ratio  $\sigma_y/\sigma_u$  in fig. 6c, except for the early part of the curve. If the curve in the early stage of plastic flow. This means that the major part of their stress-strain curves is comparatively flat 9 and 10). It should be noted then that most of these data concern materials having high work hardening rates It may be argued that certain materials with a low ratio  $\sigma_{0.2}/\sigma_u$  show a very high static efficiency (see e.g. tables this material will have lower static efficiency.

$\sigma_y/\sigma_u$ ). Consequently the average stress in the notched section is relatively lower in the more ductile material and the onset of fracture the edge of the specimen is under a relatively lower stress in the more ductile material (low by using the stress-strain curves. This has been done in fig. 6c. The conclusion to be drawn from fig. 6c is that, at Now it is possible to draw the stress distribution in the specimens on the basis of the strain distribution and

- a. The strain distributions at fracture have similar shapes for both specimens.
- b. Fracture occurs if the strain at the edge of the hole exceeds a critical value, which is different for the two specimens. For simplicity the critical value of the strain will be assumed to be the strain corresponding to  $\sigma_u$  in the stress-strain curve. The actual value of this limit is not very important for the tentative explanation of the ductility effect.
- c. The stress belonging to a certain strain can be obtained from the stress-strain curve of the material concerned.

Following assumptions will be made:

again to fig. 6. Two specimens are considered (fig. 6c) of materials with different stress-strain curves and the following explanation of the influence of ductility on the static efficiency of a tensile member reference is made and minimum values observed were 9 and 3.5 respectively.

number of 7 specimens an average strain concentration factor at fracture  $K_t = \epsilon_{max}/\epsilon_{\infty} = 5$  was found; maximum study are presented in fig. 8 for a micro-specimen and in fig. 9 for a specimen of the present investigation. For a

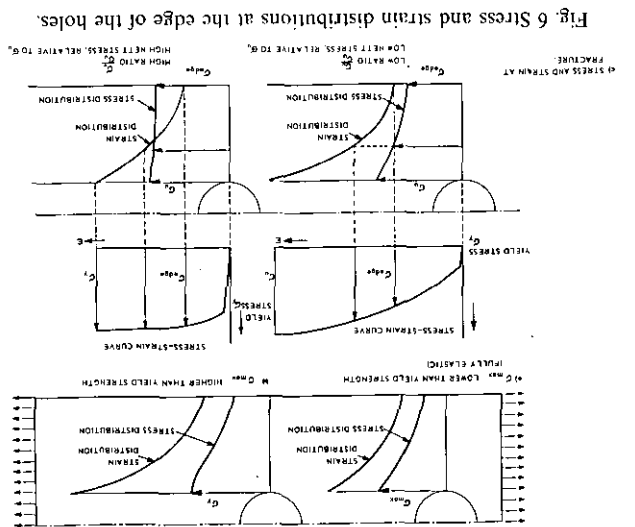
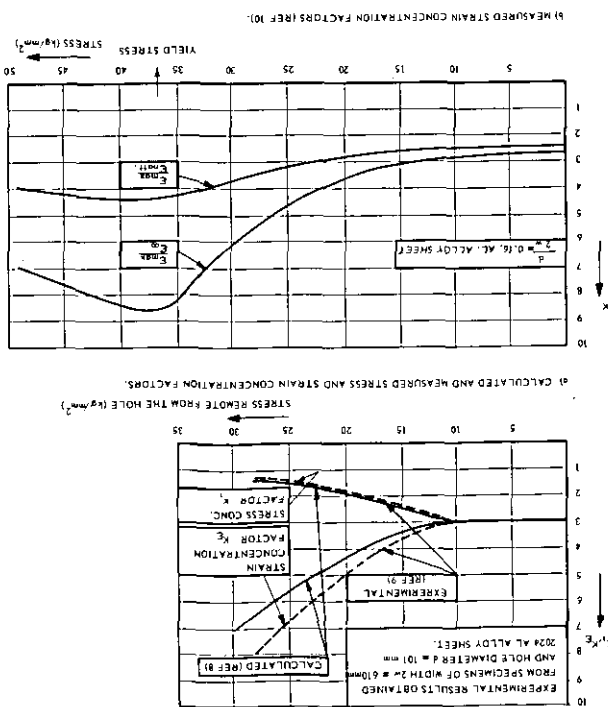


Fig. 6 Stress and strain distributions at the edge of the holes.

Fig. 7 Stress and strain concentration factors for a sheet with a circular hole loaded in tension.



consequently, will lead to a less uniform stress distribution and a lower nett fracture stress. The same reasoning as used in the previous section can be used for any form of notch, provided that the strain-concentration factors at fracture are known. A limitation is, however, that a static efficiency larger than unity cannot be explained, whereas according to the literature (see e.g. fig. 4) for the aluminium alloys a static efficiency above unity may be obtained at values of  $K_t < 3$ . Static efficiencies larger than unity are primarily obtained with edge notched specimens. This phenomenon may be related to the difference in strain distribution between an edge notched and a centrally notched specimen. This difference was shown in ref. 12, indicating that the strain concentration is lower in an edge notched specimen than in a centrally notched specimen (fig. 10).

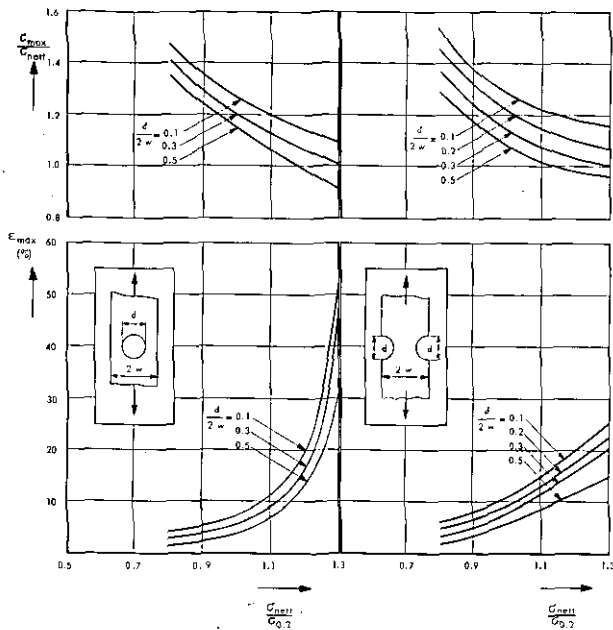


Fig. 10. The difference between centrally notched and edge notched specimens as for stress and strain concentration at different values of the stress (ref. 12).

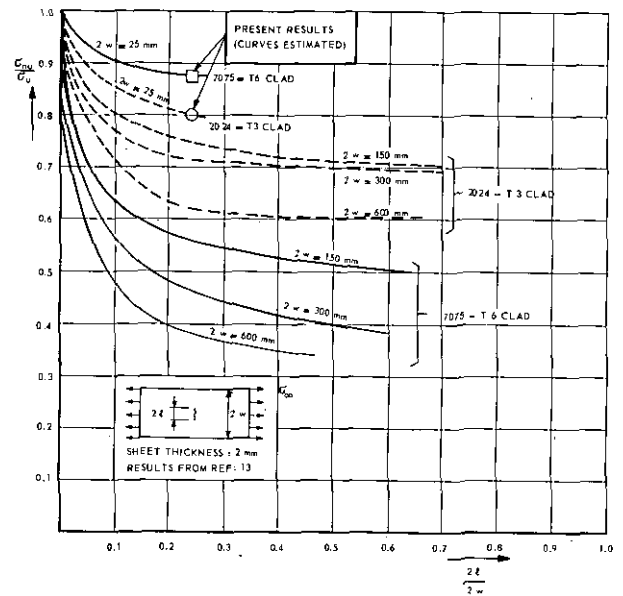


Fig. 11 The nett residual strength of sheets containing cracks (ref. 13).

An important question, which was mentioned already in sec 1, is why the influence of ductility is reversed when very sharp notches like cracks are considered. This reversal of the effect of ductility, however, did not occur in the present test series (see fig. 2). In fig. 2 the less ductile materials are still superior for the case of fatigue cracks. On the other hand results of ref. 13, presented here in fig. 11 clearly indicate that in the case of larger sheets containing cracks the ductile 2024-T3 alloy shows far better properties than the less ductile 7075-T6 alloy. In fig. 11 also the results of the fatigue cracked specimens of the present investigation are plotted. These results are compatible with the residual strength data of ref. 13 in so far that the tendency of the effect of the width is confirmed, i.e.  $\sigma_{nu}/\sigma_u$  increases for decreasing width. Since the width effect is apparently larger for the 7075 alloy than for the 2024 alloy the ductility effect has changed, i.e. the small specimens of the present investigation show higher  $\sigma_{nu}/\sigma_u$  values than 2024-T3, opposite to the trend of ref. 13.

It seems that the reversal of the ductility effect is closely related to the width effect, which is still not properly understood.

The influence of sheet thickness on the static efficiency cannot be explained properly either. It may be that the stress distribution is more uniform in thicker sheets due to the occurrence of the third principal stress which reacts plastic straining in the direction of loading.

## 5 Practical use of the results

For a large number of aluminium alloys values for the static efficiency of tensile members containing blunt notches can be obtained from the present report. Knowledge of the shape of the stress-strain curve of the material concerned is necessary for estimating a value for the static efficiency of other materials.

In practice the static efficiency of a specimen with a row of notches (rivet or bolt row) is very important. The question arises whether the static efficiency of a sheet with a transverse row of holes may be estimated by considering the sheet as a series of parallel members of width equal to the spacing of the holes, each containing one central hole. It could then be assumed that the static efficiency of the sheet is equal to that of a specimen of the dimensions of one of these parallel members. A number of data on this subject can be obtained from ref. 7. These data are

presented in table 12, which indicates that the static efficiency in the case of a row of holes is appreciably lower than the static efficiency of a specimen having a width equal to the hole spacing. Moreover, a smaller hole spacing leads to a lower static efficiency, whereas the reverse should be expected on the basis of the influence of the stress concentration factor for specimens with a single hole as observed in the present investigation. The fact that transverse deformation can occur at the edge of a specimen with a single hole and not at the edges of the imaginary parallel members with a single hole in which a specimen with a row of holes is divided was mentioned in ref. 7 as a possible cause of the different behaviour of the specimens.

Some preliminary tests on the subject have been carried out as an extension of the present test programme. A number of 4 specimens of the 7075-T6 material containing 4 holes of 4,8 mm diameter at a spacing of 25 mm (specimen width 100 mm) showed static efficiencies of 1.04, 1.04, 1.04, 1.05. According to table 6 specimens of the same material with one hole of 4.8 mm diameter and a width of 25 mm showed static efficiency of 1.01.

The results of the preliminary tests are in disagreement with the results of ref. 7. The difference might be due to a difference in ductility. Apparently the behaviour of a specimen with a row of holes cannot simply be derived from results of specimens with one hole and a width equal to the spacing of the holes. In view of its practical significance a systematical investigation on this subject should be strongly recommended.

## 6 Conclusions

From an experimental investigation on the effect of blunt notches on the tensile strength of aluminium alloy sheet specimens the following conclusions can be drawn:

- a. The static efficiency, defined as the ratio between the nett section stress at fracture  $\sigma_{nu}$  and the tensile strength of the unnotched material  $\sigma_u$ , may be larger than unity for stress concentration factors in the order of 2 to 3 if edge notches and aluminium alloys of low ductility are concerned. At larger stress concentration factors the static efficiency decreases with increasing stress concentration factor.
- b. Specimens with a circular hole show an increasing static efficiency with increasing ratio between hole diameter and specimen width, which is due to the decrease of the stress concentration factor. This conclusion is in agreement with conclusion a.
- c. At a constant ratio between hole diameter and specimen width (constant stress concentration factor) small specimens show slightly better static efficiencies than large specimens, though the data obtained on this subject are not very systematical.
- d. The static efficiency is slightly higher for thicker sheets.
- e. The static efficiency of a specimen with a transverse row of holes cannot simply be taken equal to the static efficiency of a specimen with one single hole and a width equal to the hole spacing of the first specimen. Test results indicate that a specimen with a row of holes may show a lower static efficiency than the specimen with a single hole, but that for certain materials the reverse may be true. A systematical investigation on this subject would be a valuable continuation of the present study.

## 7 References

- <sup>1</sup> Hill, H. N., Barker, R.S. Effect of open circular holes on tensile strength and elongation of sheet specimens of some aluminium alloys. NACA TN 1974, Oct. 1949.
- <sup>2</sup> Whaley, R. E., Fatigue and static strength of notched and unnotched aluminium-alloy and steel specimens. Proc. of the Soc. for Experimental Stress Analysis 19, 2 (1962) pp. 329-334.
- <sup>3</sup> Landers, C. B., Hardrath, H. F., Results of axial load fatigue tests on electropolished 2024-T3 and 7075-T6 aluminium-alloy sheet specimens with centrale holes. NACA TN 3631, March 1956.
- <sup>4</sup> Grover, H. J., Hylar, W. S., Axial load fatigue properties of 24 S-T and 75 S-T aluminium alloy as determined in several laboratories. NACA TN 2928, May 1953.
- <sup>5</sup> McEvily, A. J., Illg, W., Hardrath, H. F., Static strength of alluminium-alloy specimens containing fatigue cracks. NACA TN 3816, Oct. 1956.
- <sup>6</sup> Kaufman, J. G., Johnson, E. W., The use of notch-yield ratio to evaluate the notch sensitivity of aluminium alloy sheet A.S.T.M. Proceedings 62 (1962) pp. 778-791.
- <sup>7</sup> Jongebreur, A. A., Investigation on the effect of blunt notches on the static strength of axially loaded sheet specimens (In dutch). Fokker Report S-112 Dec. 1964.
- <sup>8</sup> Stowell, E. Z., Stress and strain concentration at a circular hole in an infinite plate. NACA TN 2073, April 1950.
- <sup>9</sup> Griffith, G. E., Experimental investigation of the effects of plastic flow in a tension panel with a circular hole. NACA TN 1705, September 1948.
- <sup>10</sup> Peterson, R. E., Engineering and design aspects of fatigue of metals. Materials Research and Standards, 3, 2 (Febr. 1962) pp. 122-139.
- <sup>11</sup> Kuhn, P., Figge, I. E., Unified notch strength analysis for wrought aluminium alloys. NASA TN D-1259, May 1962.
- <sup>12</sup> Javornicky, J., Photoplasticity and its use in the testing of materials. (In German) Materialprüfung 5, 12, (Dec. 1963) pp. 458-464
- <sup>13</sup> Broek, D., The influence of sheet width on the residual strength of sheet containing cracks. NLR report TR-H-2152.
- <sup>14</sup> Peterson, R. E., Stress concentration design factors. John Wiley and sons inc. New York. London 1953.

TABLE 1  
Outline of test programme

Test series	Object studied	Materials tested	Remarks	No. of tests
1	Influence of stress concentration factor	2024-T3 clad 7075-T6 clad RR-58	elliptical notches circular notches saw cuts fatigue cracks	80
2	Influence of hole diameter	2024-T3 clad RR-58	Constant specimen width; variable hole diameter	64
3	Influence of riveting and rivet diameter	2024-T3 clad RR-58	Constant specimen width; hole filled with hard-driven rivet	45
4	Influence of specimen width	2024-T3 clad	Constant ratio of hole diameter and specimen width	26
5	Influence of specimen thickness	2024-T3 clad	Thickness 1, 2, 3 and 4 mm	20
6	Influence of ductility	2024-T3 clad 2024-T3 after adhesive bonding cycle 2024-heat treated to max. hardness. 2024-overaged. 2024-T81 2024-T81 after adhesive bonding cycle 2024-T4 extrusion 7075-T6 clad 7075-T6 extrusion 2014-T3 bare 2014-T3 clad RR-58	similar specimens for each material	45

TABLE 2  
Influence of the stress concentration factor

Specimen thickness : 2 mm Specimen width : 25 mm Dimension of notch in width direction of specimen: 4.8 mm			2024-T3		7075-T6		RR-58	
Type	Notch	$K_t$	$\sigma_{nu}$ (kg/mm <sup>2</sup> )	$\frac{\sigma_{nu}}{\sigma_u}$	$\sigma_{nu}$ (kg/mm <sup>2</sup> )	$\frac{\sigma_{nu}}{\sigma_u}$	$\sigma_{nu}$ (kg/mm <sup>2</sup> )	$\frac{\sigma_{nu}}{\sigma_u}$
H	unnotched	1	48.32	1	55.11	1	41.34	1
A	ellipse	1.69	46.84	0.97	55.50	1.01		
B	circle	2.53	44.95	0.93	55.37	1.01	41.38	1.00
C	ellipse	4.21	41.92	0.87	53.80	0.98		
D	ellipse	5.90	40.47	0.84	53.18	0.97		
E	ellipse	7.59	40.12	0.83	51.43	0.93		
F	saw cut	—	40.23	0.83	52.29	0.95	39.13	0.95
G	crack	—	38.61	0.80	47.77	0.87	38.00	0.92

TABLE 3  
Influence of specimen width at constant  $K_t$ .

Material: 2024-T3. Specimen thickness: 2 mm  
 $K_t = 2,51$ , except for type H. Circular notch

Type	Specimen width (mm)	Notch diameter (mm)	$\sigma_{nu}$ (kg/mm <sup>2</sup> )	$\frac{\sigma_{nu}}{\sigma_u}$
H	25	unnotched	48.32	1
B	15	3.0	45.18	0.94
B	25	5.0	43.32	0.90
B	40	8.0	45.51	0.94
B	60	12.0	45.06	0.93
B	100	20.0	45.04	0.93

TABLE 5  
Influence of sheet thickness

Material: 2024-T3 Specimen width: 25 mm  
circular notch; notch diameter = 4.8 mm;  $K_t = 2.53$

Sheet thickness (mm)	$\sigma_{0.2}$ (kg/mm <sup>2</sup> )	$\sigma_u$ (kg/mm <sup>2</sup> )	$\sigma_{nu}$ (kg/mm <sup>2</sup> )	$\frac{\sigma_{nu}}{\sigma_u}$
1	32.70	44.64	41.00	0.92
2	37.68	48.32	44.95	0.93
3	36.39	47.49	45.58	0.96
4	36.15	48.43	46.04	0.95

TABLE 4  
Influence of notch diameter and riveting

Type of alloy	Notch diameter (mm)	$K_t$	Open hole		Hole filled with hard driven rivet*	
			$\sigma_{nu}$ (kg/mm <sup>2</sup> )	$\frac{\sigma_{nu}}{\sigma_u}$	$\sigma_{nu}$ (kg/mm <sup>2</sup> )	$\frac{\sigma_{nu}}{\sigma_u}$
2024-T3	0	1	48.32	1	—	—
	0.5	2.94	45.46	0.94		
	1.0	2.88	44.16	0.92		
	2.4	2.73	45.17	0.94	44.65	0.93
	3.2	2.65	45.15	0.94	44.96	0.93
	4.0	2.59	45.10	0.94	46.34	0.96
	4.8	2.53	44.95	0.93	45.82	0.95
	5.6	2.47	45.69	0.95		
	6.4	2.42	45.27	0.94	46.21	0.96
	10.0	2.25	47.50	0.98		
RR-58	0	1	41.34	1	—	—
	2.4	2.73	41.26	1.00	41.54	1.00
	4.8	2.53	41.38	1.00	41.88	1.01
	6.4	2.42	41.58	1.01	42.15	1.02

\*) The rivet connected a piece of thin sheet to the specimen.

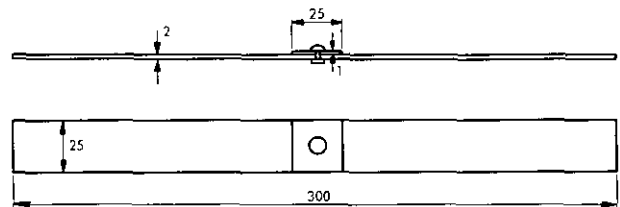


TABLE 6  
Influence of type of material and ductility

Circular notch : 4.8 mm diameter  
specimen width: 25 mm  $K_t = 2.53$

Material	$\sigma_{0.2}$ (kg/mm <sup>2</sup> )	$\sigma_u$ (kg/mm <sup>2</sup> )	$\frac{\sigma_{0.2}}{\sigma_u}$	$\delta$ (%)	$\sigma_{nu}$ (kg/mm <sup>2</sup> )	$\frac{\sigma_{nu}}{\sigma_u}$
2024-T3 clad	37.68	48.32	0.78	18	44.95	0.93
2024-T3 extrusion	37.31	50.71	0.735	17	44.45	0.88
7075-T6 clad	51.00	55.08	0.925	13	55.37	1.01
7075-T6 extrusion	47.29	53.50	0.885	12	51.25	0.96
2014-T3 clad	41.79	49.26	0.85	12	48.14	0.98
2014-T3 bare	40.14	45.34	0.885	8.5	44.56	0.99
RR-58	38.40	41.34	0.93	6.5	41.38	1.00
2024-T3 untreated	37.68	48.32	0.78	18	44.95	0.93
after adhesive bonding cycle <sup>1)</sup>	36.78	47.70	0.77	18.5	43.33	0.90
heat treated to max. hardness <sup>2)</sup>	45.31	49.74	0.91	6.5	49.78	1.00
overaged <sup>3)</sup>	45.00	49.31	0.915	9	49.46	1.00
2024-T81	43.79	48.85	0.895	13.5	49.27	1.01
2024-T81 after bonding cycle <sup>1)</sup>	46.39	49.63	0.935	6.5	49.69	1.00

<sup>1)</sup> heated to 160°C in hour, ½ hr at temp, cooling to 20°C in ½ hr  
<sup>2)</sup> 2 hrs at 195°C, <sup>3)</sup> 6 hrs at 195°C.

TABLE 7  
Individual test results

Test series	Specimen	Material	2w (mm)	d (mm)	$K_t$	t (mm)	$\sigma_{nu}$ (kg/mm <sup>2</sup> )						average $\sigma_{nu}$ (kg/mm <sup>2</sup> )	$\sigma_u$ (kg/mm <sup>2</sup> )	$\sigma_{0.2}$ (kg/mm <sup>2</sup> )		
1(a)	A	2024-T3clad	25	4.8	1.69	1.96		45.44	47.24	47.85			46.84	48.32	37.68		
	B	"	25	"	2.53	1.96	45.11	45.11	45.42	44.46	44.51	45.41	44.95				
	C	"	25	"	4.21	1.95		43.34	41.87	42.48			41.92				
	D	"	25	"	5.90	1.95	40.73	41.47	39.80	39.89			40.47				
	E	"	25	"	7.59	1.95	40.33	39.78	40.46	39.89			40.12				
	F	"	25	"	—	1.94	40.90	40.56	40.43	39.99	39.99	39.52	40.23				
	G	"	25	"	—	1.95	39.32	38.84	39.06	38.18	33.33	37.94	38.61				
1(b)	A	7075-T6clad	25	4.8	1.69	2.02	55.31	55.24	55.88	55.57			55.50	55.11	50.99		
	B	"	25	"	2.53	2.02		55.56	55.20	55.60	55.18	55.32	55.37				
	C	"	25	"	4.21	2.01	53.78	54.14	52.59	54.68			53.80				
	D	"	25	"	5.90	2.01	53.25	53.31	52.59	53.57			53.18				
	E	"	25	"	7.59	2.02	51.67	51.52	50.86	51.67			51.43				
	F	"	25	"	—	2.01	52.04	52.59	51.09	51.73	52.61	53.67	52.29				
	G	"	25	"	—	2.01	48.31	48.13	45.77	48.69	47.43	48.26	47.77				
1(c)	B	RR 58	25	4.8	2.53	2.02	41.70	41.18	41.41	41.39	41.23		41.38	41.34	38.69		
	E	"	25	—	—	2.02	38.92	39.15	39.44	38.75	39.38		39.13				
	F	"	25	—	—	2.02	35.73	38.44	39.31	38.85	37.69		39.00				
2	B	2024-T3clad	25	0.5	2.94	1.94	44.23	45.76	45.89	45.07	45.97	45.82	45.46	48.32	37.68		
	B	"	25	1.0	2.88	1.94	43.36	44.26	44.47	43.87	44.41	44.61	44.16				
	B	"	25	2.4	2.73	1.95	44.65	44.23	45.20	45.13	46.30	45.51	45.17				
	B	"	25	3.2	2.65	1.95	44.91	44.86	45.18	45.68	45.60	45.69	45.15				
	B	"	25	4.0	2.59	1.95	44.62	44.84	46.18	43.83	46.01	45.10	45.10				
	B	"	25	4.8	2.53	1.95	45.11	44.57	45.42	44.66	44.51	45.51	44.95				
	B	"	25	5.6	2.47	1.94	45.30	45.28	46.34	45.49	46.03	45.71	45.69				
	B	"	25	6.4	2.42	1.95	45.38	44.54	46.27	45.40	45.23	44.81	45.27				
	B	"	25	10.0	2.25	1.95	47.42	47.03	48.22	47.43	47.54	47.38	47.50				
	B	RR 58	25	2.4	2.73	2.02	41.72	41.16	40.99	41.03	41.42		41.26			41.34	38.69
	B	"	25	4.8	2.53	2.02							41.38				
	B	"	25	6.4	2.42	2.01	41.91	41.38	41.21	41.96	41.44		41.58				
	3	B	2024-T3clad	25.1	2.4	2.73	1.96	45.10	44.70	43.60	44.93	45.45	44.10			44.65	48.32
B		"	25	3.2	2.65	1.95	45.15	44.69	43.67	45.42	45.38	45.47	44.96				
B		"	25	4.0	2.59	1.96	46.08	46.26	44.86	46.29	47.74	46.80	46.34				
B		"	25	4.8	2.53	1.95	45.70	46.06	45.20	46.37	45.95	45.63	45.82				
B		"	25	6.4	2.42	1.95	46.54	46.67	45.93	46.95	46.95	46.95	46.95				

4	B	2024-T3clad	15	3.0	2.51	1.97	44.92	45.33	45.68	44.67	44.23	45.99	45.18	48.32	37.68
	B	"	25	5.0	2.51	1.96	42.44	43.51	43.07	43.65	43.21	44.04	43.32		
	B	"	40	8.0	2.51	1.95	46.00	45.18	45.56	46.53	45.34	44.42	45.51		
	B	"	60	12.0	2.51	1.95	44.19	44.74	45.87	45.42			45.06		
	B	"	100	20.0	2.51	1.95	44.61	44.73	45.52	45.29			45.04		
5	B	2024-T3clad	25	4.8	2.53	4.05	45.70	45.90	45.88	46.69			46.04		
	H	"	24.9	—	—	4.06	48.22	47.88	48.41	48.79	48.85			48.43	36.15
	B	"	25	4.8	2.53	3.15	45.45	45.59	45.55	45.62	45.67		45.58		
	H	"	24.9	—	—	3.16	47.41	47.06	47.39	47.54	48.03			47.49	36.39
	B	"	25	4.8	2.53	1.01	41.16	41.23	41.25	40.87	40.51		41.26		
	H	"	24.9	—	—	1.01	44.44	44.44	44.89	44.77			44.64	32.70	
6	B	2024-T3extr	25	4.8	2.53	2.19	43.41	44.80	43.79	45.22	45.15	44.31	44.45		
	H	"	24.8	—	—	2.15	50.94	51.36	50.30	50.23				50.71	37.31
	B	7075-T6extr	24.9	4.8	2.53	2.30		50.49	51.53	52.62	51.55	51.06	51.25		
	H	"	24.9	—	—	2.30	53.77	53.66	53.37	53.19				53.50	47.29
	B	2026-T3clad	24.7	4.8	2.53	1.97	48.52	47.41	48.31	48.33			48.14		
	H	"	24.8	—	—	1.93	49.03	49.49	49.18	49.35				49.26	41.79
	B	2026-T3bare	25	4.8	2.53	2.09		44.94	44.80	44.99	44.70	43.36	44.56		
	H	"	24.6	—	—	2.09	45.31	45.38	45.30	45.37				45.34	40.14
	B	RR 58	25	4.8	2.53	2.02	41.70	41.18	41.41	41.39	41.23		41.36		
	H	"	24	—	—	2.01	41.60	41.19	41.21	41.38	41.31			41.34	
	B	2024-T3clad	25	4.8	2.53	1.96	45.11	44.57	45.42	44.66	44.51	45.41	44.95		
	H	"	25	—	—	1.95	48.66	48.72	47.34	48.54				48.32	37.68
	B	7075-T6clad	25	4.8	2.53	2.02	55.56	55.20	55.60	55.18	55.32		55.37		
	H	"	24.8	—	—	2.02	54.81	55.58	54.69	55.34				55.11	50.99
	B	2024-T3clad after adh. bond	25	4.8	2.53	1.96	43.61	42.47	42.12	43.78			43.33		
	H	"	24.7	—	—	1.96	48.01	47.79	46.91	48.09				47.70	36.78
	B	2024-T81clad	25	4.8	2.53	1.98		47.70	48.08	48.91	50.27	51.40	49.27		
	H	"	24.9	—	—	1.99	48.07	48.38	48.94	49.99				48.85	43.79
	B	2024-T81clad after adh. bond	25	4.8	2.53	1.99	50.07	49.90	49.40	49.38			49.69		
	H	"	24.8	—	—	1.99	49.83	49.75	49.58	49.34				49.63	46.39
B	2024-T3clad max.hardness	25	4.8	2.53	1.95	50.32	49.48	49.15	50.32	49.94	50.46	49.78			
H	"	24.8	—	—	1.95	50.14	49.58	49.11	50.13				49.74	45.31	
B	2024-T3clad overaged	25	4.8	2.53	1.95	50.37	49.48	48.90	50.19	48.23	49.61	49.46			
H	"	24.8	—	—	1.94	49.37	49.00	48.86	50.01				49.31	45.00	

TABLE 8  
Effect of sheet width and hole diameter. Results of refs 3 and 5.

Sheet thickness: 2.3 mm Results of ref. 3 (static properties from ref. 4)				2024-T3					7075-T6				
2w (mm)	d (mm)	$\frac{d}{2w}$ (mm)	$K_t$	$\sigma_{0.2}$ (kg/mm <sup>2</sup> )	$\sigma_u$ (kg/mm <sup>2</sup> )	$\delta$ (%)	$\frac{\sigma_{nu}}{\sigma_u}$ (kg/mm <sup>2</sup> )	$\frac{\sigma_{nu}}{\sigma_u}$	$\frac{\sigma_{nu}}{\sigma_u}$	$\sigma_{nu}$ (kg/mm <sup>2</sup> )	$\delta$ (%)	$\sigma_u$ (kg/mm <sup>2</sup> )	$\sigma_{0.2}$ (kg/mm <sup>2</sup> )
102	3.2	0.03	2.91	37.6	51.1	19.9	43.6	0.85	0.97	56.2	11.9	57.8	53.3
	6.3	0.06	2.82				44.4	0.87	0.98	56.6			
	12.7	0.125	2.65				44.5	0.87					
	25.4	0.25	2.43				46.7	0.92					
	50.8	0.50	2.16				49.0	0.96	1.00	57.5			
50.8	1.6	0.03	2.91				45.0	0.88	0.99	57.3			
	3.2	0.06	2.82				43.7	0.86	0.95	54.6			
	6.3	0.125	2.65				44.4	0.87					
	12.7	0.25	2.43				46.0	0.90					
	25.4	0.50	2.16				46.9	0.92	1.00	57.8			
12.7	0.8	0.06	2.82				46.5	0.91	1.01	58.1			
	1.6	0.125	2.65				47.1	0.92					
	3.2	0.25	2.43				48.8	0.96	1.02	59.0			
	6.3	0.50	2.16				48.0	0.94	0.97	55.8			

Sheet thickness 2.5 mm; 2w = 885 mm 2 mm; 2w = 304 mm Results of ref. 5													
2w	d	$\frac{d}{2w}$	$K_t$	$\sigma_{0.2}$	$\sigma_u$	$\delta$	$\frac{\sigma_{nu}}{\sigma_u}$	$\frac{\sigma_{nu}}{\sigma_u}$	$\frac{\sigma_{nu}}{\sigma_u}$	$\sigma_{nu}$	$\delta$	$\sigma_u$	$\sigma_{0.2}$
885	25.3	0.03	2.91	37.1	50.5	19.5	40.6	0.81	52.0	56.6	12.8	56.3	1.00
304	25.3	0.08	2.76				43.8	0.87				55.0	0.97

TABLE 9  
Influence of  $K_t$  and type of material

Material	Results of ref. 1 Specimen thickness $t = 0.8$ mm circular hole				2w =	24 mm	12 mm	6 mm
	$\frac{\sigma_{0.2}}{\sigma_u}$	$\sigma_{0.2}$ (kg/mm <sup>2</sup> )	$\sigma_u$ (kg/mm <sup>2</sup> )	$\delta$ (%)	d =	2.4 mm	2.4 mm	2.4 mm
					$K_t =$	2.61	2.51	2.25
2024-O	0.43	9.3	21.6	16.0		0.97	0.96	0.97
2014-T3 clad	0.65	27.8	42.8	18.5		0.90	0.95	0.98
2024-T3	0.67	32.6	49.0	19.4		0.89	0.91	0.98
7075-T6 clad	0.85	46.5	54.5	13.0		0.96	0.97	1.00
2014-T6 clad	0.87	39.1	44.8	8.0		0.95	0.99	1.01
2024-T81	0.89	45.0	50.8	6.5		0.98	0.95	0.96
2024-T86	0.93	49.4	52.9	5.5		0.97	0.98	0.98

TABLE 10

Tests results presented in ref. 6

Sheet thickness  $t=1,5$  mm. Specimen width:  $2w=12,5$  mm. Notch depth varying from 0.63–3.2 mm. Diameter of hole:  $d=1,5$  mm

Material	Longitudinal									Transverse								
	$\sigma_{0.2}$ (kg/mm <sup>2</sup> )	$\sigma_u$ (kg/mm <sup>2</sup> )	$\delta$ (%)	$\frac{\sigma_{0.2}}{\sigma_u}$	$\frac{\sigma_{nu}}{\sigma_u}$					$\sigma_{0.2}$ (kg/mm <sup>2</sup> )	$\sigma_u$ (kg/mm <sup>2</sup> )	$\delta$ (%)	$\frac{\sigma_{0.2}}{\sigma_u}$	$\frac{\sigma_{nu}}{\sigma_u}$				
					edge notch				central hole					edge notch				central hole
					$K_t=2.5$	$K_t=2.6$	$K_t=9.8$	$K_t=12.4$	$K_t=2.7$					$K_t=2.5$	$K_t=2.6$	$K_t=9.8$	$K_t=12.4$	$K_t=2.7$
2014-T6	48.0	51.7	10	0.93	1.02	1.10	0.95	0.96	1.00	46.0	50.6	9.5	0.91	1.02	1.11	0.91	0.93	1.01
2020-T6	53.0	56.4	8	0.94	1.01	1.03	0.83	0.64	0.99	52.8	56.5	6.5	0.94	1.00	1.04	0.80	0.64	0.99
2020-T6 clad	49.8	52.2	7.5	0.95	1.01	1.05	0.85	0.77	1.00	49.1	52.6	6.5	0.93	1.00	1.06	0.84	0.72	0.99
2219-T31	31.6	39.7	17	0.80		1.05	0.92	0.98		28.8	39.8	17	0.72		1.10	0.92	0.97	
2219-T37	37.9	44.2	9	0.86		1.07	0.94	0.99		35.8	44.4	11	0.81		1.09	0.94	1.00	
2219-T62	27.6	41.6	9	0.66		1.08	0.82	0.83		27.4	41.3	9.5	0.66		1.08	0.79	0.85	
2219-T81	38.1	48.7	9	0.78		1.07	0.86	0.92		37.1	48.3	9.5	0.77		1.08	0.85	0.91	
2219-T87	42.1	50.7	9	0.83		1.08	0.90	0.94		42.6	51.2	9	0.83		1.09	0.88	0.91	
2024-T3	36.1	47.7	18	0.76	1.01	1.07	0.85	0.91	0.97	31.5	46.8	20	0.67	0.97	1.02	0.82	0.87	0.94
2024-T3 clad	37.0	48.0	18	0.77	0.99	1.08	0.85	0.93	0.98	32.8	46.6	20	0.70	0.98	1.06	0.83	0.93	0.96
2024-T86	51.2	54.0	6	0.95	1.06	1.09	0.93	0.93	1.01	50.2	53.3	5	0.94	1.02	1.09	0.87	0.85	1.00
5083-O	15.4	31.3	22	0.49	1.06	1.02	0.91	0.90	1.04	15.5	30.8	23	0.50	1.05	1.01	0.87	0.86	1.03
5083-H34	30.4	37.4	10.5	0.81	1.05	1.03	0.95	1.00	1.03	26.9	36.5	12	0.74	1.06	1.04	0.93	0.97	1.04
5086-O	13.8	28.9	22	0.48	1.05	1.02	0.96	0.92	1.02	13.9	28.4	24	0.49	1.06	1.01	0.93	0.91	1.04
5086-H34	27.2	34.2	11	0.80	1.05	1.04	0.99	1.03	1.05	26.2	34.4	13	0.76	1.08	1.07	0.89	1.04	1.05
5154-H38	30.0	34.9	10	0.86	1.02	1.05	0.99	1.05	1.02	29.9	35.1	14	0.85	1.07	1.13	1.04	1.13	1.04
5454-O	11.2	26.4	21.5	0.42	1.03	1.00	0.98	0.98	1.01	11.0	25.3	20.5	0.44	1.04	0.99	0.98	0.98	1.03
5454-H34	28.0	32.3	11	0.87	1.04	1.03	1.00	1.03	1.03	26.9	33.6	10	0.80	1.03	1.02	0.99	1.04	1.00
5456-O	17.1	33.3	22	0.51	1.04	1.05	0.87	0.87	0.99	18.1	33.0	24	0.55	1.04	1.08	0.85	0.89	1.00
5456-H24	30.2	38.5	12	0.78	0.99	1.05	0.85	0.89	0.98	27.2	38.8	14.5	0.70	0.98	1.09	0.82	0.90	0.95
6061-T6	29.1	31.3	11	0.93	1.06	1.11	1.02	1.09	1.04	28.6	31.8	11	0.90	1.05	1.11	0.99	1.07	1.02
7075-T6	53.2	58.3	10.5	0.91	1.04	1.12	0.94	0.97	1.02	51.2	57.8	10.5	0.89	1.02	1.10	0.90	0.91	1.01
7079-T6	44.7	50.8	11	0.88	1.04	1.11	0.95	1.03	1.02	44.0	51.3	11	0.86	1.20	1.10	0.93	1.00	1.01
7178-T6	57.4	62.3	11.5	0.92	1.02	1.10	0.94	0.82	1.00	55.2	62.2	11	0.89	1.01	1.08	0.87	0.70	0.99

TABLE 11  
Influence of different parameters (ref. 7)

		2024-T4 extrusion	2024-T3 clad longitudinal	2024-T3 clad transverse	2024-T3 clad longitudinal	2024-T3 clad transverse
Results of ref. 7 specimen width $2w = 20$ mm	$t$ (mm)	2,5	2	2	2,5	2,5
	$\sigma_{0.2}$ (kg/mm <sup>2</sup> )	34.8	37.2	32.9	35.9	35.3
	$\sigma_u$ (kg/mm <sup>2</sup> )	48.9	48.2	47.3	48.5	48.1
	$\delta$ (%)	14.8	16.5	17.3	16.6	16.1

notch	$d$	$d/2w$	$K_t$	$\sigma_{nu}$									
				(kg/mm <sup>2</sup> )	$\frac{\sigma_{nu}}{\sigma_u}$								
hole	10	0.5	2.15	46.5	0.95	45.5	0.95	44.6	0.94	47.2	0.97	46.0	0.96
hole	3.2	0.16	2.6	44.6	0.91	43.4	0.90	42.6	0.90	43.8	0.90	43.5	0.91
hole with bolt	3.2	0.16	2.6	44.2	0.90								
hole with rivet	3.2	0.16	2.6	45.1	0.92								
slit	10	0.5	4.15	44.1	0.90								
slit	5	0.25	4.1	43.1	0.88								
slit	10	0.5	2.8			43.0	0.89	42.7	0.90	45.4	0.93	42.4	0.88
slit	7	0.35	4.25							42.6	0.88	40.5	0.84

TABLE 12  
Static efficiency of sheet containing a row of holes (ref. 7)

material	$t$ (mm)	$2w$ (mm)	$d$ (mm)	hole spacing	$\frac{\sigma_{nu}}{\sigma_u}$		$\sigma_u$ (kg/mm <sup>2</sup> )
					open holes	holes filled with rivets	
2024-T3L	2	20	3.2	20	0.90		48.2
				(single hole) 12	0.81	0.82	
2024-T3T	2	20	3.2	20	0.90		47.3
				(single hole) 12	0.81	0.82	
2024-T3L	2.5	20	3.2	20	0.90		48.5
				(single hole) 20	0.85	0.86	
				12	0.81	0.81	
				9.4	0.80	0.81	
2024-T3T	2.5	20	3.2	20	0.91		48.1
				(single hole) 20	0.82	0.83	
				12	0.81	0.81	
				9.4	0.78	0.78	

REPORT NLR-TR M. 2152

# The effect of finite specimen width on the residual strength of light alloy sheet

by

D. Broek

## Summary

Results are given of residual strength tests on specimens of 2024-T3 and 7075-T6 aluminium alloy sheet material. Three types of specimens were used, which had a width of 150 mm, 300 mm or 600 mm.

A fracture criterion is developed for a sheet of finite size. This fracture criterion is in reasonable agreement with the test results.

## Contents

		$2L$	— length of specimen
		$2l$	— crack length from tip to tip
		$2l_c$	— critical crack length (crack length at fracture)
		$2l_0$	— initial crack length
		$t$	— sheet thickness
		$U$	— elastic energy
		$\partial U$	— energy released during a crack extension $dl$
		$W$	— plastic energy
		$dW$	— energy consumed during a crack extension $dl$
		$2w$	— specimen width
		$\alpha$	— constant (non-dimensional)
		$\beta$	— constant
		$\delta(2 \text{ in})$	— elongation on 2 inch gauge length
		$\delta_{tot}$	— total elongation of a cracked sheet
		$\sigma$	— stress (load divided by $2wt$ )
		$\sigma_c$	— critical stress (fracture stress)
		$\sigma_i$	— stress to initiate slow crack growth
		$\sigma_u$	— ultimate tensile strength of sheet material
		$\sigma_{0.2}$	— 0.2% yield stress of sheet material
			All stresses are based on gross area.
<b>Contents</b>			
<i>List of symbols</i>			
1 Introduction	1		
2 Experimental details	2		
3 Test results and comparison with results from the literature	2		
4 The width effect in residual strength tests	5		
4.1 Scope of the chapter.	5		
4.2 The fracture criterion for an infinite sheet	6		
4.3 The fracture criterion for a sheet of finite size	7		
5 Discussion	9		
5.1 The significance of the fracture criterion	9		
5.2 Some interesting features of the fracture criterion	12		
5.3 The energy consumed in crack extension	13		
6 Conclusions	14		
7 References	14		
4 tables			
21 figures			
Appendix			

## Units

length mm (1 inch = 25.4 mm).

force kg (1 lb = 0.454 kg).

stress  $\text{kg/mm}^2$  (1000 psi =  $0.703 \text{ kg/mm}^2$ ).

## 1 Introduction

The residual strength of a sheet in tension that contains a fatigue crack is not fully determined by the

## Symbols

$E$	— modulus of elasticity
$E_{\text{eff}}$	— effective overall modulus of elasticity of cracked sheet
$K$	— stress intensity factor $K = \sigma\sqrt{l}$ .

This investigation has been performed under contract with the Netherlands Aircraft Development Board (N.I.V.).

length of the crack. This would be so for an infinite sheet. For a sheet of finite size the width of the sheet together with the crack length determine the residual strength. In this case it is not even so that the relative crack length (i.e. the ratio of crack length to sheet width) fully determines the residual strength, but the residual strength depends also upon the absolute width of the specimen or the absolute length of the crack. As yet, no satisfactory theory is available which accounts for the finite width of the sheet. Consequently, the knowledge of the residual strength properties of a sheet material cannot be obtained from tests on specimens of one size only.

The present investigation was carried out in order to obtain a reliable set of residual strength curves for the aluminium alloys 2024-T3 and 7075-T6 for various values of the specimen width (ranging from 150 mm to 600 mm). The test results are used to determine the validity of the energy fracture criterion that was developed in refs 1 and 2 for an infinite sheet, the criterion being extended in the present report to sheets of finite size. The scope of the investigation is limited to specimens with one central crack transverse to the direction of loading.

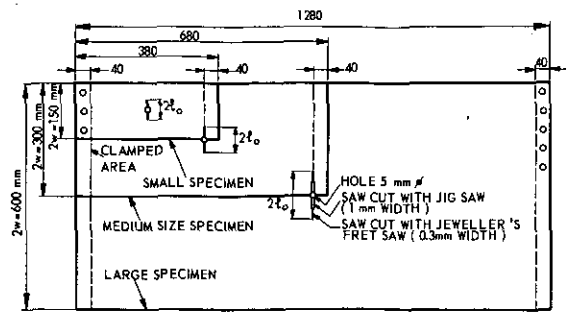
## 2 Experimental details

The materials tested were 2024-T3 and 7075-T6 clad sheet of 2 mm thickness, having the following properties (averages of 8 tests):

	$\sigma_{0.2}$ (kg/mm <sup>2</sup> )	$\sigma_u$ (kg/mm <sup>2</sup> )	$\delta$ (2 in)%
2024-T3	36.4 <sup>+1.4</sup> -1.6	47.6 <sup>+0.6</sup> -1.0	18
7075-T6	51.4 <sup>+0.8</sup> -0.9	55.2 <sup>+0.4</sup> -0.4	12

The unclamped parts of the three types of specimens used were geometrically similar but differed in size, viz. 1200 × 600 mm, 600 × 300 mm, and 300 × 150 mm. The specimens were provided with a fine central transverse sawcut (fig. 1) made by means of a jeweller's fret saw. It was shown in ref. 3 for specimens of the same materials, as used here, that this sawcut can simulate a fatigue crack for the purpose of residual strength tests. The stress to initiate slow crack growth was slightly higher for a sawcut than for a fatigue crack, but once slow crack growth had started the behaviour was the same (same  $\sigma_c$  and  $l_c$ ; see also chapter 5).

The residual strength tests were carried out in an ad hoc test set-up. The specimens were loaded in tension by means of a hydraulic jack of 50 tons capacity. A strain gauge dynamometer in combination with a strip chart recorder provided the load records.



a. The specimens

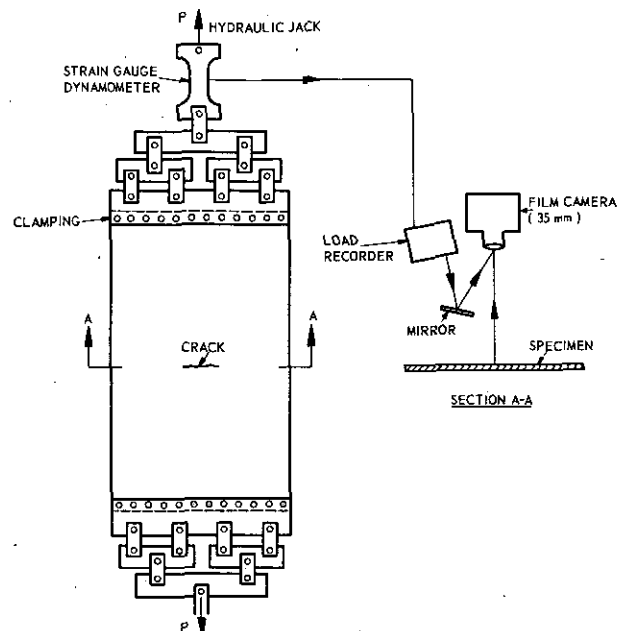


Fig. 1 Test arrangement

During the test the specimen was filmed continuously (at 14 frames per second) to record the slow crack growth. Through a mirror arrangement the load recorder was filmed simultaneously (fig. 1). From the cinematographic records the relation between stress and crack length during slow growth and the crack length at fracture could be determined. As was pointed out in ref. 3, filming gives reliable crack growth records for the thin sheets used in the present investigation.

## 3 Test results and comparison with results of other investigations.

The test results are collected in tables 1, 2 and 3. The residual strength curves (the fracture stress as a function of initial crack length) are plotted in figs 2 and 3. These data are also plotted in fig. 4 as the relative strength  $\sigma_f/\sigma_u$  versus the relative crack length. It appears from fig. 4 that for the same relative crack length (same ratio  $l_0/w$  of crack length to specimen width) a wide specimen has a lower residual strength than a narrow specimen. For the same absolute crack length the residual strength of a wide specimen is

TABLE 1  
Test results of 600 mm wide specimens

Specimen width $2w = 600$ mm		2024-T3 $\sigma_u = 47.6$ kg/mm <sup>2</sup>				7075-T6 $\sigma_u = 55.2$ kg/mm <sup>2</sup>			
$2l_0$ (mm)	$\frac{l_0}{w}$	$\sigma_i$ kg/mm <sup>2</sup>	$2l_c$ mm	$\sigma_c$ kg/mm <sup>2</sup>	$\frac{\sigma_c}{\sigma_u}$	$\sigma_i$ kg/mm <sup>2</sup>	$2l_c$ mm	$\sigma_c$ kg/mm <sup>2</sup>	$\frac{\sigma_c}{\sigma_u}$
16	0.027					32.4	22	33.7	0.61
20	0.033	*)	37	35.0	0.74	*)	25	33.4	0.60
		32.5	43	35.4	0.74	27.1	33	32.0	0.58
		30.3	36	36.8	0.77				
30	0.05	26.6	59	34.6	0.73	26.8	39	31.7	0.57
		29.4	47	34.1	0.72	26.7	35	31.7	0.57
		29.3	53	35.1	0.74	31.1	34	32.7	0.59
40	0.067	28.6	64	34.2	0.72	*)	57	28.0	0.51
		28.6	62	33.0	0.69	23.7	65	26.1	0.47
		*)	*)	32.5	0.68	25.0	48	27.9	0.51
50	0.083	22.9	81	31.7	0.67				
60	0.1					17.2	75	22.6	0.41
						20.0	68	23.2	0.42
						14.8	94	19.9	0.36
80	0.133	19.7	117	24.3	0.51	16.9	88	20.9	0.38
		18.0	113	24.9	0.52	15.9	91	20.6	0.37
		17.8	114	26.0	0.55	15.6	132	20.3	0.37
100	0.17								
120	0.2	16.8	188	26.6	0.56	11.7	127	16.0	0.29
		16.6	160	22.0	0.46	12.0	127	14.5	
		15.6	146	20.9	0.44				
160	0.27	13.2	240	21.7	0.46	11.2	174	14.9	0.27
		11.2	230	22.4	0.47	10.0	170	13.3	0.24
220	0.37	9.3	298	17.7	0.37				
300	0.5	8.9	318	14.2	0.30	7.0	336	12.7	0.23
400	0.67	*)	*)	9.6	0.20				

\*) No value obtained due to malfunction of motion picture camera.

TABLE 2  
Test results of 300 mm wide specimens

Specimen width $2w = 300$ mm		2024-T3 $\sigma_u = 47.6$ kg/mm <sup>2</sup>				7075-T6 $\sigma_u = 55.2$ kg/mm <sup>2</sup>			
$2l_0$ (mm)	$\frac{l_0}{w}$	$\sigma_i$ kg/mm <sup>2</sup>	$2l_c$ mm	$\sigma_c$ kg/mm <sup>2</sup>	$\frac{\sigma_c}{\sigma_u}$	$\sigma_i$ kg/mm <sup>2</sup>	$2l_c$ mm	$\sigma_c$ kg/mm <sup>2</sup>	$\frac{\sigma_c}{\sigma_u}$
25	0.083					29.6	35	34.3	0.62
						29.2	32	32.6	0.60
30	0.1	23.5	41	32.2	0.68				
		21.8	40	31.7	0.67				
		22.5	57	32.0	0.67				
45	0.15	22.7	63	29.6	0.62	15.4	58	24.1	0.44
		20.0	58	29.6	0.62	17.9	54	23.4	0.42
		21.4	63	29.4	0.62				
60	0.2					18.2	66	22.7	0.41
						21.2	75	22.6	0.41
90	0.3	18.1	117	23.7	0.50	13.1	107	15.7	0.28
		17.5	115	23.9	0.50	12.6	100	16.2	0.29
120	0.4	12.2	148	20.0	0.42	13.5	149	14.8	0.27
		12.1	145	19.9	0.42				

TABLE 3  
Test results of 150 mm wide specimens

Specimen width $2w = 150$ mm		2024-T3 $\sigma_u = 47.6$ kg/mm <sup>2</sup>				7075-T6 $\sigma_u = 55.2$ kg/mm <sup>2</sup>			
$2l_0$ (mm)	$\frac{l_0}{w}$	$\sigma_i$ kg/mm <sup>2</sup>	$2l_c$ mm	$\sigma_c$ kg/mm <sup>2</sup>	$\frac{\sigma_c}{\sigma_u}$	$\sigma_i$ kg/mm <sup>2</sup>	$2l_c$ mm	$\sigma_c$ kg/mm <sup>2</sup>	$\frac{\sigma_c}{\sigma_u}$
10	0.066	33.3	22	33.4	0.70	36.2	13	41.1	0.74
		34.8	16	35.1	0.74	*)	*)	40.0	0.72
		34.5	17	34.7	0.73	*)	17	41.4	0.75
20	0.13	31.8	31	32.5	0.68	27.3	25	30.1	0.55
		30.3	29	30.9	0.65	*)	25	33.3	0.60
		32.5	29	32.9	0.69	*)	25	32.7	0.59
40	0.27	23.5	53	25.7	0.54	*)	*)	22.6	0.41
		21.9	55	25.7	0.54	*)	51	22.1	0.40
		20.8	52	26.0	0.55	*)	50	25.8	0.47
80	0.53	14.5	91	15.0	0.32	*)	*)	14.1	0.26
		13.8	89	14.4	0.30	*)	*)	13.8	0.25
		14.2	89	14.9	0.31	13.7	87	13.9	0.25

\*) Not filmed.

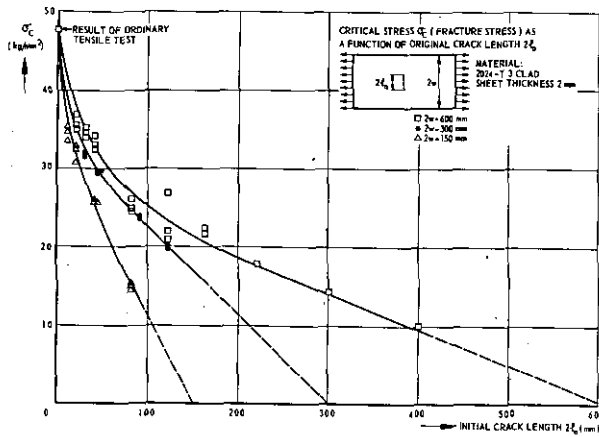


Fig. 2 Residual strength of 2024-T3 specimens.

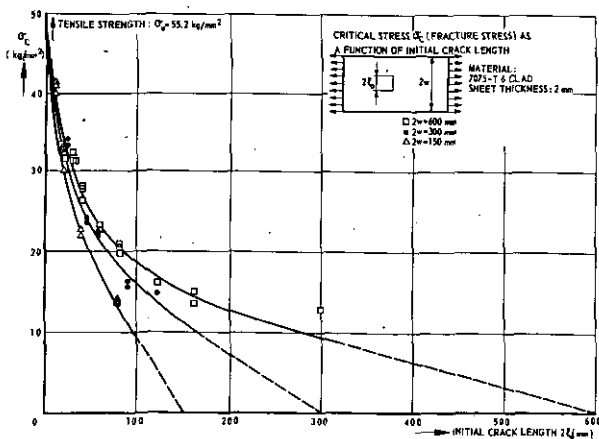


Fig. 3 Residual strength of 7075-T6 specimens.

higher than of a narrow specimen. This shows that the residual strength is a function of both crack length and specimen width and not a function of the ratio of crack length to specimen width only.

The curves for the initiation of slow crack growth

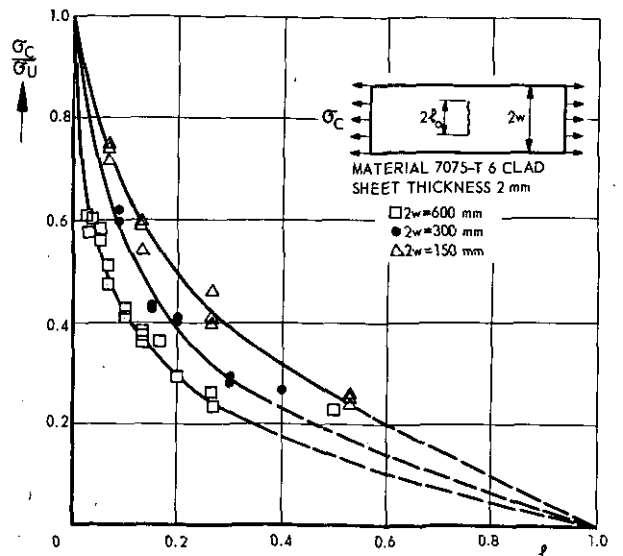
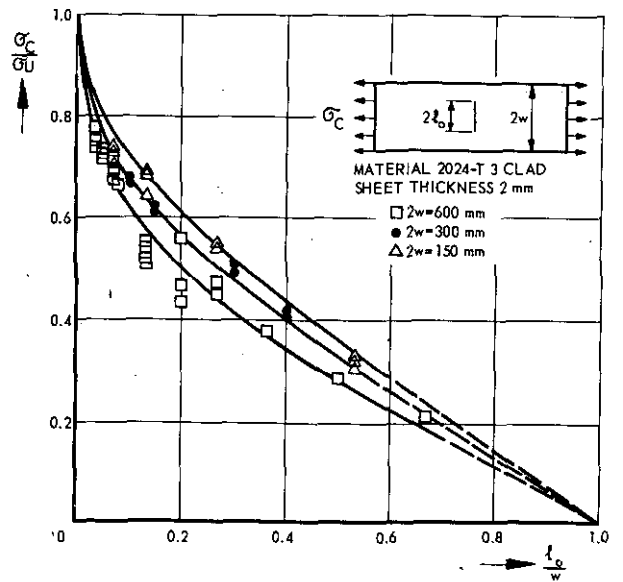


Fig. 4 Relative reduction in strength due to cracks.

are given in fig. 5. Finally, in figs 6 and 7 the critical length is plotted as a function of the initial crack

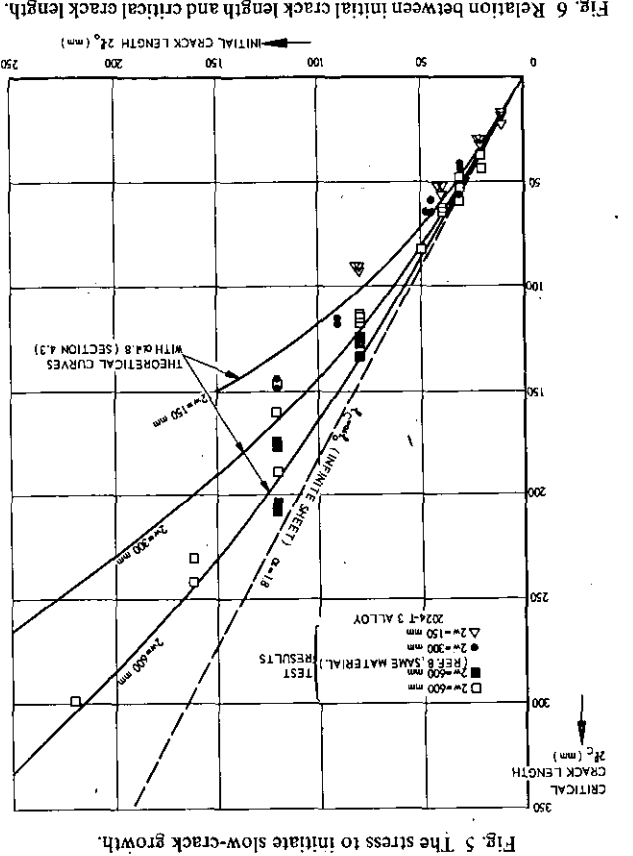
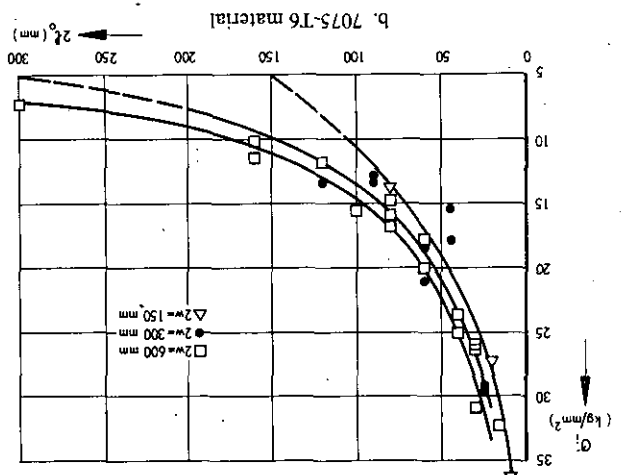
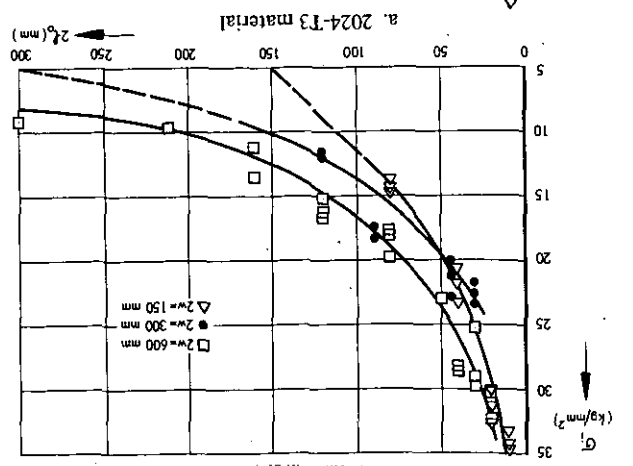


Fig. 6 Relation between initial crack length and critical crack length.

length is plotted as a function of the initial crack

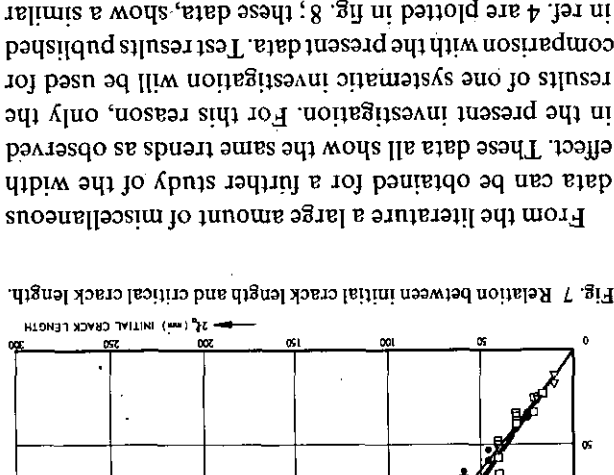
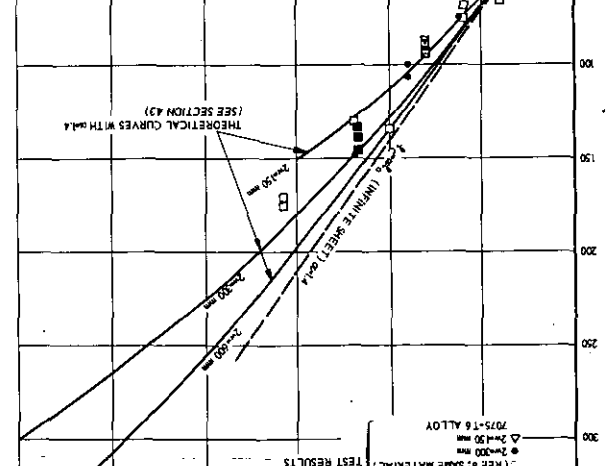


Fig. 8 Effect of finite width as observed in ref. 4.

4 The width effect in residual strength tests.

4.1 Scope of the chapter

In this chapter it will be tried to correlate the test results with an energy fracture criterion. In refs 1 and 2 an energy criterion was developed for fracture of an infinite sheet, containing a central transverse crack.

From the literature a large amount of miscellaneous data can be obtained for a further study of the width effect. These data all show the same trends as observed in the present investigation. For this reason, only the results of one systematic investigation will be used for comparison with the present data. Test results published in ref. 4 are plotted in fig. 8; these data, show a similar trend as figs 2 and 3.

The analysis presented in refs 1 and 2 will be briefly repeated in section 4.2.

In section 4.3 this fracture criterion will be extended for the application to a specimen of finite size. In the same section, the results of this analysis will be compared with the experimental data presented in the previous chapter. A discussion of the usefulness of the fracture criterion will be given in chapter 5.

It should be noted that the analysis in sections 4.2 and 4.3 will be carried out for a sheet of unit thickness.

4.2 The fracture criterion for an infinite sheet

The energy criterion postulates that crack growth occurs when the energy consumed by a crack extension  $dl$  equals the release of potential energy ( $dP/dl$ ); i.e.:

$$-\frac{dP}{dl} = \frac{dW}{dl} \tag{1a}$$

It can be shown that  $dP/dl = \partial U/\partial l$ , (see appendix) hence the energy criterion reads:

$$\frac{\partial U}{\partial l} + \frac{dW}{dl} = 0 \tag{1}$$

In eq. (1)  $dW/dl$  is the plastic work consumed during crack propagation and  $\partial U/\partial l$  is the release of elastic energy:

$$\frac{\partial U}{\partial l} = -\frac{2\pi\sigma^2 l}{E} \text{ (appendix)} \tag{2}$$

per unit thickness of the sheet. The release of energy during crack propagation is independent of whether growth occurs under constant external load or under constant displacement of the plate ends (which was shown analytically in ref. 2 and can also be seen from fig. 9 of the present report).

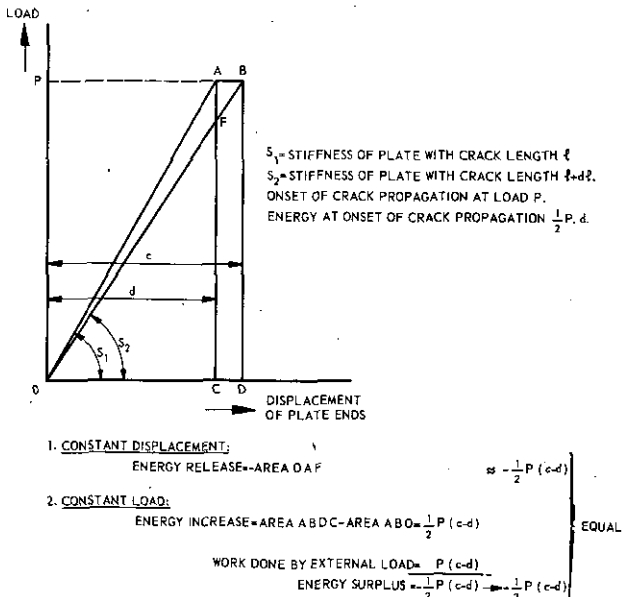


Fig. 9 Energy release due to crack growth.

In eq. (2)  $E$  is the modulus of elasticity of the sheet material,  $\sigma$  the stress and  $2l$  the crack length.

When slow crack growth starts, eq. (1) is fulfilled and during slow stable crack growth there must be a continuous balance between  $\partial U/\partial l$  and  $dW/dl$ . During slow crack growth both  $\sigma$  and  $l$  increase, and so does  $\partial U/\partial l$  according to eq. (2). Then according to eq. (1) also  $dW/dl$  increases during slow crack growth. The values of  $\sigma$  and  $l$  during crack growth can be measured in a test. Then with eqs. (1) and (2) the value of  $dW/dl$  can be calculated. Such values obtained from a large specimen (width 600 mm) with a small crack (length 30 mm) are given in fig. 10. In fig. 10 straight lines are also drawn representing the function  $-\partial U/\partial l$  (eq. 2) at constant  $\sigma$ -values. At the stress  $\sigma_1$  (crack length  $2l_0$ ) the energy release rate  $-\partial U/\partial l$  would be represented by point A in fig. 10, but this value of  $\partial U/\partial l$  is hypothetical, since there is still no crack growth. Slow crack growth starts at a stress  $\sigma_i$ ; the crack extends to the length  $2l_i$  (point B in fig. 10) where  $\partial U/\partial l$  and  $dW/dl$  are balanced (see sect. 5.2). During further increase of

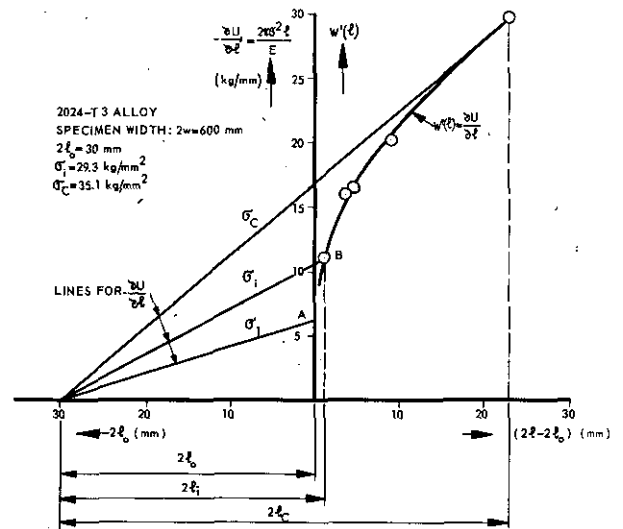


Fig. 10 Illustration of the fracture criterion.

the stress the crack extends slowly under a continuous balance of  $\partial U/\partial l$  and  $dW/dl$ , represented by the curve in fig. 10. When the stress  $\sigma_c$  is reached (crack length  $2l_c$ )  $\partial U$  can no longer be balanced by  $dW$  when the crack extends. There will be an increasing oversupply of energy and fracture instability occurs. The fracture criterion is apparently given by the point of tangency between the curve for  $dW/dl$  and the line for  $-\partial U/\partial l$ . Hence the fracture criterion reads:

$$\left. \begin{aligned} \frac{\partial^2 U}{\partial l^2} + \frac{d^2 W}{dl^2} &= 0 \\ \frac{\partial U}{\partial l} + \frac{dW}{dl} &= 0 \end{aligned} \right\} \tag{3}$$

Krafft and co-workers (ref. 5) put forward the hypothesis that  $dW/dl$  is a function of the amount of crack growth ( $l-l_0$ ) only, which means that the curve for

$dW/dl$  is the same for any value of the initial crack length. This hypothesis is reasonably well confirmed by the present tests, as will be shown in section 4.3. Therefore, this hypothesis will be used here as a basis for the evaluation of the fracture criterion of eqs (3).

From observations on slow growth of relatively small cracks in wide sheets it may be concluded that the critical crack length is proportional to the initial crack length. Figs 6 and 7 show that this is true for small cracks. Therefore it is assumed that for an infinite sheet

$$l_c = \alpha l_0 \quad (4)$$

This relation requires a distinct behaviour of  $dW/dl$  and gives a possibility to evaluate eqs (3).

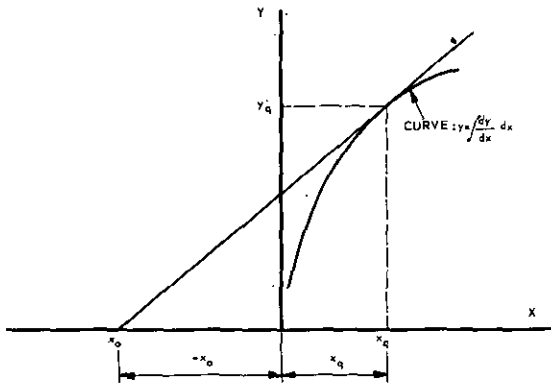


Fig. 11 Simplification of fig. 10.

Consider fig. 11, which is the same as fig. 10, but the axes are denoted by  $X$  and  $Y$  for convenience. A tangent to the curve in the point  $x_q, y_q$  is given by:

$$y = y_q + \left(\frac{dy}{dx}\right)(x - x_q) \quad (5)$$

since  $x = x_0$  at  $y = 0$ :

$$x_0 \left(\frac{dy}{dx}\right)_q = x_q \left(\frac{dy}{dx}\right)_q - y_q \quad (6)$$

and according to eq. (4):

$$-x_0 + x_q = -\alpha x_0 \quad (7)$$

Combination of eqs (6) and (7) yields:

$$(\alpha - 1)y_q = \alpha x_q \left(\frac{dy}{dx}\right)_q \quad (8)$$

Assuming eq. (4) to be valid for any value of  $l_0$ , eq. (8) can be taken to hold for any point  $(x_q, y_q)$  of the curve of fig. 11. It should be noted that to any such point, a different value of  $x_0$  is coupled according to eq. (7).

Hence eq. (8) without the subscript  $q$  will be the differential equation for the curve in fig. 11. The solution is:

$$y = \beta x^{(\alpha-1)/\alpha} \quad (9)$$

$\beta$  being an integration constant.

In the notation of fig. 10 eq. (9) reads:

$$\frac{dW}{dl} = \beta(l - l_0)^{(\alpha-1)/\alpha} \quad (10)$$

where  $\alpha$  and  $\beta$  are constants.

Eqs (2), (3) and (10) lead to:

$$\sigma_c l_c^{1/2\alpha} = \text{constant} \quad (11)$$

and, of course, also to:

$$l_c = \alpha l_0 \quad (12)$$

and then eqs (11) and (12) also give:

$$\sigma_c l_0^{1/2\alpha} = \text{constant} \quad (13)$$

$\alpha$  may be a material constant; its value is higher for a more ductile material and it has a minimum value of unity (no slow crack growth) for an ideally brittle material.

#### 4.3 The fracture criterion for a specimen of finite size

It is assumed that the plastic work required for crack extension is the same for a finite and an infinite sheet, so that eq. (10) is also valid for a specimen of finite size. However, the elastic energies of a finite and an infinite sheet are different. A solution for the elastic energy in a sheet of finite size containing a crack is not yet available.

Koiter (ref. 6) has given a solution for the stress distribution in an infinite sheet containing an infinite row of collinear cracks of spacing  $2w$ . He also calculated the elastic energy contained in such a sheet. The sheet can be divided in parallel strips of width  $2w$  and infinite length, each containing one central transverse crack. It will be assumed here that one of these strips is equivalent with a specimen of finite width  $2w$ . The shortcomings of this assumption will be discussed in chapter 5. Koiter shows that the elastic energy increase due to the crack is

$$U_{\text{crack}} = -\frac{\sigma^2}{2E} \cdot \frac{16}{\pi} w^2 \log \cos \frac{\pi l}{2w} \quad (14)$$

In order to determine whether eq. (14) gives a useful basis for the development of a fracture criterion for a finite size specimen, its validity was studied in the following way. A specimen of length  $2L$  and width  $2w$  with a central transverse crack of length  $2l$  contains, according to eq. (14), an elastic energy

$$\begin{aligned} U &= \frac{\sigma^2}{2E} \cdot 2w \cdot 2L - \frac{\sigma^2}{2E} \cdot \frac{16}{\pi} w^2 \log \cos \frac{\pi l}{2w} = \\ &= \frac{\sigma^2}{2E_{\text{eff}}} \cdot 2w \cdot 2L \end{aligned} \quad (15)$$

Eq. (15) defines an effective overall modulus of elasticity,  $E_{\text{eff}}$ , which equals

$$E_{\text{eff}} = \frac{E}{1 - \frac{4w}{L} \log \cos \frac{\pi l}{2w}} \quad (16)$$

The effective elasticity,  $E_{eff}$ , of a specimen with a crack can be determined from measurements of the total elongation of the specimen under load. When this elongation is equal to  $\delta_{tot}$  then:

$$E_{eff} = \frac{\sigma \cdot 2L}{\delta_{tot}} \quad (17)$$

The measured values of  $E_{eff}$  can be compared with the calculated value according to eq. (16). Such a comparison is presented in fig. 12, showing that the agreement between calculated and measured values is not quite satisfactory. Nevertheless, eq. (14) will be assumed to hold for a finite specimen, since no exact solution for the finite specimen is available.

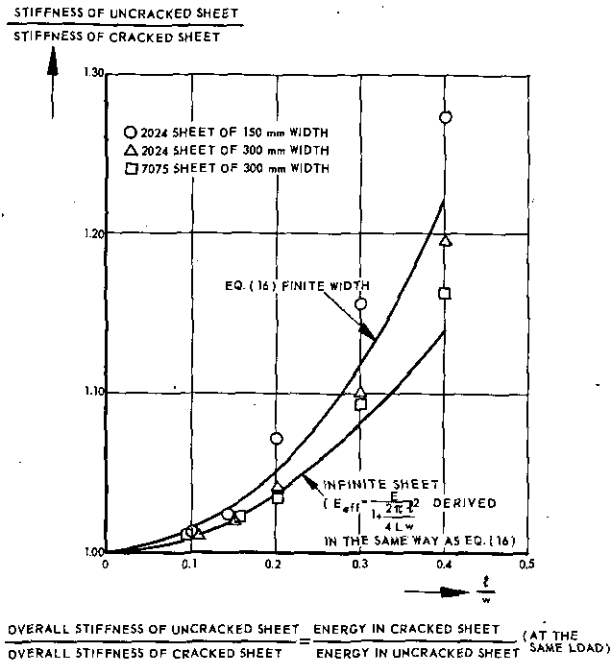


Fig. 12 Influence of finite width on elastic energy.

Then, according to eq. (14):

$$\frac{\partial U}{\partial l} = \frac{4\sigma^2 w}{E} \tan \frac{\pi l}{2w} \quad (18)$$

which is again independent of whether crack growth occurs under constant stress or under constant displacement of the specimen ends. Comparison of eqs (2) and (18) shows that the modification of eq. (2) to obtain eq. (18) for finite specimens is the same as the one proposed by Irwin (ref. 7).

The second derivative of the elastic energy is:

$$\frac{\partial^2 U}{\partial l^2} = \frac{2\pi\sigma^2}{E} \sec^2 \frac{\pi l}{2w} \quad (19)$$

The fracture criterion of eqs (3) can now be evaluated by the combination of eqs (10), (18) and (19). Eqs (3) lead to:

$$l_0 = l_c - \frac{w}{\pi} \frac{\alpha - 1}{\alpha} \sin \frac{\pi l_c}{w} \quad (20)$$

and to

$$\sigma_c^2 w^{1/\alpha} = \frac{\beta E}{2} \left( \frac{\alpha - 1}{\pi \alpha} \right)^{\alpha - 1/\alpha} \sin^{-1/\alpha} \frac{\pi l_c}{w} \cos^2 \frac{\pi l_c}{2w} \quad (21)$$

Substitution of eq. (20) in eq. (21) yields:

$$\sigma_c^2 w^{1/\alpha} = \frac{\beta E}{2} \frac{\alpha - 1}{\pi \alpha} \left( \frac{l_c}{w} - \frac{l_0}{w} \right)^{-\frac{1}{\alpha}} \cos^2 \frac{\pi l_c}{2w} \quad (22)$$

From eqs (20) and (22) it follows that

$$\sigma_c w^{1/2\alpha} = \text{constant, when } \frac{l_0}{w} = \text{constant} \quad (23)$$

The verification of eqs (20)–(23) should concern the following points:

- The relation between  $l_c$  and  $l_0$  (eq. 20). The value of  $\alpha$  appearing from this relation should also apply to the relation between crack length and strength.
- The relation between strength and crack length (sheet width) for constant values of  $l_0/w$  (eq. 23). Note that for  $l_0/w = \text{constant}$  eq. (23) is equivalent with  $\sigma_c l_0^{1/2\alpha} = \text{constant}$ , which is eq. (13) for an infinite sheet.
- The relation between strength and sheet width as given by eq. (21). The value of  $\beta$  should be obtained from plots of the type of fig. 10.

Various checks have been carried out in figs 6, 7 and 13–18, which allow the following conclusion to be made.

- The relation between  $l_c$  and  $l_0$  is reasonably well confirmed by the experimental results (figs 6 and 7), the test results systematically falling somewhat below the curves.
- According to figs 13 and 14 indeed  $\sigma_c w^{1/2\alpha} = \text{constant}$  for constant  $l/w$  and according to figs 15 and 16, also  $\sigma_c l_0^{1/2\alpha} = \text{constant}$  for small values of  $l/w$ .
- The values of  $\alpha$  for the present specimens resulting from these figures are as follows:

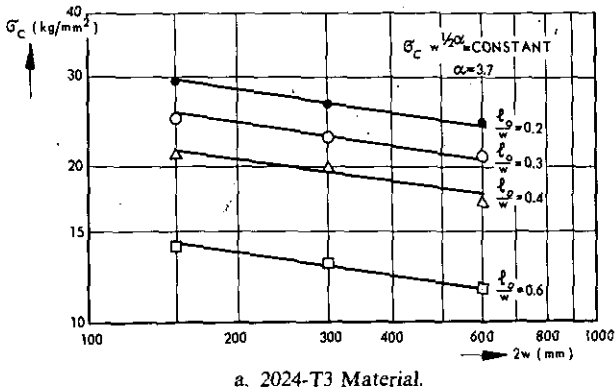
	Figs 6 and 7	Fig. 13	Figs 15 and 16
2024-T3	1.8	3.7	1.85
7075-T6	1.4	1.7	1.22

These results are somewhat contrary to what the theory would lead one to expect. The first two columns refer to constant values of  $l_0/w$ , whereas the last column was derived from tests with variable, though small values of  $l_0/w$ .

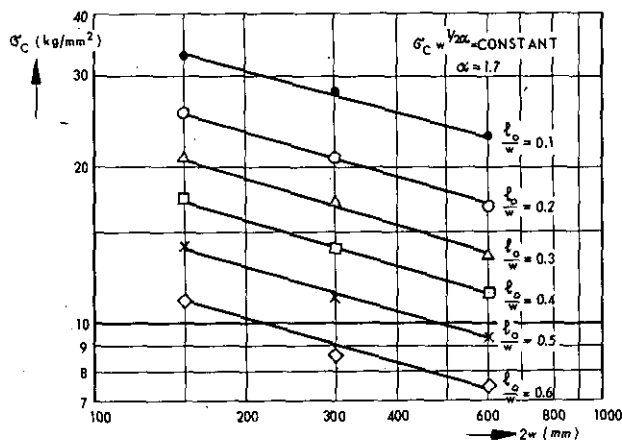
A better agreement between the first two columns could, therefore, be expected than between these two and the third one. Actually, the reverse is true.

The agreement between the first two columns is poor, but for the case of small cracks (figs 15 and 16) there is a reasonable agreement with the values observed from slow crack growth records.

One of the causes of the unsatisfactory agreement undoubtedly is that, especially in figs 6 and 7, the values  $\alpha = 1.8$  and  $\alpha = 1.4$  are no more than rough estimates.



a. 2024-T3 Material.



b. 7075-T6 Material.

Fig. 13 Relation between sheet width and strength on doubly logarithmic scale.

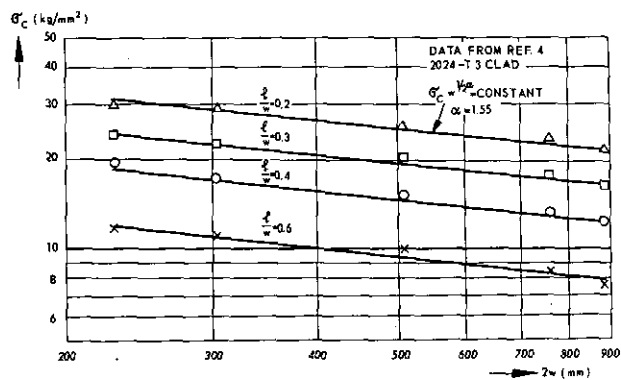


Fig. 14 Relation between sheet width and strength according to ref. 4 (see also fig. 8) on doubly-logarithmic scale

d. The point of tangency of  $\partial U/\partial l$  and  $dW/dl$  indeed gives the condition for fracture (figs 17 and 18). In figs 17 and 18 only the results are plotted of a number of arbitrarily chosen specimens of 300 mm width. The same is observed when the results of other specimens (which can be calculated from the data given in table 4) are plotted. According to the hypothesis of Krafft the curves for  $dW/dl$  should all coincide, but it is seen from figs 17 and 18 that

scatter is fairly large. This will partly be due to the scatter in the values of  $\sigma$  and  $l$  from which the curves are calculated. The values of  $\beta$  following from figs 17 and 18 show large variations. These variations are so large that the evaluation of eq. (21) can give curves that scatter by a factor of almost 2, although their shapes resemble the curves of figs 2 and 3. A prediction of these curves with eq. (21) is therefore not meaningful and is omitted.

- e. Due to the scatter of the curves in figs 17 and 18 no conclusion can be drawn upon the validity of the hypothesis of Krafft. It is felt, however, that the hypothesis can still be used as a working hypothesis.
- f. In figs 15 and 16 the stress  $\sigma_i$  for the initiation of crack growth is also plotted versus the crack length. Apparently, the relation between  $\sigma_i$  and  $l_0$  is:

$$\sigma_i l_0^{0.5} = \text{constant} \quad (24)$$

indicating that slow crack growth starts at a constant value of  $\partial U/\partial l$ .

## 5 Discussion

### 5.1 The significance of the fracture criterion

It appeared in the previous section that the basis of the fracture criterion, stating that the fracture condition is given by the point of tangency between  $\partial U/\partial l$  and  $dW/dl$ , is probably true. Not all predictions made by the fracture criterion are confirmed by test results. However, there is a reasonable agreement between the experimental results and the calculated curves for the relation between initial crack length and critical crack length (figs 6 and 7), and for an infinite sheet (or for a sheet with a small crack) the fracture criterion is reasonably well obeyed (figs 15 and 16). The values of  $\alpha$  for these two cases are in reasonable agreement. It can also be observed that the range of  $l_0/w$  values of figs 13 and 14 is of little significance for practical purposes. Therefore, there is some ground to believe that the fracture criterion is probably useful, although it requires considerable further analysis.

The hypothesis of Krafft, stating that the relation for  $dW/dl$  is independent of the absolute crack length, which was used for the mathematical development of the fracture criterion, cannot be easily defended from a physical point of view. In section 5.3 this hypothesis will be briefly considered.

Another shortcoming of the analysis in section 4.3 is the use of the formula for the elastic energy for an infinite sheet with a row of collinear cracks. A strip (of width  $2w$  containing one central crack) of this infinite sheet carries tension stresses on its edges normal to the crack, whereas a finite specimen with one single transverse crack has free longitudinal edges carrying no stress. This transverse stress system will give a contribution to the elastic energy, which was

TABLE 4  
VALUES OF STRESS AND CRACK LENGTH DURING SLOW CRACK GROWTH  
Note that the last figures for a certain specimen indicate  $2l_c$  and  $\sigma_c$   
2024-T3 alloy

2w = 600 mm									2w = 300 mm					
$2l_0$ (mm)	$2l$ (mm)	$\sigma$ (kg/mm <sup>2</sup> )												
20	21	32.5	30	31	29.3	80	81	19.7	160	161	13.2	30	31	23.5
	22	33.3		34	31.2		85	20.6		165	15.8		32	26.5
	25	34.2		36	33.2		90	21.7		172	17.9		33	28.0
	28	35.2		39	34.2		103	24.0		180	19.6		35	30.2
	30	35.3		53	35.1		107	24.1		190	20.9		36	31.2
	33	35.4					111	24.2		204	21.6		39	31.9
	43	35.4	40	41	28.6		117	24.3		222	21.7		41	32.2
				42	29.5					240	21.7			
20	21	30.3		45	30.3	80	81	17.8				30	32	21.8
	22	33.0		49	32.0		87	22.7	160	161	11.2		34	27.1
	24	34.5		53	32.6		93	24.6		166	14.6		35	29.6
	26	35.4		57	32.8		103	26.0		174	18.1		38	31.1
	29	36.4		60	32.9		114	26.0		187	21.1		40	31.7
	31	36.5		62	33.0					202	22.1			
	34	36.7				120	121	16.8		218	22.4	30	32	22.5
	36	36.8	40	41	28.6		122	18.4		230	22.4		33	25.0
				45	31.2		125	20.9					34	27.1
30	31	26.6		53	33.6		135	24.1	220	221	9.3		36	29.1
	33	29.0		57	34.0		154	26.2		230	13.5		38	30.8
	34	30.8		64	34.2		166	26.6		245	16.5		42	31.6
	38	32.6					175	26.6		261	17.5		57	32.0
	59	34.6	50	51	22.9		188	26.6		275	17.6			
				54	25.3					298	17.7	45	47	20.0
30	32	29.4		57	27.8	120	122	15.6					52	28.6
	36	31.7		60	29.8		127	18.4					55	29.3
	47	34.1		65	31.0		129	19.7					58	29.6
				70	31.6		136	20.5						
				75	31.7		140	20.9						
				81	31.7		146	20.9						

to be continued

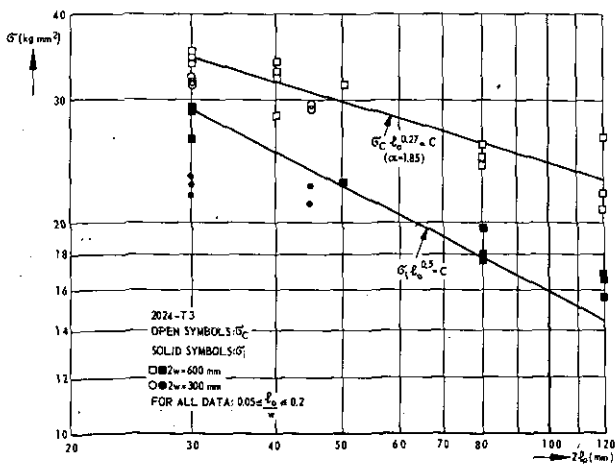


Fig. 15 Check of fracture criterion for 2024-T3 material. (Doubly-logarithmic scale)

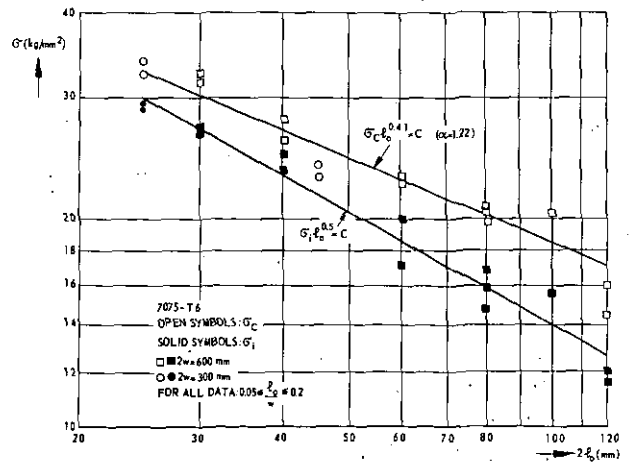


Fig. 16 Check of fracture criterion for 7075-T6 material. (Doubly-logarithmic scale)

TABLE 4 continued  
 VALUES OF STRESS AND CRACK LENGTH DURING SLOW CRACK GROWTH  
 Note that the last figures for a certain specimen indicate  $2l_c$  and  $\sigma_c$   
 7075-T6 alloy

$2w = 600$ mm			$2w = 300$ mm						$2w = 150$ mm					
$2l_0$ (mm)	$2l$ (mm)	$\sigma$ (kg/mm <sup>2</sup> )												
40	42	25.0	100	101	15.6	25	26	29.6	60	61	21.2	10	11	36.2
	44	25.8		105	18.3		29	31.5		63	21.6		12	40.3
	46	26.6		108	18.9		31	33.1		66	22.0		13	41.1
	48	27.9		132	20.3		33	34.0		74	22.2			
60	61	17.2	120	121	11.7	25	26	29.2	90	92	13.1	20	21	27.3
	63	18.9		123	14.2		28	30.4		94	13.5		22	29.7
	66	21.3		126	15.4		30	31.0		96	14.0		23	29.9
	73	22.2		127	16.0		31	31.8		97	14.8		25	30.1
	75	22.6					32	32.6		107	15.7			
60	61	20.0	120	122	12.0	45	46	15.4	90	92	12.6	80	86	13.7
	65	22.0		123	13.1		48	17.7		93	13.5		87	13.9
	67	23.0		126	13.9		50	20.2		94	14.1			
	68	23.2		127	14.5		52	21.2		95	14.9			
80	81	15.9	160	161	10.0	45	46	17.9	120	130	13.5			
	84	18.2		164	11.2		49	19.7		132	14.3			
	86	19.0		167	12.4		51	21.1		135	14.7			
	88	19.8		169	13.3		53	22.8		149	14.8			
	91	20.6		170	13.3		54	23.4						
80	81	16.9	300	301	7.0	60	62	18.2						
	82	18.1		307	10.2		64	21.5						
	83	19.7		318	11.0		65	22.3						
	84	20.2		328	11.8		66	22.7						
	86	20.4		332	12.3									
	87	20.7		336	12.7									
	88	20.9												

to be continued

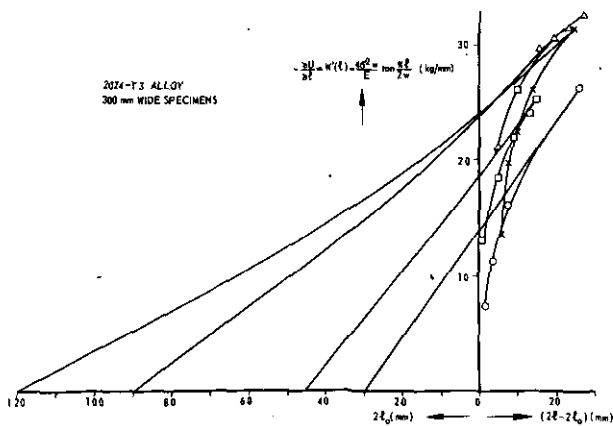


Fig. 17  $dW/dl$  as observed from the present tests.

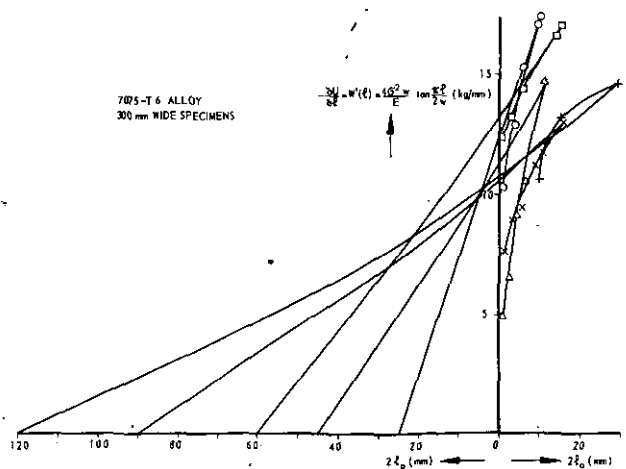


Fig. 18  $dW/dl$  as observed from the present tests.

TABLE 4 continued  
 VALUES OF STRESS AND CRACK LENGTH DURING SLOW CRACK GROWTH  
 Note that the last figures for a certain specimen indicate  $2l_c$  and  $\sigma_c$ .

2w = 300 mm 2024-T3			2w = 150 mm 2024-T3						2w = 600 mm 7075-T6							
$2l_0$ (mm)	$2l$ (mm)	$\sigma$ (kg/mm <sup>2</sup> )	$2l_0$ (mm)	$2l$ (mm)	$\sigma$ (kg/mm <sup>2</sup> )	$2l_0$ (mm)	$2l$ (mm)	$\sigma$ (kg/mm <sup>2</sup> )	$2l_0$ (mm)	$2l$ (mm)	$\sigma$ (kg/mm <sup>2</sup> )	$2l_0$ (mm)	$2l$ (mm)	$\sigma$ (kg/mm <sup>2</sup> )		
90	90	18.1	10	11	33.3	20	21	32.5	80	82	14.5	16	18	32.4		
	95	21.3		12	33.4		23	32.6		83	14.7		20	33.6		
	101	23.0		13	33.4		24	32.8		85	14.7		22	33.7		
	107	23.7		16	33.4		25	32.9		86	14.8					
	110	23.7		20	33.4		29	32.9		88	14.9		20	21	27.1	
	113	23.7		22	33.4					91	15.0		23	28.1		
	117	23.7					40	41		23.5			24	29.3		
							42	24.2		80	81		13.8	26	31.3	
90	91	17.5	10	12	35.0	40	44	25.0	80	82	13.9	30	31	26.8		
	94	21.2		16	35.1		46	25.5		83	14.1		33	32.0		
	99	23.3					47	25.7		84	14.2					
	102	23.3		10	10		34.5	49		25.7	85		14.3	30	31	26.8
	106	23.7		11	34.6		50	25.7		86	14.3		33	28.5		
	115	23.9		12	34.6		53	25.7		89	14.4		35	30.2		
				17	34.7								37	31.6		
120	121	12.2	20	21	31.8	40	46	21.9	80	81	14.2	30	31	26.7		
	125	14.7		22	32.2		47	24.1		82	14.3		33	30.0		
	133	18.4		25	31.3		48	24.7		83	14.5		34	31.3		
	138	19.3		31	32.5		50	25.6		84	14.6		35	31.7		
	143	19.9					55	25.7		85	14.7					
	148	20.0								87	14.7					
							40	41		20.8	89		14.9	40	42	23.7
120	123	12.1	20	22	30.7	40	42	23.6	80			40	65	26.1		
	126	14.4		23	30.8		43	25.1								
	127	17.3		25	30.9		52	26.0								
	130	18.1		26	30.9											
	134	18.9		29	30.9											
	145	19.9														

not accounted for in eq. (14). A correct formula for the energy in a finite sheet might result in a better relation for the residual strength curve.

It should be noted, finally, that the criterion cannot be applied when the nett mean stress in the cracked section exceeds the yield stress of the material, since then general yielding of the nett section occurs, making the formula for the elastic energy meaningless. In almost none of the present tests general yielding has occurred.

As for the practical significance of the criterion it can be stated that the relation  $\sigma_c l_0^{1/2} = \text{constant}$  can be used quite well (see figs 15 and 16). Residual strength problems in aircraft structures generally concern very wide sheets such as wing skins or tailplane skins. Furthermore, large cracks cannot be tolerated in practice and therefore in general only relatively small cracks will be of interest. From figs 15 and 16 it may be concluded that then the panel can be treated as an infinite sheet.

### 5.2 Some interesting features of the fracture criterion.

In fig. 19,  $\partial U/\partial l$  and  $dW/dl$  are again shown diagrammatically. According to eq. (10)  $dW/dl = 0$  at  $l = l_0$ . This seems to imply that crack extension can occur at any stress different from zero. For the onset of crack propagation it is necessary, however, that the

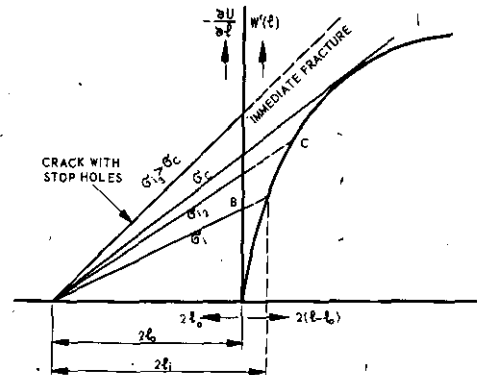


Fig. 19 Different behaviours for a crack with a blunt tip.

stress at the crack tip exceeds a certain critical value (ref. 2). The stress at the crack tip can be described by one parameter, the stress intensity factor, defined as:

$$\bar{K} = \sigma \sqrt{l} \sqrt{\frac{2w}{\pi l} \tan \frac{\pi l}{2w}} \quad (25)$$

Slow crack growth occurs when this parameter exceeds a critical value. Since  $K^2 = (E/\pi)(\partial U/\partial l)$  (eq. 18) this criterion is equivalent to eq. (24), which was shown to be true in figs 17 and 18.

Returning to fig. 19 it is seen that if slow crack growth starts at  $\sigma_i$  the instantaneous value of  $\partial U/\partial l$  is represented by point B. The crack now can extend suddenly to the length  $2l_i$ , where for the first time  $\partial U/\partial l$  and  $dW/dl$  are balanced. This sudden crack extension with a discrete increase of the crack length, associated with a sound effect, was often observed in the tests and is well known as the 'pop-in' effect.

Now a crack can be considered with a blunt tip (e.g. if stop holes are drilled at the crack tip). The stress at the crack tip should exceed a critical value for the onset of crack extension to occur. This critical value corresponds to higher nominal stress than  $\sigma_i$ , say  $\sigma_{i2}$  (fig. 19). The crack then extends suddenly to point C and from there on the behaviour is the same as that of sharp initial crack. This behaviour, which was confirmed by test results (ref. 3), explains why a saw cut can simulate a fatigue crack in a residual strength test; it requires a higher nominal stress for the onset of slow crack growth but shows the same  $\sigma_c$  and  $l_c$  as a fatigue crack.

When the stop-holes drilled at a crack tip are so large that crack growth is postponed to a stress  $\sigma_{i3} > \sigma_c$  it is clear that immediate fracture occurs as soon as the crack starts to grow and no slow stable crack growth will be observed (fig. 19). This was confirmed by test results of ref. 3 and it shows that stop holes should have a large size in order to have an effect on the residual strength.

In the literature the value  $K_c$  is often used, which is the stress intensity factor of eq. (25) for the case when  $\sigma = \sigma_c$  and  $l = l_c$ , i.e. fracture. It is clear that the point of tangency of  $\partial U/\partial l$  and  $dW/dl$  gives  $K_c$  as the square root of  $(E/\pi)(\partial U/\partial l)$  at fracture. There has been some

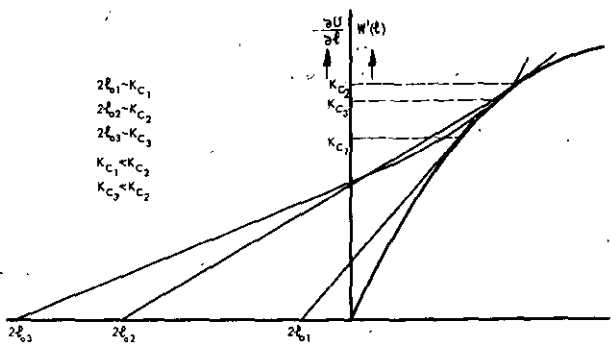


Fig. 20 The maximum of  $K_c$ .

confusion in the literature about the fact that  $K_c$  is not a constant but increases with crack length until a certain maximum and then decreases again. The present fracture criterion predicts that  $K_c$  cannot be a constant and can even explain the observed variation of  $K_c$ , as is shown in fig. 20. For increasing crack lengths the point of tangency rises along the curve of  $dW/dl$ , but for large cracks it returns again, due to the fact that the lines for  $\partial U/\partial l$  deviate more and more from straight lines (see eq. 18).

5.3 The energy consumed in crack extension.

It has been tentatively assumed in chapter 4 that the energy that is consumed during crack extension is mainly composed of plastic energy. Of course energy is required also for the occurrence of fracture per se, namely for the breaking of atomic bonds. This energy, however, would be independent of crack growth, whereas  $dW/dl$  apparently depends strongly upon the amount of crack growth. Moreover, the energy required for the breaking of the atomic bonds is very small in comparison with  $\partial U/\partial l$ . Probably more mechanisms of energy consumption can be mentioned, but it is quite certain that the plastic energy is by far the most important part of the total amount consumed in crack propagation.

As was shown in section 4.3 slow crack growth starts at a constant value of  $\partial U/\partial l$  or  $K^2$ , i.e. at a constant value of  $\sigma_i^2 l_0$  if the correction for finite width is ignored. It can be easily shown that the size of the plastic zone at the crack tip is also proportional to  $\sigma^2 l$ . Then it follows that at the onset of slow crack growth the plastic zone at the crack tip has a constant size, independent of the crack length (fig. 21).

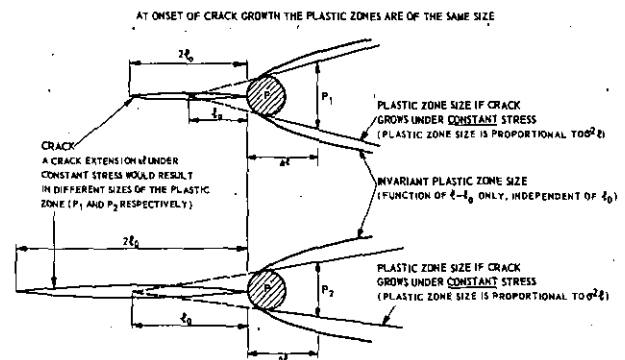


Fig. 21 Plastic zone size during crack growth.

Since both  $dW/dl$  and the plastic zone size depend in the same way on stress and crack length, the hypothesis that  $dW/dl$  is a function of the amount of crack growth only implies that also the size of the plastic zone is a function of the amount of crack growth only.

During crack extension under constant stress the plastic zone size would be proportional to  $l$ . In that

case the size of the plastic zone would be given by the straight lines drawn in fig. 21. Then the sizes of the plastic zones of the two cracks shown in fig. 21 would be different during crack growth. If, however, the zones are of the same size at the onset of slow crack growth it might be conjectured that the continuation of crack growth would also require plastic zones of the same size (fig. 21). Continuation of crack growth then would require an increasing stress. Measurement of the size of the plastic zone during slow crack growth would be of interest for the verification of the hypothesis of an invariant curve for  $dW/dl$ .

## 6 Conclusions.

From an experimental investigation on the residual strength of aluminium alloy sheet specimens containing central cracks it can be concluded that for the same relative crack length (same ratio between crack length and sheet width) a wide sheet has a lower gross fracture stress than a narrow sheet. For the same absolute crack length the wide sheet fractures at a higher stress.

It was pointed out that the energy criterion for fracture is determined by the second derivatives of consumed and released energy. This criterion was evaluated both for an infinite sheet and a sheet of finite size. It turned out that for an infinite sheet the relation between the fracture stress and the initial crack length is given by

$$\sigma_c l_0^{1/2\alpha} = \text{constant},$$

where  $\alpha$  is a constant which has a higher value for a more ductile material. This relation can also be used for small cracks in wide sheets ( $l_0/w < 0.2$ ); this means that it is applicable in most cases where aircraft sheet structures are concerned. The equation is not valid if the stresses are so high that general yielding occurs.

No satisfactory relation was arrived at for the residual strength of sheets containing long cracks. Yet, certain tendencies in the test results could be explained by the use of an approximative solution.

## Appendix

The elastic energy in a cracked plate is equal to:

$$U = \frac{\sigma^2}{2E} (A + 2\pi l^2) \quad (\text{A})$$

per unit thickness in which  $A$  is the surface of the sheet (length  $\times$  width). Eq. (A) can be written as:

$$U = \frac{\sigma^2}{2E_{\text{eff}}} \cdot A \quad \text{where } E_{\text{eff}} = \frac{AE}{A + 2\pi l^2} \quad (\text{B})$$

The average strain in the cracked plate is:

$$\bar{\epsilon} = \frac{\sigma}{E_{\text{eff}}} = \frac{\sigma}{E} \left( 1 + \frac{2\pi l^2}{A} \right) \quad (\text{C})$$

From this it follows for the elastic energy:

$$U(\bar{\epsilon}, l) = \frac{1}{2} \frac{\bar{\epsilon}^2 EA}{1 + \frac{2\pi l^2}{A}} \quad (\text{D})$$

The potential energy of the plate at constant stress can be written as:

$$P = U(\bar{\epsilon}, l) - \sigma \bar{\epsilon} A \quad (\text{E})$$

The potential energy is a minimum as a function of  $\bar{\epsilon}$ , hence:

$$\frac{\partial P}{\partial \bar{\epsilon}} = \frac{\partial U(\bar{\epsilon}, l)}{\partial \bar{\epsilon}} - \sigma A = 0 \quad (\text{F})$$

Combination of eqs (E) and (F) leads to:

$$\frac{dP}{dl} = \frac{\partial U(\bar{\epsilon}, l)}{\partial l} \quad (\text{G})$$

at constant stress.

From eq. (D) it follows that

$$\frac{dP}{dl} = \frac{\partial U(\bar{\epsilon}, l)}{\partial l} = - \frac{2\pi\sigma^2 l}{E} \quad (\text{H})$$

## 7 References.

- <sup>1</sup> Broek, D., The energy criterion for fracture of sheets containing cracks. *Applied Materials Research* 4, 3 (July 1965) pp. 188-189.
- <sup>2</sup> Broek, D., The residual strength of cracked sheet and structures. N.L.R. report TM-M. 2135, Aug. 1964.
- <sup>3</sup> Broek, D., The residual strength of aluminium alloy sheet specimens containing fatigue cracks or saw cuts. N.L.R. report TN-M. 2143, Febr. 1965.
- <sup>4</sup> Christensen, R. H. Denke, P. H., Crack strength and crack propagation characteristics of high strength metals. Techn. Doc. Rep. ASD-TR-61-207. Jan. 1962.
- <sup>5</sup> Krafft, J. M. Sullivan, A. M. Boyle, R. W., Effect of dimensions on fast fracture instability of notched sheets. *Proceedings of the crack-propagation symposium, Cranfield 1961, Vol I* pp. 8-28. Cranfield, The College of Aeronautics, 1962.
- <sup>6</sup> Koiter, W. T., An infinite row of collinear cracks in an infinite elastic sheet. *Ingenieur Archiv*, 28. Band, 1959, pp. 168-172.
- <sup>7</sup> Irwin, G. R., *Fracture. Handbuch der Physik*, Ed by S. Flügge pp. 551-590. Springer Verlag 1958.
- <sup>8</sup> Broek, D., The residual strength of cracked sheet. Tests interrupted after intermediate slow crack growth. N.L.R. report M. 2145, July 1965.

## REPORT NLR-TR M.2154

# The influence of the loading rate on the residual strength of aluminium alloy sheet specimens

by

D. BROEK AND A. NEDERVEEN

## Summary

Residual strength tests with a duration ranging from 30 minutes to about 0.4 seconds were carried out on 2024-T3 alclad sheet specimens containing a central transverse saw cut. It turned out that the stress to initiate slow crack growth decreased at increasing loading rate, but in the range of loading rates tested the residual strength did not depend upon the rate of loading.

Some incidental results were obtained on the rate of crack propagation during fracture instability.

Contents	Page	$2l_0$	— initial crack length
List of symbols.	1	$\frac{\partial U}{\partial l}$	— energy released during a crack extension $dl$
1 Introduction.	1	$v_c$	— rate of crack propagation
2 Experimental details.	2	$v_s$	— velocity of sound
2.1 Materials and specimens.	2	$2w$	— specimen width
2.2 Testing technique.	2	$\frac{dW}{dl}$	— energy consumed during a crack extension $dl$
3 Test results and discussion.	3	$\alpha$	— constant
4 The rate of crack propagation during fracture instability.	5	$\beta$	— constant
4.1 Test results.	5	$\delta(2 \text{ in})$	— elongation on 2 in gauge length
4.2 Predictions by fracture dynamics.	5	$\rho$	— specific mass of sheet material
5 Conclusions.	7	$\sigma$	— stress
6 References.	7	$\sigma_c$	— fracture stress; residual strength
1 table		$\sigma_i$	— stress to initiate slow crack growth
5 figures		$\sigma_u$	— ultimate tensile strength
		$\sigma_{0.2}$	— 0.2% yield stress
		All stresses are based on gross area.	

## Symbols

$E$  — modulus of elasticity  
 $H$  — kinetic energy  
 $k$  — numerical constant  
 $2l$  — crack length  
 $2l_c$  — crack length at fracture (critical crack length)

## Units

length mm (1 inch = 25.4 mm)  
 force kg (1 lb = 0.454 kg)  
 stress kg/mm<sup>2</sup> (1000 psi = 0.703 kg/mm<sup>2</sup>)

## 1 Introduction

The loading rates encountered in engineering practice can vary by several orders of magnitude. Structures subjected to impact loadings may attain their maximum load in a fraction of a second, whereas the load-bearing elements of a large building under construction may attain their maximum load in a period of about a year. Though for the special case of an aircraft structure the extreme loading rates are closer together than in the previous example, they may still vary by a factor in the order of  $10^4$  for the primary structure. The most important parts for the fail-safe

problem are the pressure cabin and the wing. The pressure cabin reaches its maximum load in a time in the order of 30 minutes, whereas the wing of a civil aircraft may experience gust loads built up in a few tenths of a second.

The loading rate could very well affect the residual strength in the presence of fatigue cracks. Residual strength tests on sheet material usually have a duration of about 2 minutes and it would be worthwhile to know whether the data obtained from such tests are of general applicability for the estimation of the fail-safe properties of aircraft structures. For this reason a limited number of residual strength tests were carried out on sheet specimens of 2024-T3 alclad sheet material. A few tests were performed on specimens of 7075-T6 alclad sheet material. The duration of the tests ranged from 30 minutes to about 0.4 seconds. The results of this experimental investigation are presented in this report.

A few specimens were filmed with a high-speed camera during testing. From the films some data were obtained on the rate of crack propagation during fracture instability. In chapter 4 of this report the observed crack propagation velocities are presented and an attempt is made to compare them with values predicted by fracture dynamics.

## 2 Experimental details

### 2.1 Materials and specimens

The specimens were cut from 2024-T3 alclad sheet material of 2 mm thickness. Two tests were carried out on specimens of 7075-T6 alclad sheet of 2 mm thickness. The static properties of the sheet materials are (averages of 8 tests for each type of material):

	$\sigma_{0.2}$ (kg/mm <sup>2</sup> )	$\sigma_u$ (kg/mm <sup>2</sup> )	$\delta$ (2 in) (%)
2024-T3	36.4 +1.4 -1.6	47.6 +0.6 -1.0	18
7075-T6	51.4 +0.8 -0.9	55.2 +0.4 -0.4	12

The size of the specimens was 680 × 300 mm. They were provided with a central transverse saw-cut (fig. 1) made by means of a jeweller's fret saw. It was shown in ref. 1 for the same materials that this saw-cut can simulate a fatigue crack for the purpose of residual strength tests. The stress to initiate slow crack growth was slightly higher for a saw-cut than for a fatigue crack of equal length, but once slow crack growth had started the behaviour was the same (same fracture stress and same critical crack length).

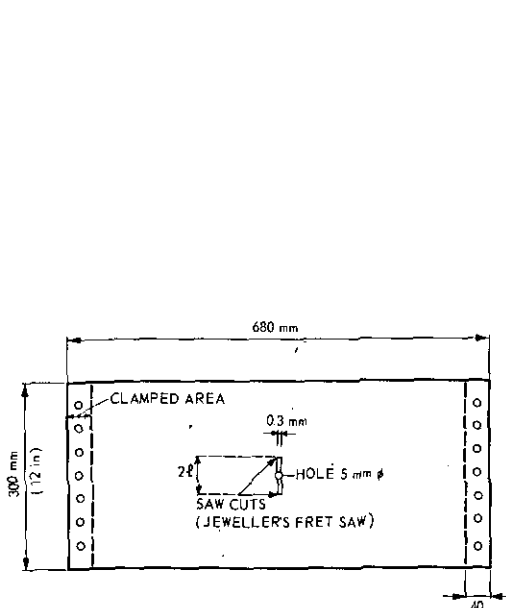


Fig. 1 The specimen.

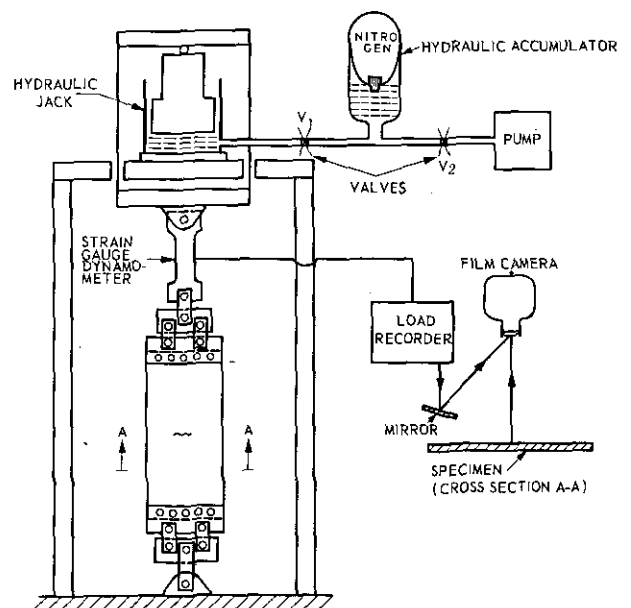


Fig. 2 Arrangement of tests.

### 2.2 Testing technique

Four test series were carried out with testing times of 30 minutes, 2 minutes, 2 seconds and about 0.4 seconds, respectively.



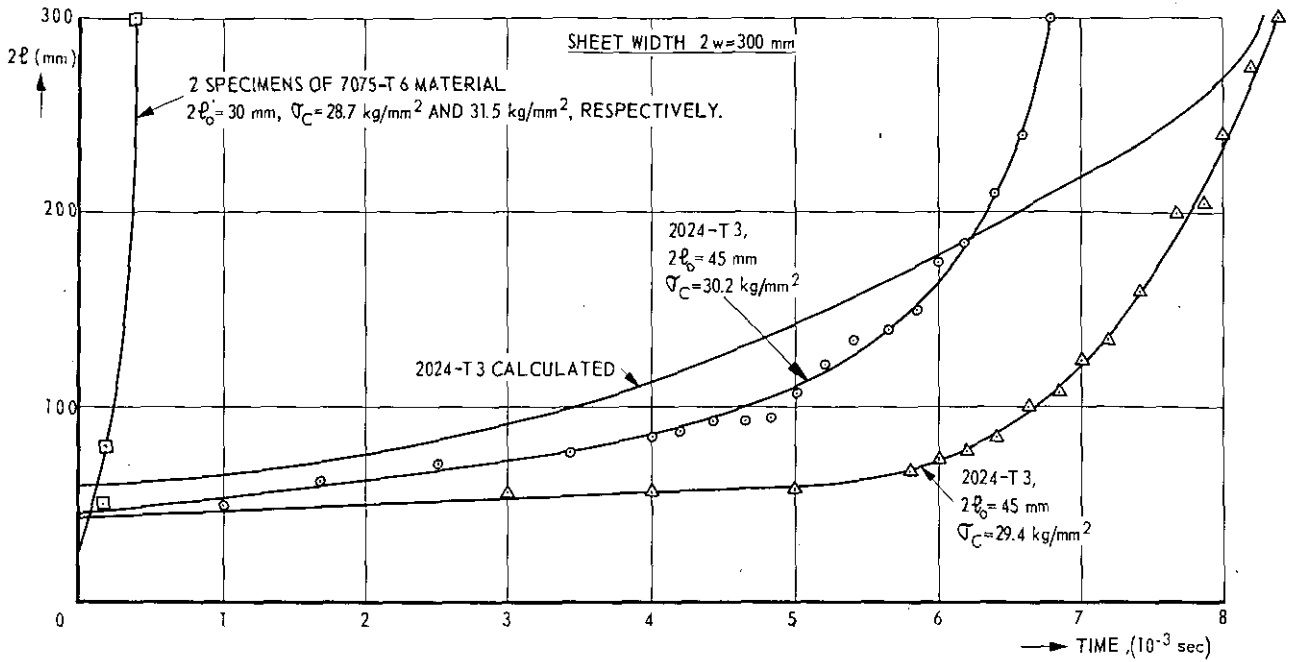


Fig. 3 Crack propagation curves as observed from high-speed motion pictures.

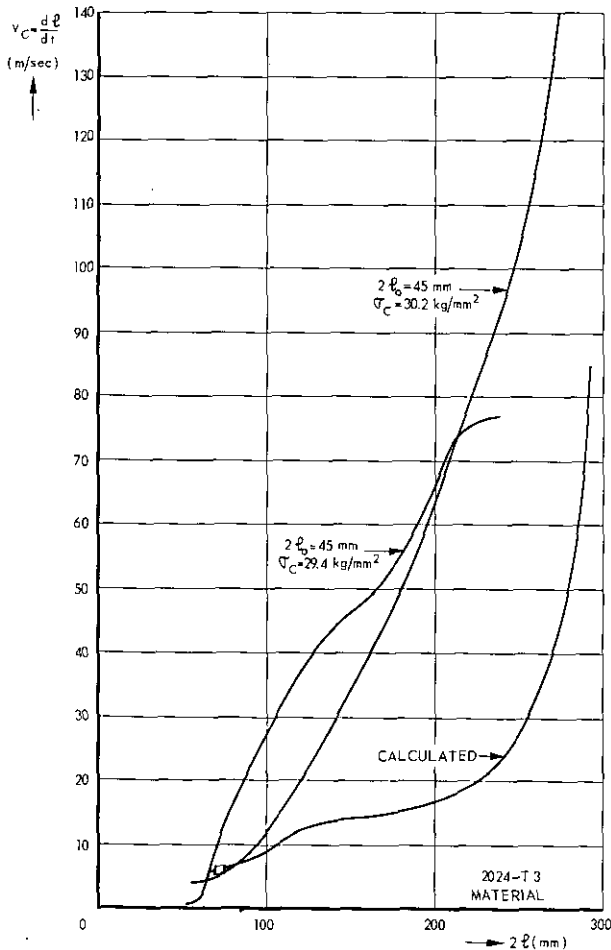


Fig. 4 Velocity of crack propagation during fracture.

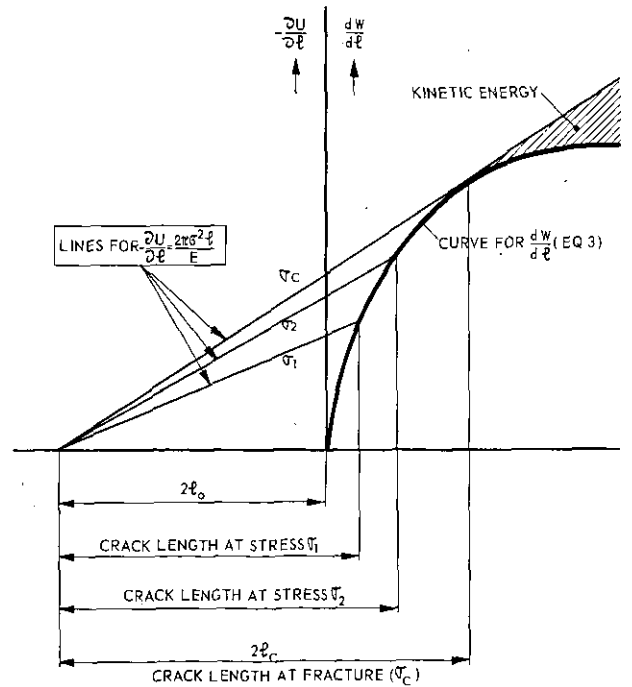


Fig. 5 The energy criterion for fracture.

loading rates in the fast tests were in the order of magnitude of the loading rates attained in bending of the wing of a civil aircraft due to gusts. It can be said that these are the practical limits for residual strength problems in aircraft structures. The duration of normal residual strength tests is in between these limits (about 2 minutes) and it may be concluded that results obtained from such tests are of general applicability in aircraft design.

#### 4 The rate of crack propagation during fracture instability

##### 4.1 Test results

The films obtained from the high-speed camera give some data on the rate of crack propagation during fracture. These data are presented in figs. 3 and 4. (The calculated curves shown in figs. 3 and 4 will be discussed later in this chapter). It was concluded from fig. 4 that fracture occurred at a critical crack length  $2l_c \approx 60$  mm, the point where the crack propagation rate increases suddenly. (Of course, also during "slow" crack growth the rate of crack propagation was high due to the high rate of loading).

Figs. 3 and 4 indicate that the velocity of the crack tip during fracture in the 2024-T3 alloy reaches values in the order of 100 m/sec. The velocity in the 7075-T6 alloy is about 15 times higher; no sufficient data could be obtained for this material, since fracture occurred within 2 frames of the high-speed film. In ref. 4 pictures are given of a high-speed film record of crack propagation as a result of a particle impact on a water filled steel tank. From these pictures it appears that the rate of crack propagation was in the order of 500 m/sec.

##### 4.2 Predictions by fracture dynamics

It is possible to make a prediction of the crack-tip velocity during fracture by the use of fracture dynamics, as will be treated in this section. It should be realized, however, that the analysis given can yield no more than a qualitative estimate, because it is based on elastic formulas and quantitative results are derived from very limited test data.

The energy criterion for fracture of sheets containing cracks as developed in refs. 2 and 5 predicts that fracture occurs when:

$$\left. \begin{aligned} \frac{\partial U}{\partial l} + \frac{dW}{dl} &= 0 \\ \frac{\partial^2 U}{\partial l^2} + \frac{d^2 W}{dl^2} &= 0 \end{aligned} \right\} \quad (1)$$

In eqs. (1)  $\partial U/\partial l$  is the energy released during a crack extension  $dl$  and  $dW/dl$  is the energy consumed during this crack extension.  $\partial U/\partial l$  is mainly composed of elastic energy and for an infinite sheet it is given by

$$\frac{\partial U}{\partial l} = -\frac{2\pi\sigma^2 l}{E} \quad (2)$$

where  $E$  is the modulus of elasticity. It was pointed out in ref. 5 that

$$\frac{dW}{dl} = \beta(l-l_0)^{(\alpha-1)/\alpha} \quad (3)$$

in which  $l_0$  is the semi-initial-crack length and  $\alpha$  is a constant. For an infinite sheet  $\beta$  can be given by (ref.2)

$$\beta = \frac{2\pi\sigma_c^2}{E} \left( \frac{\alpha}{\alpha-1} \right)^{(\alpha-1)/\alpha} l_c^{1/\alpha} \quad (4)$$

(The fracture criterion yields that  $\sigma_c^2 l_c^{1/\alpha} = \text{constant}$ ; i.e.  $\beta$  is a constant). In this equation  $\sigma_c$  is the fracture stress and  $l_c$  the crack length at fracture. For an infinite sheet ref. 2 also shows that

$$l_c = \alpha l_0 \quad (5)$$

The fracture criterion is illustrated in fig. 5. During slow crack propagation the energy released is completely consumed for crack extension ( $\partial U/\partial l + dW/dl = 0$ ) and an increase of the stress is necessary for the continuation of crack growth. When the stress is raised to  $\sigma_c$  the crack has obtained a length  $2l_c$ . Now  $\partial U/\partial l$  can no longer be balanced by  $dW/dl$  and there is an increasing oversupply of energy, indicating that fracture occurs.

The oversupply of energy is probably converted into kinetic energy incorporated in the rapid splitting motion of the material at the crack tip. The kinetic energy  $H$  is then given by:

$$H = - \int_{l_c}^l \left( \frac{\partial U}{\partial l} + \frac{dW}{dl} \right) dl \quad (6)$$

Based on dimensional arguments Mott (ref. 6) pointed out that the kinetic energy can also be given by:

$$H = \frac{k\rho\sigma_c^2 l^2 v_c^2}{2E^2} \quad (7)$$

in which  $\rho$  is the specific mass of the material,  $v_c$  is the crack tip velocity and  $k$  is a numerical constant.

Combining eqs. (6) and (7) and substituting eqs. (2), (3) and (4) yields:

$$\frac{k\rho\sigma_c^2 l^2 v_c^2}{2E^2} = \frac{2\pi\sigma_c^2}{E} \int_{l_c}^l \left\{ 1 - \left( \frac{\alpha}{\alpha-1} \right)^{(\alpha-1)/\alpha} l_c^{1/\alpha} (l-l_0)^{(\alpha-1)/\alpha} \right\} dl \quad (8)$$

Since  $\sqrt{E/\rho} = v_s$ , the velocity of sound:

$$\frac{v_c^2}{v_s^2} \cdot l^2 = \frac{4\pi}{k} \int_{l_c}^l \left\{ 1 - \left( \frac{\alpha}{\alpha-1} \right)^{(\alpha-1)/\alpha} l_c^{1/\alpha} (l-l_0)^{(\alpha-1)/\alpha} \right\} dl \quad (9)$$

Eq. (9) in combination with eq. (5) can be manipulated to give:

$$\frac{v_c^2}{v_s^2} = \frac{4\pi}{k} \left[ \frac{1}{2} \left( 1 - \frac{l_c^2}{l^2} \right) - \left( \frac{\alpha}{\alpha-1} \right)^{(\alpha-1)/\alpha} \frac{\alpha}{2\alpha-1} \left( 1 - \frac{l_c}{\alpha l} \right)^2 \left( \frac{\alpha l_c}{\alpha l - l_c} \right)^{1/\alpha} + \frac{\alpha-1}{2\alpha-1} \frac{l_c^2}{l^2} \right] \quad (10)$$

or:

$$\frac{v_c^2}{v_s^2} = \frac{4\pi}{k} \left[ \frac{1}{2} - \frac{1}{4\alpha-2} \frac{l_c^2}{l^2} - \left( \frac{\alpha}{\alpha-1} \right)^{(\alpha-1)/\alpha} \frac{\alpha}{2\alpha-1} \left( 1 - \frac{l_c}{\alpha l} \right)^2 \left( \frac{\alpha l_c}{\alpha l - l_c} \right)^{1/\alpha} \right] \quad (11)$$

Eq. (11) predicts that  $v_c = 0$  for  $l = l_c$  and that the velocity of crack propagation is limited (for large values of  $l$ ) to:

$$v_c^2 = \frac{2\pi}{k} v_s^2 \quad (12)$$

For the particular case when  $\alpha = 1$  Berry (ref. 7) also arrived at eq. (12).

For the case of a sheet of finite size the relation of eq. (2) for  $\frac{\partial U}{\partial l}$  changes (ref. 2) to:

$$\frac{\partial U}{\partial l} = \frac{4\sigma^2 w}{E} \tan \frac{\pi l}{2w} \quad (13)$$

in which  $2w$  is the width of the specimen. The relation between  $l_0$  and  $l_c$  becomes:

$$l_0 = l_c - \frac{w}{\pi} \frac{\alpha-1}{\alpha} \sin \frac{\pi l_c}{w} \quad (14)$$

For the case of a wide sheet with a small initial crack eqs. (4) and (5) are still approximately valid. By using eq. (13) in the evaluation of eq. (6) the following relation is obtained for the rate of crack propagation in a sheet of finite size:

$$\frac{v_c^2}{v_s^2} = \frac{4\pi}{k} \left[ - \frac{4w^2}{\pi^2 l^2} \log \frac{\cos \frac{\pi l}{2w}}{\cos \frac{\pi l_c}{2w}} - \left( \frac{\alpha}{\alpha-1} \right)^{(\alpha-1)/\alpha} \frac{\alpha}{2\alpha-1} \left( 1 - \frac{l_c}{\alpha l} \right)^2 \left( \frac{\alpha l_c}{\alpha l - l_c} \right)^{1/\alpha} + \frac{\alpha-1}{2\alpha-1} \frac{l_c^2}{l^2} \right] \quad (15)$$

which is the same as eq. (10) except for the first term between the square brackets. For small values of  $l/\omega$  eq. (15) reduces to eq. (10). For large values of  $l/\omega$  (if fracture is almost complete) the logarithm of the first term approaches  $-\infty$ , which indicates that the crack tip velocity tends to infinity (of course this velocity cannot exceed  $v_s$ ).

For the 2024-T3 material used in the present tests a reasonable estimate for the value of the constant  $\alpha$  seems to be  $\alpha = 1.8$  (ref. 2). The numerical constant  $k$  was calculated by inserting a value of  $v_c = 7.5$  m/sec in eq. (15) for the case when  $2l = 90$  mm and  $2l_c = 60$  mm, values estimated from the films. Then by the use of eq. (15) the curves in figs. 3 and 4 were calculated. It is seen, however, that the agreement with the measured curves is rather poor. This is hardly surprising in view of the facts mentioned in the first paragraph of this section.

The fact that the 7075-T6 alloy showed much higher crack propagation rates cannot be explained by a different value of  $\alpha$  ( $\alpha = 1.3$ ) since  $v_c$  is only slightly affected by  $\alpha$ . This different crack rate can be due to a different numerical constant  $k$ , which should then strongly depend on the material of the specimen.

## 5. Conclusions

Residual strength tests with a duration ranging from 30 minutes to about 0.4 second were carried out on 2024-T3 clad sheet specimens. A few specimens were filmed during fracture by a high-speed camera. The results allow the following conclusions to be made:

- a. The stress to initiate crack-growth decreases slightly at increasing testing speed.
- b. In the range of loading rates investigated the residual strength was not affected by the testing speed.
- c. Results of normal residual strength tests on aluminium alloys are of general applicability in aircraft design, since the extreme loading rates in aircraft structures are between the limits applied in the present investigation.
- d. The velocity of crack propagation during fracture is in the order of 100 m/sec. A few tests carried out on 7075-T6 material showed that the crack propagation rate in this material is an order of magnitude higher.

## 6 References

- <sup>1</sup> Broek, D., The residual strength of aluminium alloy sheet specimens containing fatigue cracks or saw cuts. N.L.R. report M.2143, Febr. 1965.
- <sup>2</sup> Broek, D., The effect of finite specimen width on the residual strength of light alloy sheet. N.L.R. report M.2152, Nov. 1965.
- <sup>3</sup> Hoskin, B.C., Time effects in the tension test. ARL structures and materials Note 271 Melbourne, June 1961.
- <sup>4</sup> Kemp, R. H., Flow and fracture problems in aerospace vehicles. Materials for space operation pp. 31-38. NASA S.P. 27. Dec. 1962.
- <sup>5</sup> Broek, D., The energy criterion for fracture of sheets containing cracks. Applied Materials Research 4 3 (July 1965) pp. 188-189.
- <sup>6</sup> Mott, N. F., Fracture of metals: some theoretical considerations. Engineering 165 (Jan. 2, 1948) pp. 16-18.
- <sup>7</sup> Berry, J. P., Some kinetic considerations of the Griffith criterion for fracture. J. Mech. and Phys. of Solids 8 (1960), 3, pp. 194-216.



# The crack propagation in two aluminium alloys in an indoor and an outdoor environment under random and programmed load sequences

by

J. SCHIJVE and P. DE RIJK

## Summary

Sheet specimens of 2024-T3 Alclad and 7075-T6 Clad were tested in a test hall and outside this hall. Each specimen contained five cracks. The crack growth data allow comparisons to be made (1) between indoors and outdoors (2) between random and program loading (3) between these loadings with and without ground-to-air cycles and (4) between the two alloys. Damage calculations are made.

Contents	Page nb.	List of symbols	
List of symbols	1	$l$	— half length of crack, see fig. 1
1 Introduction.	2	$n$	— number of applied load cycles
2 The materials, the specimens and the experimental procedures.	3	$N$	— fatigue life or crack propagation life for a certain amount of crack propagation
3 The test set-up.	4	$S$	— stress
4 The fatigue loads.	5	$S_a$	— stress amplitude
5 The environmental conditions.	7	$S_m$	— mean stress
6 The crack propagation data.	8	$S_{0.2}$	— 0.2% yield stress
7 Fractographic examination and some additional observations.	8	$S_u$	— ultimate stress
8 Damage calculations.	10	I	— tested indoors
9 Summary of two NASA investigations.	11	O	— tested outdoors
10 Discussion.	13	R	— random load sequence
10.1. The trends of the present results.	13	Pr	— programmed load sequence
10.2. The technical consequences of the present results.	15	GTAC	— ground-to-air cycle(s)
11 Conclusions.	18	R+GTAC	— random load sequence with GTAC inserted
12 References.	19	Pr+GTAC	— programmed load sequence with GTAC inserted
12 tables		kg/mm <sup>2</sup>	— 1 kg/mm <sup>2</sup> = 1422 psi (1000 psi = 0.703 kg/mm <sup>2</sup> )
14 figures		mm	— 1 mm = 0.04" (1 inch = 25.4 mm)
		cpm	— cycles per minute
		kc	— kilocycle = 1000 cycles

This investigation has been performed under contract with the Netherlands Aircraft Development Board (NIV).

## 1 Introduction

The rate of propagation of a fatigue crack in an aircraft structure is of major importance for its fail safe performance. Fatigue testing of a prototype structure of a commercial aircraft usually includes measurements of the crack rates at various locations in the structure. In general such tests are carried out in a test hall i.e. *indoors*. It may be questioned whether crack rates under service conditions, i.e. *outdoors*, will be the same, they might be larger. The aim of the present investigation is to explore this question by comparative experiments indoors and outdoors.

Comparisons of the fatigue behaviour of aluminium alloys indoors and outdoors were made by NASA (refs. 1 and 2). These investigations, which are summarized in chapter 9, were concerned with the fatigue lives of notched specimens of 2024-T3 and 7075-T6 sheet material in both the bare and the clad conditions. In the present investigation the propagation of macro-cracks is studied in the same sheet materials; however, in the clad condition only. The tests were carried out concurrently with full-scale fatigue tests on tension skins (ref. 3). Since the hydraulic pressure applied in the latter tests was also used for the present tests, the same random and programmed load sequences with and without ground-to-air cycles were used. Moreover, the loading rate and the interruptions of the tests thus had a similar character as in full-scale testing of aircraft structures.

Although the atmospheric influence on crack propagation was the prime object of the investigation, the

results also permit comparisons to be made between crack propagation under random and programmed load sequences and between the crack propagation in the 2024 and the 7075 alloys. Damage calculations are also made.

At the end of the report the trends of the results are discussed and the technical consequences are briefly commented upon.

## 2 The materials, the specimens and the experimental procedures

All specimens were cut from sheets with a nominal thickness of 2 mm (0.08"). The static properties of the two alloys 2024-T3 Alclad and 7075-T6 Clad are given in table 1.

The dimensions of the specimens are given in fig. 1. The specimens were provided with five central notches for crack initiation. This allows cracks to grow simultaneously at five locations, which increases the amount of data becoming available during a test. The spacing of the cracks is 2.3 times the width of the specimen. For the values of the crack length considered in the evaluation of the crack propagation data, a mutual interference of the growth of neighbouring cracks is not to be expected.

In order to avoid a time loss due to a slow crack initiation at the saw cuts, the specimens were first cycled at a low stress amplitude in a hydraulic pulsator, the frequency being 500 cycles per minute. After small cracks were present at all five notches the specimens were taken from the pulsator and mounted in the test rigs indoors and outdoors. The half length  $l$  of the cracks at the beginning of the comparative testing in the rigs ranged from 2 to 5 mm, see table 3, which also shows the values of  $l$  at the end of the test. The specimens were provided with scribe line markings for recording the crack length. Both these line markings and the central notches have been used in several previous NLR investigations (for instance refs. 6, 7 and 9).

The period during which crack growth was observed ranged from 1 to 3 months. The tests were running concurrently with the tests on the tension skins in the day time only, viz. from 8.30 a.m. to 5.30 p.m. In the

TABLE 1

Static properties of the two sheet materials  
Results are averages of 8 tests.  
Sheet thickness 2 mm (0.08")

Material	$S_{0.2}$		$S_u$		Elongation (2" gage length)
	(kg/mm <sup>2</sup> )	(ksi)	(kg/mm <sup>2</sup> )	(ksi)	
2024-T3 Alclad	37.1	52.8	48.3	68.7	18.9%
7075-T6 Clad	47.3	67.3	53.0	75.4	9.4%

TABLE 2

Survey of the tests

Material	Specimen no.		Load sequence	Simultaneous testing of tension skin no.
	Indoors	Outdoors		
2024	C5	C8	Random	1 and 4
	C2	C1	Program	5
	C4	C3	Random+GTAC	6
	C6	C9	Program+GTAC	7
7075	C74	C73	Program	2
	C76	C71	Random+GTAC	3
	C79	C74	Program+GTAC	8

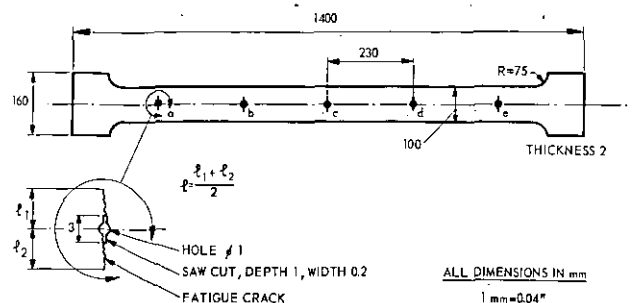


Fig. 1. Sheet specimen with 5 central notches for crack initiation.

night time, only a small tensile load on the specimens was maintained. In general, the crack length was measured twice a day. In a few tests the specimens

fractured completely. A simple riveted double strap joint was then made to connect the two parts of the specimen and testing was continued.

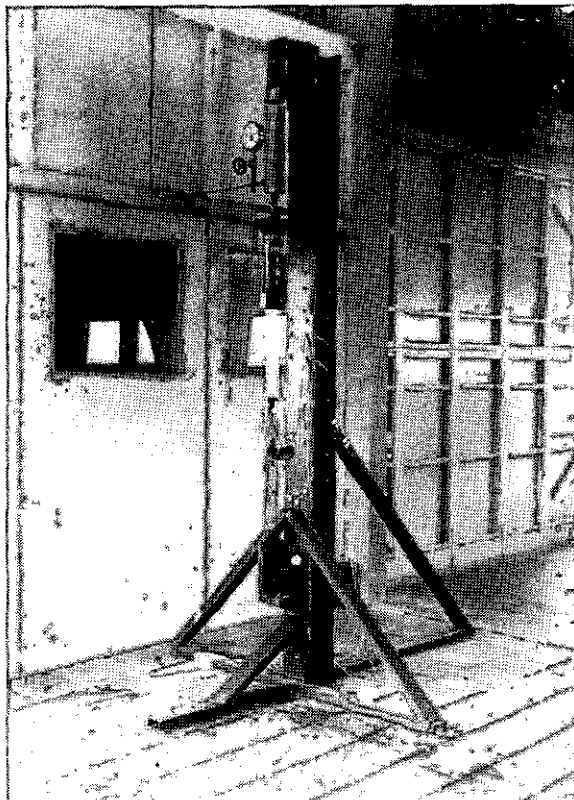
TABLE 3  
Survey of the crack propagation observed.

Material	Specimen no.	Tested <sup>1</sup>	Load sequence <sup>2</sup>	Half crack length <sup>l</sup> <sub>3</sub> at beginning and of the test (mm)				
				a	b	c	d	e
2024	C5	I	R	2.45-5.5	2.25-5.5	2.7-6.25	2.3-5.3	2.3-5.9
	C8	O		2.3-6.05	3.1-8.65	2.25-5.8	3.1-9.05	3.2-8.5
	C2	I	Pr	3.1-6.9	2.8-6.45	3.75-10.0	4.05-11.55	4.2-11.75
	C1	O		4.45-50	3.05-9.35	2.3-4.6	2.45-6.95	2.4-7.2
	C4	I	R+GTAC	4.35-7.65	5.1-9.15	4.35-8.0	4.0-6.8	4.7-8.1
	C3	O		4.9-7.65	2.7-6.0	6.9-11.5	2.75-6.35	3.0-6.55
	C6	I	Pr+GTAC	3.0-6.2	4.2-8.5	2.95-6.0	2.35-4.4	3.4-6.7
	C9	O		3.1-6.85	2.95-6.45	2.55-6.2	3.15-7.05	2.95-6.25
	C74	I	Pr	1.95-4.05	1.8-3.35	1.85-3.75	2.0-4.1	2.25-4.45
C73	O		2.25-50	2.0-50	1.55-12.0	1.75-15.4	1.75-15.1	
7075	C76	I	R+GTAC	2.15-9.85	2.0-9.4	2.15-11.15	2.5-11.7	2.7-50
	C71	O		2.55-17.0	2.2-6.65	2.35-50	2.3-50	2.05-15.0
	C79	I	Pr+GTAC	2.2-6.8	3.4-10.4	3.0-6.7	4.15-11.9	3.1-7.85
	C74	O		2.2-7.9	2.3-9.05	2.75-11.2	2.05-7.8	2.15-50

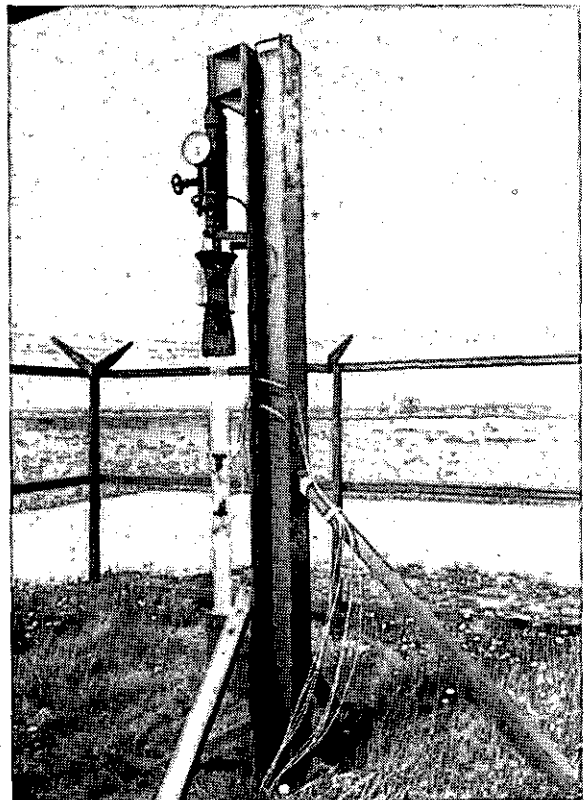
<sup>1</sup> I = indoors, O = outdoors

<sup>2</sup> R = random, Pr = program, GTAC = ground-to-air cycle

<sup>3</sup> *l* = half length, see fig. 1.



THE TEST RIG IN THE TEST HALL



THE TEST RIG OUTSIDE THE TEST HALL

Fig. 2 The test rigs indoors and outdoors.

### 3 The test set-up

Two simple tests rigs were built with the specimen and the loading jack in series, see fig. 2. The jacks were supplied with the same oil pressure as used in full-scale tests on tension skins. A schematic picture of the test set-up and the load control is given in fig. 3. The random load machine CARLA is primarily controlling the load in the full-scale test. The desired load sequence is punched into a binary digit tape. The tape is fed into a tape reader, which selects one of 32 preset potentiometers. The output of the selected potentiometer is compared with the feed-back signal of a dynamometer. As soon as a zero difference between the two signals is obtained, the zero detector reverses the direction of the oil flow delivered by the pump and at the same time the tape reader selects the following load level. The pump delivery was constant for both loading and unloading, implying constant loading rates. The average loading frequency was about 20 cpm. More details on the fatigue machine can be found in ref. 4.

During the full-scale tests, additional oil lines connected the main system with the two test rigs for the present test series (see fig. 3), which consumed only a minor part of the oil delivery of the pump. The oil lines to the two test rigs had the same length and the same number of bends in order to secure equal loads on the specimens indoors and outdoors. Dynamic strain gage measurements indicated that the differences between the strains simultaneously measured indoors and outdoors were less than 1%, i.e. the strains were equal within the accuracy of the strain gage measurements. The strain gage measurements further indicated that the strains were about 3% lower than the expected values, based on the hydraulic pressure as derived from the loads applied in the tests on the tension skins. This difference has to be attributed to friction in the jacks.

### 4 The fatigue loads

The load sequences applied are the same as for the full-scale tests on the tension skins (ref. 3). They were based on a strain-gage record of the bending moment at the root of a wing of a large aircraft flying in turbulent air. The record covered 96 min. of flying and showed the typical features of random gust loads as well as the first wing bending mode frequency, see fig. 4. It is clear that 96 min. of flying cannot be representative for a complete gust spectrum. The record obtained is indicated as tape A1. Other tapes B1, C1, D1 and E1 were obtained from tape A1 by increasing the maximum peak loads by different amounts (highly non-linear amplification). Subsequently five tapes A2 to E2 were produced by reducing all load peaks of the tapes A1 to E1 to a ratio of 75 percent (linear amplification). From the ten tapes a sequence was composed consisting of

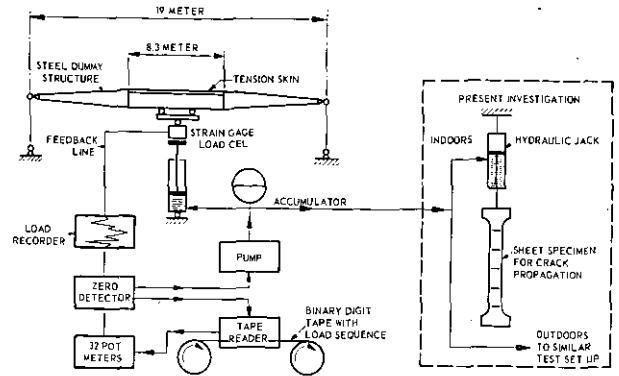


Fig. 3 Schematic principle of the NLR random load machine carla (code actuated random load apparatus) developed for full-scale tests on tension skins.

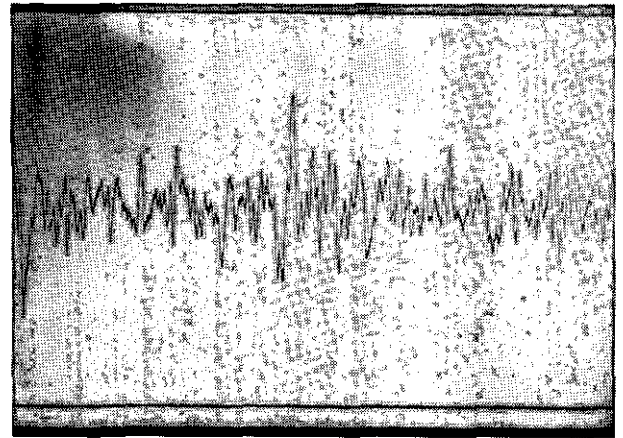


Fig. 4 Sample of a strain gage record on which the load sequence in the random tests was based.

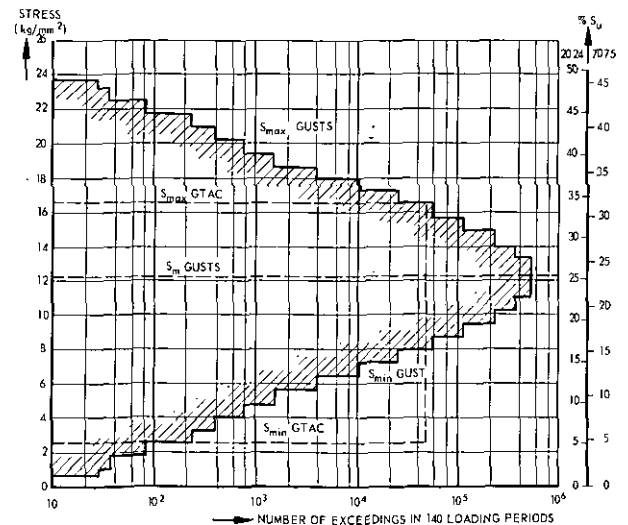


Fig. 5 Load spectrum for 140 loading periods as counted by the mean-crossing-peak-count method.

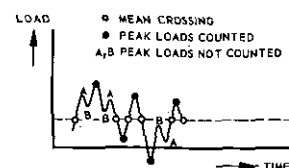


Fig. 6 Principle of the mean-crossing-peak-count method.

49 × A1, 14 × B1, 4 × C1, 2 × D1, 1 × E1 and the same numbers of tapes A2 to E2, making a total of 140 tapes. The sequence of the tapes and full data of the load statistics for each tape are given in ref. 5.

In the random-load tests the load sequence of the gust record is exactly simulated. Since the number of load levels is limited, viz. 32, all peaks, maxima and minima, had to shift a little bit to coincide with the nearest level of the 32 available ones.

The magnitudes of the stresses follow from the selected cross sectional area of the specimens (200 mm<sup>2</sup>). The stress spectrum for the 140 tapes (or test periods) has been plotted in fig. 5. Actually the stresses are about 3% lower due to friction in the jacks as pointed out in the previous chapter. The mean stress was 12.1 kg/mm<sup>2</sup>.

The spectrum was obtained by adopting the so-called mean-crossing-peak-count method. Between two successive mean crossings only one count is made. The method is further explained in fig. 6. From all the peak loads applied in the random tests only 69.2 percent is counted with this method.

For the random tests with ground-to-air cycles (GTAC) the minimum stress of these cycles was 12.6 kg/mm<sup>2</sup>. Some touch-down load variations were added. Further it was assumed that one of the two flights was a smooth flight without gusts. In other words GTAC were applied in pairs, as indicated in fig. 7. Such pairs were inserted in the random load tapes at regular intervals. The average number of gust cycles (according to the mean-crossing-peak-count method) was 24 per interval. Apart from the GTAC the load sequence remained exactly the same.

In the program tests the number of cycles in one period was the same as the average number for the random tapes as counted by the mean-crossing-peak-count method, viz. 3865 cycles. Consequently the frequency of the highest amplitudes was lower than once per period. Three different tapes P1, P2 and P3 were made, which differed for the highest amplitudes only and which were combined such that fig. 5 applies to both the random and the program test. Moreover, if it was assumed that the mean-crossing-peak-count method is the correct counting method, one program tape (containing one program period) represents one random tape. So the fatigue life in all types of testing can be compared on the basis of numbers of tapes. Since in the program tests the mean load was not used as a load level for reversal of the loading direction, the 31 load levels of the random load test lead to 15 different values of the load amplitude in the program tests. Load amplitudes were applied in increasing and decreasing order of succession in each period.

In the program tests with ground-to-air cycles the GTAC were inserted in each period as six batches of 56 cycles each, see fig. 8. The minimum load is the

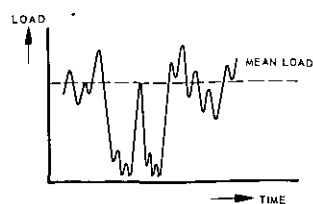


Fig. 7 Two ground-to-air cycles in the random tests with GTAC.

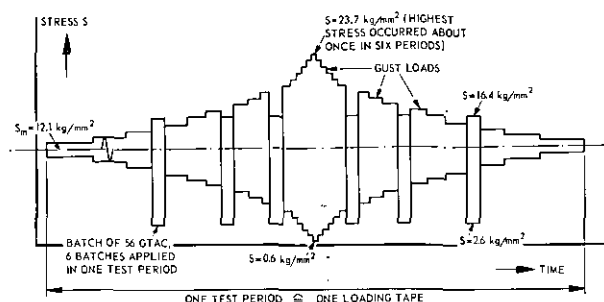


Fig. 8 Schematic picture of load sequence in one test period of a program test with ground-to-air cycles (GTAC).

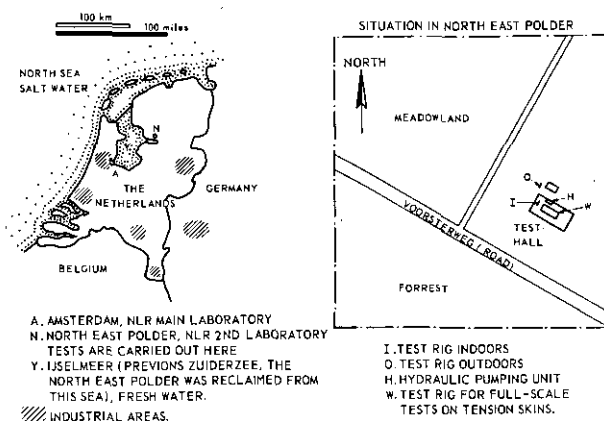


Fig. 9 Location and environment of the laboratory.

same as in the random tests with GTAC, but the touch-down loads are omitted. The maximum load is the load which on the average was exceeded once per flight in the random tests with GTAC.

## 5 The environmental conditions

The location of the test site at the NLR's second laboratory in the North East Polder has been indicated in fig. 9. The site is at a distance of 85 km (53 miles) from the salt water of the North Sea. There are no industrial areas in the immediate vicinity, which is mainly agrarian. The outdoor environment is therefore considered as being rural and non-aggressive.

Meteorologic data for this part of the country were provided for each day by the Koninklijk Nederlands Meteorologisch Instituut (the Royal Netherlands Meteorological Institute). Average values drawn from these data for the periods of testing are presented in table 4. The table shows that the duration of the tests ranged from 31 to 106 days. The proportion of days

with precipitation is in the order of 60%. The temperatures are normal for the times of the year.

The relative humidity hardly varied from test to test. One should keep in mind, however, that the water vapour contents of the air for a certain relative humidity strongly depends on the temperature. Consequently, the amount of water vapour was much higher in summer time than in winter time. The outdoor specimens frequently were somewhat wettish, which was due to a remainder of rain or dew. They were then wiped before the crack length was measured. The specimens indoors always had a dry surface.

The indoor conditions are roughly characterized by temperatures between 15 and 20°C and a relative humidity which was equal to or somewhat lower than the outdoor humidity. In winter time this meant that the water vapour content was higher inside than outside the test hall.

### 6 The crack propagation data

The crack propagation data were evaluated by calculating  $l = \frac{1}{2}(l_1 + l_2)$ , see fig. 1, for all observations and plotting  $l$  as a function of the number of load cycles applied. Curves were then drawn through the data points and from the curves the numbers of load cycles corresponding to several values ( $l_i$ ) of the crack length were read for each crack. By subtraction the number of load cycles ( $\Delta n$ ) corresponding to a crack extension from  $l_i$  to  $l_{i+1}$  was derived. An example of a graph with crack growth data points is shown in fig. 10.

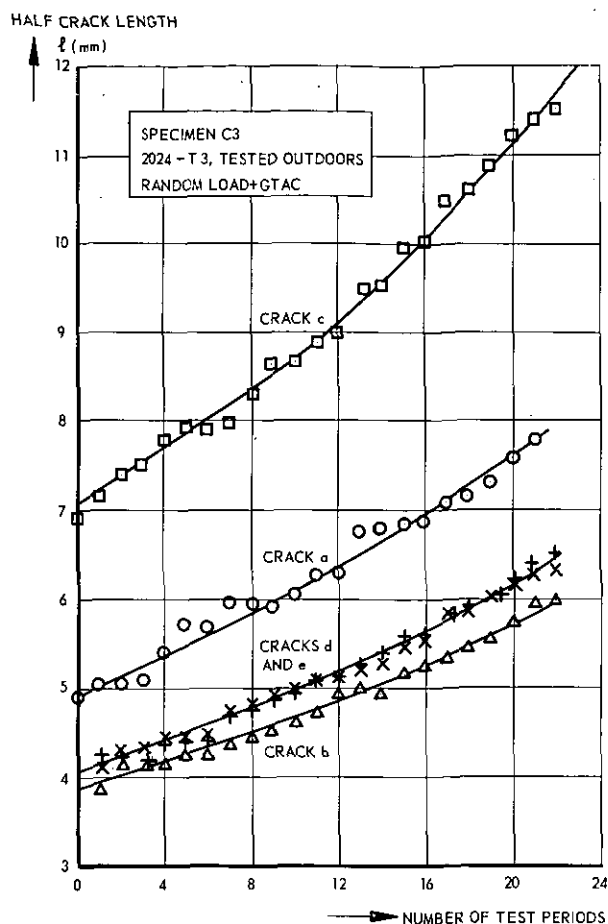


Fig. 10 Example of plotted crack growth observations.

TABLE 4  
Outdoor atmospheric conditions

Material	Specimens no.	Load sequence	Period of testing <sup>1</sup>			Precipitation <sup>2</sup>			Temperature <sup>3</sup> (°C)			Relative humidity (%)	direction of wind <sup>5</sup>	
			Start	End	Days	Days	Quantity (mm)	Type	Mean	Max	Min			
2024-T3	C5/C8	R	Feb. 28-'62	Mar. 15-'62	16	12	1.1	snow	0.9	3.4	-1.6	82	variable	
			Aug. 7-'62	Aug. 30-'62	40	24	17	2.8	rain	16.0	18.4	12.3	75	SW
	C2/C1	Pr	Oct. 4-'62	Jan. 17-'63	106	64/12	2.1/2.4	rain/snow	2.7	5.3	1.8	88	SSW/NE	
	C4/C3	R+GTAC	Feb. 8-'63	Mar. 14-'63	35	9/7	1.5/3.7	snow/rain	-0.5	2.7	-4.5	89	EbNE	
	C6/C9	Pr+GTAC	Apr. 10-'63	June 12-'63	64	30	3.5	rain	13.2	16.0	7.9	72	SSW	
7075-T6	C74/C73	Pr	Apr. 3-'62	May 3-'62	31	22	3.8	rain	8.4	11.0	5.0	78	WbNW	
	C76/C71	R+GTAC	June 4-'62	July 18-'62	45	21	2.2	rain	15.5	17.9	10.9	69	WbNW	
	C79/C74	Pr+GTAC	June 16-'63	July 24-'63	39	24	4.1	rain	16.8	19.6	12.2	77	SW	

<sup>1</sup> Period of testing: Last column gives the duration of the tests.

<sup>2</sup> Precipitation: First column gives the days that precipitation occurred. Second column gives the daily average of precipitation for the days that precipitation occurred. The third column gives the predominant type of precipitation. During the tests on specimens was C2/C1 and C4/C3 a marked change of the type of weather occurred and the precipitation data are given separately for the first and second part of the test.

<sup>3</sup> Temperatures given are test period averages of the mean, the maximum and the minimum temperatures occurring each day.

<sup>4</sup> Relative humidity data are test period averages of the humidity measured every day at 8.40, 14.40 and 19.40 hours.

<sup>5</sup> The indicated direction of wind is the predominant wind direction during the test period.

The  $\Delta n$ -values for all tests have been compiled in tables 5a through 5g.

The five cracks in one specimen did not have the same initial length and they therefore showed different amounts of crack propagation, see table 3. The  $\Delta n$ -

values as presented in table 5 allowed a simple composing of the data for the five cracks by averaging the available  $\Delta n$ -values. These mean values of  $\Delta n$  are also presented in table 5. In general the scatter was small, as is usual for crack propagation. In a few cases, the

TABLE 5  
Crack propagation data

The tables give the incremental number of cycles ( $\Delta n$ , unit: loading periods, see chapter 6) to extend the crack over a small crack length interval (from  $l_i$  to  $l_{i+1}$ ). The  $\Delta n$ -values were obtained from curves faired through the plotted test results, see for an example fig. 10. The letters a, b, c, d and e refer to the five cracks in one specimen (fig. 1).

TABLE 5a  
Material 2024-T3 Alclad, random loading

$l_i-l_{i+1}$ (mm)	$\Delta n$ for specimen C5 (indoors)						$\Delta n$ for specimen C8 (outdoors)					
	a	b	c	d	e	mean	a	b	c	d	e	mean
2.5-2.75	6.6	5.4		5.8	5.7	5.9	6.8		5.2			6.0
2.75-3	6.3	4.9	4.6	5.7	5.4	5.4	4.5		4.1			4.3
3-3.25	5.4	4.2	4.4	5.8	5.2	5.0	4.1		4.2			4.2
3.25-3.5	4.3	4.2	4.6	5.6	4.7	4.8	3.9	4.0	4.2	4.6	7.1	4.2
3.5-3.75	4.1	4.2	4.6	5.4	4.1	4.5	3.4	3.0	3.7	3.7	4.8	3.7
3.75-4	3.8	4.0	4.4	4.5	3.6	4.1	3.5	2.8	3.2	2.6	2.7	3.0
4-4.25	3.8	3.9	4.1	3.6	3.2	3.7	3.0	2.6	2.7	2.5	2.6	2.7
4.25-4.5	3.6	3.6	3.6	3.3	3.0	3.4	2.7	2.7	2.7	2.5	2.8	2.7
4.5-5	6.1	6.1	5.9	5.9	5.1	5.8	5.4	5.0	4.9	4.5	5.6	5.1
5-5.5	5.4	5.3	5.5		4.6	5.2	4.8	4.8	4.2	4.8	5.1	4.7
5.5-6			5.1		4.2	4.7	3.9	4.0		4.7	4.2	4.2
6-6.5								3.6		3.7	3.9	3.7
6.5-7								3.4		3.3	4.0	3.6
7-7.5								3.2		2.9	3.5	3.2
7.5-8								3.1		3.3	3.1	3.2
8-8.5								3.1		3.1	2.6	2.9
8.5-9										2.8		2.8

TABLE 5b  
Material 2024-T3 Alclad, program loading

$l_i-l_{i+1}$ (mm)	$\Delta n$ for specimen C2 (indoors)						$\Delta n$ for specimen C1 (outdoors)					
	a	b	c	d	e	mean	a	b	c	d	e	mean
2.5-3	—	—	—	—	—	—	—	—	20.6	—	—	20.6
3-3.5	10.1	11.5	—	—	—	10.8	—	—	14.4	10.4	9.1	10.4
3.5-4	10.7	11.9	—	—	—	11.3	—	7.5	12.2	10.2	9.2	9.7
4-4.5	10.5	11.5	7.7	—	—	10.5	—	8.0	10.8	9.7	9.3	9.5
4.5-5	9.9	11.0	7.4	—	—	9.9	—	7.7	—	8.7	8.8	8.7
5-5.5	9.6	9.3	7.5	7.2	7.2	7.5	5.1	7.6	—	7.8	8.0	7.7
5.5-6	8.6	7.8	7.2	6.9	6.9	7.2	4.9	7.1	—	7.6	7.9	7.3
6-6.5	7.3	6.4	7.2	7.0	6.9	7.0	5.1	6.3	—	6.7	6.9	6.5
6.5-7	6.7	—	6.3	6.6	6.5	6.5	5.0	5.6	—	5.5	6.5	5.6
7-7.5	—	—	5.8	5.8	5.9	5.8	5.0	5.3	—	—	—	5.2
7.5-8	—	—	5.5	5.5	5.5	5.5	4.9	5.1	—	—	—	5.0
8-8.5	—	—	4.9	5.1	5.2	5.1	5.0	4.4	—	—	—	4.7
8.5-9	—	—	4.9	4.7	4.3	4.6	4.1	4.1	—	—	—	4.1
9-9.5	—	—	4.3	4.1	4.0	4.1	3.5	3.9	—	—	—	3.7
9.5-10	—	—	3.9	3.7	3.6	3.7	3.1	—	—	—	—	3.1
10-11	—	—	—	6.2	6.5	6.4	5.3	—	—	—	—	5.3
11-12	—	—	—	4.9	5.2	5.0	4.4	—	—	—	—	4.4
12-13	—	—	—	—	—	—	3.6	—	—	—	—	3.6
13-14	—	—	—	—	—	—	3.1	—	—	—	—	3.1
14-15	—	—	—	—	—	—	2.4	—	—	—	—	2.4
15-16	—	—	—	—	—	—	1.9	—	—	—	—	1.9
16-17	—	—	—	—	—	—	1.7	—	—	—	—	1.7
17-18	—	—	—	—	—	—	1.8	—	—	—	—	1.8

TABLE 5c  
Material 2024-T3 Alclad, random loading with GTAC

$l_i-l_{i+1}$ (mm)	$\Delta n$ for specimen C6 (indoors)						$\Delta n$ for specimen C1 (outdoors)					
	a	b	c	d	e	mean	a	b	c	d	e	mean
4 -4.5	—	—	—	4.8	—	4.8	—	6.5	—	—	—	6.5
4.5 -5	4.0	—	—	4.6	—	4.3	—	5.2	—	5.1	5.1	5.1
5 -5.5	3.9	—	3.9	4.2	3.8	4.0	4.3	4.4	—	4.7	4.7	4.5
5.5-6	3.5	3.3	3.7	3.8	3.7	3.6	3.9	3.7	—	3.9	3.9	3.8
6 -6.5	3.3	3.2	3.4	3.6	3.6	3.4	3.7	—	—	3.3	3.3	3.4
6.5-7	3.2	3.2	3.2	—	3.4	3.2	3.5	—	—	—	—	3.5
7 -7.5	2.9	2.9	3.0	—	3.2	3.0	3.3	—	2.9	—	—	3.1
7.5-8	—	2.7	2.8	—	3.0	2.8	2.8	—	2.9	—	—	2.9
8 -8.5	—	2.6	—	—	—	2.6	—	—	2.8	—	—	2.8
8.5-9	—	2.5	—	—	—	2.5	—	—	2.5	—	—	2.5
9 -9.5	—	—	—	—	—	—	—	—	2.2	—	—	2.2
9.5-10	—	—	—	—	—	—	—	—	2.1	—	—	2.1
10 -10.5	—	—	—	—	—	—	—	—	1.9	—	—	1.9
10.5-11	—	—	—	—	—	—	—	—	1.9	—	—	1.9
11 -11.5	—	—	—	—	—	—	—	—	1.8	—	—	1.8

TABLE 5d  
Material 2024-T3 Alclad, program loading with GTAC

$l_i-l_{i+1}$ (mm)	$\Delta n$ for specimen C6 (indoors)						$\Delta n$ for specimen C9 (outdoors)					
	a	b	c	d	e	mean	a	b	c	d	e	mean
3 -3.5	—	—	—	10.1	—	10.1	—	—	5.3	—	—	5.7
3.5-4	7.2	—	7.0	8.0	—	7.4	6.0	5.8	5.3	—	5.7	5.7
4 -4.5	6.7	—	6.8	6.6	7.4	6.9	5.6	5.6	5.2	6.2	5.5	5.6
4.5-5	6.1	4.7	6.2	—	6.4	5.8	5.4	5.4	5.0	5.6	5.3	5.3
5 -5.5	5.4	4.5	5.8	—	5.8	5.4	5.4	5.1	5.2	5.2	5.2	5.2
5.5-6	5.0	4.4	5.1	—	5.2	4.9	5.2	4.4	4.9	4.7	5.0	4.8
6 -6.5	—	4.4	—	—	4.6	4.5	5.2	—	—	4.3	—	4.7
6.5-7	—	4.1	—	—	4.0	4.1	—	—	—	3.8	—	3.8
7 -7.5	—	3.9	—	—	—	3.9	—	—	—	—	—	3.9
7.5-8	—	3.8	—	—	—	3.8	—	—	—	—	—	3.8
8 -8.5	—	3.2	—	—	—	3.2	—	—	—	—	—	3.2

TABLE 5e  
Material 7075-T6 Clad, program loading

$l_i-l_{i+1}$ (mm)	$\Delta n$ for specimen C74 (indoors)						$l_i-l_{i+1}$ (mm)	$\Delta n$ for specimen C73 (outdoors)				
	a	b	c	d	e	mean		a	b	c	d+e	mean
1.75-2	—	4.4	—	—	—	4.4	1.75-2	—	—	2.9	3.0	3.0
2 -2.25	4.1	4.2	3.8	4.1	—	4.0	2-2.5	—	5.0	2.9	4.0	4.0
2.25-2.5	3.0	3.8	2.9	3.0	3.7	3.3	2.5-3	2.5	2.3	2.5	2.5	2.5
2.5 -2.75	2.7	3.3	2.6	2.7	2.8	2.8	3-3.5	2.0	2.3	1.9	2.0	2.0
2.75-3	2.6	2.8	2.5	2.6	2.5	2.6	3.5-4	1.5	1.5	1.8	1.6	1.6
3 -3.25	2.3	2.6	2.5	2.3	2.4	2.4	4-4.5	1.4	1.4	1.5	1.5	1.5
3.25-3.5	2.1	—	2.3	2.1	2.2	2.2	4.5-5	1.3	1.2	1.4	1.4	1.3
3.5 -3.75	1.8	—	2.1	1.8	2.2	2.0	5-6	2.3	2.0	2.3	2.4	2.3
3.75-4	1.6	—	—	1.6	1.7	1.6	6-7	2.2	1.9	1.9	1.7	1.9
4 -4.25	1.5	—	—	1.5	1.5	1.5	7-8	1.7	1.7	1.4	1.5	1.6
4.25-4.5	—	—	—	—	1.5	1.5	8-9	—	1.5	1.0	1.2	1.2
							9-10		1.3	0.8	0.9	1.0
							10-12		1.7	1.1	1.1	1.2
							12-14		0.9	—	0.7	0.8
							14-16		0.5	—	—	0.5
							16-18		0.3	—	—	0.3

TABLE 5f  
Material 7075-T6 Clad, random loading with GTAC

$l_i-l_{i+1}$ (mm)	$\Delta n$ for specimen C76 (indoors)						$\Delta n$ for specimen C71 (outdoors)					
	a	b	c	d	e	mean	a	b	c	d	e	mean
2 -2.5	—	2.9	—	—	—	2.9	—	—	—	—	1.8	1.8
2.5-3	2.2	2.2	2.1	2.5	—	2.3	—	2.0	2.0	1.4	1.4	1.7
3 -3.5	2.0	2.1	2.0	2.1	2.0	2.0	1.5	3.5	1.6	0.9	1.2	1.35
3.5-4	1.7	2.0	1.8	1.8	1.6	1.8	1.1	1.9	1.1	0.8	0.9	1.0
4 -4.5	1.5	1.5	1.6	1.7	1.5	1.6	1.0	1.3	0.9	0.7	0.8	0.85
4.5-5	1.3	1.4	1.3	1.4	1.5	1.4	0.9	1.2	0.8	0.6	0.7	0.75
5 -6	2.2	2.3	2.2	2.3	2.4	2.3	1.5	1.9	1.3	1.2	1.3	1.4
6 -7	2.1	2.2	2.0	1.9	2.1	2.1	1.5	—	1.4	1.1	1.3	1.3
7 -8	1.6	1.6	1.7	1.7	1.7	1.7	1.1	—	1.1	1.1	1.1	1.1
8 -9	1.3	1.4	1.5	1.6	1.5	1.5	0.9	—	0.8	1.0	0.9	0.9
9 -10	1.3	—	1.3	1.3	1.5	1.3	0.9	—	0.7	0.8	0.7	0.8
10 -12	—	—	—	1.8	1.8	1.8	—	—	1.4	1.2	1.3	1.3
12 -14	—	—	—	—	1.2	1.2	—	—	—	1.0	0.7	0.8

TABLE 5g  
Material 7075-T6 Clad, program loading with GTAC

$l_i-l_{i+1}$ (mm)	$\Delta n$ for specimen C79 (indoors)						$\Delta n$ for specimen C74 (outdoors)					
	a	b	c	d	e	mean	a	b	c	d	e	mean
2.5-3	—	—	—	—	—	—	1.0	0.9	—	1.1	0.6	0.9
3 -3.5	1.1	—	—	—	—	1.1	1.0	0.9	0.9	0.9	0.6	0.9
3.5-4	1.1	—	1.4	—	—	1.3	1.0	0.9	0.8	1.0	0.5	0.8
4 -4.5	1.1	—	1.4	—	1.2	1.2	0.9	0.8	0.7	0.9	0.5	0.8
4.5-5	1.0	0.8	1.3	—	1.1	1.1	0.8	0.8	0.7	0.9	0.5	0.8
5 -5.5	1.0	0.9	1.3	0.7	1.1	1.0	0.8	0.7	0.7	0.8	0.5	0.7
5.5-6	1.0	0.8	1.3	0.7	1.1	1.0	0.8	0.7	0.6	0.7	0.4	0.6
6 -6.5	1.0	0.8	1.2	0.7	1.0	0.9	0.7	0.7	0.6	0.7	0.5	0.6
6.5-7	0.9	0.7	1.1	0.7	1.0	0.9	0.7	0.6	0.6	0.7	0.4	0.6
7 -7.5	0.9	0.7	—	0.7	0.9	0.8	0.6	0.5	0.5	0.6	0.4	0.5
7.5-8	—	0.7	—	0.6	0.9	0.7	0.5	0.5	0.5	0.6	0.4	0.5
8 -8.5	—	0.6	—	0.7	—	0.7	—	0.5	0.5	—	0.4	0.5
8.5-9	—	0.6	—	0.5	—	0.6	—	0.3	0.4	—	0.4	0.4
9 -9.5	—	0.5	—	0.6	—	0.6	—	—	0.4	—	0.3	0.4
9.5-10	—	0.6	—	0.5	—	0.5	—	—	0.4	—	0.4	0.4
10 -10.5	—	0.4	—	0.5	—	0.5	—	—	0.3	—	0.3	0.3
10.5-11	—	—	—	0.5	—	—	—	—	0.3	—	0.2	0.3
11 -11.5	—	—	—	—	—	—	—	—	0.3	—	0.3	0.3

TABLE 6

Comparison of the crack propagation indoors and outdoors

$$\text{Ratio} = \frac{\text{crack propagation life indoors}}{\text{crack propagation life outdoors}}$$

Material	Type of loading	Ratio	Crack growth from $l_a-l_b$ (mm)
2024	R	1.17	2.5-6
	R + GTAC	0.90	4-9
	Pr	1.11	3.5-12
	Pr+GTAC	1.20	3-7
7075	R + GTAC	1.58	2-14
	Pr	2.06	2-4.5
	Pr+GTAC	1.49	3-11

TABLE 7

Comparison of the crack propagation under program and random loading.

$$\text{Ratio} = \frac{\text{crack propagation life under program loading}}{\text{crack propagation life under random loading}}$$

Material	GTAC	Environment	Ratio	Crack growth from $l_a-l_b$ (mm)
2024	No	I	1.48	3.5-6
		O	1.63	3.5-9
	Yes	I	1.34	4-8.5
		O	1.10	4-7
7075	Yes	I	0.82	3-11
		O	0.91	3-11.5

TABLE 8

Effect of the GTAC on the crack propagation

$$\text{Ratio} = \frac{\text{crack propagation life with GTAC}}{\text{crack propagation life without GTAC}}$$

Material	Type of loading	Environment	Ratio	Crack growth from $l_a-l_b$ (mm)
2024	Random	I	0.73	4-6
		O	0.98	4-9
	Program	I	0.65	3.5-8.5
		O	0.45	3-7
7075	Program	I	0.32	3-4.5
		O	0.47	2.5-11.5

TABLE 9

Comparison between the crack propagation lives of the 2024 alloy and the 7075 alloy.

$$\text{Ratio} = \frac{\text{crack propagation life of 2024}}{\text{crack propagation life of 7075}}$$

Type of loading	Environment	Ratio	Crack growth from $l_a-l_b$ (mm)
Pr	I	3.0	3.5-4.5
	O	6.9	3.5-18
R+GTAC	I	3.2	4-9
	O	5.9	4-11.5
Pr+GTAC	I	5.6	3-8.5
	O	7.0	3-7

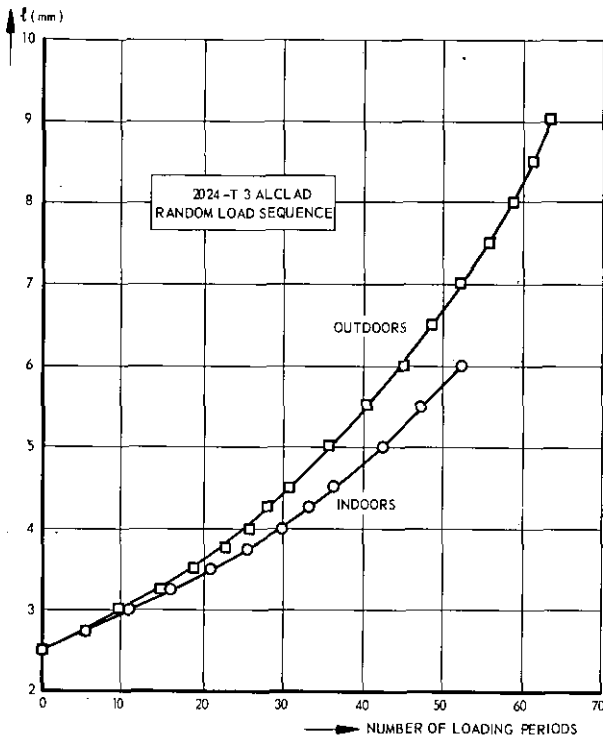


Fig. 11a

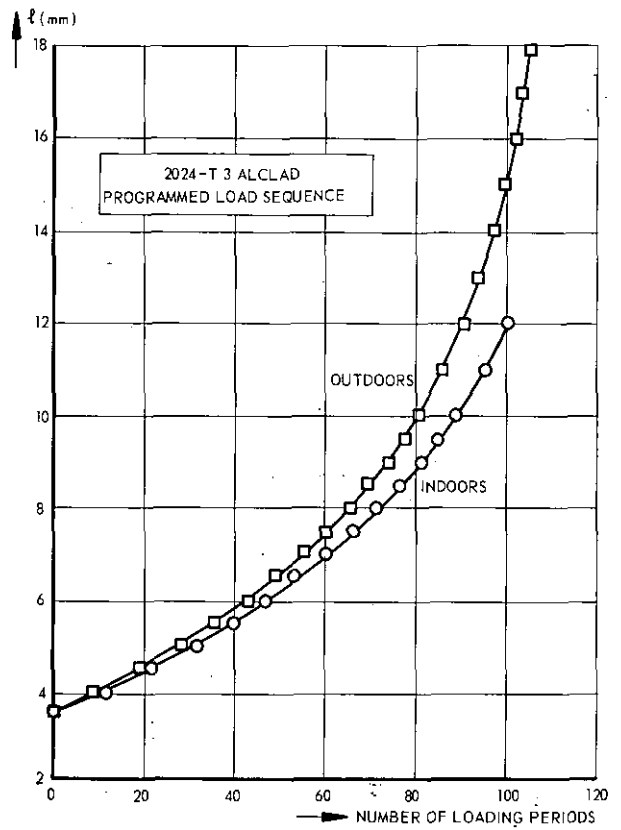


Fig. 11b

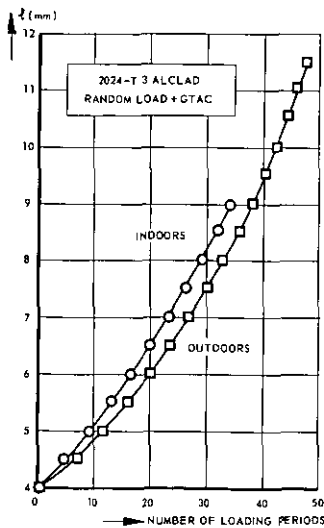


Fig. 11c

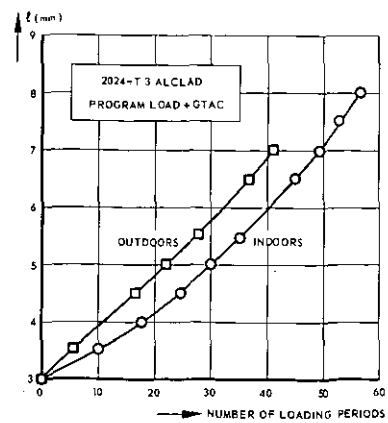


Fig. 11d

Fig. 11 Comparison of the crack propagation indoors and outdoors for the 2024 alloy.

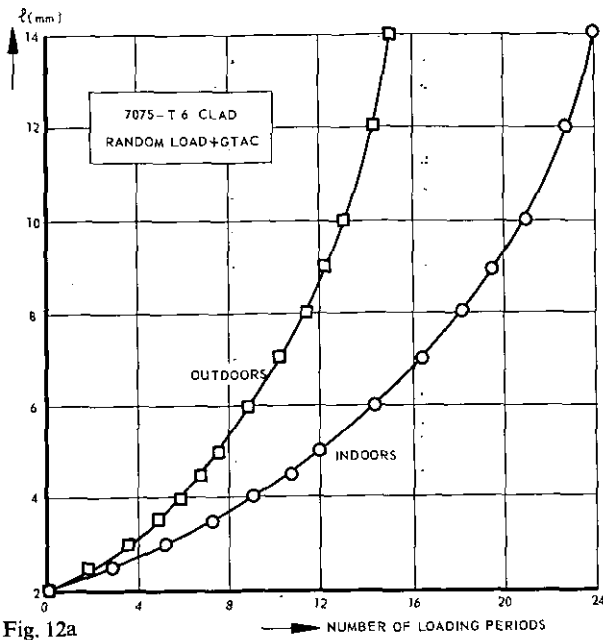


Fig. 12a

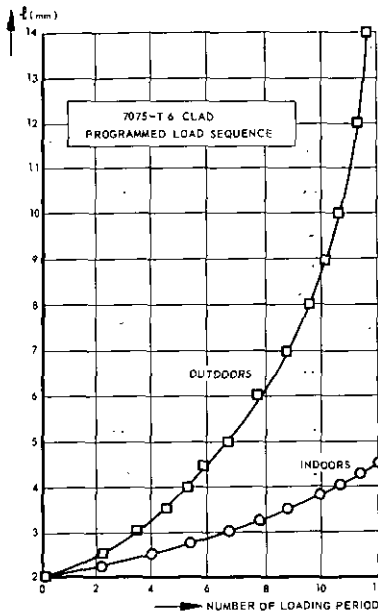


Fig. 12b

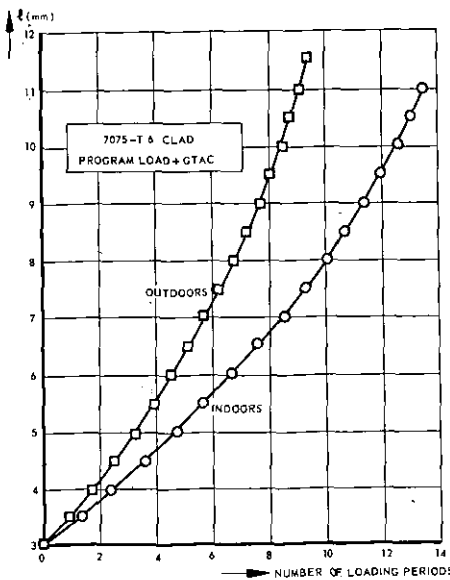


Fig. 12c

Fig. 12 Comparison of the crack propagation indoors and outdoors for the 7075 alloy.

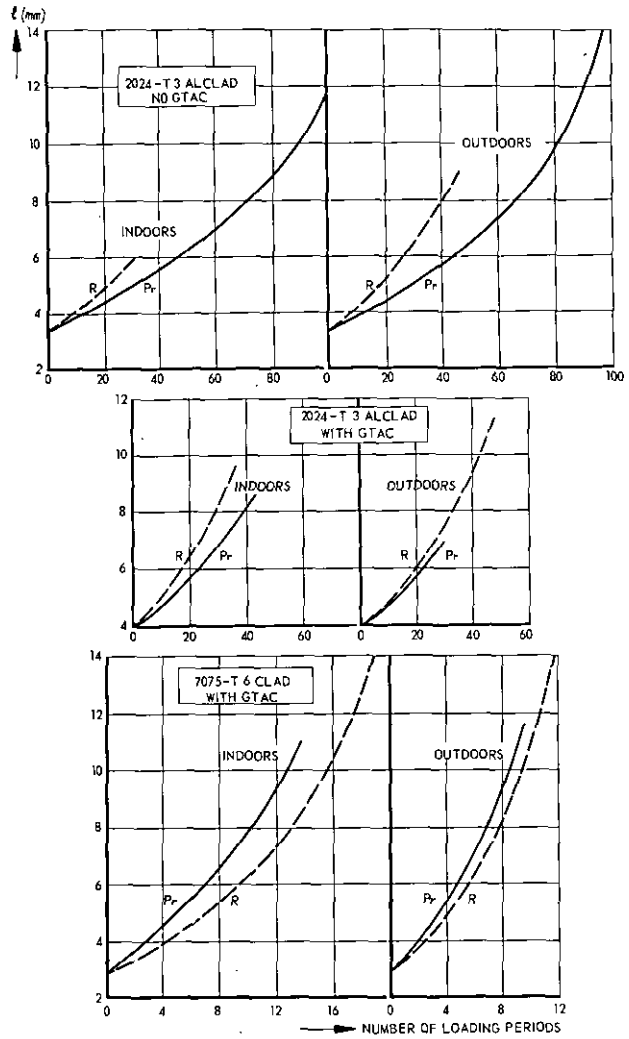


Fig. 13 Comparison of the crack propagation under random loading and programmed loading.

scatter was larger than expected. The median value of  $\Delta n$  rather than the mean was then calculated to avoid an excessive influence of a single outlying result.

Average crack propagation curves were obtained by summing the mean values of  $\Delta n$  and plotting  $l_i$  as a function of this sum. The average crack propagation curves are shown in figs. 11 and 12 for the 2024-T3 and the 7075-T6 alloy, respectively. The curves are partly replotted in fig. 13 to allow a comparison between random and program loading.

The crack propagation lives under two different conditions are compared in tables 6 to 9. In these tables the crack growth interval was selected as large as possible for a useful comparison.

### 7 Fractographic examination and some additional observations

Several parts of the specimens containing one crack each were loaded to fracture in a tensile testing machine in order to enable examination of the fracture surfaces.

The transition from the 90°-mode fracture (tensile

mode) to the 45°-mode (shear mode) as described in several previous NLR reports (see for instance ref. 6) was noticed in the specimens with the larger cracks. The average crack rate, disregarding the variable-amplitude character of the loading, at completion of the transition was in the order of  $0.15 \mu/c$  and  $0.5 \mu/c$  for the 2024 and the 7075 alloy, respectively. In constant-amplitude tests on specimens cut from the same sheets loaded at the same mean stress these values were about  $0.3 \mu/c$  and  $1.8 \mu/c$  respectively (ref. 6). Since the crack propagation in variable-amplitude tests occurs predominantly at the higher stress amplitudes (ref. 7) the lower (average) values of the present test series are not unexpected.

With respect to the colour of the fracture surfaces no differences could be detected between the 2024-T3 specimens tested indoors and outdoors. However, for the 7075-T6 specimens the colour appeared to be somewhat duller for the specimens tested outdoors. This applies to the tests under program loading and random loading with GTAC. For the third test series with program loading including GTAC such a difference was not systematically present. In this test series the ratio between the crack rates outdoors and indoors was somewhat smaller than for the other two series, see table 6 and fig. 12.

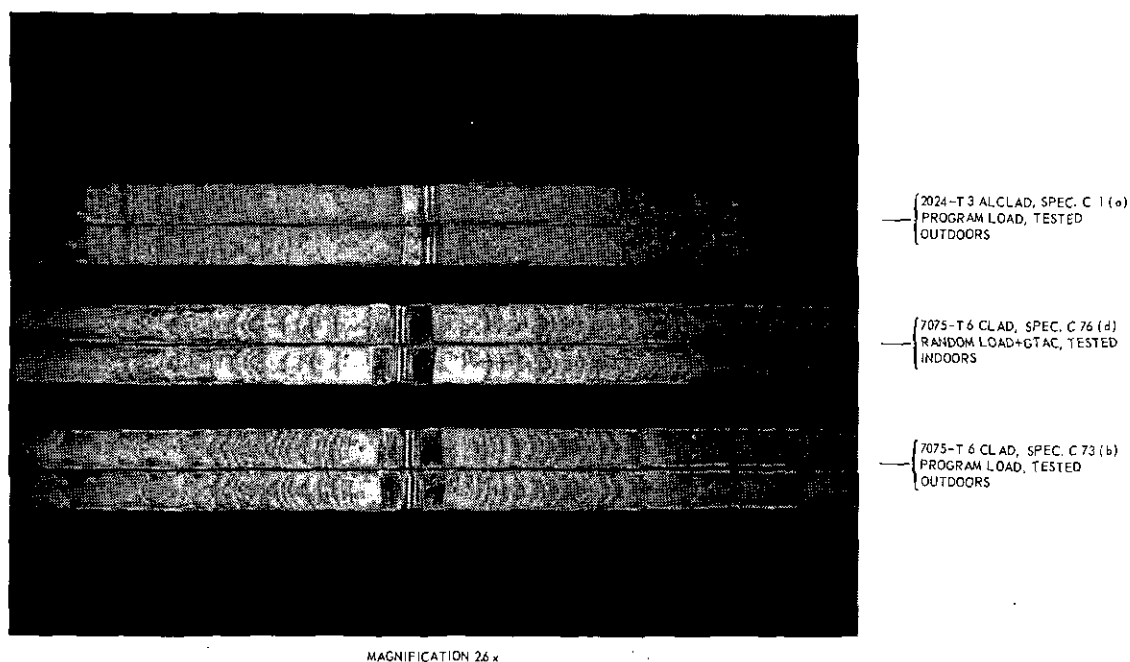
On the fractures of the 2024 specimens tested under random loading, either with or without GTAC, faint lines were visible, probably corresponding to the highest loads of the random sequence. The specimens with program loading more clearly showed lines and bands, see fig. 14. Note that the bands are practically straight, implying that the crack front was macroscopically straight.

The 7075 specimens all showed dark tongue-shaped bands, see fig. 14 for examples of random and program loading. These bands were previously mentioned in the literature, see the papers of Forsyth, of Hardrath and Mc Evily, of Christensen, and of Frost, Holden and Phillips presented at the Cranfield Crack Propagation Symposium (ref. 8). Hardrath and Mc Evily noticed in variable-amplitude tests that the dark bands were crack extensions occurring in a single cycle with the highest maximum load of a test period. This is in agreement with the present experience, since the dark bands in the lower specimen of fig. 14 (program loading) could easily be traced back to the successive loading periods. The bands were not observed in the constant-amplitude tests on the same sheet material (ref. 6); however, the highest stress was much lower in those tests ( $18.5 \text{ kg/mm}^2$  instead of  $23.7 \text{ kg/mm}^2$  in the present test series).

The absence of the tongue-shaped bands in the 2024 specimens might be a consequence of the higher ductility of this alloy but also of a different fatigue mechanism.

After the tests, the surfaces of the cladding layer of the outdoor specimens had a somewhat duller and less reflective appearance than the surfaces of the indoor specimens. The appearance for the 2024-T3 specimens was also a bit spotty.

Microscopic specimens were prepared from two cracks in the outdoor specimen C 73 (7075-T6) which showed a much higher crack rate than the concurrently tested indoor specimen. Microscopical examinations of the cracks showed that the growth had been transcrystalline. Exceptional features could not be detected.



MAGNIFICATION 26 x

Fig. 14 The two fracture surfaces of three cracks.

TABLE 10

Example of damage calculation

Material: 2024-T3 Alclad.

Crack growth interval from  $l=4$  mm to  $l=8$  mm; corresponding crack propagation life under constant amplitude loading:  $N_{4-8}$ Data for  $N_{4-8}$  from ref. 6 (tables 1-6).

$S_m$	$N_{4-8}$ (kc)			$S_m$ and $S_a$ in kg/mm <sup>2</sup>
	$S_a=2.5$	$S_a=4$	$S_a=6.5$	
12	74.57	26.09	9.38	
9	91.15	32.23	12.98	

The above data were used to plot  $S-N$  data used in the table below.

Loads	$S_m$	$S_a$	$n^1$ (cycles)	$N_{4-8}$ (kc)	$n/N_{4-8}$
Gusts	12.1	1.15	174160	550	0.317
		1.93	152880	135	1.132
		2.70	98280	62	1.586
		3.48	59080	35	1.692
		4.23	31640	23	1.376
		5.00	14968	16	0.936
		5.76	5948	12	0.496
		6.53	2620	9.2	0.285
		7.30	772	7.4	0.104
		8.09	438	6	0.073
		8.86	148	5	0.030
		9.60	140	4.2	0.033
		10.35	52	3.6	0.014
11.08	8	3.2	0.002		
11.57	26	2.9	0.009		
			$\Sigma = 8.085$		
GTAC	9.5	6.9	47040	11.8	3.986
					$\Sigma = 12.071$

Fatigue life in program test = 59.9 test periods (indoors)

$$\Sigma n/N = (59.9/140) \times 8.085 = 3.46$$

Fatigue life in program test with GTAC = 39.3 test periods (indoors)

$$\Sigma n/N = (39.3/140) \times 12.071 = 3.39$$

<sup>1</sup> number of load cycles in 140 test periods (chapter 4)

## 8 Damage calculations

In ref. 6 specimens cut from the same sheets were tested under constant-amplitude loading at three values of the mean stress. The highest mean stress adopted was 12 kg/mm<sup>2</sup> which is practically the same value as applied in the present test series. At the three mean stresses crack propagation tests were carried out at three values of the stress amplitude, viz.  $S_a=2.5$ , 4 and 6.5 kg/mm<sup>2</sup>. From these tests the crack propagation life corresponding to a certain amount of crack propagation could be obtained. The crack propagation life was plotted as a function of  $S_a$  and a curve was drawn through the three data points. Such curves, and the load spectrum as discussed in chapter 4, were then used for damage calculations. An example of a calculation is shown in table 10. A summary of the calculated  $\Sigma n/N$  values is given in table 11. For all tests with GTAC the contribution to  $\Sigma n/N$  from the GTAC was about half the contribution of the gust cycles. The crack growth intervals in table 11 were selected in such a way as to cover a large part of the crack propagation occurring in most tests on the same material. In the program tests indoors on the 7075-T6 specimen crack propaga-

tion extended to slightly over 4 mm only (fig. 12b) and for this loading calculations were also made for  $l=2$  mm to  $l=4$  mm.

TABLE 11  
Damage values for the crack propagation

Material	Type of loading	Environment	Crack growth interval $l_b$ to $l_e$ (mm)	$\Sigma n/N$
2024-T3	R	O	4 to 8	1.9
	Pr	I		3.5
	R+GTAC	O		3.2
		I		2.5
	Pr+GTAC	O		2.8
		I		3.4
7075-T6	R+GTAC	I	3 to 10	3.7
		O		2.2
	Pr	O		2.2
		I		2.9
	Pr+GTAC	O		2.0
		I		3.6
	O	1.7		

For the random loading the stress spectrum was assumed to be the same as for the program loading, see chapter 4.

The  $S-N$  data used were partly obtained by extrapolation, see table 10. Although this might imply a certain inaccuracy, the major portion of the damage (calculated as  $\Sigma n/N$ ) stems from stress amplitudes for which the determination of the  $N$ -values did not require extrapolation. In other words this source of inaccuracy is not important.

The  $S-N$  data were obtained on specimens with a width of 160 mm (100 mm in the present tests) loaded at a frequency of 2000 cpm (average frequency in the present tests 20 cpm). In ref. 9 it was shown that the width effect on crack propagation was negligible as long as the crack was smaller than about 30% of the sheet width. This limit is not exceeded in table 11. With respect to the frequency, an approximately 20 to 30% faster crack rate at 20 cpm as compared with 2000 cpm was found for the 2024-T3 alloy in a previous investigation (ref. 10). Application of this percentage to the present results would have yielded 30% higher  $\Sigma n/N$ -values. Finally, the 3% error on the loads due to friction in the jacks has to be mentioned, see chapter 3. This implies that the  $S_a$ -values were actually 3% lower, which roughly corresponds to about 7% higher  $N$ -values and hence to 7% lower  $\Sigma n/N$ -values. Consequently, the  $\Sigma n/N$ -values will be about 20% higher than indicated in table 11. This implies that for the tests indoors  $\Sigma n/N$  is about 4 and for the tests outdoors it is about 3.3 for the 2024-T3 specimens and 2.5 for the 7075-T6 specimens. It was actually not completely fair to calculate  $\Sigma n/N$  for the outdoor tests, since  $N$ -values obtained indoors were used.

Although the  $\Sigma n/N$  values appear to be high, similar values, viz. 3.6 to 4.1, were obtained in a previous investigation (ref. 7) during program tests on 2024-T3 Alclad specimens, employing 5 load amplitudes. The high values were explained by referring to the ease of setting up favourable residual stresses around cracks.

## 9 Summary of two NASA investigations

Two investigations on notched sheet specimens were carried out by the NASA (refs. 1 and 2). They are both concerned with the effect of outdoor exposure on the fatigue life of sheet bending specimens notched by a hole ( $K_t = 1.6$ ). The environmental conditions were similar to those of the present tests, except for the salt content of the air which was probably higher since the test site was situated near the seacoast.

A survey of the first investigation has been compiled in table 12. For the two alloys 2024-T3 and 7075-T6 tested in the bare condition the fatigue lives obtained outdoors were in the order of 40% of the lives obtained indoors, i.e. considerably shorter. In the clad condition the 7075-T6 alloy showed a reduction to approximately 70% when tested outdoors, whereas the reduction for the 2024-T3 alloy was negligible. Although one might

think that the results for the clad material are in qualitative agreement with those of the present test series (table 6), one should recognize that when the values of the crack length considered in the present tests were obtained in the NASA specimens the final failure was imminent.

In the second NASA test series (ref. 2) the effect of outdoor exposure under load on the subsequent fatigue life obtained in tests in the laboratory was investigated. The same type of specimen and the same materials were used. Exposure under load (stress corrosion environment) occurred during times varying from  $\frac{1}{2}$  year to 4 years and the bending stresses corresponding to the exposure loads were 0,8,4 and 21.1 kg/mm<sup>2</sup> respectively. The fatigue lives obtained after the exposure were similar for the three values of the preload stress and the reductions of the fatigue lives had therefore to be attributed to the corrosion per se and not to stress corrosion.

For the 2024-T3 and the 7075-T6 alloys in the bare condition the fatigue lives were reduced by the outdoor exposure to approximately 25% of the fatigue lives of the unexposed materials. The reduction was almost fully effectuated after the shortest exposure time ( $\frac{1}{2}$  year). In the clad condition the reduction for the 7075-T6 alloy was small and for the 2024-T3 alloy a reduction could not be noticed. Unfortunately, the scatter of data for the clad material was fairly large.

Also in this second investigation it appeared that the 7075-T6 alloy in the clad condition is more sensitive to outdoor exposure than the 2024-T3 Alclad. It is also remarkable that stress corrosion did not affect the results.

## 10 Discussion

The discussion in this chapter will be concerned with two questions: (1) Is it possible to understand qualitatively the trends of the present results? (2)

TABLE 12

Survey of a NASA investigation concerning the effect of outdoor exposure on the fatigue life (ref. 1)

Tests were carried out at the Langley Station. Cantilever sheet bending specimens were notched by a hole (diameter 6.3 mm, width 25.4 mm,  $K_t = 1.6$ ). Sheet thickness 1.3 mm. Frequency for tests outdoor 430 cpm, specimens being loaded for 4000 cycles each working day. The duration of the outdoor tests varied from 3 weeks to 6 months. Frequency for tests indoors 575 cpm, specimens being loaded uninterruptedly till failure.

Material	$S_m \pm S_a$ (kg/mm <sup>2</sup> )	Geometric mean fatigue lives (kc)		Ratio (I/O)
		Indoors	Outdoors	
2024-T3 bare	8.4 ± 17.6	399	145	2.8
2024-T3 clad	8.4 ± 10.5	541	546	1.0
7075-T6 bare	8.4 ± 17.6	211	90	2.3
7075-T6 clad	8.4 ± 10.2	389	280	1.4

Which are the technical consequences of the present results? The first question is important for recognizing the applicability of the results beyond the circumstances valid for the present investigation and is therefore also important with respect to the second question.

#### 10.1 *The trends of the present results*

According to table 6 and figs. 12 and 13 the atmospheric effect on the crack propagation was small if not negligible for the 2024-T3 Alclad whereas a consistent accelerating effect was found for the 7075-T6 Clad material. The differences between the outdoor and indoor environments are concerned with temperature, humidity, precipitation and possibly the chemical composition of the air.

The temperature outdoors was at most some 20°C lower than indoors in winter time, whereas in summer time the temperature difference between outdoors and indoors is practically negligible. Temperature is not considered to be important since the atmospheric effect was found in summer time as well, and since the 2024-T3 alloy did not show this effect in winter time.

The vapour pressure of water at 0°C is 4.6 mm Hg and at 20°C it is 17.5 mm Hg. In view of the relative humidities measured it can be said that the absolute amount of water vapour indoors was probably always larger than or at least equal to the amount outdoors. Water vapour has an accelerating effect on the crack propagation in 2024-T3 Alclad as shown by Hartman and Jacobs (ref. 11) and a similar effect has been noticed for 7075-T6 Clad (to be published). One should then expect a faster crack-rate in the indoor tests and hence it seems to be difficult to attribute the trends observed to an influence of humidity.

An apparent difference between the outdoor and the indoor circumstances is the presence of water on the outdoor specimens which did not occur on the indoor specimens. The 7075 alloy is known to be more susceptible to stress corrosion than the 2024 alloy (ref. 12) and one might say that the water will assist the contribution of stress corrosion to the crack propagation\*. Although this may be correct it has to be admitted that the explanation is rather superficial and it cannot be said that the atmospheric influence is really understood. Since the 7075 alloy specimens tested outdoors had a somewhat duller fracture appearance than the indoor specimens, it is still thought that corrosion was a predominant factor in causing the atmospheric influence. Since high stresses are always present around growing cracks one could say that it was stress corrosion by definition.

It is thought unlikely (although not a priori impos-

sible) that other chemical constituents of the atmosphere have been active. It is somewhat difficult to see that such constituents were present outdoors and not indoors.

The NASA results summarized in chapter 9 are concerned with fatigue lives of small specimens, i.e. with crack nucleation and propagation of very minute cracks. They are helpful in showing that aluminium alloys are sensitive to atmospheric attack. Unfortunately in the bare condition the two alloys 2024-T3 and 7075-T6 both exhibited this sensitivity to a similar degree. In the present tests the crack rate is mainly controlled by the core of the sheet. One could only speculate that for the 2024-T3 alloy the cladding layer has still been acting as an anodic layer and has given some protection to the core, whereas for the 7075-T6 alloy, this protection is probably less effective. This speculation finds some confirmation from the NASA investigations.

Although the prime purpose of the investigation was the comparison of the fatigue crack behaviour outdoor and indoor the results also allow a comparison of crack propagation under different load sequences and a comparison of the crack rates in the 2024-T3 and the 7075-T6 sheet material.

A comparison of the crack propagation under random and programmed load sequences is made in table 7 and fig. 13. It is remarkable that the two alloys show a different behaviour, viz. a faster crack rate under random loading for the 2024-T3 alloy and a faster crack rate under program loading for the 7075-T6 alloy. The latter trend was the expected one. Although the number of peak loads per test period is lower for the program loading (about 30%), only the smaller load excursions are neglected by the mean-crossing-peak count method used for deriving the program loading from the random loading (ref. 13). On the other hand, in the program loading positive and negative load amplitudes of equal size are combined to complete cycles, which was thought to lead to a somewhat more severe load sequence. The latter effect did indeed prevail for the 7075 alloy, but for the 2024 alloy the omission of a number of peak loads had apparently a larger influence. It should be recognized that the differences between the lives under random and program loading are small for the tests with GTAC, but it is somewhat disappointing to see ratios of about 1.5 for the tests without GTAC.

The effect of adding GTAC to either the random or programmed load sequence was of course a reduction of the fatigue life. According to the damage calculations a reduction to about  $\frac{2}{3}$  of the fatigue life without GTAC had to be expected. Although the average value in table 8 is 0.60, lower values were found in some tests, indicating that the damage was larger than expected on the basis of the linear cumula-

\* It should be kept in mind that the stress on the specimen is practically zero when the fatigue loading is not applied, viz. in the night time and during interruptions of the tests.

tive damage rule. This is not unexpected in view of previous experience in cumulative damage tests (refs. 14 and 15). It is the more gratifying to see that  $\Sigma n/N$  values are still clearly beyond one in tests with GTAC (see table 11).

A comparison between the crack propagation lives for the two alloys has been made in table 9. Indoors the average ratio between the lives for the 2024-T3 alloy and the 7075-T6 alloy is about 4 and outdoors about 6.5. In a previous investigation (ref. 6), under constant-amplitude loading indoors, ratios of 3 to 4 were found in agreement with the present results. The higher ratio for the outdoor tests is due to the higher sensitivity to atmospheric exposure of the 7075 alloy.

#### 10.2 *The technical consequences of the present results*

A full-scale test is generally made in a test hall under similar conditions as the present indoor tests. For a fail-safe structure crack propagation data are obtained in such a test for establishing safe inspection periods. Safety factors are applied on the crack propagation lives obtained in the test. A reasonable value for this factor may be 3. The factor has to cover atmospheric influences amongst other things. According to the evidence of the present test series the factor required for these influences only, may be of the order of 1.5 to 2 for the 7075 alloy, whereas for the 2024 alloy such a factor may not be necessary. Actually the generalizing of the present data is not justified. Smaller or larger factors may be necessary depending on the environmental circumstances. This is a somewhat disquieting result of the present tests. The atmospheric influence under service conditions may be larger than found in the present test series if service conditions involve a more corrosive environment than at the NLR test site. There are reasons to believe that the conditions at the NLR test site are indeed not particularly corrosive.

Another obvious consequence of the present results is that further study is urgently required. On one hand comparative tests under various possible service and full-scale testing conditions should be carried out. On the other hand tests under closely controlled environments are equally necessary to improve the understanding of the mechanism, which is a prerequisite for generalizing of the results of the former tests.

One might also consider the question of simulating the corrosive atmosphere occurring in service in a full-scale test, for instance by performing the test outdoors. This question will not be further discussed here.

Finally some comments will be given on the crack propagation under random and program loading. Fortunately the differences between the crack rates under the two types of loading were not larger than 30% if both types of loading included GTAC. One cannot guarantee, of course, that a full-scale test with a programmed flight simulation will always yield a

similar small difference as compared with a random service loading. In this respect, however, there appears to be a more pertinent problem which is the assessment of the highest load of the load spectrum still to be included in the full-scale test. The influence of the magnitude of this load on the crack rate is of predominant importance (ref. 7) and one may only take comfort in the thought that infrequent high loads usually omitted in a full-scale test are probably favourable for the crack propagation, i.e. they will have a retarding effect. The problem of establishing the loadings for a full-scale test are further discussed in ref. 3.

### 11 Conclusions

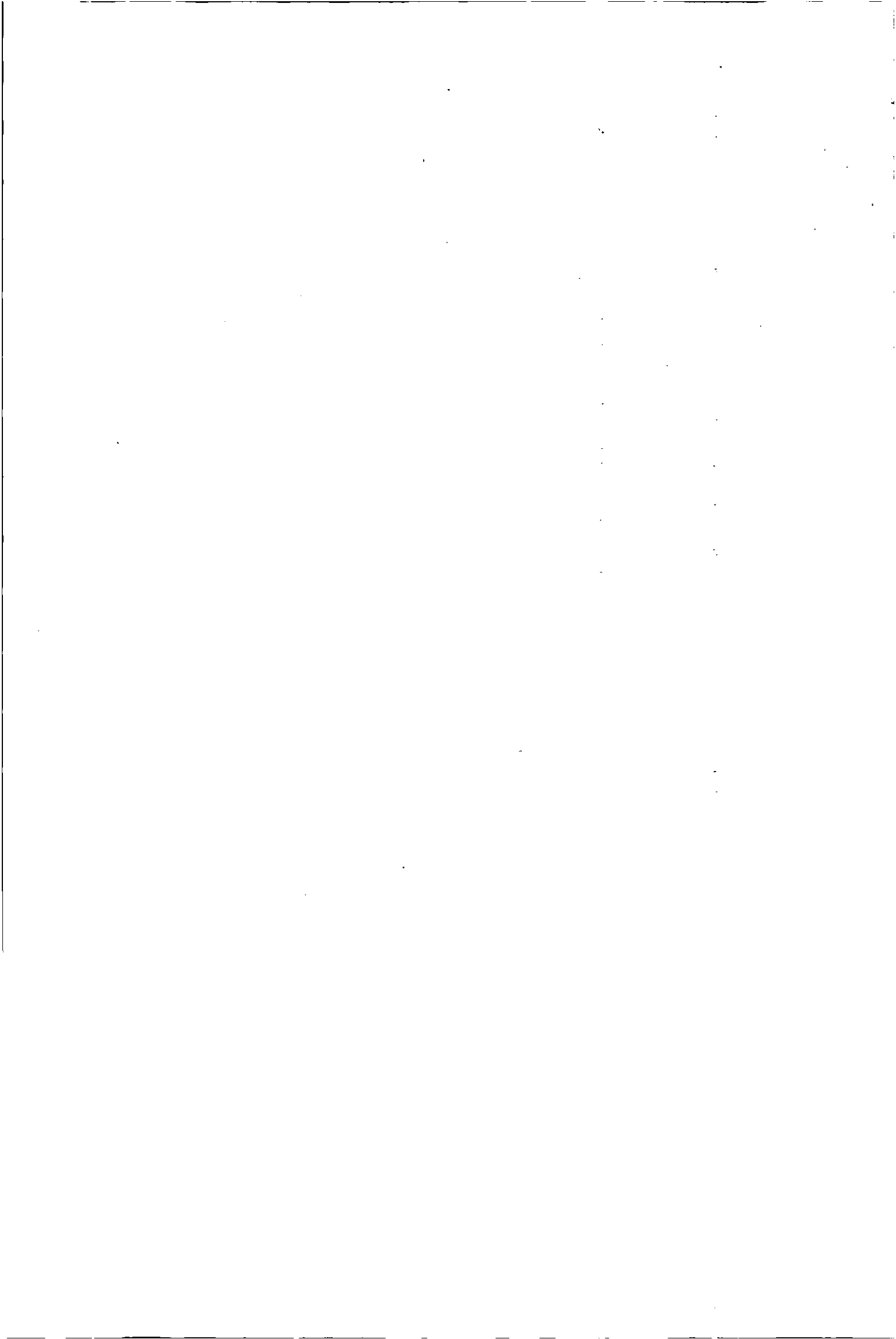
An investigation was carried out on the influence of atmospheric exposure during the propagation of (macro) fatigue cracks in sheet specimens of 2024-T3 Alclad and 7075-T6 Clad material. Tests were conducted in two test rigs, one located indoors and the other one outdoors. The tests were run concurrently with full-scale fatigue tests on tension skins and the same random and programmed load sequences, representing a severe gust spectrum, were employed. Tests with and without ground-to-air cycles (GTAC) were performed. The main results can be summarized in the following conclusions.

1. The differences between the crack propagation rates in the 2024-material tested indoors and tested outdoors were small. However, for the 7075 material the crack propagation outdoors was about 1.5 to 2 times faster than indoors.
2. For the 7075 alloy the crack propagation under program loading was about 15% faster than under random loading. For the 2024 alloy it was from 10 to 40% slower.
3. As a result of damage calculations relating to the fatigue crack propagation lives,  $\Sigma n/N$  values in the order of 4 were obtained for the specimens tested indoors.
4. The ratios between the crack propagation lives for the 2024 alloy and the 7075 alloy were in the order of 4 for the indoor tests and in the order of 6.5 for the outdoor tests. The stress spectra were the same for the two materials.
5. It is possible that the ratio between the crack rates in an aircraft structure in service and the crack rates observed in a full-scale test on the same structure is larger than observed in the present tests, especially if the service conditions are more corrosive than the present outdoor environment.
6. The atmospheric influence on crack propagation noticed for the 7075 alloy and practically absent in the 2024 alloy was tentatively attributed to stress corrosion. Nevertheless, it cannot be said that the

atmospheric influence is reasonable well understood and additional investigations are strongly recommended.

## 12 References

- <sup>1</sup> LEYBOLD, H. A., HARDRATH, H. F. AND MOORE, R. L., An investigation of the effect of atmospheric corrosion on the fatigue life of aluminium alloys. NACA Techn. Note 4331, Sep. 1958.
- <sup>2</sup> LEYBOLD, H. A., *The effects of combined prior stress and atmospheric corrosion on the fatigue life of aluminium alloy.* NASA Techn. Note D-2359. Aug. 1964.
- <sup>3</sup> SCHIJVE, J., BROEK, D., DE RIJK, P., NEDERVEEN, A. AND SEVENHUYSEN, P., Fatigue tests with random and programmed load sequences, with and without ground-to-air cycles. A comparative study on full-scale wing center sections. NLR report S. 613, Dec. 1965.
- <sup>4</sup> NEDERVEEN, A., DE RIJK, P., BROEK, D. AND SCHIJVE, J., Experimental details of testing a full-scale structure with random and programmed fatigue load sequences. NLR report S.608, Jan. 1964.
- <sup>5</sup> SCHIJVE, J., Fatigue loads applied on a full-scale structure in random and programmed sequences. NLR report S.609, April 1964.
- <sup>6</sup> BROEK, D. AND SCHIJVE, J., The influence of the mean stress on the propagation of fatigue cracks in aluminium alloy sheet. NLR-TR M.2111, Jan. 1963.
- <sup>7</sup> SCHIJVE, J. AND BROEK, D., Crack propagation, the results of a test programme based on a gust spectrum with variable amplitude loading. *Aircraft Engineering*, Vol. 34, p. 314, 1962.
- <sup>8</sup> Proceedings of the Crack Propagation Symposium, Vols. 1 and 2, Cranfield 1961.
- <sup>9</sup> SCHIJVE, J., NEDERVEEN, A. AND JACOBS, F. A., The effect of the sheet width on the fatigue crack propagation in 2024-T3 Alclad material. NLR-TR M.2142, March 1965.
- <sup>10</sup> SCHIJVE, J., Fatigue crack propagation in light alloy sheet material and structures. *Advances in Aero-Sciences*, Vol. 3, p. 387. Pergamon, 1962.
- <sup>11</sup> HARTMAN, A. AND JACOBS, F. A., *An investigation into the effect of oxygen and watervapour on the propagation of fatigue cracks in 2024-T3 Alclad sheet.* NLR Report M.2123, Jan. 1964.
- <sup>12</sup> SHREIR, L. L., *Corrosion. Vol. 1: Corrosion of metals and alloys.* George Newnes Lim., London 1963.
- <sup>13</sup> SCHIJVE, J., The analysis of random load-time histories with relation to fatigue tests and life calculations. *Fatigue of Aircraft Structures*, Proc. 2nd ICAF-AGARD Symposium, May 1961. Edited by W. Barrois and E. L. Ripley, Pergamon 1963, p. 403. Also NLR-report MP. 201, May 1961.
- <sup>14</sup> SCHIJVE, J. AND JACOBS, F. A., Program-fatigue tests on notched light alloy specimens of 2024 and 7075 material. NLR-TR M.2070, March 1960.
- <sup>15</sup> NAUMANN, E. C., *Evaluation of the influence of load randomization and of ground-air-ground cycles on fatigue life.* NASA TN D-1584, Oct. 1964.



REPORT NLR-TR M. 2160

# The effect of the sheet thickness on the fracture toughness of cracked sheet

by

D. Broek

## Summary

Results are presented on the effect of thickness on the residual strength of aluminium alloy sheet specimens.

It could be explained why a state of plane stress at the crack-tip results in a slant fracture and why a state of plane strain results in a square fracture (flat tensile mode). It could also be explained why a plane strain fracture occurs at a lower stress than a plane stress fracture. Explanations are based on the observation that crack growth is a mechanism of void coalescence and that void initiation and growth are governed by shear stresses, whereas void coalescence is governed by the tensile stress acting on the plane of maximum void concentration.

## Contents

	P. Nr.
List of symbols	1
1 Introduction	1
2 Experimental details	2
3 Test results and results of other investigations	2
4 The relation between fracture appearance and state of stress	3
4.1 Scope	3
4.2 The thickness effect and the fracture appearance	3
4.3 The mechanism of crack propagation	3
4.4 Explanation of the fracture mode transition	4
5 The influence of the thickness on residual strength	5
6 The criterion for the transition of the state of stress	5
7 Conclusions	6
8 References	6
1 table	
17 figures	

## Symbols

$2l_0$	— initial crack length
$2l_c$	— (critical) crack length at fracture instability
$r_p$	— width of the plastic zone at the crack tip

$s$	— width of slant part of fracture surface
$t$	— sheet thickness
$2w$	— specimen width
$\delta(2 \text{ in})$	— elongation on 2 in gauge length
$\eta$	— $2s/t$
$\sigma_c$	— fracture stress (residual strength; fracture toughness)
$\sigma_i$	— stress to initiate crack growth
$\sigma_u$	— ultimate tensile strength
$\sigma_y$	— yield strength
$\sigma_{0.2}$	— 0.2% yield stress
$\sigma_1, \sigma_2, \sigma_3$	— principal stresses
$\tau$	— shear stress
$\tau_{\max}$	— maximum shear stress

## 1 Introduction

Experimental data on the effect of sheet thickness on the residual strength are scarce. The thickness effect is very complicated and is generally believed to be related with a variation of the state of stress at the crack tip. Its relation with the mode of fracture suggests that the thickness effect is of fundamental interest and, therefore, a study of this effect seemed to be worthwhile.

A number of tests were carried out on 300 mm wide sheets of thickness ranging from 1 to 4 mm. A supplementary test series was performed on 100 mm wide specimens of thicknesses ranging from 0.5 to 20 mm. The test results are presented in this report.

After the discussion of the relation between specimen thickness, fracture mode and state of stress and of the mechanism of crack growth, tentative explanations will be offered for the influence of the state of stress on fracture mode and fracture toughness. Finally, the criterion for the transition of the state of stress from plane strain to plane stress will be briefly discussed.

## 2 Experimental details

The material tested was 2024-T3 alclad sheet of 1,2,3 and 4 mm thickness (in a subsequent test series also a number of small specimens were tested with thicknesses up to 20 mm; see sec 3) having the following static properties:

Thickness $t$ (mm)	$\sigma_{0.2}$ (kg/mm <sup>2</sup> )	$\sigma_u$ (kg/mm <sup>2</sup> )	$\delta(2 \text{ in})$ (%)	Number of specimens
1	31.6	44.8 <sup>+0.7</sup> -0.9	19	4
2	36.4	47.6 <sup>+0.6</sup> -1.0	18	8
3	37.4	47.9 <sup>+0.5</sup> -0.3	19	6
4	36.6	48.2 <sup>+0.7</sup> -0.3	20	4

The specimens were cut to a size of 680 × 300 mm, with the longest dimension parallel to the rolling direction, and were provided with a fine central transverse saw cut made by means of a jeweller's fret saw. It was shown in ref. 1 that this saw cut can simulate a fatigue crack for the purpose of residual strength tests. The

stress to initiate slow crack growth was slightly higher for a saw cut than for a fatigue crack, but once slow crack growth had started the behaviour was the same (same  $\sigma_c$  and  $l_c$ ).

The specimens were loaded by a hydraulic jack. A strain gauge dynamometer in combination with a strip chart recorder provided the load records. During the test the specimen was filmed at 14 frames per second to record the slow crack growth preceding fracture. The recorder was filmed simultaneously via a mirror, which gave the possibility to determine the load at which crack growth was initiated.

## 3 Test results and results of other investigations

The test results have been collected in table 1. The fracture stress as a function of sheet thickness for different values of the initial crack length is shown in fig. 1. A plot of the stress to initiate slow crack growth is shown in fig. 2. Finally, fig. 3 shows the relation between critical crack length and initial crack length as observed from the film records.

The typical relation between fracture stress and sheet thickness (fig. 1) was confirmed by a supplementary test series on smaller (100 mm wide) specimens. In this test series a wider range of gauges was investigated. The results of these tests are given in fig. 4 (The lower part of this figure will be discussed in sec. 4.2). No data on crack initiation and propagation are available, since film records have not been made of these tests.

Test results of other investigations are given in figs. 5,6 and 7. For the data of refs. 4 and 5 (fig. 7) no values for the crack length are available and, therefore, the results are given on the basis of  $\sigma_c/\sqrt{l_c}$  as in the original

TABLE I  
TEST RESULTS

Influence of sheet thickness on residual-strength of sheet specimens.

Initial crack length $2l_0$ (mm)	$\sigma_t$ Stress to initiate slow crack growth (kg/mm <sup>2</sup> )				$2l_c$ Critical crack length at instability (mm)				$\sigma_c$ Critical stress (at instability) (kg/mm <sup>2</sup> )			
	$t=$ 1 mm	$t=$ 2 mm	$t=$ 3 mm	$t=$ 4 mm	$t=$ 1 mm	$t=$ 2 mm	$t=$ 3 mm	$t=$ 4 mm	$t=$ 1 mm	$t=$ 2 mm	$t=$ 3 mm	$t=$ 4 mm
	30	24.7	23.5	27.2	27.0	41	41	44	41	28.0	32.2	31.6
30	23.7	21.8	26.6	26.8	49	40	46	41	28.2	31.7	31.1	31.1
30		22.5					57			32.0		
45	18.0	20.0	22.4	24.5	66	58	69	76	25.3	29.6	29.2	28.9
45	20.9	21.4	23.9	23.8	75	63	64	62	25.4	29.4	29.1	29.2
45	21.4	22.7	25.1	23.9	61	63	63	64	25.4	29.6	29.4	29.0
90	14.3	18.1	16.4	18.5	133	117	119	117	20.5	23.7	22.6	22.8
90	14.5	17.5	17.7	16.4	131	115	116	107	20.7	23.9	22.6	22.6
120	12.1	12.2	14.3	13.9	157	148	137	154	16.8	20.0	18.0	18.9
120	12.7	12.1	14.5	14.7	166	145	141	143	17.0	19.9	17.7	18.6

papers. This will be no objection if it is assumed all data are for the same length of the initial crack, since for small cracks  $l_c$  is almost proportional to  $l_0$  (fig. 3) and, hence,  $l_c$  will be almost a constant for constant  $l_0$ .

From figs. 1 and 5-7 it can be concluded that (starting with thin sheets) the residual strength increases with thickness until at a particular thickness a maximum strength is obtained. Further increase of the thickness gives a decreasing strength. In fig. 5-7 some materials show either the ascending or the descending part of the curve only. It may be assumed that a similar behaviour as for the other materials would have been obtained if a larger range of gauges had been tested. This will become plausible in the course of this report.

#### 4 The relation between fracture appearance and state of stress

##### 4.1 Scope

The thickness effect is not the result of metallurgical processing involved in rolling the sheet to thickness, since the effect is the same when the specimens are machined to thickness from a thick plate (ref. 6).

At least some aspects of the thickness effect can be reasonably explained. These explanations are largely based on the relation between fracture appearance and the state of stress at the crack tip. This relation will be considered in sec. 4.2. The mechanism by which cracks in ductile materials propagate, which is essential in the discussion, will be outlined in sec. 4.3, based both upon what is known from the literature and on direct observations made during the present investigation. Finally, in sec. 4.4 the conclusions of the discussions will lead to a reasonable explanation of the relation between fracture appearance and state of stress.

##### 4.2 The thickness effect and the fracture appearance

In thin sheets (ascending part of the curves in figs. 1 and 4), the fracture is completely of the so called shear type: the fracture surface makes an angle of  $45^\circ$  with the sheet surface. Beyond the maximum in the curves the fracture surfaces have a part at mid-thickness that is perpendicular to the sheet surface, and is generally denoted as the flat tensile fracture mode. The thicker the sheet, the larger the flat tensile part of the fracture surface (see fig. 8).

Following Srawley and Brown (ref. 6), the shear fracture mode will be denoted here as a slant fracture and the flat tensile fracture as a square fracture, because the slant fracture is not necessarily the result of a shearing apart of the two fracture surfaces and because the square fracture is as much a result of shear as is the slant fracture (secs 4.3 and 4.4).

The width of the slant portion of the fracture relative

to the sheet thickness is defined as the slant fraction  $\eta$ . It varies from 100% in thin sheets to values as low as 5% in thick plates. Data for  $\eta$  are given in figs. 4 and 7. Values lower than 100% occur only beyond the maximum of the strength curve (see also fig. 8).

It was tried in the present investigation to force a slant fracture in two specimens of a thickness that was known to produce a square fracture. These specimens were provided with a central saw-cut simulated crack making an angle of  $45^\circ$  with the sheet surface. Indeed, macroscopically the specimens showed a fully slant fracture, but cross sections examined in the optical microscope showed that on a microscale the fracture consisted of square portions, forming a stepped fracture surface; only the shear lips were really slant (see figs. 9 and 10).

The mode of fracture is usually claimed to be related with the state of stress at the crack tip. The slant fracture occurs where the state of stress is plane stress and the square fracture where it is plane strain. At the sheet surface there is always plane stress, since the third principal stress cannot exist at the surface. This correlates with the fact that slant portions (shear lips) are always present. At the crack tip local plastic deformation occurs, but yielding cannot take place freely due to constraint of the surrounding elastic material. As a result a triaxial state of stress can occur in the plastic zone, which is ultimately a state of plane strain. When the state of stress is triaxial, this will be at mid-thickness and triaxiality will occur over a larger part of the thickness as the sheet is thicker, which correlates with a decreasing slant fraction.

The correlation between fracture mode and state of stress indicates that the state of stress can be responsible for the fracture mode transition and for the related thickness effect on strength. Therefore, it will be a starting point for the discussion of fracture mechanisms and the thickness effect.

##### 4.3 The mechanism of crack propagation

Fractographic observations made by means of the electron microscope have greatly contributed to the understanding of the mechanism of crack propagation. Excellent work on this subject has been performed by Beachem (refs. 7-11), Pelloux (refs. 11 and 12) and Crussard et al (ref. 13).

The electron microscope has revealed that surfaces of ductile fractures consist of dimples or cupules. Fig. 11 shows dimples in fracture surfaces of specimens of the present investigation\*. These dimples are thought to be the halves of micro-voids that were initiated in the highly stressed region at the crack tip. Crack growth is a result of growth and coalescence of these voids,

\* The electron micrographs were made on the Hitachi E.M. of the 'Metaalinstuut TNO' at Delft.

and linking up with the main crack. As a result of the local stress conditions the dimples can be either equiaxed or shear or tear dimples (refs 7-13), which is illustrated in fig. 12.

Generally, all types of dimples can be observed in square fractures as well as in slant fractures. Therefore it cannot be concluded from the dimple configurations on an electron micrograph whether the fracture surface was slant or square, though in certain cases a correlation between the dimple configuration and the macro fracture-appearance can be observed, as is probably the case in fig. 11a. In that figure a sort of plateau can be seen, which can possibly be identified as a square part of the forced slant fracture (figs. 9 and 10). The middle of the plateau consists of equiaxed dimples, whereas tear dimples were formed when the crack front reached the edges of the plateau.

In general, however, all types of dimples were observed close together in slant as well as in square fracture surfaces. The shape of the dimples depends on local irregularities in the stress distribution due to neighbouring voids. For example, an intermetallic particle may cleave or loose coherency with the matrix, giving rise to a large void (fig. 11b), which will probably affect the mechanism of coalescence of neighbouring voids.

During the present investigation it was tried to learn something on void growth and coalescence from a soap bubble raft model. The two-dimensional bubble raft was produced according to the method developed by Bragg and Nye (ref. 14). Void growth and coalescence in this model are illustrated in figs. 13 and 14. The way in which the models were loaded by means of diagonally compressing an open square with hinges at the corners is shown in fig. 13. In this way a system of true shear was applied; the void was located transversely to the largest tensile stress. Fig. 15 may be of help in following the dislocation movements in figs 13 and 14.

Fig. 14 shows a mechanism in agreement with the formation of shear dimples as presented in fig. 12. From motion pictures of the model it could be concluded that void growth occurs mainly by slip (i.e. dislocations are emitted from the void or run into the void), which can also be appreciated from fig. 13. Sometimes a short cleavage crack formed, but when it did the sharp tip was soon blunted by slip.

Of course, a two-dimensional bubble raft is only of limited value for the study of processes occurring in real crystalline structures. It is felt, however, that also in metals shear stresses are of primary importance for void growth. Direct evidence for the growth of voids by slip are smoothed slip steps (serpentine glide or pencil glide) of glide plane decohesion (ref. 9), which can often be observed in voids (see fig. 11a and b).

So far the mechanism of void initiation has not been considered. Also void initiation could be a result of

slip when it occurs in accordance with the models as proposed by Stroh (ref. 15), Cottrell (ref. 16) and others. Dislocations may pile up against grain boundaries or inclusions or may intersect, giving way to the formation of a tiny crack. Void initiation can also occur without slip, simply when an intermetallic particle cleaves or loses coherency with the matrix.

As far as dislocation mechanisms are responsible for void initiation, the voids will occur most abundantly on planes of intensive slip. Since void growth is primarily a mechanism of slip, it may be stated that the largest concentration of voids and the largest voids are to be found in planes of maximum shear stress.

#### 4.4 Explanation of the fracture mode transition.

From the foregoing, two important points can be summarized:

- a. Square fractures occur when the state of stress is macroscopically plane strain. Slant fractures occur in the case of plane stress.
- b. Cracks propagate by a mechanism of void coalescence. Void growth and possibly void initiation are a result of slip. Consequently the largest void concentration and the largest voids occur in planes of maximum shear stress. Tensile stresses may affect the way in which voids coalesce.

For the case when all stresses at the tip of the crack are elastic, Schijve (ref. 17) has shown by numerical calculations that the planes of maximum shear stress are different in plane strain and plane stress situations. When the state of stress is plane stress the maximum shear stress occurs on planes making angles of  $45^\circ$  with both the sheet surface and the loading direction. In case of plane strain the planes of maximum shear stress are perpendicular to the sheet surface and make an angle with the crack.

It may be assumed that these results hold also for the case when plastic deformation occurs at the tip of the crack. For a small region in front of the crack tip this assumption can be made plausible as follows. The material at the crack tip is far beyond the yield strain. Hence, Poisson's ratio will approach the value 0.5. This means that in the case of plane strain the third principal stress, very roughly, will be  $\sigma_3 \approx (\sigma_1 + \sigma_2)/2$ . In the region very close to the crack tip and close to the plane of the crack the first principal stress acts in the direction of the tensile load (longitudinal) and  $\sigma_2$  is positive. Therefore, the state of stress will be very close to what is diagrammatically shown in fig. 16a. From fig. 16a it follows that in the case of plane stress the maximum shear stress at the crack tip is at planes making an angle of  $45^\circ$  with the sheet surface. In the case of plane strain the maximum shear stress is at planes perpendicular to the sheet surface, but making an angle of about  $45^\circ$  with the loading direction (see also fig. 16b).

Since shear stresses are responsible for (initiation

and) growth of voids this will lead to void concentrations at different planes in the two cases (fig. 16c). The crack follows a path through the regions with the largest void concentrations, which leads to a square fracture in the case of plane strain and to a slant fracture in the case of plane stress (fig. 16c).

### 5 The influence of thickness on residual strength

Considering now the influence of thickness on the fracture strength, two things have to be explained:

- a. A lower strength in the case when plane strain dominates at the crack tip than in the case where there is a state of plane stress.
- b. A lower strength of sheets thinner than the optimum thickness.

A tentative explanation can be offered for item *a*, but only some speculations can be made on item *b*. Therefore, item *b* will be only briefly considered at the end of this section.

In the previous sections it has been pointed out that void initiation and void growth is a result of slip and as such is governed by shear stresses. It was further shown why the largest void concentrations occur on different planes in the case of plane stress and the case of plane strain.

It may be concluded from fig. 12 that the mechanisms of void coalescence are dominated by tensile stresses. Of course, void coalescence in itself will probably still be a slip mechanism, but in planes of large void concentration the stress distribution will be very complicated and from fig. 12, which is based on electron-microscopical observations, it must be concluded that the shear stresses responsible for void coalescence are governed by the tensile stress acting on the plane of largest void concentration. Then it must be concluded that void coalescence and, hence, crack growth are governed by this tensile stress.

This point of view is confirmed by results obtained from specimens with blunted crack tips (ref. 1) and from tests with interrupted loading (ref. 29). These tests indicated that crack growth is governed by the tensile stress at the crack tip, but that crack growth is slow and stable as long as the released energy is balanced by the energy consumed in crack growth. Fracture instability occurs when the energy released during crack extension is larger than the energy consumed in crack extension (refs. 20, 21) (the latter energy is necessary for plastic deformations and void growth by slip).

Using these arguments a tentative explanation can be given for the influence of sheet thickness on fracture toughness. Consider fig. 17. In the lower line of this figure five specimens are compared of thicknesses  $t_1$ - $t_5$ . All specimens are loaded to the same nominal stress  $\sigma_a$ . In all specimens the planes of largest void concentration are indicated (see also fig. 16). Also the

size of the plastic zone is indicated, which for a certain nominal stress is roughly twice as large in the case of plane stress as in the case of plane strain (ref. 17). As can be seen from fig. 16a the tensile stress on the plane of largest void concentration is smaller in the case of plane stress ( $\sigma_p$ ) than in the case of plane strain ( $\sigma_q$ ). This indicates that crack growth and eventually fracture will occur in specimens  $t_4$  and  $t_5$  and not yet in specimens  $t_1$  and  $t_2$ . The specimen  $t_3$ , where plane stress occupies a relatively large fraction of the thickness, will be at an intermediate stage.

The stress in specimens  $t_1$  and  $t_2$  can still be increased, since the tensile stress on the plane of maximum void concentration is not yet critical.

It is felt that these considerations give a reasonable explanation for the lower fracture strength in the case of plane strain than in the case of plane stress.

As for the maximum in the strength curve (i.e. the lower strength of the very thin sheets) it might be believed that this is due to the fact that the normal tensile strength of unnotched test coupons is somewhat lower for the thin sheets (compare the strength values in the table in sec. 2), though this latter effect could very well be due to the same cause as the lower fracture toughness of the thin sheet. A speculative explanation can be given when it is assumed that the distribution of plastic strain is the same in specimens  $t_1$  and  $t_2$  (fig. 17). Then also the distribution and size of the voids are the same and then it can be understood that the critical plane in specimen  $t_1$  will be somewhat earlier 'filled in' with voids than in specimen  $t_2$  (Fig. 17).

It might be argued that fig. 2 is a serious objection against the previous reasoning, since beyond the optimum thickness hardly any influence of thickness was found on the stress to initiate crack growth. Two arguments should be kept in mind, however:

- a. Fig. 2 concerns only a small range of thickness.
- b. The values for  $\sigma_i$  were obtained from film records, which are difficult to interpret due to the presence of a plastic zone at the crack tip, and which are increasingly in error as the specimens are thicker. This is because crack propagation starts at mid-thickness and especially in thick specimens the crack may tunnel appreciably. This could be observed indirectly in the specimens used for compiling fig. 4, where pop-in and cracking could be heard as an indication of crack growth far before crack growth was observed at the surface of the specimen.

### 6 The criterion for the transition of the state of stress

As a result of the previous considerations one might feel a temptation to speculate on a criterion for the fracture mode transition and for the maximum in the strength curve, which of course should be a criterion for the transition of the state of stress. Different authors

(refs. 4, 18, 22) have proposed more or less the same criterion, stating that plane stress will be constrained until the width of the plastic zone at the crack tip is at least equal to the plate thickness.

A criterion based on the size of the plastic zone is probably found. At the same nominal stress a plane stress plastic zone is roughly twice as large as a plane strain plastic zone (ref. 17). Hence, in thick specimens where the state of stress changes from plane strain in the interior of the specimen to plane stress at the surface, the size of the plastic zone cannot properly be defined. The presence of plane stress at the surface of the specimen could lead one to expect that full plane stress might occur already when the size of the plane strain plastic zone is still appreciably smaller than the sheet thickness.

According to ref. 17 the width  $r_p$  of the plastic zone is equal to  $r_p = C(\sigma^2/\sigma_y^2)l$ , where  $\sigma$  is the nominal gross section stress,  $\sigma_y$  the yield stress and  $l$  the semi-crack length. The value of  $C$  is about 0.3 for plane strain and about 0.6 for plane stress.

Now, consider the data for the 2014 alloy in fig. 4 and assume that the specimen of 20 mm thickness was the first to have almost completely plane strain through the thickness. (In thinner specimens the slant fraction is appreciably larger). This specimen fractured at a stress of 22 kg/mm<sup>2</sup>. Then the size of the plastic zone was  $r_p \approx 0.3 \cdot (22^2 \cdot 15)/40^2 = 1.35$  mm. Fully slant fractures (maximum of strength curve) occurred at 2 mm thickness, i.e. in a 2 mm sheet full plane stress could develop.

This leads to the conclusion that plane stress can develop at  $r_p \approx 1.35/2 = 0.7 t$  ( $t$  = sheet thickness).

A suitable set of data to check this point is available for the  $\beta$ -titanium alloy in fig. 7. Assuming fully plane strain at  $t = 2.5$  mm gives a critical plane strain plastic zone size of  $r_p \approx 0.22$  mm. Then plane stress would occur at  $t \leq 0.3$  mm, which is in good agreement with the data (100% slant fracture at  $t = 0.3$  mm).

In conclusion, it can be said that the criteria of refs. (4, 18, 22) for the transition in the state of stress and the fracture mode are in reasonable agreement with test results.

## 7 Conclusions

From an experimental investigation of the effect of specimen thickness on the fracture toughness of aluminium alloy specimens with central cracks the following conclusions can be drawn.

a. The fracture strength as a function of thickness shows a maximum at a particular thickness. Closely related to this phenomenon is the mode of fracture. Specimens thinner than the optimum thickness show slant fractures, whereas thicker specimens show square fractures with shear lips.

- b. The observations mentioned sub *a* are a consequence of the state of stress at the crack tip, which is plane strain in thick plates, but develops into plane stress in thin sheets.
- c. Crack growth is a result of initiation, growth and coalescence of microvoids. Micro-void initiation and growth are slip mechanisms.
- d. The largest concentration of voids occurs on planes that have different orientations in the case of plane stress and in the case of plane strain. This can explain the fracture mode transition.
- e. The coalescence of micro-voids to a crack is probably governed by the tensile stress acting on the plane of maximum void concentrations. This can explain why plane strain fractures occur at lower gross stresses than plane stress fractures.
- f. Conclusion *e* confirms results of previous investigations (refs. 1, 21) which indicate that crack growth is governed by the tensile stress at the crack tip, but fracture cannot occur as long as there is a balance of released and consumed energy. Fracture instability is governed by an energy criterion and it occurs when more energy is released than consumed in crack extension.
- g. The criterion based on the size of the plastic zone for the transition from plane strain to plane stress, as presented by various authors, is probably correct.

## 8 References

- <sup>1</sup> BROEK, D., The residual strength of aluminium alloy sheet specimens containing fatigue cracks or saw cuts. NLR report TN-M.2143, Febr. 1965.
- <sup>2</sup> CHRISTENSEN, R.H., DENKE, P.H., Crack strength and crack propagation characteristics of high strength metals. Techn. Doc. Rep. ASD. TR-61-207, Jan. 1962.
- <sup>3</sup> HARPUR, N.F., Crack propagation and residual strength characteristics of some aircraft structural materials. Proc. of the Crack-propagation symposium, Cranfield, 1961, Vol. II, pp. 442-466.
- <sup>4</sup> IRWIN, G.R., Fracture mode transition for a crack traversing a plate. ASME Trans., J. of Basic Engineering 82 (June 1960) pp. 417-425.
- <sup>5</sup> REPKO, R.J., JONES, M.H., BROWN, W.F., Influence of sheet thickness on sharp-edge notch properties of a  $\beta$ -titanium alloy at room and low temperatures. Symposium on evaluation of metallic materials in design for low-temperature service. A.S.T.M. S.T.P. No. 302 (1962) pp. 213-229.
- <sup>6</sup> SRAWLEY, J.E., BROWN, W.F. Fracture toughness testing. NASA TN D-2599, January 1965.
- <sup>7</sup> BEACHEM, C.D., Electron fractographic studies of mechanical fracture processes in metals. ASME Trans., J. of Basic Engng 87 D, 2, (June 1965)
- <sup>8</sup> BEACHEM, C.D., An electron fractographic study of the mechanisms of ductile rupture in metals. U.S. Naval Res. Lab. Report 5871, Dec. 1962.
- <sup>9</sup> BEACHEM, C.D., MEYN, D.A., Illustrated glossary of fractographic terms. Section 2. U.S. Naval Res. Lab. Memorandum Report 1547, June 1964.

<sup>10</sup> BEACHEM, C.D., An electron fractographic study of the influence of plastic strain conditions upon ductile rupture processes in metals A.S.M. Trans. Quarterly 56, 3 (Sept. 1963) pp. 318-326.

<sup>11</sup> BEACHEM, C.D., PELLOUX, R.M.N., Electron fractography - A tool for the study of micromechanisms of fracturing processes. A.S.T.M. Spec. Techn. Publ. No. 381, pp. 210-245 (1965).

<sup>12</sup> PELLOUX, R.M.N., The analysis of fracture surfaces by electron microscopy. Metals Engng Quarterly 5, 4 (Nov. 1965) pp. 26-37.

<sup>13</sup> CRUSSARD, C., PLATEAU, J., TAMHANKAR, R., HENRY, G., LAJEUNESSE, D., A comparison of ductile and fatigue fracture. Fracture, Proceedings of the Swampscott Conference (1959) pp. 524-561. John Wiley and Sons, N.Y.

<sup>14</sup> BRAGG, L., NIJE, J.F., A dynamical model of a crystal structure. Proc. Roy. Soc. A. Vol. 190 (1948) pp. 474-481.

<sup>15</sup> STROH, A.N. The formation of cracks as a result of plastic flow. Proc. Roy Soc. A, Vol. 223 (1954) p. 404 and Vol. 232 (1955) p. 548.

<sup>16</sup> COTTRELL, A.H. Theory of brittle fracture in steels and similar metals. AIME Trans., Vol. 212 (April 1958) pp. 192-203.

<sup>17</sup> SCHIJVE, J. Analysis of the fatigue phenomenon in aluminium alloys. NLR-Tech. Rep. M. 2122, April 1964.

<sup>18</sup> HAHN, G.T., ROSENFELD, A.R. Local yielding and extension of a crack under plane stress. Acta Metallurgica, 13, 3 (March 1965) pp. 293-306.

<sup>19</sup> BROEK, D. The residual strength of cracked sheet-Tests interrupted after intermediate slow crack growth. NLR Report TR M. 2145, July 1965.

<sup>20</sup> BROEK, D., The energy criterion for fracture of sheets containing cracks. Applied Materials Research, 4, 3 (July 1965) pp. 188-189

<sup>21</sup> BROEK, D. The effect of finite specimen width on the residual strength of light alloy sheet. NLR Report M. 2142, Sep. 1965.

<sup>22</sup> LIU, H.W. Discussion in Proceedings of the crack propagation Symposium at Cranfield, 1961. Vol. II, pp. 514-517. Cranfield The College of Aeronautics, 1962.

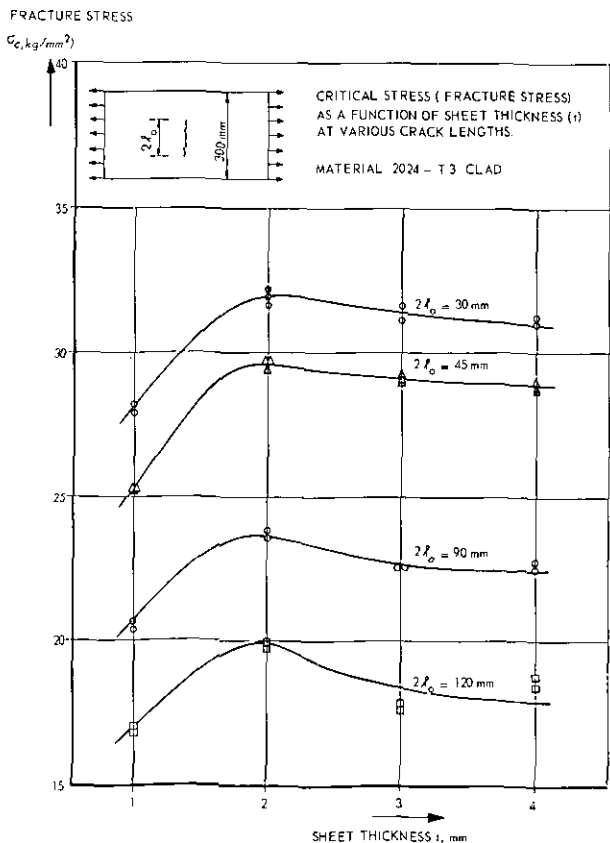


Fig. 1 Influence of sheet thickness on residual strength.

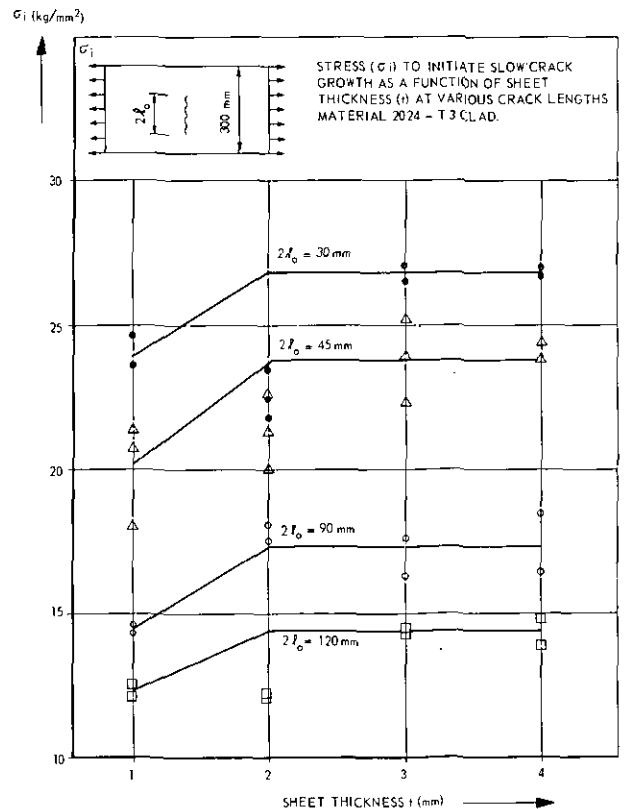


Fig. 2 The stress to initiate slow crack growth as a function of sheet thickness.

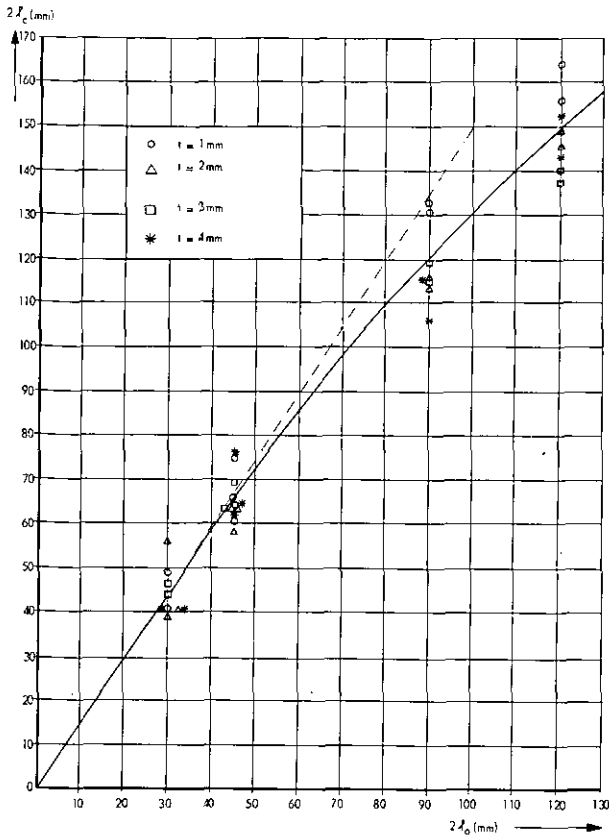


Fig. 3 Relation between critical crack length and initial crack length.

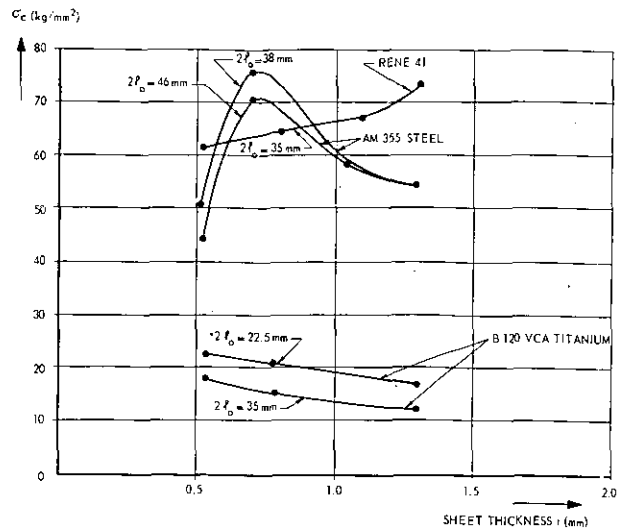


Fig. 5 Effect of sheet thickness as found by Christensen and Denke (ref. 2) in 150 mm wide specimens.

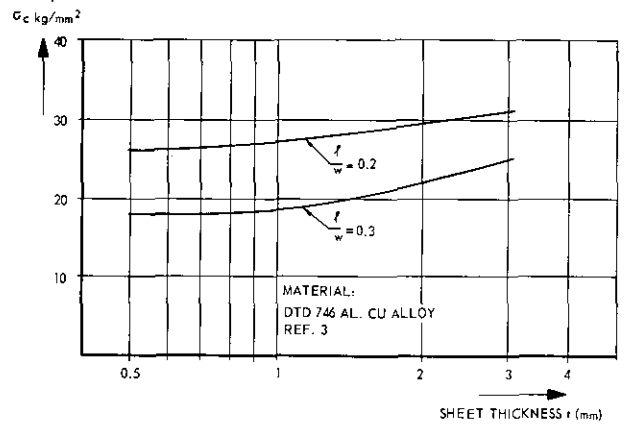


Fig. 6 Effect of thickness as found by Harpur (ref. 3).

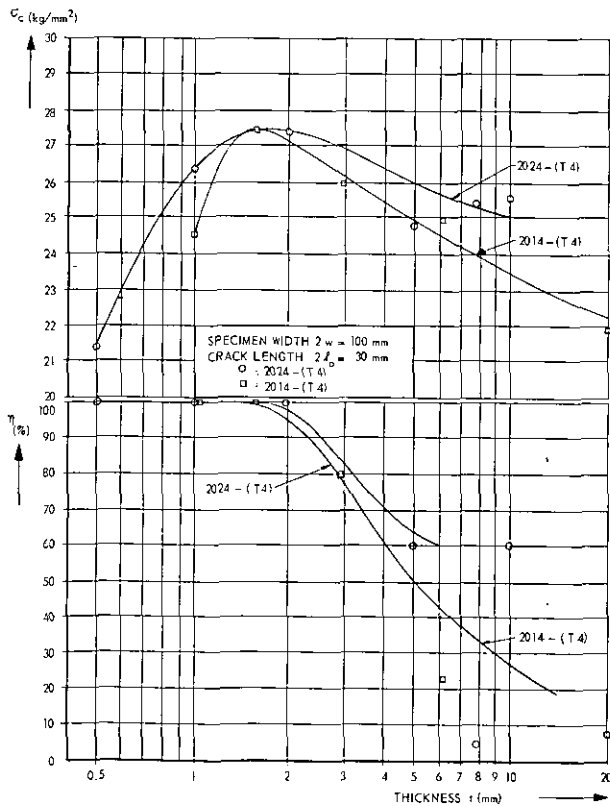


Fig. 4 Influence of thickness on residual strength and fracture mode

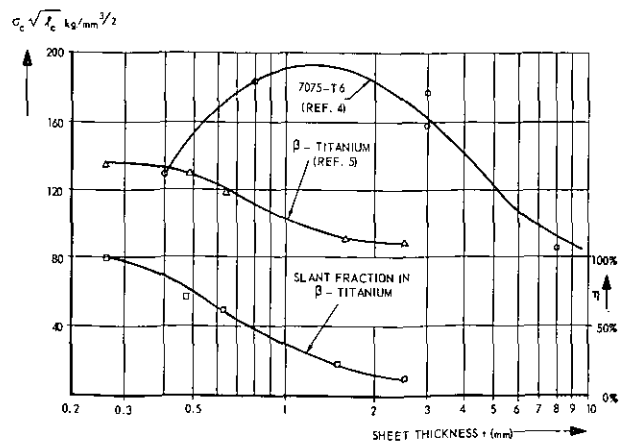


Fig. 7 Effect of thickness as found in refs. 4 and 5.

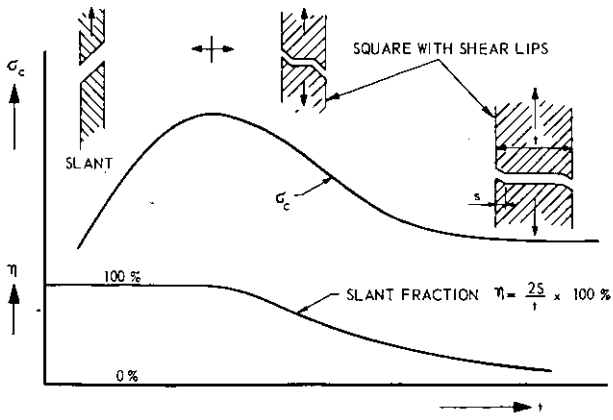


Fig. 8 Fracture appearance as affected by sheet thickness.

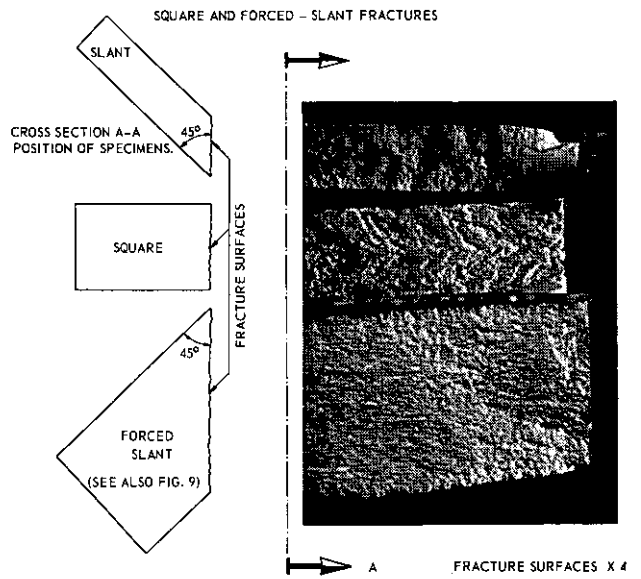
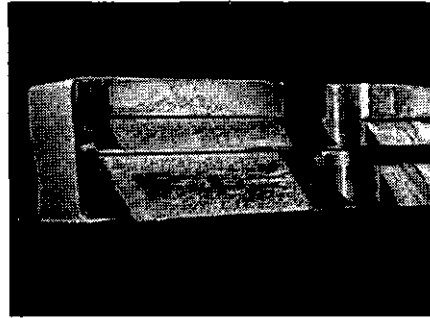
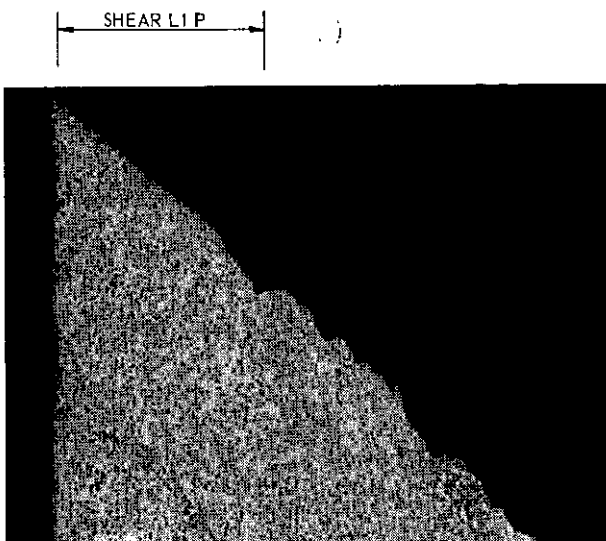
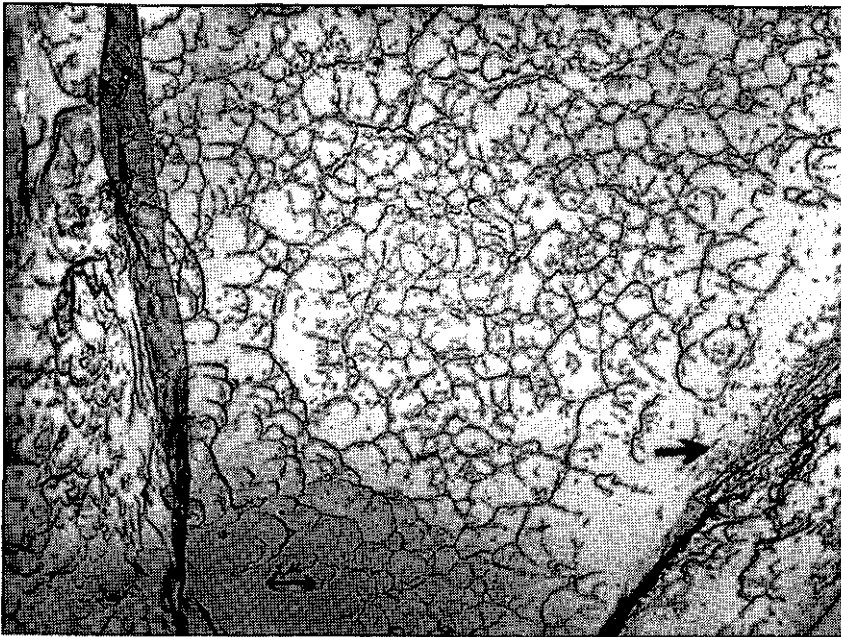


Fig. 10 Square, slant and forced-slant fractures (2024 material)



FRACTURE CONSISTS OF SQUARE PARTS, EXCEPT IN SHEAR LIP  
(SEE ALSO FIG. 10)

Fig. 9 Forced slant fracture; cross section  $\times 50$ .



ELECTRON MICROGRAPH  
X 6000  
ARROW POINTS TO  
SMOOTHED SLIP STEPS.



a. FORCED SLANT FRACTURE



ELECTRON MICROGRAPH  
X 6000  
A. INTERMETALLIC  
PARTICLE, THE CAUSE  
OF A LARGE VOID.

B AND C VOIDS OPENED  
UP BY TEARING  
(REF. 9), SEE SKETCH



D. SMOOTHED SLIP STEPS.

b. SQUARE FRACTURE.

Fig. 11 Fracture surfaces.

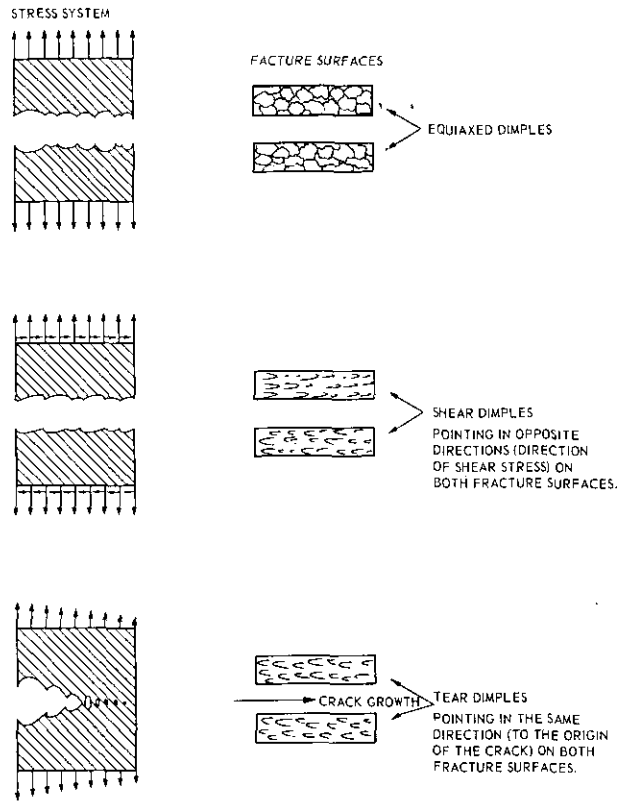
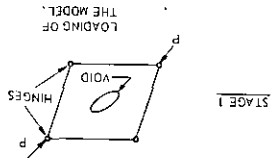
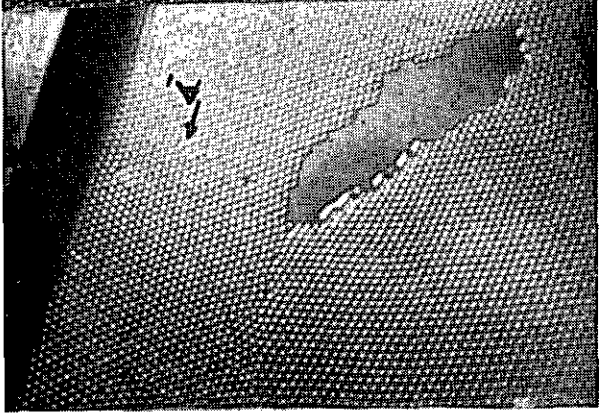


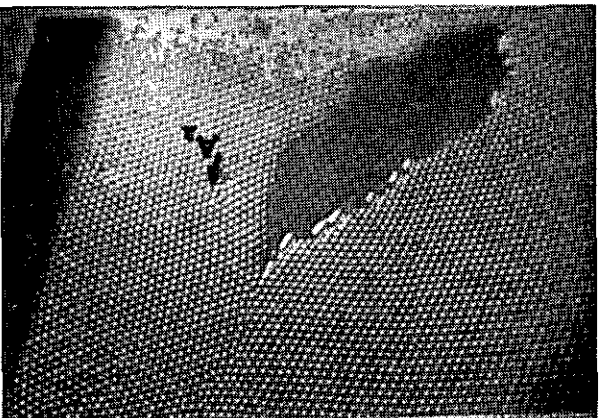
Fig. 12 Mechanisms of micro-void coalescence after Beachem (refs. 7-11).



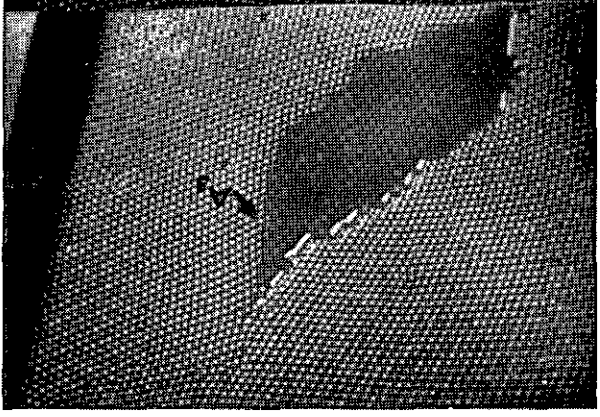
NOTE DISLOCATION AT ARROW A WHICH WILL RUN INTO THE VOID, (SEE ALSO FIG. 15)



STAGE 2  
DISLOCATION MENTIONED ABOVE IS NOW JUST ABOVE THE VACANCY (ARROW A<sub>2</sub>)



STAGE 3  
DISLOCATION MENTIONED ABOVE HAS RUN INTO THE VOID AND HAS FORMED A SLIP STEP AT A<sub>3</sub> (COMPARE WITH STAGE 2)



STAGE 4  
VOID GROWTH AND BLUNTING OF TIP DUE TO SLIP. DISLOCATION AT ARROW B WAS EMITTED FROM THE VOID TIP AND DISLOCATION AT ARROW C IS UP TO RUN INTO THE VOID. AT THE LEFT OF THE VOID (IN THE MIDDLE OF THE PICTURE) A DISLOCATION HAS JUST BEEN EMITTED.



Fig. 13 Void growth in a bubble raft model.





## REPORT TR M.2162

# The fatigue crack propagation in 2024-T3 Alclad sheet materials from seven different manufacturers

by

J. SCHIJVE AND P. DE RIJK

## Summary

Constant-amplitude and program tests were carried out at  $S_m = 7 \text{ kg/mm}^2$  and  $S_a = 2.5, 4$  and  $6.5 \text{ kg/mm}^2$ . Sheet specimens were loaded parallel and transverse to the rolling direction. Two materials were also tested with additional heat treatments. Various comparisons between the crack growth data are made, including a batch to batch variation. Additional measurements are concerned with static properties, chemical composition, data on grains and inclusions, electrical conductivity and fractographic observations. The discussion is concerned with correlation between the crack growth results and other material properties, technical implications of the results and improvements of the 2024-alloy.

Contents	Page	5.3 Some comments on fatigue crack propagation in 2024-T3.	Page
List of symbols and units.	1	6 Conclusions.	15
1 Introduction.	2	7 References.	16
2 Experimental details.	2	6 Tables.	
2.1 Survey of the tests.	2	16 Figures.	
2.2 Materials tested.	2	Appendix A: Crack propagation records.	
2.3 Testing procedures.	3	(1 page, 10 tables).	
3 Test results	3	<b>List of symbols and units</b>	
3.1 Crack propagation data.	3	$\delta$ elongation	
3.2 Damage calculations.	6	$S_{0.2}$ 0.2% yield stress	} of material
3.3 The microscopic structures.	7	$S_u$ ultimate stress	
3.4 Fractographic observations.	8	$S$ stress	} gross stress in test specimen
3.4.1 The transition.	8	$S_a$ stress amplitude	
3.4.2 Growth lines.	9	$S_m$ mean stress	
3.4.3 Inclusions.	10	$H_V$ Vickers hardness	
3.5 Measurements of the electrical conductivity.	11	$l$ half length of crack, see fig. 2	
4 Results from other investigations.	11	$l_{tr}$ crack length $l$ at the completion of the transition from the tensile mode fracture to the shear mode	
4.1 The effect of the manufacture on the crack propagation properties.	11	$n$ number of load cycles	
4.2 The batch to batch variation of the crack propagation properties.	12	$dl/dn$ crack rate	
4.3 The effect of the rolling direction on the crack propagation.	13	$n_t$ number of cycles to reach a crack length $l$	
5 Discussion.	13	$t$ sheet thickness	
5.1 Introduction.	13	$\text{kg/mm}^2$ $1 \text{ kg/mm}^2 = 1422 \text{ psi}$ ( $1000 \text{ psi} = 0.703 \text{ kg/mm}^2$ )	
5.2 Practical aspects of the present results.	13	$\text{mm}$ $1 \text{ mm} = 0.04 \text{ inch}$ ( $1 \text{ inch} = 25.4 \text{ mm}$ )	
		$\mu$ micron, $1 \text{ mm} = 1000 \mu$	
		$\text{kc}$ kilocycle = 1000 cycles	
		$\text{cpm}$ cycles per minute	

This investigation has been performed under contract with the Netherlands Aircraft Development Board (NIV).

## 1 Introduction

The NLR has carried out several test series concerning fatigue crack propagation in aluminum alloy sheet material. The purpose of the tests was to indicate the possible influences of several variables, such as mean stress, type of alloy, heat treatment, frequency, environment, sheet thickness and sheet width. It turned out from some of these test series that crack propagation in nominally identical material from different manufacturers could be systematically different. This finding initiated the present test series.

Sheet material of the alloy 2024-T3 Alclad with a thickness of 2 mm was procured from 7 different manufacturers. Comparative crack propagation tests were carried out on sheet specimens loaded parallel to the rolling direction and also on specimens loaded transverse to the rolling directions. For two manufacturers data were available for sheets from two different batches. Some data for other heat treatment conditions than the T3 condition were also available.

Tests were carried out at a mean stress of  $7 \text{ kg/mm}^2$  (10 ksi) and three values of the stress amplitude. Program tests employing the three amplitudes were also performed. The crack propagation results and various comparisons are presented in this report. The prime purpose was to compare crack propagation rates in sheet material from different manufacturers and to determine any directionality effect on the crack rate. Since the crack rates in the sheet material from one manufacturer were consistently lower than for the other materials, it was tried to explore the possible cause of this finding. For this purpose microscopic and fractographic observations were made. Attention is drawn to relevant information from the literature. In the discussion of the results several implications of the present investigation are mentioned.

## 2 Experimental details

### 2.1 Survey of the tests

A survey of the present test series is given in table 1. The manufacturers and their materials are indicated by capitals A to G. Specimens loaded transverse to the rolling direction were tested with constant-amplitude loading only. Program tests were restricted to specimens loaded parallel to the rolling direction.

Comparisons can be made (1) between sheets from different manufacturers, (2) between the results for specimens loaded parallel and transverse to the rolling direction and (3) between constant-amplitude and program loading (damage calculations).

Sheet materials of manufacturers B and E were also tested after some additional heat treatments, see table 1. Sheet materials of manufacturers C and F were used in previous NLR crack propagation tests. Hence it was

possible to study the effects of the additional heat treatments and a batch to batch variation.

### 2.2 Materials tested

Sheet material according to specifications for 2024-T3 Alclad was obtained from 7 different manufacturers, namely 3 from the United States and one from England, France, Germany and the Netherlands respectively. The manufacturers as well as their sheet materials are indicated by capitals A to G. The nominal thickness of the sheets was 2 mm except for material B which was slightly thicker, namely 2.4 instead of 2 mm.

Material B was also given an additional temperature cycle, consisting of 3 hours at  $170^\circ\text{C}$  (see table 7). This corresponds to an extreme adhesive curing cycle. The material is then indicated by B'. Specimens of B and B' were cut from the same sheet. Sheets with an artificial aging were obtained from manufacturer E (see table 1). Material E'', which corresponds to 2024-T81, was aged at  $190^\circ\text{C}$  for 9 hours. Material E' was aged for 6 hours at the same temperature, which is not long enough to reach the T8 condition. Materials E' and E'' are from the same batch, material E was from another batch.

All specimens from one manufacturer and with the same heat treatment were cut from the same sheet, that means that specimens loaded parallel or transverse to the rolling direction originated from the same sheet.

The chemical composition was checked for six materials by X-ray fluorescence analysis. The measurements were made at the Metals Institute TNO at Delft. The results are presented in table 2, which shows little variation between the materials and in general a good agreement with the composition limits mentioned in the Metals Handbook of the American Society for Metals. The copper contents of materials A and C are fairly high. Although the absolute contents for chromium are unknown it appears that material F contains more of this element than the other materials.

The results of tensile tests and hardness measurements have been compiled in table 3. All properties were determined for specimens located parallel and transverse to the rolling direction. The table shows that there is little variation between the materials A-G, when comparing the ultimate strength and the elongation. With respect to the yield stress and the hardness, material E is slightly above the average and material B is clearly beyond it. The ratio  $S_{0.2}/S_u$  is relatively high for material B. It is thought that the extreme data for material B are due to a fairly high amount of stretching, applied by the manufacturer for flattening after quenching.

In agreement with the temperature cycles the static strength properties for materials B', E' and E'' were raised accordingly while the elongation decreased.

The directionality of the sheet materials is illustrated

by the ratios between the properties in the longitudinal and the transverse directions of the sheets. The directionality is the most pronounced for the yield stress, but even in that case it is quite moderate (average ratio 0.90).

### 2.3 Testing procedures

The mean stress in all tests was  $S_m = 7.0 \text{ kg/mm}^2$  (10.0 ksi). Three values of the stress amplitude were adopted in both the constant-amplitude tests and the program tests, viz.  $S_a = 2.5, 4.0$  and  $6.5 \text{ kg/mm}^2$  (3.6, 5.7 and 9.3 ksi, respectively). The load sequence for one period of the program tests is shown in fig. 1. This period was repeated until failure.

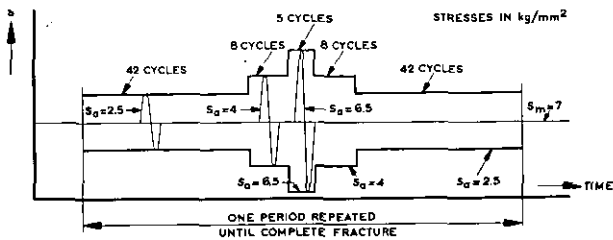


Fig. 1 Load sequence in the program tests.

All constant-amplitude tests were carried out on a vertical Schenck pulsator (PVQ 002S, resonance machine) at a frequency of about 3200 cpm. The program tests were performed on a horizontal Schenck pulsator (PP6D) equipped with a quick drive (resonance) and a slow drive (reversible screw drive). The slow drive had to be used in order to apply a program as indicated in figure 1. The machine was modified for the program tests by installing three pairs of limit switches instead of one. The selection of the pairs was made by the small Amsler programming apparatus belonging to the Amsler Vibraphore. Since this implied a programming of time spent at the three load levels the actual numbers of cycles could deviate slightly from the average numbers indicated in fig. 1. The question whether the first or the last half cycle of a load level was a positive or a negative load increment (relative to the mean load) was a matter of chance. The frequencies for the three amplitudes were about 18, 11 and 7.5 cpm. The nominal capacities of the two Schenck machines were the same, namely 6 tons.

The specimens were cut to a size of  $160 \times 400 \text{ mm}$  ( $6.3'' \times 15.7''$ ) and provided with a small central notch for crack initiation, see fig. 2. This type of specimen was used in several previous NLR investigations. Fine line markings were inscribed on the surface for facilitating the recording of the crack propagation. During the constant-amplitude tests the number of applied cycles was noted each time that a tip of a crack reached a line marking. The program tests required a long testing time due to the low frequency. Recording of the

crack growth was made automatically by taking pictures of the crack at specific intervals, a usual period being 3 hours. A Robot camera was used for this purpose. The cycle counter of the fatigue machine was simultaneously photographed. Pictures were taken when the load was at its maximum to obtain a maximum of crack opening. The crack propagation data were deduced from the film after completion of the tests.

The specimens for the program tests were precracked with the quick drive of the fatigue machine at  $S_m = 7 \text{ kg/mm}^2$  and  $S_a = 4 \text{ kg/mm}^2$  until the half length of the crack was slightly smaller than 5 mm. Propagation records during program loading were made from  $l = 5 \text{ mm}$  onwards.

The majority of tests were carried out three times. The program tests were performed in duplicate in view of their long duration. Also tests with the loading transverse to the rolling direction could be carried out only twice for some materials due to insufficient sheet material being available.

## 3 Test results

### 3.1 Crack propagation data

The central notch initiated two cracks, which are considered as one crack with a half length  $l$  defined by  $2l = l_1 + l_2 = \text{length from tip to tip}$ , see fig. 2. The differences between  $l_1$  and  $l_2$  were always small. The crack propagation data for all specimens have been compiled in Appendix A. Average crack propagation

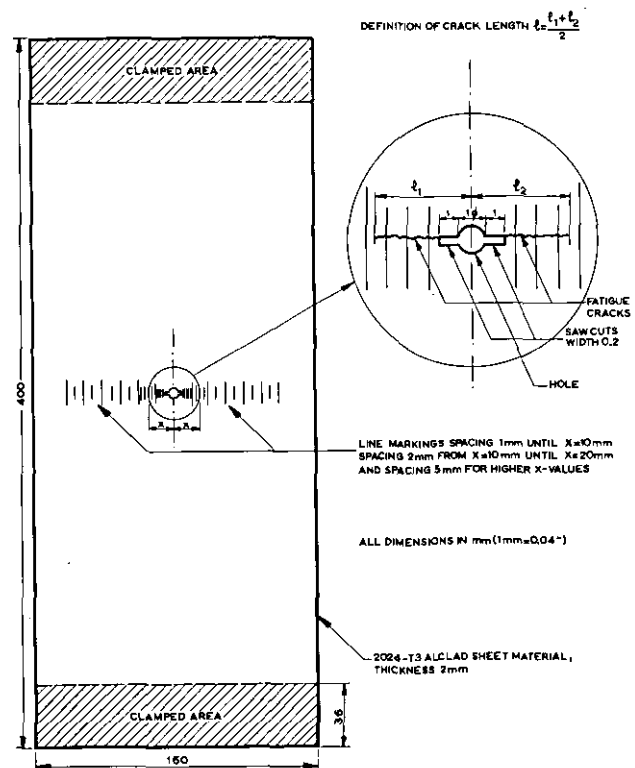


Fig. 2 Sheet specimen for crack propagation.

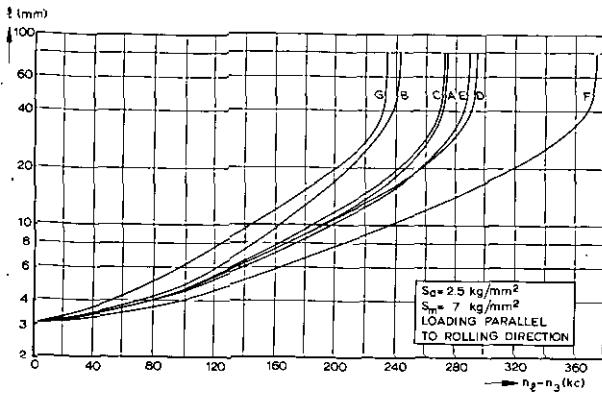


Fig. 3a Crack propagation curves for 2024-T3 Alclad ( $t = 2$  mm) from seven different manufacturers (A-G). Loading parallel to the rolling direction.

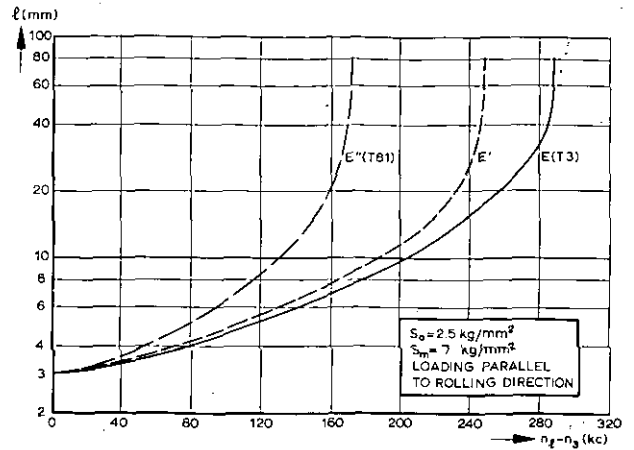


Fig. 4a Crack propagation curves for 2024-T3 Alclad ( $t = 2$  mm) from manufacturer E in three different conditions.

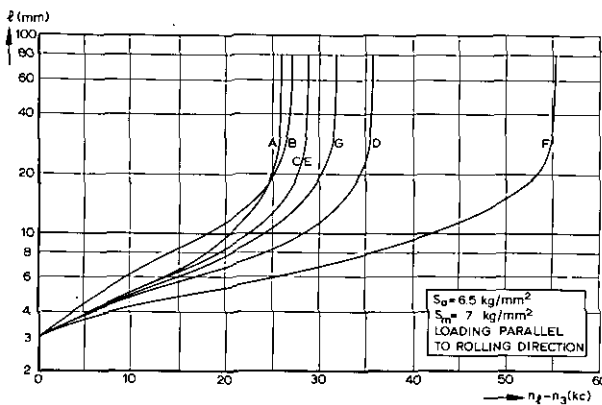


Fig. 3c

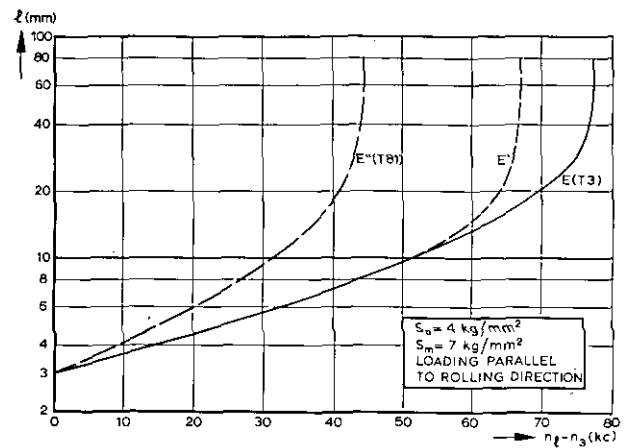


Fig. 4b

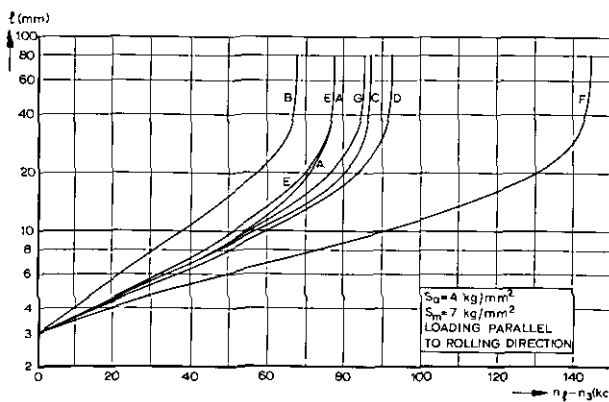


Fig. 3b

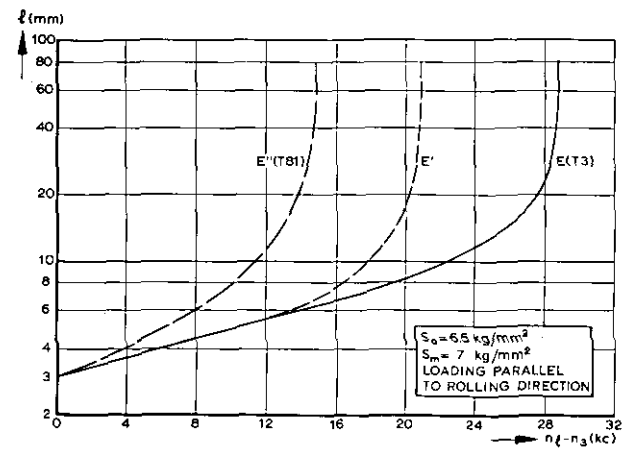


Fig. 4c

curves for each group of similarly tested specimens are presented in figs 3-6 except for the constant-amplitude tests on material B'. For the latter material the curves almost coincide with those for material B.

Figs 3, 5 and 6 show that material F was superior to all the other materials for all loading cases. Materials A and B generally were among the more inferior materials. Fig. 11 shows the effect of different heat treatments for material E of manufacturer E. For

material B the two heat treatments (B and B', see table 1) yielded almost the same results, in the constant-amplitude tests as well as in the program tests (see fig. 6).

For a more detailed comparison the crack propagation was split up in three intervals, namely  $l = 3-8$  mm,  $l = 8-16$  mm and  $l = 16-80$  mm. The last interval terminated by complete fracture of the specimen. The crack propagation lives for the three intervals are

Fig. 5 Crack propagation curves for 2024-T3 Alclad ( $t=2$  mm) from six different manufacturers. Loading transverse to the rolling direction.

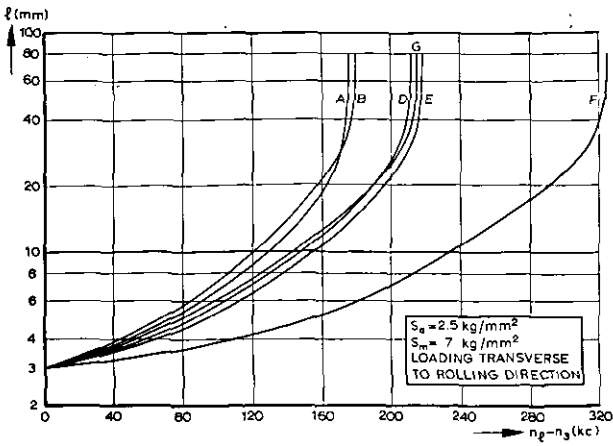


Fig. 5a

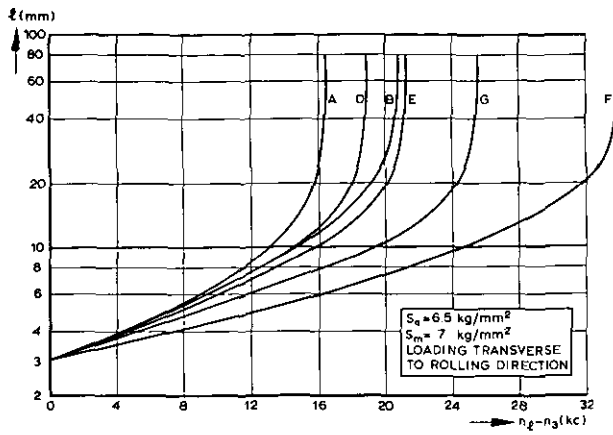


Fig. 5c

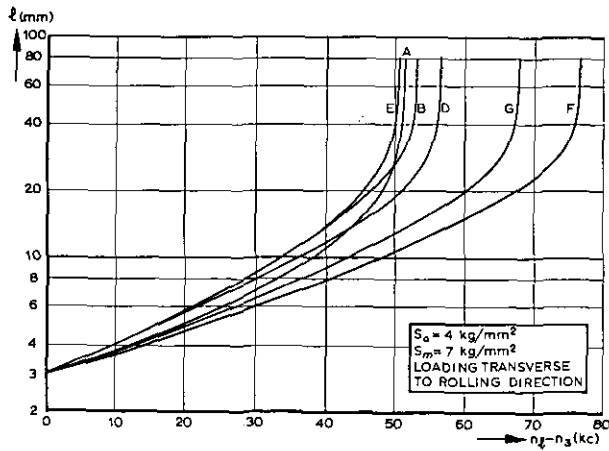


Fig. 5b

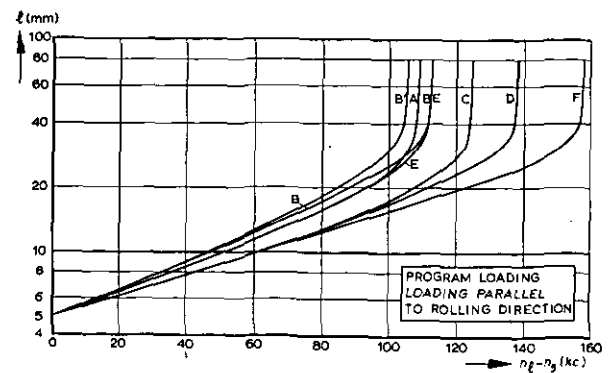


Fig. 6 Crack propagation curves for 2024-T3 Alclad ( $t=2$  mm) from six different manufacturers (A-F). Program Loading.

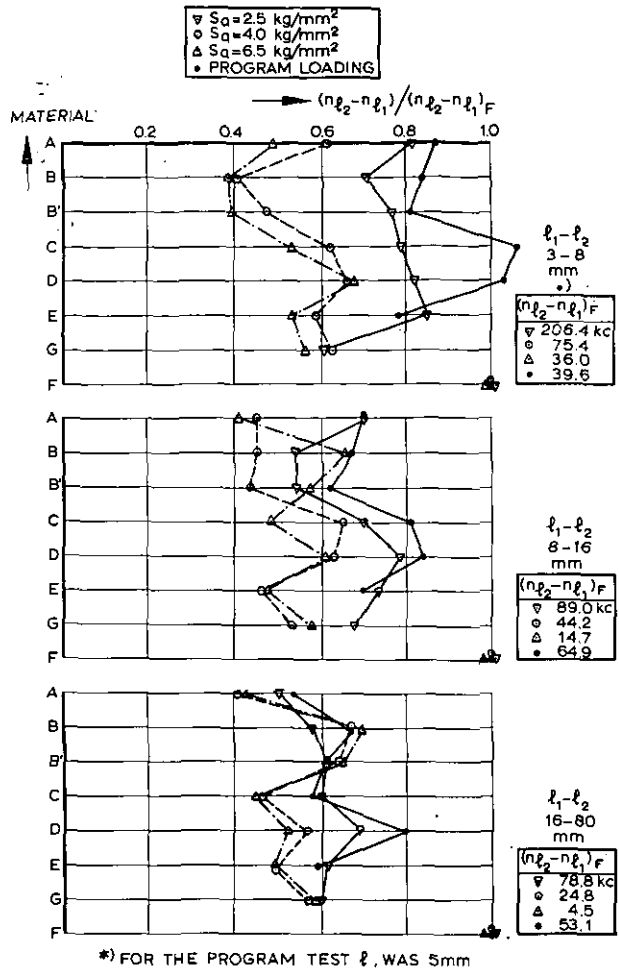


Fig. 7 Relative fatigue lives for three crack propagation intervals, loading parallel to the rolling direction.

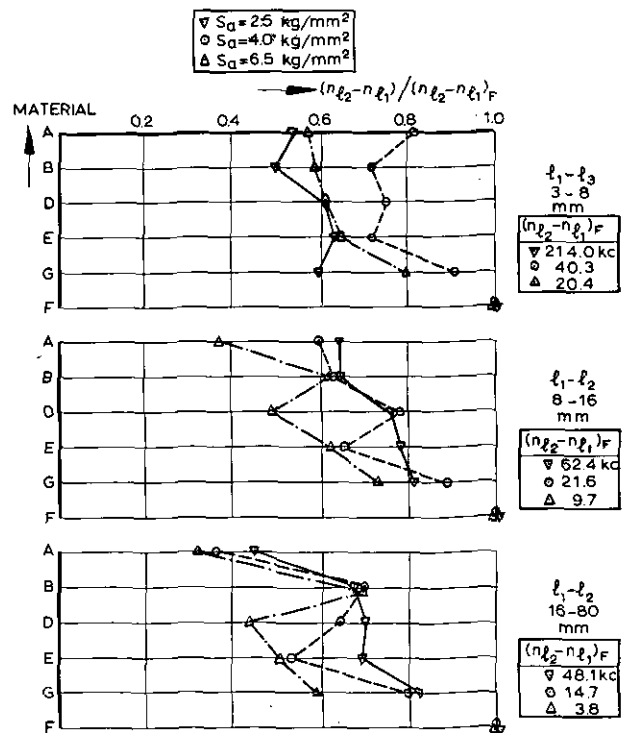


Fig. 8 Relative fatigue lives for three crack propagation intervals, loading transverse to rolling direction.

compared in figs. 7 and 8 for the two loading directions, respectively. The lives were divided by the lives for material F, thus making the results of material F equal to unity per definition. The two figures were drawn to permit a systematic effect of either the crack propagation interval or the stress amplitude to be noted. Such effects, however, are hardly indicated by figs. 7 and 8.

In fig. 9 a comparison is made between the crack propagation lives for specimens loaded transverse and parallel to the loading direction. The ratio of these two lives has been plotted. The comparison is made for the three crack propagation intervals mentioned above and for the three stress amplitudes. Fig. 9 again shows no

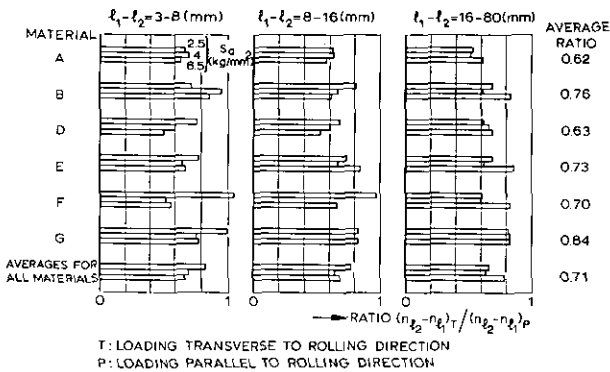


Fig. 9 Ratio's between the crack propagation lives of specimens loaded transverse and parallel to the loading direction.

systematic influence of the interval or the amplitude. The general trend of the figure is that the crack propagation lives are reduced to about 70% if the sheet material is loaded transverse to the loading direction instead of parallel to that direction. Stated in the reverse way: the life is about 40% longer if the material is loaded in the rolling direction as compared with the life for transversely loaded specimens.

The question how significant are the differences between the various materials is difficult to answer quantitatively. Although most tests were carried out three times, this number is rather small for indicating the statistical significance of small differences between two materials. For instance, the differences between materials C, A, E and D in fig. 3a are too small to be considered significant.

The differences between the various materials can be appreciated in another way by plotting the crack propagation lives as a function of the stress amplitude. This has been done in fig. 10 for the four materials A, B, D and F loaded parallel to the rolling direction. Material F is the most superior material, materials A and B were generally among the poorest materials, whereas material D was at an intermediate position. In fig. 10 straight lines were drawn between the three data points for  $S_a = 2.5, 4$  and  $6.5 \text{ kg/mm}^2$ . The figure illustrates that the differences in crack propagation lives correspond to considerable differences in crack

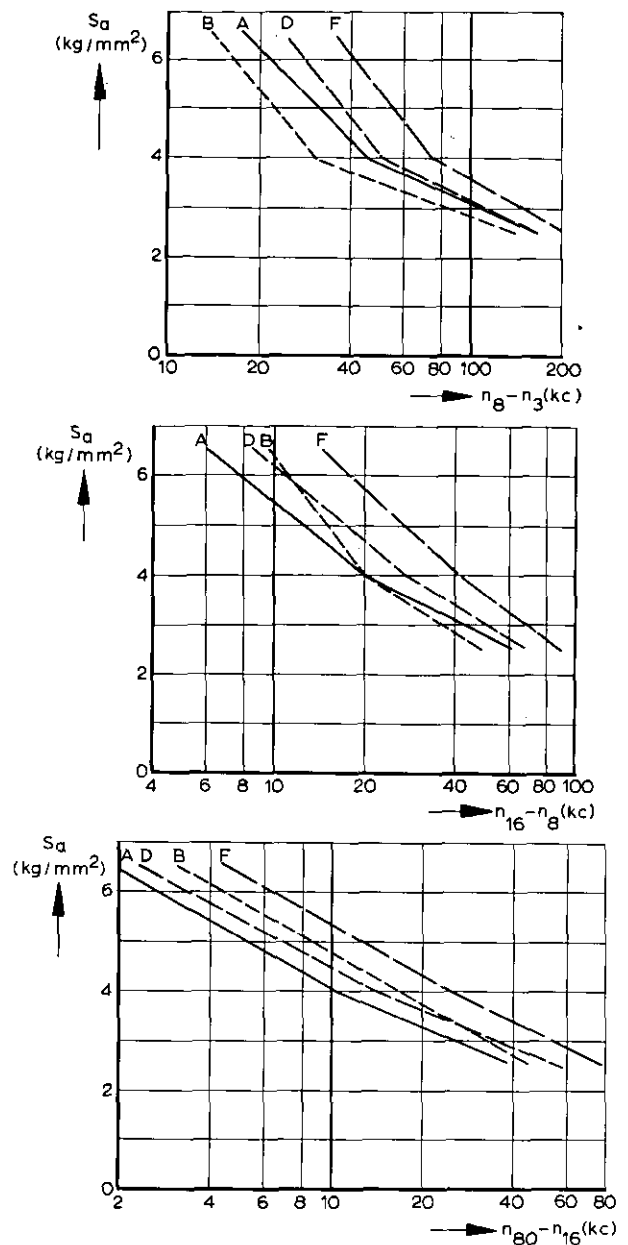


Fig. 10 The crack propagation lives as a function of the stress amplitude for three propagation intervals (loading parallel to rolling direction).

propagation strength and certainly cannot be due to inaccuracies of the fatigue load.

### 3.2 Damage calculations

For the program tests damage calculations were made for three crack propagation intervals, namely 5-8 mm, 8-16 mm and 16 mm to complete failure. The  $\Sigma n/N$ -values have been compiled in table 4. The  $N$ -values were taken from the average results in tables A1-A3 for the constant-amplitude tests.

Table 4 shows  $\Sigma n/N$ -values ranging from 0.72 to 1.94. It should be recognized that the  $N$ -values were obtained at a high loading frequency ( $\sim 3000 \text{ cpm}$ ) whereas the program tests were carried out at low frequencies (7.5 to 18 cpm). In a previous test series

(ref. 1) on material of manufacturer C the crack rate at the low frequencies was approximately 30% faster than at the high frequency. An indication of the frequency effect for material F can be obtained by comparing the results from two NLR investigations carried out at 2000 cpm and 15 cpm, respectively (refs 1 and 20). In both test series specimens cut from the same sheets were used. The same value for  $S_m$  was adopted (9 kg/mm<sup>2</sup>) but the  $S_a$ -values were different. The comparison of the results for the two frequencies is made in fig. 11. The graphs indicate that the crack rate at the low frequency was 45–85% faster than the crack rate at the high frequency. It thus appears that the frequency effect may be different for nominally identical materials from different manufacturers.

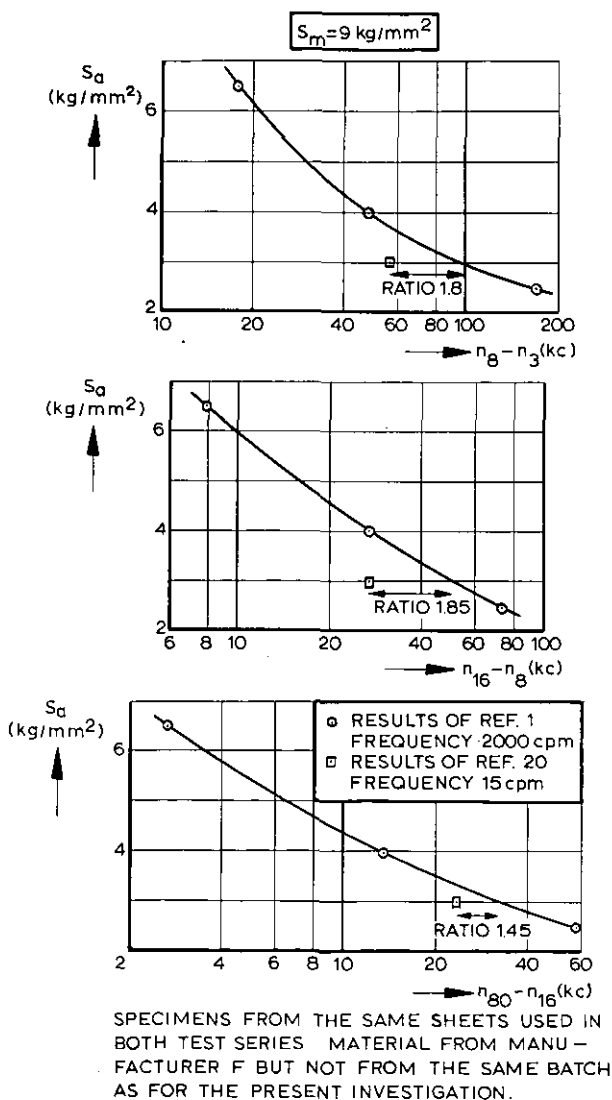


Fig. 11 The effect of the frequency on the crack propagation life for three propagation intervals.

As a consequence of the frequency effect the  $N$ -values adopted for the calculation of  $\Sigma n/N$  were too high. If the correct  $N$ -values had been available, it is expected that  $\Sigma n/N$ -values in the range from 1–3 would have been obtained. Values for  $\Sigma n/N$  were

found in a previous NLR test series on program loading (ref. 18).

It is noteworthy that table 4 does not show the same order of the results as the propagation data (fig. 7). The most striking feature is that material F shows the lowest  $\Sigma n/N$  values, whereas it was clearly superior in the constant-amplitude tests. This reflects the fact that its superiority in the program tests was less pronounced than in the constant-amplitude tests, see fig. 7.

### 3.3 The microstructures

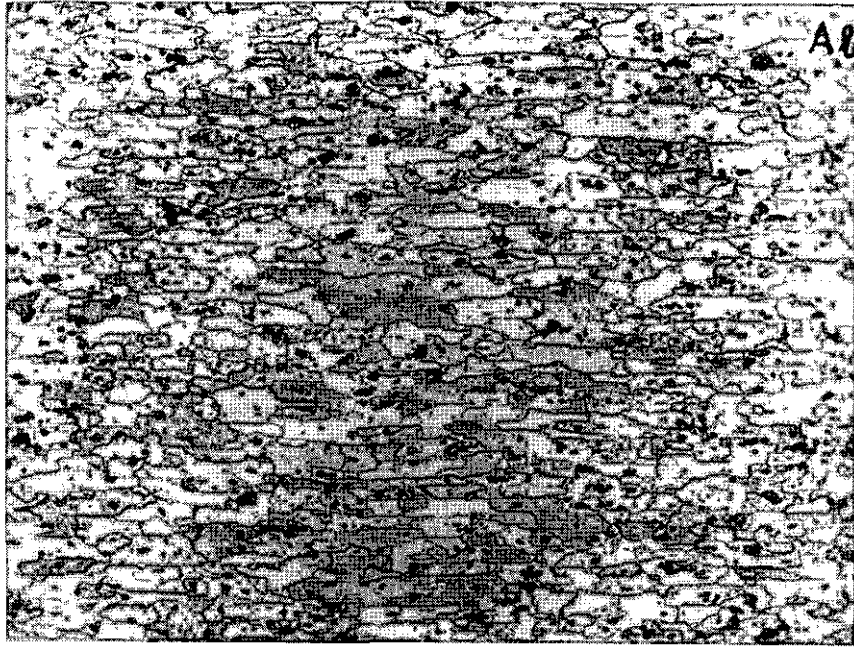
Specimens were prepared from the sheet materials for microscopic examination. Cross sections parallel and transverse to the rolling direction were polished and etched. The microscopic examination was concerned with grain size and shape, inclusions, and thickness of the cladding layer. The results are summarized in tables 5 and 6. The inclusions were observed on the polished but unetched specimens. The data regarding grain size and inclusions have to be regarded as estimates, lacking great accuracy.

In all materials the grains were flattened parallel to the sheet surface, as is usual for aluminum sheet material. The size of the grains varies considerably from one material to another. The largest grains were exhibited by material B and the smallest ones by material A. Micrographs from these materials are shown in fig. 12. There was no apparent correlation between the grain size and the crack propagation properties.

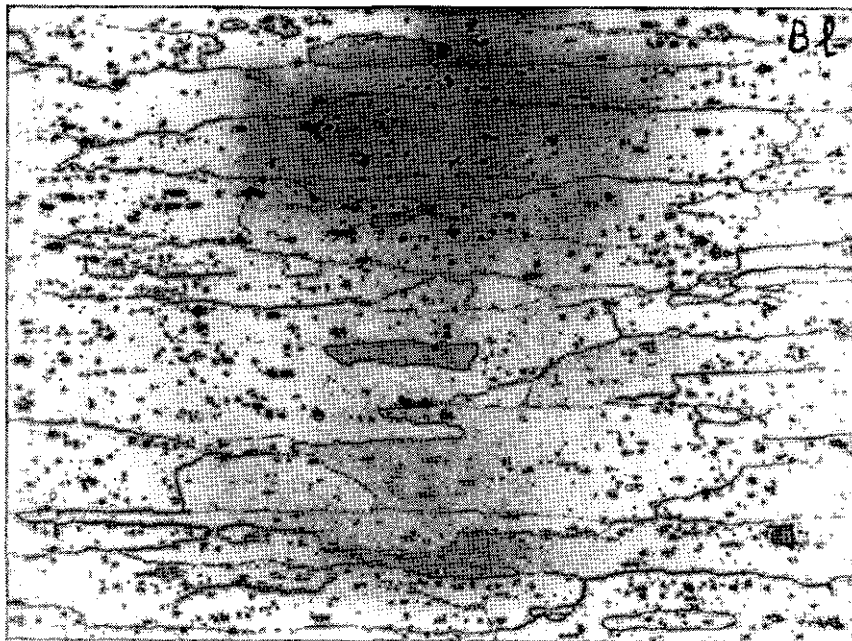
Inclusions were the most numerous in materials E and E', whereas the smallest numbers apply to materials B and F. The size of the inclusions did not vary a great deal. Some materials showed a slight tendency towards an elongated or flattened shape of the inclusions parallel to the sheet surface. Also a slight tendency towards an arrangement of inclusions in strings parallel to the sheet surface was observed. An exceptional material appears to be material F since the tendencies towards elongated inclusions and strings are both absent, see table 5. One could guess that this is a favorable feature for crack propagation, which could then account for the superior crack propagation results of this material. The effect of inclusions on the path of the growing crack would also lead one to expect that the ratios between the fatigue lives for specimens loaded transverse and parallel to the rolling direction would be the most favorable for materials A, D and G (see table 5). This is certainly not confirmed by fig. 9. Therefore, the suggested relation between the superior crack growth data for material F and the number, the shape and the distribution of its inclusions is a rather tentative one.

A chemical analysis of the microconstituents has not been made as yet. The inclusions are believed to be intermetallic particles.

For both pictures: Magnification 200×. Cross section parallel to rolling direction.



Material from manufacturer A



Material from manufacturer B

Fig. 12 Examples of microstructures with small and with large grains.

The thicknesses of the cladding layer range from about 2.5% to 6% of the sheet thickness. The variation of the thickness of the layer cannot be correlated with the variation of the crack propagation data. Thin layers were found on materials A and F with widely different propagation results.

#### 3.4 Fractographic observations

Observations were concerned with three aspects, namely:

1. The transition of the fracture surface from the tensile mode to the shear mode.
2. Growth lines.
3. Inclusions.

The results will be summarized below.

##### 3.4.1 The transition

The transition of the fracture surface from the tensile mode (90°-mode) to the shear mode (45°-mode) was described in several previous NLR-reports (for

instance, refs. 1, 2 and 19). The following observations were made on the present specimens.

In the constant-amplitude tests about half the number of cracks made a transition to a double-shear fracture and the other half to a single shear fracture. A systematic effect on this percentage from either the manufacture, the stress amplitude or the direction of loading with respect to the rolling direction could not be observed. It appeared to be a matter of pure chance whether the transition would produce a single or a double shear fracture. Therefore it was surprising to see that almost all program-loaded specimens revealed a single shear fracture.

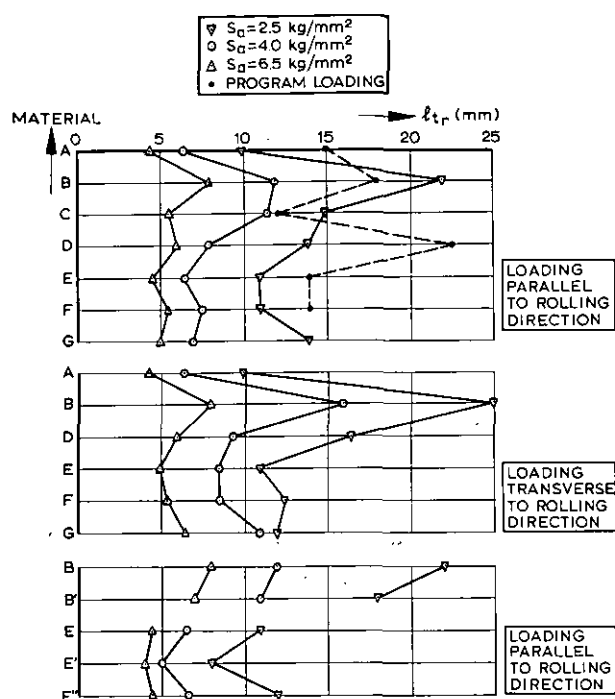


Fig. 13 The crack length,  $l_{tr}$ , at the completion of the transition from tensile mode fracture to shear mode fracture.

The crack length at the moment when the transition had been completed is shown in fig. 13. Except for material B there appear to be no noteworthy differences between the sheet materials. For material B the value of  $l_{tr}$  was generally larger, which is thought to be due to the high yield stress of this material. As a consequence the plastic zone at the tip of the crack will be smaller, which postpones the transition from plane strain to plane stress and hence the transition from the tensile mode to the shear mode fracture (ref. 19). It was therefore surprising to see small values for  $l_{tr}$  for material E'' (2024-T81). It is apparently not the same whether the high yield stress is obtained by aging (E'') or by deformation (B'). This once again emphasized the complexity of fatigue in aluminum alloys.

Fig. 13a shows that  $l_{tr}$  for the program tests was of the same order of magnitude as for the constant-amplitude tests with the lowest  $S_a$ -value. It has to be

said that the transition of the fracture surface occurred very gradually during the program tests and it was hard to indicate the completion of the transition. Nevertheless, this also is a surprising result, since the load cycles at the highest stress amplitude played such a predominating part in the crack propagation.

### 3.4.2 Growth lines

Observations were mainly made with the light microscope. A few replicas were made for observation in the electron microscope.

Growth lines indicating the successive stages of the crack front could be detected on all specimens. It was again observed that in the core of the sheet the growth lines were clearly visible on the tensile mode part of the fracture, whereas they were hard to see on the shear mode part. In the cladding the growth lines were easily observed also when the propagation occurred according to the shear mode. The latter indicated that also in this stage of the propagation, crack extension occurred in practically all load cycles if not in all.

A comparison of the microscopic observations of the growth lines for sheets of different manufacturers did not reveal systematic differences. The impression was obtained that the growth lines were somewhat more clearly defined in sheets of manufacturer B.

Interesting observations could be made on the fractures of program-loaded specimens. The periods of the program loading could be easily indicated under the microscope, since the 5 cycles of the highest of the three amplitudes left 5 clearly defined growth lines. Batches of these 5 lines recurred periodically with almost no visible growth lines between them. On the average about 50% of the crack propagation occurred at the highest stress amplitude. The crack rate at this amplitude, deduced from that percentage was about twice as high as the crack rate in the constant-amplitude tests at the same amplitude. There may be two causes for this. In the first place the program tests were carried out at a much lower frequency as compared with the constant-amplitude tests.

Second, an unfavorable effect of the two lower amplitudes may have accelerated the crack growth at the highest amplitude. It is difficult to say which of the two contributions was the most important one.

The average crack rate at the two lower amplitudes as deduced from the growth lines was about 50% slower than expected on the basis of the constant-amplitude tests. Also this result will have been affected by the frequency difference, and the favorable interaction from the highest stress amplitude on the two lower amplitudes was certainly larger than 50%.

For one program-loaded specimen (no. S3) a comparison was made between the average crack rate as deduced from the spacings between the batches of

growth lines of the highest stress amplitude and the average crack rate calculated from the crack propagation record. The results, applying from  $l=5$  mm to  $l=15$  mm, are shown in fig. 14. The graph confirms that crack growth occurred in almost every period if not in all. Similar graphs were shown in refs. 19 and 20.

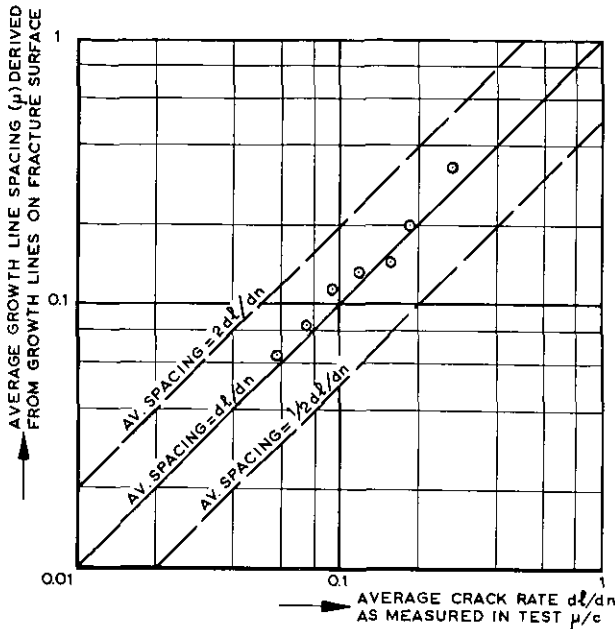


Fig. 14 Comparison of the crack rates derived from the propagation records and from the growth line spacings.

### 3.4.3 Inclusions

Under the light microscope inclusions were detected on the fracture surface. Identification occurred by noting that the colour was exactly the same as for inclusions in the microscopic specimens that were polished but still unetched. Also the size and even the shape were similar. It appeared to be impossible to find systematic differences between the number of inclusions on the fracture surfaces of sheets of different manufacturers.

In view of the significance inclusions could have for crack propagation the discussion on this aspect will be carried on a little further. With the light microscope inclusions could be revealed with a small number of more or less concentric growth lines or growth rings around them. Similar growth rings in the 7178-T6 alloy were found by Pelloux (ref. 14), who suggested that cracking of the inclusions initiated secondary cracks in the matrix just ahead of the crack front of the main crack. This may obviously lead to acceleration of the crack growth. In the present test series the majority of inclusions, however, did not show such rings. In general the impression was obtained that the effect of the inclusions on the pattern of growth lines was small and of a rather local nature. This especially applies to small cracks and low crack rates. At larger values of the crack length the crack appeared to pick up more

inclusions and at the same time the growth lines were more rarely observed. The inclusions are then found at pits and hills, suggesting that they considerably affect the path of the main crack.

Similar observations were published in the literature. Forsyth (ref. 9) mentioned the cracking of inclusions in both Al-Cu and Al-Zn type alloys. This occurred just ahead of the main crack if the crack was near final failure. The cracking of the particles could lead to deep voids on the fracture surfaces.

Glassman and McEvily (ref. 11) compared two AlZn alloys differing in the Fe and Si contents only, which noticeably affected the number and the size of the intermetallic particles. The alloy with the larger amount of particles showed a lower crack rate for low values of the crack length and a higher crack rate for large values of the crack length (see also ref. 15).

Pelloux (ref. 14) and Piper, Quist and Anderson (ref. 15), who studied various types of the alloy 7178-T6, came to the conclusion that the crack propagation was not accelerated by inclusions as long as the crack rate was low. Acceleration should occur at high crack rates when the plastic zone size becomes of the order of the particle spacings and void formation sets in.

The cracking of particles in RR58 and Au2GN, two Al-Cu type alloys, is mentioned by de Leiris, Mencarelli and Poulignier (ref. 13).

There cannot exist doubt that particles in the 2024-T3 alloy can be cracked by plastic deformation of the matrix. Glassman and McEvily show several micrographs of cracked particles. According to them such cracks can be present after sheet rolling and a 3% stretching in a tensile test also produced the cracks. In the present investigation the microscopic specimens of the unloaded sheet never showed cracked particles. However, in microscopic specimens from tensile test specimens loaded until failure the majority of the particles were cracked. It therefore may be concluded that particles in the plastic zone of a crack tip will be fractured. The problem remains, however, whether this accelerates or decelerates the crack growth. The examination of the fractures of the present test series and of a previous NLR test series on 2024-T3 sheet material suggests that neither acceleration nor deceleration occurs as long as the crack is still in the tensile mode, that means as long as the crack rate is relatively small. Whether the inclusions cause an acceleration after the transition to the shear mode has occurred could not be deduced from the present observations.

Acceleration of crack growth was suggested in refs. 14 and 15 to be a consequence of void formation between particles. On the other hand, a deceleration effect was suggested by de Leiris, Mencarelli and Poulignier (ref. 13) because the crack had to follow a rather irregular path through the particles. One might indeed think that a rough topography of the two fracture

surfaces will hinder a relative shear movement of one fracture surface over the mating one and thus relieve the stress concentration at the tip of the crack. A decelerating influence of cracked particles was also suggested by Glassman and McEvily (ref. 11) based on the idea that the cracked particle may act as a crack stopper like a hole. Since cracked particles will not be found over the complete crack front but at a smaller part of the crack front only, the crack stopping action is not expected to be very effective. The present observations regarding the effect of inclusions on growth lines do not support the crack stopping idea. Another aspect of inclusions acting as a crack stopper is the adherence between the inclusion and the matrix. If the inclusion should act as a stop hole, the adherence has to be largely destroyed and it is not sure whether this occurs.

The survey of the fracture surfaces has made the impression that the number of inclusions on the fracture was larger for specimens loaded transverse to the rolling direction as compared with specimens loaded parallel to the rolling direction. One might expect this result since there was a weak tendency for inclusions to be situated in strings in the rolling direction. If inclusions have an unfavorable effect on the propagation it would also explain the higher crack rates for the transversely loaded specimens as illustrated by fig. 9. However, the unfavorable effect should then be expected to be a maximum for the highest stress amplitude and at large cracks, and this is contradicted by fig. 9. It appears that the effect of the inclusions is not as simple as one might expect.

### 3.5 Measurements of the electrical conductivity

Measurements were made with the non-destructive apparatus Sigmatest-T made by the Institut Dr. Förster. The apparatus is operating according to the eddy current principle. A layer of about 20% of the sheet thickness was ground from samples of the sheet materials in order to remove the cladding layer and to allow measurements on the core material. Test results are shown in table 6, including the results of measurements on the cladding layer. Since the cladding material is pure aluminum, the results of the latter measurements revealed higher conductivities. It is noteworthy that the differences between the conductivities as measured on the cladding layer and on the core are clearly correlated with the thickness of the cladding layer. This is illustrated in fig. 15. The correlation is not further explored here. It is given since it might open certain possibilities for non-destructive measurements of the thickness of the cladding.

The data on the electrical conductivity in table 6 do not indicate any correlation between this property and the crack propagation properties. Four specimens were given a renewed heat treatment, that means a solution

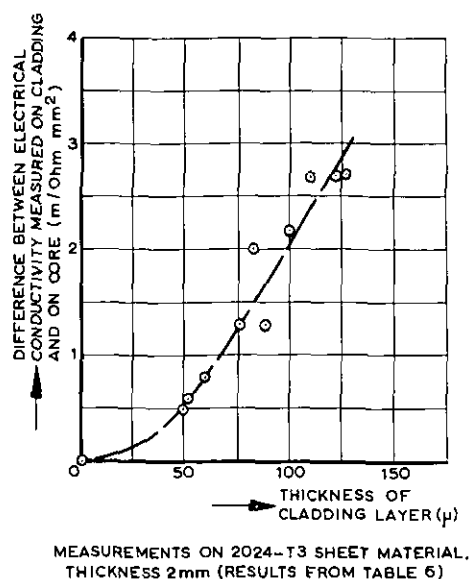


Fig. 15 Increase of the electrical conductivity as measured by the Sigmatest apparatus due to the presence of the cladding layer.

heating (495°C), quenching, but no flattening, and aging at room temperature. The electrical conductivities have changed noticeably then, see table 6, last column. It is remarkable that the conductivity, varying from 16.6 to 18.6 m/Ohm mm<sup>2</sup> before the re-heat treatment, did not vary more than from 16.1 to 16.6 after this treatment. Apparently, the structure of some of the materials has changed. This applies especially to material B for which the conductivity changed from 18.6 to 16.6. Since this material was believed to be stretched more than is usually done, it is thought that the initial, large variation of the conductivities may be due to differences of the flattening procedures between the manufacturers. As a consequence the dislocation densities and configurations may have been different. That will also effect the locations and probably the sizes of the precipitated zones during subsequent aging. Since the re-heat treatment did not include any flattening operation, such differences are eliminated then. If the above reasoning is correct it should be recognized that differences between the densities and the configurations of dislocations and precipitated zones could be of some importance for the behavior of the material under cyclic plastic strain and thus for crack propagation.

## 4 Results from other investigations

### 4.1 The effect of the manufacture on the crack propagation properties

Crack propagation tests on aluminum alloy sheet materials have been carried out by several laboratories and it may be assumed that materials from different manufacturers were used. Unfortunately a comparison of results in order to detect an effect of the manufacture

is not feasible in view of the large number of other variables that may also affect the crack propagation and that were usually different for different investigations. Variables for which it was shown that they have a noticeable effect on the propagation are: the type of aluminum alloy, the mean stress or stress ratio, the loading frequency, the sheet width and the sheet thickness. Therefore, it has not been attempted to discover from the literature any effect of the manufacture on the fatigue crack propagation.

#### 4.2 The batch to batch variation of the crack propagation properties

In the previous section reference was made to different variables that may affect the fatigue crack propagation. Since these effects could overshadow an effect of a batch to batch variation, the latter can only be studied if all other test conditions are the same. Some laboratories have selected their own standard type of crack propagation specimen. However, if they have in stock many sheets of the same batch, which is advantageous for many reasons, their results cannot be used for indicating the effect of the batch. It appears that for 2024-T3 sheet material only some NLR results are available for studying the effect of the batch on the crack propagation. For 7178-T6 sheet material some results were presented in ref. 15, which will be discussed afterwards.

For several NLR investigations the sheet material was ordered separately for each test series. This permits the effect of the batch to be studied for 2024-T3 Alclad sheet material ordered from manufacturers C and F. Results were available for two batches from each manufacturer.

In fig. 16 comparative results are presented for three crack propagation intervals, viz.  $l=4-8$  mm,  $l=8-16$  mm and  $l=16-40$  mm. The dimensions of the specimens were the same for all test series. All tests were carried out in Schenck machines at frequencies of 2000 or 3000 cpm. For all test series  $S_m=7$  kg/mm<sup>2</sup> and  $S_a=2.5, 4$  and  $6.5$  kg/mm<sup>2</sup>, except for test series 1 for which  $S_m=8.2$  kg/mm<sup>2</sup> and  $S_a=2.4, 3.3$  and  $5.5$  kg/mm<sup>2</sup>. The results were corrected to  $S_m=7$  kg/mm<sup>2</sup> with the aid of the data from ref. 1. Correction factors on life were 1.1 to 1.4, which are very small. The crack propagation lives were then plotted as a function of  $S_a$  and from these plots the lives at  $S_a=2.5, 4$  and  $6.5$  kg/mm<sup>2</sup> were read. It is thought that the interpolations introduced unimportant inaccuracies as compared with the scatter shown in fig. 16. A conclusion to be drawn from the figure is that two batches of one manufacturer have yielded noticeably different crack propagation results and this applies to both manufacturers C and F. Minimum to maximum life ratios at the same stress amplitude are in the order of 1:3. This is a higher ratio than found in the present test series

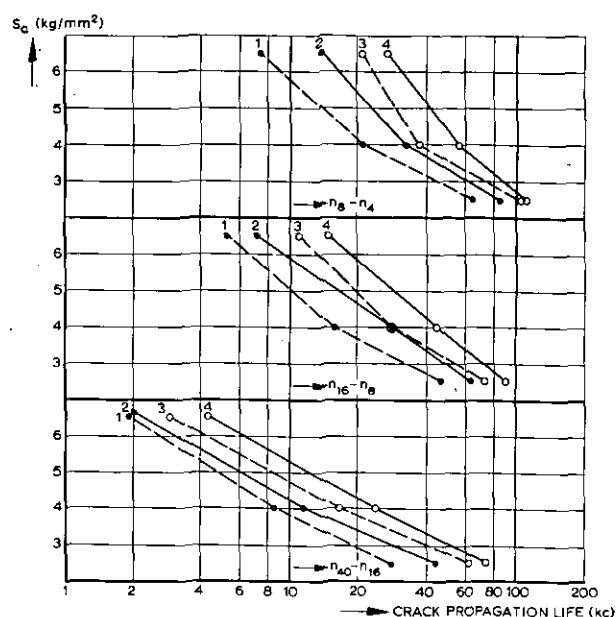


Fig. 16 The crack propagation life for three crack propagation intervals and two batches of manufacturers C and F.

Testseries	Manufacturer	Static properties			Reference
		$S_u$	$S_{0.2}$	$\delta(2'')$	
1	C	48.5	36.9	16	This report
2		46.9	34.4	23	
3	F	48.3	37.1	19	This report
4		46.3	35.2	22	

2024-T3 Alclad sheet specimens, width 160 mm, thickness 2 mm

between different manufacturers. The influence of the batch is an additional source for scatter of the crack propagation.

The static properties of the two batches from one manufacturer are somewhat different, see the table in fig. 16. It is noteworthy that the better crack propagation data are shown by the batch with the higher elongation and the lower yield stress, that means the higher ductility. This is in agreement with previous findings (see, for instance, refs. 1, 3 and 12) and with the present results for materials E, E' and E'', namely that a lower ductility is associated with higher crack rates. Fig. 16 then also confirms that the ductility alone does not determine the propagation results. The static properties of test series 1 and 3 are almost the same and still the propagation lives are significantly different. The same applies to test series 2 and 4.

Piper, Quist and Anderson (ref. 15) compared the crack propagation in 18 experimental alloys with chemical compositions more or less similar to that of the 7178 alloy. Four of the alloys had the same composition and practically the same static properties. The fatigue crack propagation rates for the four alloys were different, the ratio between the maximum and minimum value at a certain crack length varying from about 1.2

to about 2 for small and large cracks, respectively. The manufacturing procedure appeared to be the only variable that could be responsible for these differences.

#### 4.3 The effect of the rolling direction on the crack propagation

A few data are scattered through the literature. According to Donaldson and Anderson (ref. 8) the crack propagation life ( $2l=10$  mm to  $2l=50$  mm) was about 5% shorter for 2024-T81 material if loaded transverse to the rolling direction as compared with loading in the rolling direction. For 2618-T6 material (AlCuMg alloy for high temperature application) it was about 15% shorter. For both materials the cyclic stress was  $7.4 \pm 3.2$  kg/mm<sup>2</sup>. The static properties in the two directions were not very much different.

Rooke, Gunn, Ballett and Bradshaw (ref. 16) performed tests on DTD 5070 A material (2.5% Cu, 1.5% Mg, 1.2% Ni, 1.0% Fe, balance Al), the cyclic stresses being  $3.1 \pm 2.5$  and  $6.2 \pm 5.1$  kg/mm<sup>2</sup>. The results presented as crack propagation rates showed the rates to be 0–20% higher if the specimens were loaded transverse to the rolling direction. For this material the static properties were also similar for the longitudinal and transverse directions of the sheet.

Christensen and Bellinfante (ref. 7) found a 20% shorter life for 2014-T6 material loaded transverse to rolling direction as compared with the material loaded in the rolling direction. The maximum stress was 9.8 kg/mm<sup>2</sup> ( $\sigma_{min}$  or R not quoted) and the crack growth interval was from  $2l=15$  mm to  $2l=48$  mm. Static properties were not given.

The reductions of the crack propagation life mentioned above for Al-Cu type alloys are of the same order as or smaller than those found in the present test series (average 30%, see fig. 9). A large reduction for an Al-Zn type alloy (DTD 687A) was found by Frost (ref. 10), who employed high mean stresses (about 23 kg/mm<sup>2</sup>) and low stress amplitudes (1.2, 2.0 and 2.4 kg/mm<sup>2</sup>). Crack propagation ( $2l$  values in the order from 10–25 mm) in the transversely loaded specimens was 2–2.5 times faster than in the longitudinally loaded specimens. This material alternately exhibited fast brittle and slow fatigue cracking (sheet thickness 3.25 mm). More investigations on the 7075 type alloys seem to be warranted.

## 5 Discussion

### 5.1 Introduction

The significance of the present results is partly of a direct practical nature, while other information obtained is related to fatigue crack propagation as a phenomenon, thus having a more indirect relation to practical problems. Practical aspects are such questions as: how large is the variability of the crack rate in

materials from different manufacturers, how large is the batch to batch variation and how large is the influence of the directionality caused by rolling. With respect to the crack propagation phenomenon the central problem is: can differences between crack rates under nominally identical conditions be understood. If this were possible, it might be helpful to select materials for better crack propagation properties and perhaps to produce materials with an improved fatigue cracking behavior. The two types of aspects will be briefly discussed in the following sections.

### 5.2 Practical aspects of the present results

The maximum ratios between the crack propagation lives for sheet materials from different manufacturers as found in the present tests were in the order of 1:2. Adding results from previous NLR test series and hence including a batch to batch variation, the maximum ratios were in the order of 1:3. For fatigue crack propagation this really is a large variation, the more so since the above ratios are concerned with average results of test series.

The ratios mentioned were obtained in constant-amplitude tests. Fortunately the variation of the fatigue life due to different manufactures was smaller in the program tests. The explanation for this is unknown. It may be assumed that a local loss of ductility occurs in the crack tip region, caused by the cyclic plastic deformation and its effect on the precipitates. This loss may be larger for some materials, which could then show higher crack rates in constant-amplitude tests. In variable-amplitude tests it may cause a more favorable interaction from high-amplitude cycles on the crack extension at low-amplitude cycles and this could partly compensate for the former effect. This qualitative explanation that is obviously tentative still emphasizes a most important question, that is: which kind of loading should be adopted for comparing the fatigue crack propagation properties of different materials. Knowing that interaction effects between load cycles of different magnitudes may be important (refs. 17 and 18) the only practical answer seems to be that the load sequence adopted for comparative testing should be a very realistic one. In a recent NLR investigation (ref. 21) on program and random load testing it was advised that realistic load sequences had to be used for this purpose rather than simplified load sequences. It was questioned whether a simple program loading could be considered as a realistic load sequence for an aircraft structure. This aspect will not be discussed any further here.

Although the variation of crack propagation lives under realistic load sequences may be smaller than the 1:3 ratio mentioned before, it has to be recognized that the variations between manufactures and batches are a potential source of scatter for the crack rate. A practical

problem for a fail-safe structure is the assessment of safe inspection periods. Crack propagation data have to be used to that end and the possible variation of these data as mentioned above is obviously a rather disturbing aspect. The most relevant crack propagation data are obtained in a full-scale test on a complete structure. Safety factors have to be applied to the results of such a test. It now appears that a considerable part of the safety factor is necessary cover the scatter due to the effect of the manufacture and the batch variation. Since the safety factor has also to cover scatter of the fatigue loads, environmental effects, etc. a factor of 3 as sometimes adopted does not seem to be overdone.

The authors cannot but make a plea for a periodic checking of the uniformity of crack propagation properties of sheet materials that are used for the line production of tension skins of aircraft structures. For this purpose it may be sufficient to test a small number of specimens from each batch that is received.

In general, sheet material is applied in a structure with the rolling direction parallel to the maximum tensile stress. The present results show that this is also favorable for crack propagation, since then the crack propagation life may be some 40% longer than for sheet loaded transverse to the rolling direction. Such a gain in life may be of practical importance. In a pressurized fuselage the sheets for the skinning may be applied in two ways, namely (1) with the rolling direction parallel to the hoop stress and (2) with the rolling direction parallel to the axis of the fuselage. In view of crack propagation the former should be preferred.

### 5.3 *Some comments on fatigue crack propagation in 2024-T3*

It was the prime purpose of the present test series to provide experimental data on crack propagation in 2024-T3 Alclad sheet material from different manufacturers. In addition a number of other characteristics of the materials were determined, in order to see whether any correlation with the crack propagation data could be found. Although conclusive indications of such a correlation were not obtained, a few observations are worth mentioning. They are summarized below.

The results did not indicate any correlation between the crack propagation rates and the grain size, the grain shape, the thickness of the cladding layer and the electrical conductivity. The correlation with the static properties appeared to be more complicated than thought previously. A comparison of the crack rates in sheets from different batches from the same manufacturer (see fig. 16), confirmed that the crack rate was larger in the less ductile material. However, tests on sheet materials from different manufacturers with about the same static properties could still show signif-

icantly different crack propagation results. In this respect it should be recognized that cyclic plastic strain will considerably modify the stress-strain curve of 2024-T3 alloy (ref. 19). The modifications need not be the same for all materials. An indication of the latter is perhaps the transition of the tensile mode fracture to the shear mode in materials E' and E'', which occurred at an unexpectedly short crack length. It was already said in section 3.4.1 that it is apparently the same for fatigue crack propagation whether a high yield stress was obtained by aging or by deformation. Cyclic deformation may further complicate the behavior of the material. The cyclic plastic deformation depends on dislocations, precipitated zones and their interactions, but unfortunately there is not very much known in detail about the latter phenomenon in the 2024-T3 alloy. It would not be surprising if there were differences between the "as received" conditions of the 2024-T3 materials concerning the dislocation densities, the number and the size of the zones and the positions of the zones with respect to the dislocations. The differences need not noticeably affect the static stress-strain curve, but they could imply a different cyclic strain behavior. If the chemical compositions for two materials are the same, the above differences are caused by different heat treatment procedures concerning the solution heating, quenching and flattening. An indication that flattening (which involves plastic deformation between quenching and aging) may be important comes from the electrical conductivity measurements presented in section 3.5.

The chemical compositions of the materials tested did not vary a great deal. The chromium content was relatively large for material F, which also showed the most superior crack propagation data. It is not known whether a correlation with the chromium exists, but it cannot a priori be excluded that small amounts of certain elements have a significant effect on the precipitation and thus on the crack growth data.

Coming now to the role played by inclusions, a clear correlation between the crack propagation and the amount of inclusions could hardly be indicated. It is true that material F with the most superior crack growth data had a somewhat smaller amount of inclusions. Some other results, for instance the directionality effect, were contradicting an effect of the inclusions. The fractographic observations and some information of the literature suggest that the role of the inclusions was probably of minor importance for the major part of the present results. Inclusions are believed to be important for fast crack propagation and residual strength of cracked sheets. This was shown in the literature for Al-Zn type alloys (refs 6, 14 and 15). It probably also applies to the 2024-T3 alloys since plastic deformation causes cracked particles in these alloys. Residual strength tests were recently carried out (ref. 5) on specimens of materials

B, D, E, F and G cut from the same sheets as the present crack propagation specimens. The results showed the following order of increasing residual strength: D, E, G, F, B which is noticeably different from the order of increasing crack propagation lives. This implies that good crack propagation properties and good residual strength properties are not necessarily associated properties. A similar warning was already given by Harpur (ref. 12).

Recapitulating the above discussion and considering the possibilities of improving the properties of the 2024-T3 sheet material, it is thought that the two important variables are heat treatment and inclusions. The heat treatment variables are concerned with the solution heating, quenching and flattening, and also the addition of minor quantities of certain elements (for instance chromium) might be important. The heat treatment affects the properties of the matrix and is probably more important for fatigue crack propagation than for residual strength. It may also be important for corrosion properties. The elimination of inclusions, which may be obtained by reducing the contents of certain elements (probably Si and Fe), is thought to improve the material with respect to both fast fatigue crack propagation and residual strength. Of course, it is possible that improvements of different properties will require conflicting modifications of the manufacturing process. Since this is not known as yet, there appears to be ample room for a further exploration, which may well yield results of great technical importance.

## 6 Conclusions

Fatigue crack propagation tests were carried out on 2024-T3 Alclad sheet material with a nominal thickness of 2 mm. Sheets were obtained from seven different manufacturers, materials A-G, which all met the specifications for the 2024 alloy. Materials B and E were also tested after artificial aging (materials B', E' and E'' = T81 condition). Crack propagation tests were carried out on specimens loaded in the rolling direction and on specimens loaded transverse to that direction. Mean stress and stress amplitudes were:  $S_m = 7 \text{ kg/mm}^2$  and  $S_a = 2.5, 4 \text{ and } 6.5 \text{ kg/mm}^2$ . The loading frequency in the constant-amplitude tests was approximately 3000 cpm. In addition to the constant-amplitude tests, a number of program tests were performed with the same stress amplitudes in a programmed sequence. The frequency in these tests was low, namely 7.5 to 18 cpm. The width of all specimens was 160 mm. Various characteristics of the materials were determined and fractographic observations were made. The results and the conclusions are summarized below.

1. Systematic differences between the crack propaga-

tion lives of the seven materials A-G were found. The most outstanding result was that material F excelled above all the other materials under practically all loading conditions. The indication of the most inferior material was depending on the type of test, although materials A and B generally yielded poor results. For material B this could be attributed to its low ductility, which did not apply to material A. The ratios between the fatigue lives for the most superior material (F) and the most inferior material were in the order of 1:2 for the constant-amplitude tests and in the order of 1:1.5 for the program tests.

2. The aging of material E implied a reduction of ductility and a reduction of the crack propagation lives to about 50-60%. The aging of the low ductility material B did not noticeably effect the crack propagation life.
3. The crack propagation life for sheet specimens loaded transverse to the rolling direction was on the average about 30% shorter than the life of specimens loaded parallel to the rolling direction. The directionality effect was hardly affected by the stress amplitude, the crack length and the manufacture of the material.
4. In a previous investigation on 2024-T3 Alclad sheet material of manufacturer C the crack rates at 20 cpm were about 30% faster than the crack rate at 2000 cpm. For similar frequencies this percentage ranged from 45% to 85% for material F of the present investigation.
5. For materials from manufacturers C and F data from two different batches were available, which indicated ratios between the crack propagation lives for the two batches in the order of 1:1.5. This batch effect appeared to be correlated with the ductility.
6. The  $\Sigma n/N$ -values for the program tests were in the order of 1-3 if estimated corrections for the frequency difference between the constant-amplitude tests and the program tests were applied.
7. There was no apparent correlation between the crack propagation rates and the grain size, the thickness of the cladding layer and the electrical conductivity.
8. The correlation between the crack propagation rates and the ductilities of the materials appeared to be more complicated than thought previously. Although a low ductility is unfavorable for crack propagation, materials with the same ductility (as determined in a tensile test) can still give noticeably different crack growth rates. It is thought that this probably has to be associated with the differences in the heat treatment regarding solution heating, quenching and flattening before aging. Also the presence of minor quantities of certain elements may be important.

9. Although the good crack propagation results of material F could be related to the slightly lower contents of inclusions, the fractographic observations suggest that inclusions had little effect on the propagation that occurs according to the tensile mode fracture. Inclusions are believed to be important for fast fatigue crack propagation and residual strength.

## 7 References

- <sup>1</sup> BROEK, D. AND SCHIJVE, J., The influence of the mean stress on the propagation of fatigue crack in aluminium alloy sheet. NLR-TR M.2111, Jan. 1963.
- <sup>2</sup> BROEK, D. AND SCHIJVE, J., The effect of sheet thickness on the fatigue crack propagation in 2024-T3 Alclad sheet material. NLR-TR M.2129, April 1963.
- <sup>3</sup> BROEK, D., SCHIJVE, J. AND NEDERVEEN, A., The effect of heat treatment on the propagation of fatigue cracks in light alloy sheet material. NLR-TR M.2134, May 1963.
- <sup>4</sup> BROEK, D., Crack propagation of 2024-T8 sheet under static and dynamic loads. NLR-Report M.2161, March 1966.
- <sup>5</sup> BROEK, D., Static tests on cracked panels of 2024-T3 Alclad sheet materials from different manufacturers. NLR-Report to be published in 1966.
- <sup>6</sup> CARMAN, C. M., ARMIENTO, D. F. AND MARKUS, H., Plane-strain fracture toughness of high-strength aluminium alloys. J. Basic Engng. Vol. 87, Series D, p. 904, 1965.
- <sup>7</sup> CHRISTENSEN, R. H. AND BELLINFANTE, R. J., Some considerations in the fatigue design of launch and spacecraft structures. NASA CR-242, June 1965.
- <sup>8</sup> DONALDSON, D. R. AND ANDERSON, W. E., Crack propagation behaviour of some airframe materials. Proc. Crack Propagation Symposium, Cranfield, 1961, Vol. II, p. 375. The College of Aeronautics 1962.
- <sup>9</sup> FORSYTH, P. J. E., A two stage process of fatigue crack growth. Proc. Crack Propagation Symposium, Cranfield 1961, Vol. I, p. 76. The College of Aeronautics 1962.
- <sup>10</sup> FROST, N. E., Effect of mean stress on the rate of growth of fatigue cracks in sheet materials. J. Mech. Engng. Science, Vol. 4, p. 22, 1962.
- <sup>11</sup> GLASSMAN, L. H. AND MCEVILY, A. J., Effects of constituent particles on the notch-sensitivity and fatigue-crack-propagation characteristics of Al-Zn-Mg alloys. NASA TN D-928, April 1962.
- <sup>12</sup> HARPUR, N. F., Material selection for crack resistance. Proc. Crack Propagation Symposium, Cranfield 1961, Vol. II, p. 442. The College of Aeronautics, 1962.
- <sup>13</sup> DE LEIRIS, H., MENCARELLI, E. AND POULIGNIER, J., Contribution de la microfractographie électronique à l'étude de l'influence de la fréquence des cycles sur le développement des cassures dans les alliages d'aluminium. ONERA, T.P. No. 117, 1964.
- <sup>14</sup> PELLOUX, R. M. N., Fractographic analysis of the influence of constituent particles on fatigue crack propagation in aluminum alloys. Trans. ASM, Vol. 57, p. 511, June 1964.
- <sup>15</sup> PIPER, D. E., QUIST, W. E. AND ANDERSON, W. E., The effect of composition on the fracture properties of 7178-T6 aluminum alloy sheet. Paper presented at the Fall Meeting of the Metallurgical Society of AIME, Oct. 1964.
- <sup>16</sup> ROOKE, P. D., GUNN, N. J. F., BALLETT, J. T. AND BRADSHAW, F. J., Crack propagation in fatigue. Some experiments with DTD 5070A aluminium alloy sheet. RAE Techn. Report No. 64025, Oct. 1964.
- <sup>17</sup> SCHIJVE, J., Fatigue crack propagation in light alloy sheet material and structures. Advances in Aeronautical Sciences, Vol. 3, p. 387. Pergamon Press, 1961. Also NLR-Report MP.195.
- <sup>18</sup> SCHIJVE, J. AND BROEK, D., Crack propagation. The results of a test programme based on a gust spectrum with variable amplitude loading. Aircraft Engineering, Vol. 34, p. 314, 1962. Also NLR-Report MP.208.
- <sup>19</sup> SCHIJVE, J., Analysis of the fatigue phenomenon in aluminium alloys. NLR-TR M.2122, April 1964.
- <sup>20</sup> SCHIJVE, J. AND DE RIJK, P., The effect of ground-to-air cycles on the fatigue crack propagation in 2024-T3 Alclad sheet material. NLR-TR M.2148, July 1965.
- <sup>21</sup> SCHIJVE, J., BROEK, D., DE RIJK, P., NEDERVEEN, A. AND SEVENHUYSEN, P. J., Fatigue tests with random and programmed load sequences with and without ground-to-air cycles. A comparative study on full-scale wing center sections. NLR-Report S.613, Dec. 1965.

TABLE 1  
Survey of the present test series on 2024-T3 Alclad sheet material

Loading	Loading and rolling direction	Tests on sheets of manufacturers <sup>1)</sup>									
constant-amplitude program	parallel	A	B	C	D	E	F	G	B'	E'	E''
	transverse	A	B		D	E	F	G			
	parallel	A	B	C	D	E	F			B'	

<sup>1)</sup> The manufacturers are indicated by capitals A to G. B', E' and E'' refer to material with an additional heat treatment specified below.

Material	Additional heat treatment	Note on batch
B'	3 hours at 170°C	Same as B
E'	6 hours at 190°C	} Not the same as E, E' and E'' from the same batch
E''	9 hours at 190°C (T81-condition)	

TABLE 2  
Chemical compositions of the core material of the 2024-T3 sheet materials

Material		A	B	C	D	E	F	ASM Metals Handbook
Alloying elements (% by weight)	Cu	4.90	4.45	5.07	4.50	4.49	4.72	3.8-4.9
	Mg	1.63	1.69	1.77	1.61	1.70	1.55	1.2-1.8
	Mn	0.70	0.58	0.58	0.71	0.68	0.63	0.3-0.9
	Si	0.14	0.16	0.26	0.21	0.24	0.16	0.50 max
	Fe	0.23	0.23	0.29	0.33	0.37	0.32	0.50 max
	Zn	0.08	0.07	0.10	0.20	0.02	0.06	0.25 max
	Cr <sup>1)</sup>	455	566	392	657	799	1189	0.05 max
	Ti	0.03	0.02	0.01	0.04	0.02	0.02	0.05 max

<sup>1)</sup> Relative values are given. Absolute contents were not determined since the monitor sample did not contain chromium.

TABLE 3

Material	Results of tensile tests									Hardness measurements (500 grams)				
	$S_{0.2}$ (kg/mm <sup>2</sup> )			$S_u$ (kg/mm <sup>2</sup> )			Elongation (%) (2 in gage length)			$S_{0.2}/S_u$		$H_v$		
	P	T	Ratio	P	T	Ratio	P	T	Ratio	P	T	P <sup>1)</sup>	T <sup>2)</sup>	Ratio
A	36.7	31.6	0.86	46.2	44.6	0.97	20	20	1.00	0.79	0.71	138.2	139.5	1.01
B	39.4	36.5	0.92	46.5	44.0	0.95	19	20	1.05	0.85	0.83	151.0	152.2	1.01
C	34.4	32.3	0.94	46.9	45.7	0.97	23	22.5	0.98	0.73	0.71	139.6	137.5	0.98
D	35.4	32.3	0.91	48.3	46.7	0.97	22.5	20.5	0.91	0.73	0.69	137.5	135.7	0.99
E	37.2	34.3	0.92	47.7	46.8	0.98	21	21	1.00	0.74	0.73	147.5	144.8	0.98
F	35.2	31.5	0.89	46.3	45.5	0.98	22	21	0.95	0.76	0.69	135.3	133.7	0.99
G	36.4	31.5	0.87	47.6	46.0	0.97	18	18	1.00	0.76	0.68	139.5	138.6	0.99
B'	43.0	39.2	0.91	48.5	45.1	0.93	13	15	1.15	0.91	0.87	151.7	153.5	1.01
E'	41.7	37.2	0.89	48.0	46.7	0.97	14.5	13	0.90	0.87	0.80	152.1	153.6	1.01
E''(T8)	46.5	46.0	0.99	48.7	48.1	0.99	6.5	7	1.08	0.95	0.96	159.7	159.8	1.00

P: Loaded in the rolling direction; average results of 4 tensile tests or 6 hardness measurements.

T: Loaded transverse to the rolling direction; average results of 2 tensile tests or 6 hardness measurements.

Ratio: Ratio of the two preceding columns.

<sup>1)</sup> Hardness measured on cross section of sheet, located in the rolling direction.

<sup>2)</sup> Hardness measured on cross section of sheet transversely located to the rolling direction.

TABLE 4

Damage calculations for three crack propagation intervals

Manufacturer	$\Sigma n/N$		
	$l=5-8$ mm	$l=8-16$ mm	$l=16-80$ mm
A	0.92	1.29	1.68
B	1.26	1.24	1.50
B'	1.14	1.20	1.40
C	1.12	1.29	1.63
D	0.96	1.21	1.94
E	0.92	1.19	1.61
F	0.72	1.02	1.43

TABLE 5

Some data on grain sizes and inclusions

Manufacturer	Grain size <sup>1)</sup> (microns)			Cross <sup>2)</sup> section	Inclusions			
	Length	Width	Thickness		Number <sup>3)</sup> per mm <sup>2</sup>	Size <sup>4)</sup> (micron)	Tendency to	
							Elongated shape	Strings
A	50	50	20	P	1300	8	no	no
				T	1300	6	slight	slight
B	250	200	50	P	1100	8	slight	no
				T	1100	8	slight	slight
C	125	100	35	P	1500	6	slight	slight
				T	1500	6	slight	slight
D	175	100	25	P	1250	8	no	no
				T	1100	8	slight	slight
E	100	75	20	P	2000	6	slight	slight
				T	2000	6	slight	slight
E''	100	75	20	P	1850	6	no	no
				T	1850	6	no	slight
F	150	100	35	P	1100	6	no	no
				T	1100	8	no	no
G	150	100	25	P	1200	8	no	no
				T	1300	6	slight	slight

1) Characteristic values estimated from microscopic picture.

3) Rough estimate made under the microscope.

2) P: cross section parallel to rolling direction

4) Characteristic size of the larger inclusions.

T: cross section transverse to rolling direction.

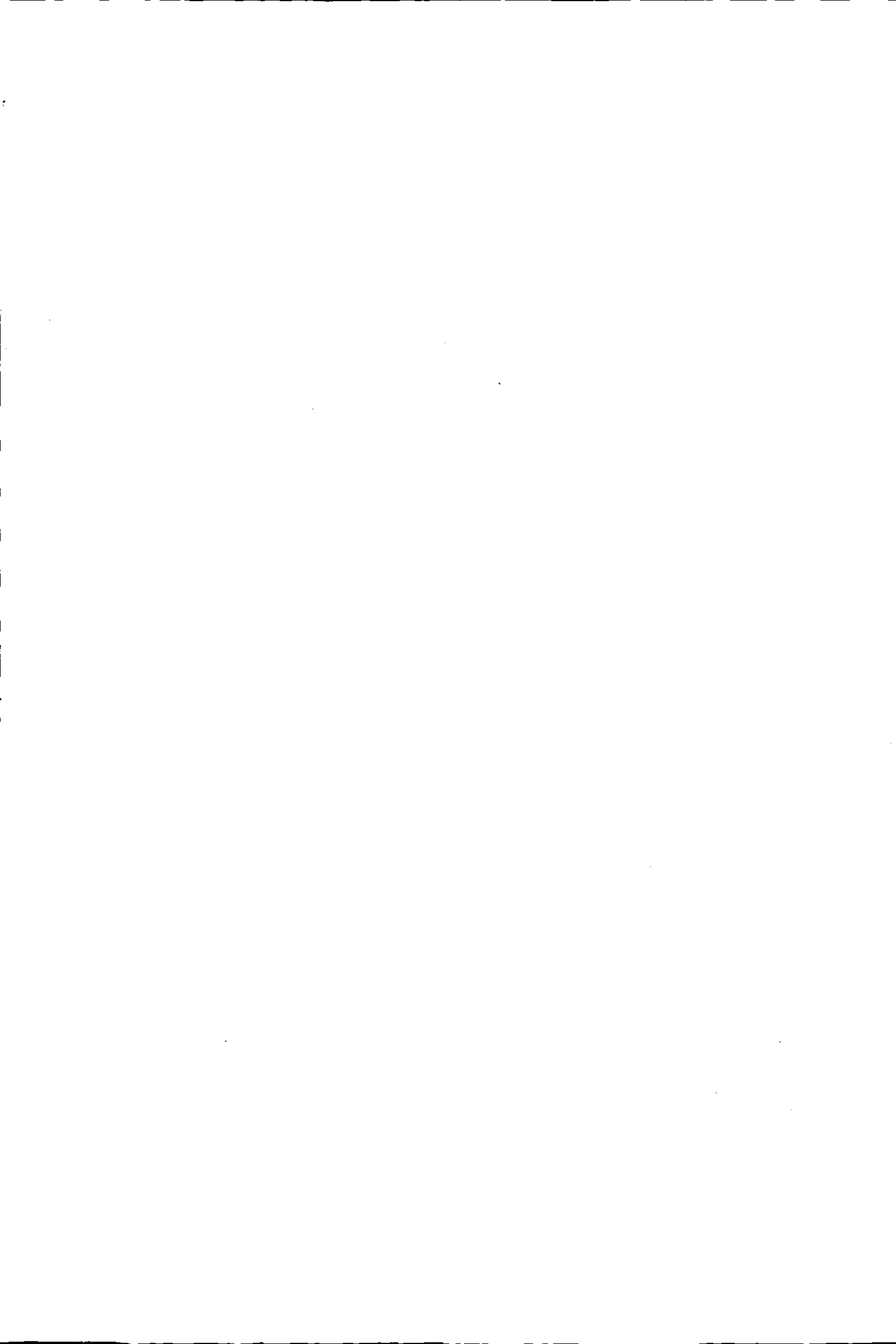
TABLE 6

Measurements of the electrical conductivity

Material	Thickness of cladding layer <sup>1)</sup> (micron)	Electrical conductivity (m/Ohm mm <sup>2</sup> )			
		on core	on cladding	difference	after re-heat treatment <sup>2)</sup> on core
A	59	17.4	18.2	0.8	16.1
B	126	18.6	21.3	2.7	16.6
C	82	16.6	18.6	2.0	
D	75	16.3	17.6	1.3	
E	88	16.6	17.9	1.3	16.6
F	50	17.2	17.7	0.5	16.6
G	52	16.6	17.2	0.6	
B'	122	19.1	21.8	2.7	
E'	100	17.0	19.2	2.2	
E''	110	19.6	22.3	2.7	

1) measured on etched microscopic specimen.

2) re-heat treatment consisted of solution heating at 495°C, water quenching and room temperature aging for 14 days.



## APPENDIX A

## Crack propagation records

The crack propagation records for all specimens have been compiled in tables 1-10, which also contain

the mean results for each group of similarly tested specimens.

Results for the constant-amplitude tests for  $S_a = 2.5$ , 4 and 6.5 kg/mm<sup>2</sup>, respectively, are to be found in: Tables 1-3: Materials A-G, specimens loaded in the rolling direction.

Crack propagation for  $S_a = 2.5$  kg/t  
 $n_1 - n_3$  is the number of cycles for extension

Material Specimen	A				F				E				U2
	A2	A10	A11	mean	K2	K6	K10	mean	N2	N6	N10	mean	
$l$ (mm)													$n_1 - n_3$ (k)
3	0	0	0	0	0	0	0	0	0	0	0	0	0
4	73.85	66.80	64.25	68.30	98.00	80.00	108.75	95.58	85.60	77.80	71.85	78.42	72.0
5	111.25	105.80	106.85	107.97	135.50	116.40	165.75	139.22	126.00	118.95	104.15	116.37	108.0
6	135.95	132.30	137.00	135.08	164.55	139.30	188.25	164.03	150.20	132.70	132.35	138.42	136.0
7	157.50	148.40	151.00	152.30	185.50	161.85	211.35	186.23	167.60	155.80	150.35	157.92	156.0
8	170.75	168.00	170.00	169.58	206.10	179.90	233.25	206.42	185.20	172.35	166.60	174.72	172.0
9	184.00	178.00	180.50	180.83	222.40	193.90	247.75	221.35	198.80	185.65	177.60	187.35	186.0
10	194.55	188.55	192.55	191.88	235.60	206.40	262.80	234.93	206.50	195.60	189.05	197.05	200.0
12	211.40	206.50	209.65	209.18	262.20	228.85	289.85	260.30	225.10	214.60	208.35	216.02	219.0
14	224.50	220.10	222.75	222.45	281.50	245.40	308.90	278.60	236.00	228.60	228.35	230.98	234.0
16	235.25	231.60	232.55	233.13	299.65	261.05	325.65	295.45	246.70	237.55	237.65	240.63	246.0
18	244.00	239.45	240.75	241.40	315.00	273.20	339.35	309.18	254.60	246.05	247.10	249.25	255.0
20	249.55	245.90	247.40	247.62	326.00	282.30	348.10	318.80	260.35	252.85	254.35	255.85	264.0
25	259.95	256.65	259.50	258.70	349.00	301.95	370.75	340.57	272.20	265.10	269.25	268.85	280.0
30	266.05	262.90	266.00	264.98	361.00	313.45	385.50	353.32	280.50	272.20	279.85	277.52	289.0
35	269.95	266.85	270.00	268.93	368.80	321.45	395.95	362.07	285.75	276.95	285.70	282.80	295.0
40	272.35	269.50	272.10	271.32	374.70	326.85	403.70	368.42	288.65	279.75	289.00	285.80	298.0
45	273.70	270.85	273.65	272.73	378.05	330.55	407.30	371.97	290.15	281.55	291.00	287.57	300.0
50	274.45	271.60	274.30	273.45	379.20	332.15	409.10	373.48	291.10	282.40	291.85	288.45	301.0
55		271.90	274.45		379.75	332.75	409.50	374.00	291.40	282.65			301.0
80	274.70	271.90	274.50	273.70	380.40	332.80	409.65	374.28	291.40	282.75	292.05	288.73	301.0

Crack propagation records for  $S_a = 4$  kg/t  
 $n_1 - n_3$  is the number of cycles for extension

Material specimen	A				F				E				U1
	A1	A5	A9	mean	K1	K5	K9	mean	N1	N5	N9	mean	
$l$ (mm)													$n_1 - n_3$ (k)
3	0	0	0	0	0	0	0	0	0	0	0	0	0
4	12.00	24.90	14.10	17.00	15.20	24.00	19.70	19.63	13.85	14.50	16.75	15.03	15.5
5	24.00	32.15	23.60	26.58	30.20	39.45	32.20	33.95	22.95	26.15	22.75	23.95	26.0
6	31.45	38.85	31.60	33.97	39.00	57.30	52.00	49.43	32.00	33.00	31.20	32.07	35.0
7	39.70	45.50	38.30	41.17	49.90	68.70	68.20	62.27	38.05	40.05	37.05	38.38	44.0
8	45.60	50.50	43.40	46.50	59.50	78.10	88.50	75.37	43.40	45.90	43.10	44.13	48.0
9	50.40	54.50	47.60	50.83	65.60	86.25	97.10	82.98	47.45	48.60	46.60	47.55	52.0
10	53.95	58.50	51.20	54.55	71.35	92.05	105.00	89.47	50.85	51.70	50.20	50.92	57.0
12	59.60	62.30	58.45	60.12	83.60	105.00	121.55	103.38	56.65	58.15	55.60	56.80	66.0
14	64.30	66.00	62.25	64.18	93.45	113.65	129.60	112.23	60.70	63.00	60.00	61.23	72.0
16	65.80	69.30	65.35	66.82	99.40	120.00	139.25	119.55	64.60	67.25	63.40	65.08	77.0
18	69.40	71.50	67.50	69.47	104.70	125.50	146.25	125.48	67.30	69.70	65.90	67.63	81.0
20	71.35	72.50	69.40	71.08	108.40	130.10	151.25	129.92	69.15	71.65	68.10	69.63	83.0
25	74.05	75.45	72.40	73.97	115.70	136.70	158.15	136.85	72.10	75.90	72.50	73.50	87.0
30	75.75	76.65	73.95	75.42	119.25	140.30	162.05	140.53	73.70	78.45	74.55	75.57	90.0
35	76.75	77.40	74.85	76.33	121.30	142.00	164.30	142.53	74.55	79.60	75.70	76.66	92.0
40	77.15	77.80	75.30	76.75	122.30	143.00	165.50	143.60	75.10	80.25	76.20	77.18	92.0
45	77.30	77.95	75.45	76.90	122.60	143.40	165.95	143.98	75.30	80.50	76.40	77.40	92.0
50		75.50			122.90	143.50	166.10	144.17					
80	77.30	78.10	75.50	76.97	123.20	143.60	166.10	144.30	75.35	80.55	76.50	77.47	93.0

Tables 4-6: Materials B', E' and E'', specimens loaded in the rolling direction.

Tables 7-9: Materials A, B, D-G, specimens loaded transverse to the loading direction.

The results of the program tests are presented in

table 10. The results for material B'' (2024-T81) were drawn from another NLR-investigation (ref. 4) regarding the fatigue crack propagation and the residual strength properties of this material as compared with those for 2024-T3.

ing direction parallel to rolling direction:  
crack from  $l=3$  mm to the indicated  $l$ -value

D			C				B				G			
U6	U10	mean	V2	V6	V10	mean	S2	S6	S10	mean	R5	R8	R3	mean
0	0	0	0	0	0	0	0	0	0	0	0	0	0	0
7.00	60.75	73.48	76.00	99.65	59.75	78.47	90.15	54.75	65.00	69.97	51.45	59.30	46.25	52.33
2.50	95.75	108.92	107.45	134.15	85.50	109.03	137.00	88.85	96.00	107.28	82.3	80.85	68.75	77.30
4.65	122.35	134.48	127.25	161.15	105.30	131.23	155.45	100.15	112.30	122.63	103.2	100.80	88.05	97.35
9.50	140.65	152.27	144.50	179.20	122.30	148.67	172.30	114.55	126.20	137.68	120.1	112.45	107.45	113.33
6.40	157.25	168.85	158.60	194.90	135.05	162.85	181.95	122.95	138.10	147.67	132.35	124.60	119.40	125.45
8.40	171.60	182.03	169.60	208.80	147.00	175.13	191.80	132.15	146.20	156.72	142.6	133.80	130.65	135.68
9.50	181.80	193.82	179.80	219.60	154.25	184.55	200.25	140.05	154.70	165.00	153.4	141.30	140.35	145.02
6.50	201.15	212.22	195.20	237.50	170.50	201.07	213.15	153.40	168.00	178.18	170.9	157.50	157.25	161.88
2.30	216.60	227.68	208.20	252.80	183.85	214.95	226.25	163.60	177.60	189.15	186.7	170.10	171.35	176.05
2.40	228.70	239.15	220.15	263.45	193.00	225.53	233.05	170.75	186.15	196.65	196.55	179.60	182.05	186.07
3.40	237.65	248.88	230.50	272.95	201.00	234.82	239.05	176.45	192.25	202.58	205.45	187.00	191.20	194.55
0.90	246.35	257.10	236.30	280.55	207.00	241.28	245.65	183.35	198.15	209.05	213.9	192.90	198.40	201.73
5.40	260.50	272.22	249.35	294.15	220.00	254.50	256.75	194.40	209.45	220.20	228.25	204.65	212.70	215.20
4.20	269.35	281.13	257.35	302.40	225.80	261.85	264.95	201.80	217.55	228.10	236.0	211.30	221.05	222.78
0.45	274.70	286.90	261.95	307.35	230.75	266.68	270.65	207.20	223.30	233.72	241.4	215.75	226.85	228.00
4.05	278.10	290.33	264.75	310.80	233.50	269.68	274.45	211.35	227.90	237.90	244.45	218.25	229.85	230.85
6.20	280.30	292.35	266.55	312.80	235.20	271.52	276.70	213.10	230.70	240.17	246.45	219.80	231.55	232.60
7.50	281.40	293.47	267.45	313.95	236.10	272.50	277.95	214.20	232.30	241.48	247.55	220.45	232.45	233.48
7.90	281.65	293.72	267.55	314.25			278.85	214.70	233.15	242.23	247.95		232.65	
8.20	281.80	293.93	267.60	314.40	236.20	272.73	278.95	214.70	233.30	242.32	247.95	220.55	232.75	233.75

ing direction parallel to rolling direction  
crack from  $l=3$  mm to the indicated  $l$ -value

D			C				B				G			
U5	U9	mean	V1	V5	V9	mean	S1	S5	S9	mean	R10	R4	R1	mean
0	0	0	0	0	0	0	0	0	0	0	0	0	0	0
5.55	14.40	15.28	12.70	13.65	15.75	14.03	8.05	10.35	9.95	9.45	13.9	18.8	17.0	16.75
5.00	26.90	26.33	21.65	22.25	29.55	24.48	15.55	16.40	18.80	16.92	23.0	28.25	26.5	25.92
7.10	36.70	36.47	29.10	32.10	37.20	32.80	21.10	22.50	23.90	22.50	31.85	37.35	35.2	34.80
4.70	44.10	44.57	35.60	41.25	44.30	40.38	26.70	26.45	28.95	27.37	39.7	43.85	41.65	41.73
0.75	50.60	50.08	41.75	47.70	50.05	46.50	29.90	30.35	31.85	30.70	45.5	48.85	47.7	47.35
5.90	55.90	55.17	46.00	54.50	54.60	51.70	33.45	33.85	35.75	34.35	50.7	52.80	52.5	52.00
0.35	59.65	59.22	50.25	59.45	59.70	56.47	36.45	36.85	38.15	37.15	55.4	56.1	56.0	55.83
3.75	66.50	67.22	56.80	69.15	67.10	64.35	41.10	41.65	43.95	42.23	62.3	61.75	63.5	62.52
3.85	72.05	72.88	63.10	75.40	72.50	70.33	45.50	46.55	49.15	47.07	67.15	66.1	68.7	67.32
0.20	76.15	77.98	67.40	80.00	77.90	75.10	48.80	50.95	53.60	51.12	71.35	69.55	72.7	71.20
3.30	78.90	81.07	70.40	83.20	80.15	77.92	51.80	54.85	57.25	54.63	74.2	72.3	75.9	74.13
5.65	81.85	83.70	72.85	85.20	82.30	80.12	54.80	57.85	60.35	57.67	76.45	74.5	78.1	76.35
9.45	86.15	87.83	75.80	88.50	86.05	83.45	59.15	62.30	65.80	62.42	80.4	78.65	82.35	80.47
1.40	87.85	89.95	77.45	90.15	88.05	85.22	61.50	64.75	69.05	65.10	82.6	81.0	84.65	82.75
2.65	88.95	91.23	78.35	91.00	89.20	86.18	62.65	65.90	70.35	66.30	83.8	82.4	86.0	84.07
3.15	89.50	91.80	78.80	91.50	89.70	86.67	63.50	66.45	71.15	67.03	84.55	83.2	86.6	84.78
3.35	89.70	92.00	79.00	91.60	89.90	86.83	63.95	66.80	71.50	67.42	84.85	83.7	86.9	85.15
3.45	89.75						64.10	66.95	71.55	67.53		83.85	87.05	
3.55	89.80	92.15	79.00	91.60	89.95	86.85	64.20	66.95	71.55	67.59	85.0	83.85	87.1	85.32

Crack propagation records for  $S_a = 6.5$  kg/r  
 $n_1 - n_3$  is the number of cycles for extension

Material specimen	A				F				E				U
	A4	A6	A12	mean	K4	K8	K12	mean	N4	N8	N12	mean	
$l$ (mm)													$n_1 - n_3$ (k)
3	0	0	0	0	0	0	0	0	0	0	0	0	0
4	6.20	5.45	5.35	5.67	7.65	6.50	10.25	8.13	5.70	4.45	5.80	5.32	5.
5	10.00	9.95	9.85	9.93	17.50	16.10	18.05	17.22	10.90	9.20	10.30	10.13	10.
6	13.40	13.55	13.85	13.60	24.70	27.20	26.30	26.07	14.15	13.00	14.80	13.98	12.
7	15.60	15.85	16.40	15.95	31.10	31.55	32.05	31.57	16.80	15.50	19.00	17.10	15.
8	17.55	17.95	17.95	17.82	35.90	35.90	36.10	35.97	19.40	16.80	22.20	19.47	18.
9	19.30	19.65	19.35	19.43	39.20	40.05	39.65	39.63	21.45	18.10	24.30	21.28	19.
10	20.30	20.55	20.40	20.42	41.40	42.15	42.80	42.12	22.75	18.90	26.20	22.62	21.
12	21.85	22.40	21.95	22.07	45.50	46.40	47.05	46.32	24.80	20.40	28.05	24.42	24.
14	22.85	23.50	23.00	23.12	48.10	49.50	49.65	49.08	26.30	21.40	29.40	25.70	25.
16	23.65	24.40	23.80	23.95	49.50	50.90	51.65	50.68	27.35	21.90	30.25	26.50	26.
18	24.20	24.85	24.35	24.47	51.45	52.40	52.90	52.25	28.15	22.35	30.85	27.12	27.
20	24.50	25.35	24.65	24.83	52.30	53.55	53.75	53.20	28.75	22.70	31.30	27.80	27.
25	25.10	26.00	25.30	25.47	53.80	53.95	55.35	54.37	29.65	23.30	31.90	28.28	28.
30	25.35	26.35	25.60	25.77	54.50	54.05	56.00	54.85	30.05	23.50	32.25	28.60	28.
35		26.50	25.70		54.75		56.25		30.15	23.60	32.30	28.68	29.
40			25.75				56.35						
45													
80	25.40	26.55	25.75	25.90	54.90	54.20	56.40	55.17	30.20	23.60	32.40	28.73	29.

TABLE A4

Crack propagation records for  $S_a = 2.5$  kg/mm<sup>2</sup> loading direction parallel to rolling direction, materials with additional heat treatments.  
 $n_1 - n_3$  is the number of cycles for extending the crack from  $l = 3$  mm to the indicated  $l$ -value.

Material specimen	B'				E'				E''			
	S <sub>L</sub> 2	S <sub>L</sub> 6	S <sub>L</sub> 10	mean	1T81	4T81	9T81	mean	1/5	2/2	6/2	mean
$l$ (mm)	$n_1 - n_3$ (kc)											
3	0	0	0	0	0	0	0	0	0	0	0	0
4	78.0	52.0	89.15	73.05	63.5	66.3	73.8	67.87	50.75	53.55	55.00	53.10
5	114.0	94.0	131.00	113.0	99.3	108.9	120.8	109.67	73.40	79.55	85.10	79.35
6	136.0	114.8	149.1	133.30	123.15	128.1	142.8	131.35	88.35	95.55	97.00	93.63
7	147.0	126.7	165.95	146.55	141.25	146.85	156.9	148.33	100.85	109.55	108.90	106.43
8	158.0	137.0	178.85	157.95	152.3	167.0	171.1	163.47	109.45	118.60	115.80	114.62
9	167.8	147.1	186.35	167.08	168.15	180.05	183.0	177.07	117.15	125.80	124.50	122.48
10	174.0	157.0	194.70	175.23	178.55	188.5	192.0	186.35	123.25	132.75	129.80	128.60
12	187.8	169.0	209.25	188.68	192.95	205.05	205.6	201.20	133.20	141.75	137.85	137.93
14	197.9	179.8	220.90	199.53	207.85	219.25	217.7	214.93	140.65	149.10	145.70	145.15
16	204.8	186.2	229.8	206.93	216.3	228.35	228.2	224.28	145.45	156.00	150.30	150.58
18	211.5	193.5	237.25	214.08	220.75	233.15	232.95	228.95	149.30	160.20	154.50	153.67
20	216.5	199.2	243.35	219.68	224.9	237.25	236.4	232.85	152.40	163.65	157.50	157.85
25	227.15	210.4	256.85	231.47	230.7	243.35	242.9	238.98	157.00	169.45	162.40	162.95
30	234.95	218.8	266.50	240.08	234.2	246.7	247.1	242.67	160.35	173.55	165.75	166.55
35	240.40	225.6	273.5	246.50	236.3	248.85	248.95	244.70	162.45	175.55	167.95	168.65
40	244.45	229.5	277.8	250.25	237.7	250.3	250.4	246.13	163.50	177.35	169.25	170.03
45	246.50	231.5	280.05	252.68	238.6	251.0	251.15	246.92	164.65	178.30	170.05	171.00
50	247.55	232.75	281.55	253.95		251.55	251.7		165.20	178.75	170.50	171.45
55	248.20	233.40	282.00	254.53						178.95		
80	248.30	233.50	282.10	254.63	239.3	251.65	251.8	247.58	165.40	179.05	170.70	171.87

loading direction parallel to rolling direction  
 crack from  $l=3$  mm to the indicated  $l$ -value

l	D		C				B				G			
	U12	mean	V4	V8	V12	mean	S4	S8	S12	mean	R12	R6	R2	mean
0	0	0	0	0	0	0	0	0	0	0	0	0	0	0
4.40	7.35	6.32	6.35	4.80	5.50	5.55	4.70	4.15	4.05	4.30	6.4	6.15	5.75	6.00
4.70	13.15	11.42	10.10	8.60	9.75	9.48	7.90	7.15	6.50	7.18	11.05	11.3	9.25	10.00
4.70	19.05	16.18	14.20	11.95	14.85	13.67	10.35	9.60	8.90	9.62	14.7	15.55	13.2	14.00
4.90	26.50	21.10	17.25	15.10	18.10	16.82	13.35	11.60	11.10	12.02	18.3	19.25	16.05	17.00
5.05	29.90	24.35	20.00	17.90	20.45	19.45	15.05	13.35	13.90	14.10	21.35	22.05	18.15	20.00
5.00	32.75	26.78	21.80	20.00	22.30	21.37	17.50	16.05	16.40	16.65	23.4	24.2	20.45	22.00
5.60	34.50	28.57	23.10	21.45	23.55	22.70	18.95	17.85	17.70	18.17	24.9	25.55	22.05	24.00
5.85	36.95	30.93	24.90	23.65	25.50	24.68	21.15	21.50	19.65	20.77	27.15	27.80	24.75	26.00
6.15	38.25	32.30	26.00	24.90	26.50	25.80	23.10	23.60	21.45	22.72	28.55	29.35	26.35	28.00
6.05	39.20	33.27	26.75	25.80	27.40	26.65	23.95	25.05	22.50	23.83	29.4	30.35	27.3	29.00
6.55	39.90	33.87	27.35	26.30	27.90	27.18	24.75	26.05	23.15	24.65	30.15	30.95	27.85	29.00
6.05	40.30	34.38	27.80	26.80	28.30	27.63	25.20	26.65	23.65	25.17	30.6	31.55	28.35	30.00
6.80	41.05	35.13	28.40	27.50	28.85	28.25	25.95	27.75	24.40	26.03	31.4	32.2	29.1	30.00
6.05	41.30	35.42	28.60	27.80	29.10	28.53	26.30	28.25	24.80	26.45	31.8	32.7	29.4	31.00
6.10	41.55	35.55	28.85	27.95	29.20	28.67	26.55	28.60	25.10	26.75	32.0	32.8	29.6	31.00
								28.85	25.20		32.1	32.9	29.7	31.00
											32.2	33.0	29.8	31.00
6.15	41.55	35.63	28.85	28.00	29.20	28.68	26.55	29.15	25.20	26.97	32.2	33.0	29.8	31.00

TABLE A5

Crack propagation records for  $S_a = 4$  kg/mm<sup>2</sup>; loading direction parallel to rolling direction, materials with additional heat treatments.  
 $m_1 - m_3$  is the number of cycles for extending the crack from  $l = 3$  mm to the indicated  $l$ -value

Material Specimen	B'				E'				E''			
	S <sub>L1</sub>	S <sub>L5</sub>	S <sub>L9</sub>	mean	2T81	5T81	7T81	mean	6/5	3/2	4/5	mean
$l$ (mm)	$m_1 - m_3$ (kc)											
3	0	0	0	0	0	0	0	0	0	0	0	0
4	16.35	9.05	15.45	13.62	15.7	14.15	10.25	13.37	8.35	11.35	9.40	9.70
5	23.95	18.00	22.20	21.38	26.3	24.2	27.35	25.95	15.05	17.30	15.45	15.93
6	29.65	23.25	30.0	27.63	32.8	32.05	35.2	33.35	19.55	22.30	20.25	20.70
7	34.60	28.45	33.7	32.25	41.1	36.5	40.5	39.37	23.30	25.45	23.80	24.18
8	39.4	32.40	37.8	36.53	46.4	42.45	45.3	44.72	26.30	28.40	26.55	27.08
9	42.5	35.55	41.3	39.78	49.95	47.95	49.8	49.23	29.05	30.60	29.35	29.67
10	44.8	38.85	44.1	42.58	52.7	50.9	52.85	52.15	30.50	32.60	31.25	31.45
12	49.65	43.50	48.45	47.20	56.25	56.45	57.85	56.85	33.80	35.30	34.35	34.45
14	54.40	48.25	52.90	51.85	59.2	59.15	60.7	59.68	36.65	37.70	36.30	36.88
16	59.1	51.80	57.1	56.0	61.05	60.9	62.65	61.53	38.30	39.35	37.95	38.53
18	62.1	55.6	60.6	59.43	61.95	62.0	64.1	62.68	39.50	40.50	39.15	39.72
20	64.35	58.2	63.2	61.92	62.95	62.85	65.15	63.65	40.50	41.35	40.05	40.63
25	68.20	63.4	67.6	66.40	64.65	64.45	66.75	65.28	42.15	42.80	41.55	42.17
30	70.6	65.75	70.45	68.93	65.25	65.3	67.55	66.03	43.10	43.65	42.65	43.13
35	71.9	67.10	72.15	70.38	65.80	65.75	67.95	66.50	43.65	44.25	43.30	43.73
40	72.8	67.75	72.95	71.17	66.0	66.0	68.15	66.72	44.05	44.55	43.65	44.05
45	73.1	68.20	73.20	71.5					44.25	44.65	43.80	44.20
50	73.2	68.4	73.3	71.63								
80	73.3	68.5	73.4	71.73	66.20	66.20	68.3	66.90	44.45	44.90	43.95	44.47

TABLE A6

Crack propagation records for  $S_a = 6.5 \text{ kg/mm}^2$ , loading direction parallel to the rolling direction, materials with additional heat treatments.  
 $n_l - n_3$  is the number of cycles for extending the crack length from  $l = 3 \text{ mm}$  to the indicated  $l$ -value.

Material specimen	B'				E'				E''			
	S <sub>L</sub> 4	S <sub>L</sub> 8	S <sub>L</sub> 12	mean	3T81	6T81	8T81	mean	5/2	2/5	1/2	mean
$l$ (mm)	$n_l - n_3$ (kc)											
3	0	0	0	0	0	0	0	0	0	0	0	0
4	5.45	5.25	3.85	4.85	5.45	7.05	4.15	5.55	3.70	3.30	3.70	3.57
5	9.20	7.85	6.55	7.87	10.65	12.9	7.25	10.27	6.15	5.50	6.20	5.95
6	11.15	10.45	8.45	10.02	14.35	17.4	9.65	13.8	7.95	7.30	8.10	7.78
7	12.65	12.45	11.10	12.07	16.5	19.1	11.25	15.62	9.35	8.65	9.55	9.18
8	14.60	14.70	13.55	14.28	17.75	20.1	12.35	16.73	10.55	9.70	10.40	10.22
9	17.25	16.9	15.45	16.53	18.3	20.8	13.15	17.42	11.40	10.35	11.10	10.95
10	18.80	18.55	16.80	18.05	18.95	21.4	13.6	17.98	11.95	10.85	11.60	11.47
12	20.95	21.10	18.85	20.3	19.85	22.3	14.2	18.78	12.70	11.60	12.40	12.23
14	22.40	22.75	20.45	21.87	20.4	22.9	14.75	19.35	13.35	12.10	13.00	12.82
16	23.45	23.50	21.70	22.88	20.8	23.3	15.15	19.75	13.85	12.50	13.50	13.28
18	24.35	24.2	22.5	23.68	21.05	23.65	15.3	20.00	14.20	12.80	13.90	13.63
20	24.80	24.7	22.9	24.13	21.3	23.95	15.55	20.27	14.45	13.10	14.20	13.92
25	25.4	25.45	23.6	24.82	21.5	24.35	15.9	20.58	14.90	13.30	14.70	14.30
30	25.8	25.80	24.1	25.23		24.6	16.1		15.15	13.50	15.05	14.57
35	26.1	26.0	24.4	25.5		24.75	16.2				15.20	
40	26.2	26.2	24.6	25.7								
80	26.3	26.3	24.7	25.8	21.65	24.8	16.3	20.92	15.35	13.75	15.30	14.80

TABLE A7  
 Crack propagation records for  $S_a = 2.5 \text{ kg/mm}^2$ , loading direction parallel to the rolling direction, materials with additional heat treatments.  
 $n_l - n_3$  is the number of cycles for extending the crack length from  $l = 3 \text{ mm}$  to the indicated  $l$ -value.

Material specimen	A				F			
	A7	A5	A2	mean	K3	K5	mean	N5
$l$ (mm)	$n_l - n_3$ (kc)							
3	0	0	0	0	0	0	0	0
4	52.5	61.75	32.7	48.98	127.0	102.75	114.88	80.0
5	81.8	77.50	55.1	71.47	176.4	138.50	157.45	110.9
6	100.9	100.7	68.9	90.17	206.4	160.10	183.25	137.45
7	115.9	114.7	80.95	103.85	222.95	174.00	198.48	151.50
8	127.0	127.3	89.2	114.50	238.65	189.30	213.98	160.45
9	137.45	134.7	97.2	123.12	252.00	199.75	225.88	170.30
10	144.35	141.9	102.3	129.52	261.15	207.30	234.23	178.20
12	156.45	153.2	113.2	140.95	283.00	222.25	252.63	193.95
14	165.5	162.35	119.3	149.05	300.3	233.90	267.10	206.40
16	171.75	167.8	123.9	154.48	310.5	242.15	276.33	215.05
18	176.25	172.45	127.7	158.80	319.6	249.65	284.63	221.40
20	179.9	176.5	130.3	162.23	327.0	255.95	291.48	227.95
25	186.55	182.15	135.7	168.13	341.15	266.65	303.90	237.25
30	190.4	185.75	138.7	171.62	350.95	274.20	312.58	243.95
35	192.65	188.0	140.4	173.68	356.70	278.90	317.80	247.95
40	193.9	189.2	141.4	174.83	360.60	281.75	321.18	250.30
45	194.6	190.0	142.0	175.53	363.00	283.40	323.20	251.75
50	195.0	190.45	142.2	175.88	364.25	284.10	324.18	252.25
55	195.0		142.3			284.20		
80	195.0	190.5	142.3	175.93	364.70	284.20	324.45	252.40

ding direction transverse to rolling direction  
crack from  $l=3$  mm to the indicated  $l$ -value

E		D			B	G			
N3	mean	U3	U5	mean	S3	R4	R7	R3	mean
0	0	0	0	0	0	0	0	0	0
48.55	64.28	62.15	57.2	59.68	43.4	41.45	61.20	47.00	49.88
80.65	95.78	96.75	77.5	87.13	70.35	75.05	89.70	77.05	80.60
94.75	116.10	116.15	98.4	107.28	86.65	89.85	106.10	95.85	97.27
101.85	126.68	130.15	110.6	120.38	97.85	105.90	122.45	110.95	113.10
115.15	135.80	140.20	120.5	130.35	107.80	118.90	135.15	123.15	125.73
119.00	144.65	149.65	132.3	140.98	115.35	127.15	144.80	131.50	134.48
125.20	151.70	158.25	136.8	147.53	120.95	136.70	152.95	140.55	143.40
137.00	165.48	171.10	149.1	160.10	132.15	149.35	168.00	153.40	156.92
146.90	176.65	180.95	158.65	169.80	140.70	159.05	180.15	164.45	167.88
153.75	184.40	189.15	166.75	177.95	147.85	167.05	189.00	172.85	176.30
158.70	190.05	194.75	172.50	183.63	153.50	173.35	195.95	179.30	182.87
163.65	195.80	199.75	177.15	188.45	157.95	179.65	201.60	186.35	188.87
171.75	204.50	208.70	186.65	197.68	165.85	189.20	211.70	195.95	198.95
176.25	210.10	215.20	192.65	203.93	171.25	195.80	219.25	202.95	206.00
179.60	213.80	218.45	196.50	207.48	175.10	200.05	223.90	207.75	210.57
181.55	215.93	220.60	198.70	209.65	177.35	202.55	226.45	210.80	213.27
182.65	217.20	221.85	199.80	210.83	178.80	203.95	228.15	212.40	214.83
183.20	217.73	222.55	200.55	211.55	179.45	204.75	229.05	213.20	215.67
		222.75	200.60	211.68	179.85	204.95	229.25	213.40	215.87
183.25	217.83	222.75	200.60	211.68	179.95	204.95	229.25	213.40	215.87

Crack propagation records for  $S_a = 4$  kg/m  
 $n_1 - n_3$  is the number of cycles for extend

Material specimen	A			F			E			U2
	A3	A6	mean	K6	K2	mean	N6	N2	mean	
$l$ (mm)										$n_1 - n_3$ (kc)
3	0	0	0	0	0	0	0	0	0	0
4	11.65	14.25	12.95	12.90	16.50	14.70	10.00	10.50	10.25	14.50
5	18.95	20.35	19.65	20.05	24.05	22.05	15.50	15.65	15.58	18.70
6	24.60	26.75	25.68	27.90	30.80	29.35	21.40	20.25	20.83	24.65
7	28.90	30.40	29.65	33.00	37.15	35.08	26.10	25.10	25.60	29.30
8	32.15	34.05	33.10	38.20	42.35	40.28	29.90	28.30	29.10	33.70
9	34.80	36.85	35.83	41.45	47.25	44.35	32.50	30.90	31.70	36.80
10	36.70	38.40	37.55	44.05	50.65	47.35	34.90	33.20	34.05	39.90
12	40.50	42.00	41.25	49.60	57.20	53.40	38.70	37.15	37.93	44.30
14	43.20	44.90	44.05	53.60	62.35	57.98	41.70	40.25	40.98	47.90
16	45.05	46.75	45.90	56.90	66.80	61.85	44.00	42.20	43.10	50.90
18	46.25	48.00	47.13	59.30	70.20	64.75	45.60	43.95	44.78	52.90
20	47.05	48.90	47.98	61.30	72.40	66.85	46.70	45.35	46.03	54.90
25	48.40	50.75	49.58	65.20	77.50	71.35	48.85	48.05	48.45	57.30
30	49.20	51.60	50.40	67.65	80.30	73.98	50.00	49.25	49.63	58.60
35	49.60	52.00	50.80	68.95	81.80	75.38	50.55	49.90	50.23	59.30
40	49.85	52.20	51.03	69.70	82.55	76.13	50.90	50.35	50.63	59.70
45	49.95	52.35	51.15	70.05	82.95	76.50	51.10	50.55	50.83	59.90
50				70.10						
80	49.95	52.35	51.15	70.10	83.10	76.60	51.10	50.60	50.85	59.90

Crack propagation records for  $S_a = 6.5$  kg/m  
 $n_1 - n_3$  is the number of cycles for extend

Material specimen	A				F			N1
	A8	A4	A1	mean	K4	K1	mean	
$l$ (mm)								$n_1 - n_3$ (kc)
3	0	0	0	0	0	0	0	0
4	4.30	4.90	2.80	4.00	6.70	8.35	7.53	5.30
5	7.35	7.40	4.60	6.45	10.90	12.30	11.60	8.10
6	9.90	9.90	6.50	8.77	14.00	16.00	15.00	10.30
7	11.70	11.55	7.80	10.35	16.40	19.15	17.78	12.30
8	12.85	13.00	8.90	11.58	19.00	21.90	20.45	13.70
9	13.95	14.00	9.60	12.52	21.30	24.05	22.68	14.90
10	14.50	14.80	10.15	13.15	23.00	25.55	24.28	16.00
12	15.45	15.95	11.00	14.13	25.80	28.05	26.93	18.05
14	16.00	16.65	11.55	14.73	27.80	29.85	28.83	19.35
16	16.40	17.15	11.90	15.15	29.15	31.15	30.15	19.95
18	16.70	17.50	12.15	14.55	30.25	32.00	31.13	20.50
20	16.90	17.75	12.40	15.68	30.80	32.75	31.78	20.90
25	17.30	18.10	12.70	16.03	32.25	33.70	32.98	21.55
30	17.40	18.30	12.85	16.18	32.90	34.10	33.50	21.85
35	17.50	18.40	12.95	16.28	33.20	34.30	33.75	22.00
40	17.60	18.45			33.30	34.40	33.85	
45					33.40			
80	17.60	18.45	13.00	16.35	33.40	34.45	33.93	22.10

ing direction transverse to rolling direction  
crack from  $l=3$  mm to the indicated  $l$ -value

D		B					G			
U6	mean	S6	S2	S4	SJ	mean	R6	R8	R1	mean
0	0	0	0	0	0	0	0	0	0	0
6.96	10.73	14.0	7.80	11.70	10.95	11.11	13.30	13.45	12.95	13.23
13.20	15.95	20.80	14.70	17.05	17.20	17.44	20.60	21.45	21.15	21.07
18.95	21.80	26.00	18.85	23.45	22.00	22.58	26.40	27.45	27.10	26.98
24.40	26.85	31.00	21.45	27.50	26.15	26.63	31.80	32.70	32.20	32.23
26.90	30.30	32.00	23.55	31.05	30.00	29.15	36.45	36.65	36.50	36.53
30.60	33.70	34.30	25.50	33.75	32.25	31.45	40.50	40.30	39.35	40.05
32.75	36.33	37.10	26.80	36.25	34.25	33.60	43.70	43.00	41.90	42.87
37.45	40.88	40.50	29.50	40.95	38.00	37.24	48.80	48.00	47.20	48.00
40.90	44.40	44.20	31.65	44.45	41.30	40.40	53.15	53.20	50.85	52.40
43.30	47.10	46.20	33.60	47.10	44.10	42.75	56.30	56.70	54.15	55.72
43.30	49.10	48.60	34.90	49.85	46.25	44.90	59.25	59.45	56.45	58.38
47.10	51.00	50.60	35.90	51.85	47.85	46.55	61.40	61.85	58.25	60.50
49.85	53.58	54.45	37.30	55.10	51.35	49.55	65.80	65.65	61.25	63.90
51.35	54.98	56.80	38.30	57.00	53.10	51.30	66.85	67.55	62.80	65.73
52.30	55.80	57.80	38.60	58.05	54.05	52.13	67.80	68.65	63.65	66.70
52.85	56.28	58.30	38.90	58.60	54.55	52.59	68.35	69.15	64.15	67.22
53.15	56.53	58.50	39.20	58.95	54.70	52.84	68.60	69.40		
		58.65			54.90					
53.20	56.55	58.70	39.20	59.15	55.00	53.01	68.70	69.55	64.40	67.55

ing direction transverse to the rolling direction  
crack from  $l=3$  mm to the indicated  $l$ -value

E		D			B	G			
N4	mean	U4	U1	mean	S5	R10	R12	R5	mean
0	0	0	0	0	0	0	0	0	0
4.75	5.03	4.90	2.45	3.68	4.25	5.30	4.75	5.40	5.15
7.55	7.83	7.95	6.00	6.98	7.00	8.75	8.35	8.25	8.45
10.30	10.30	9.80	7.90	8.85	9.00	11.65	11.20	11.55	11.47
11.70	12.00	11.90	10.20	11.05	10.65	14.50	13.35	14.10	13.98
12.90	13.30	13.50	11.60	12.55	12.15	16.95	15.80	16.10	16.28
14.40	14.65	14.70	12.40	13.55	13.20	18.60	17.50	17.90	18.00
15.35	15.68	15.55	13.25	14.40	14.20	20.10	18.80	19.15	19.68
16.95	17.50	17.00	14.80	15.90	15.95	22.00	20.75	21.05	21.27
18.05	18.70	17.90	15.60	16.75	17.10	23.35	22.00	22.30	22.55
18.65	19.30	18.45	16.15	17.30	18.15	24.25	22.90	22.95	23.37
19.10	19.80	18.85	16.55	17.70	18.70	24.85	23.40	23.40	23.88
19.30	20.10	19.20	16.85	18.03	19.20	25.35	23.80	23.75	24.30
19.85	20.70	19.70	17.25	18.48	20.00	26.15	24.30	24.25	24.90
20.05	20.95	19.95	17.40	18.68	20.35	26.45	24.60	24.50	25.18
20.15	21.08	20.05	17.50	18.78	20.60	26.55	24.70	24.70	25.32
20.25					20.75	26.65	24.80	24.75	25.40
						26.75			
20.35	21.23	20.20	17.70	18.95	20.80	27.80	24.85	24.75	25.60

Crack propagation records for the program □  
 $n_1 - n_5$  is the number of cycles for extension

Material specimen	A				F			D			U3
	A3	A7	A8	mean	K7	K3	mean	N11	N3	N7	
$l$ (mm)											$n_1 - n_5$ (kc)
5	0	0	0	0	0	0	0	0	0	0	0
6	14.38	13.88	12.50	13.19	17.98	12.75	15.37	14.78	14.53	13.78	16.1
7	26.43	25.86	22.88	24.37	31.88	24.43	28.06	27.01	26.28	25.93	28.2
8	36.18	36.59	32.11	34.35	43.41	35.88	39.05	37.41	38.11	35.03	41.9
9	44.46	45.62	39.74	42.68	54.79	46.28	50.04	45.66	47.96	43.08	52.3
10		53.27	46.54	49.91	64.97	55.26	60.02	52.59	55.64	50.21	59.9
12		66.12	59.32	62.72	80.30	76.74	78.02		68.04	61.79	71.6
14		76.62	68.35	72.49	93.20	91.89	92.09			72.22	82.8
16		84.52	76.73	80.63	105.15	103.94	104.05			80.52	92.9
18		91.65	83.53	87.59	115.83	115.52	115.08			87.35	100.7
20		97.58	88.56	93.07	124.46	123.07	123.07			93.35	107.0
25		105.91	96.34	101.13	140.84	138.72	139.08			102.60	119.3
30		109.74	100.79	105.27	152.62	147.27	150.00			107.65	126.9
35		112.04	103.47	107.76	157.17	151.97	154.07			110.30	130.8
40			104.06		159.38	154.10	156.04				
45					160.16	154.95	157.06				
80		114.07	104.06	109.07	160.23	155.06	157.05			112.60	132.3

g direction parallel to rolling direction  
 tick from  $l=5$  mm to the indicated  $l$ -value

l	D		C			B			B'		
	U7	mean	V3	V7	mean	S3	S7	mean	SL7	SL3	mean
0	0	0	0	0	0	0	0	0	0	0	0
1.63	15.15	15.89	17.83	14.68	16.26	14.93	11.70	13.32	12.90	12.31	12.61
1.76	28.45	27.98	32.96	27.93	30.45	26.83	21.93	24.38	23.68	22.69	23.19
1.91	39.50	40.90	45.04	38.98	42.01	35.96	30.86	33.41	32.58	31.97	32.28
1.06	47.85	51.70	54.34	48.96	51.65	43.36	38.26	40.81	40.08	39.60	39.84
1.98	55.15	59.55	63.37	57.04	60.21	49.84	44.81	47.33	46.48	45.85	46.17
1.44	69.20	73.52	77.17	71.07	74.12	61.42	56.51	58.97	56.61	56.38	56.50
1.92	81.35	84.35	88.42	81.67	85.05	70.97	66.11	68.54	65.31	65.31	65.31
1.79	91.80	95.44	97.80	90.82	94.31	79.20	73.96	76.58	73.19	72.41	72.80
1.76		104.20	105.03	98.35	101.69	85.50	80.46	82.98	79.87	78.36	79.12
1.56		111.34	110.98	104.10	107.54	90.80	86.01	88.41	85.15	83.74	84.45
1.83		124.60	121.01	114.00	117.51	101.68	97.56	99.62	94.63	93.44	94.04
1.73		132.12	125.24	119.03	122.14	107.83	104.16	106.00	100.21	98.72	99.47
1.31		136.09		121.33		111.53	107.51	109.52	103.86	101.70	102.78
1.279							109.44		105.79		
							110.07				
1.378		138.05	126.71	123.02	124.87	114.38	110.19	112.29	106.71	104.18	105.4

